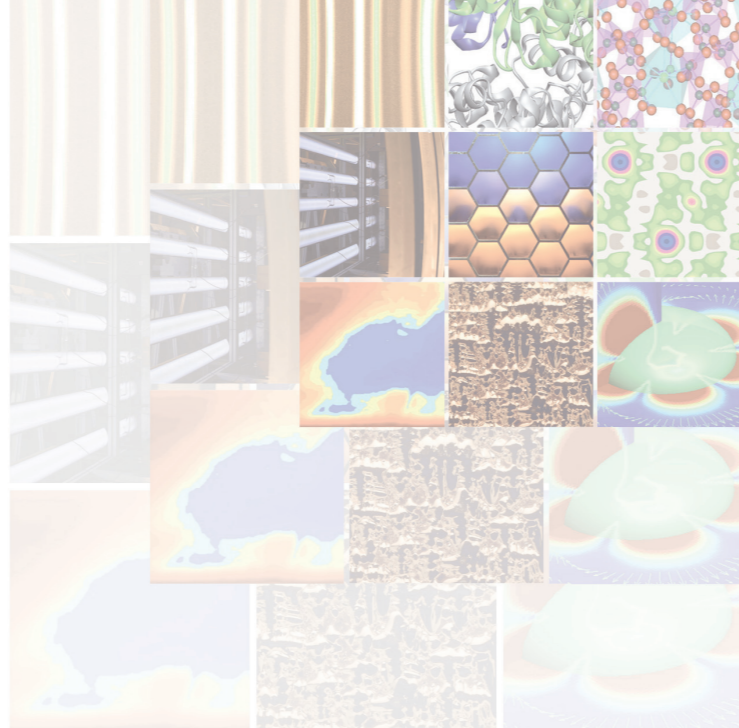


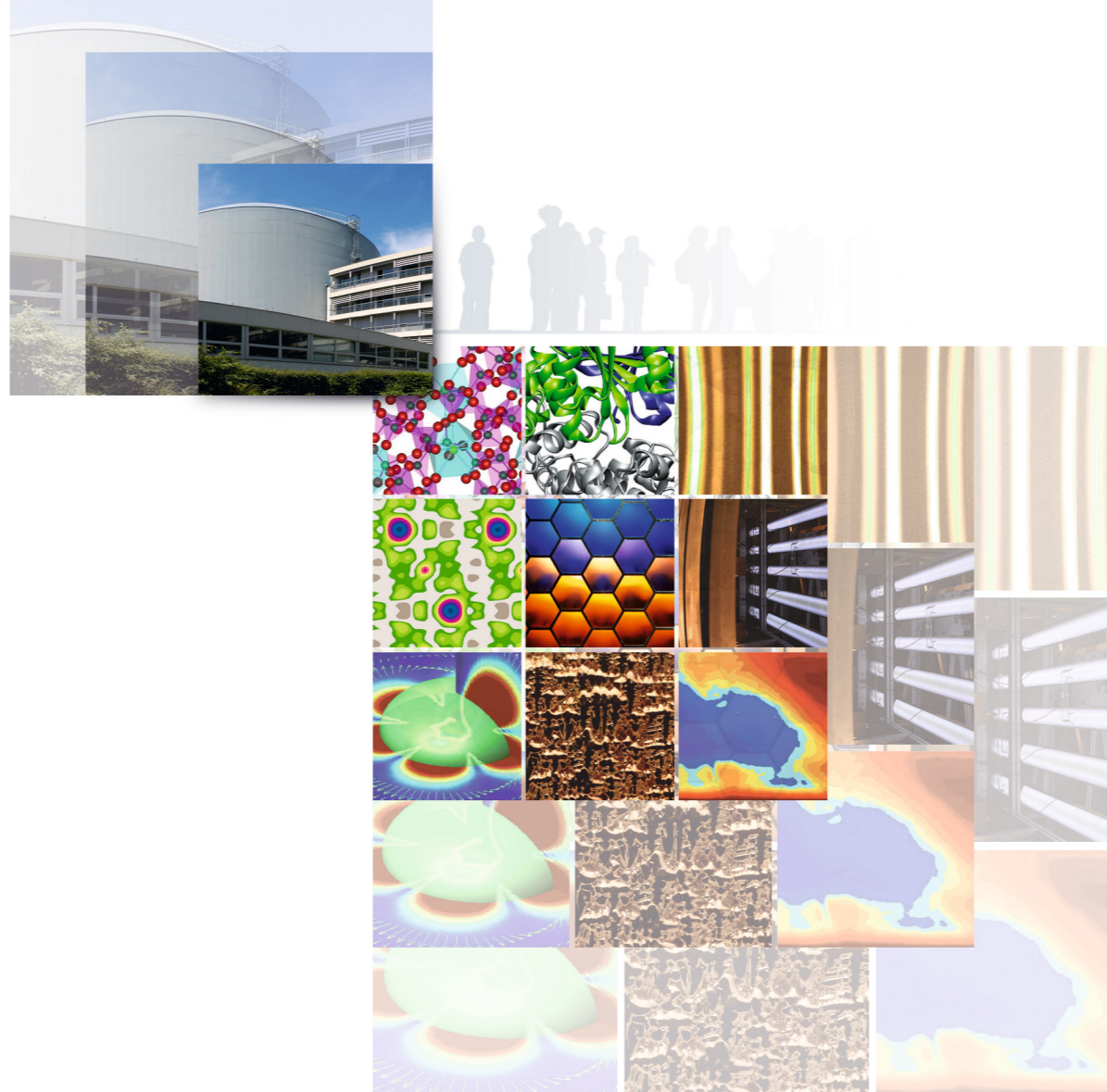
A n n u a l R e p o r t
2 0 0 8



Institut Laue - Langevin
6, rue Horowitz - BP 150 - 38042 Grenoble Cedex - France - <http://www.ill.fr>



ANNUAL REPORT 2008



A n n u a l R e p o r t
2 0 0 8

I n s t i t u t L a u e - L a n g e v i n





The world's leading facility in neutron science and technology ■



■ The Institut Laue-Langevin





The Institut Laue-Langevin (ILL) is an international research centre where neutrons are used to probe the microscopic structure and dynamics of a broad range of materials from the molecular, atomic and nuclear point of view. The ILL is owned and operated by three founding countries - France, Germany and the United Kingdom.

The 3 Associate countries contributed a total of almost 60 M€ to the Institute in 2008, a sum enhanced by significant contributions from the ILL's Scientific Member countries, Austria, Belgium, the Czech Republic, Hungary, Italy, Poland, Spain, Sweden and Switzerland. ILL's overall budget in 2008 amounted to almost 83 M€.

The ILL was founded to provide scientific communities in its member countries with a unique flux of slow neutrons and a matching suite of experimental facilities (some 40 instruments) for use in fields as varied as solid-state physics, materials science, chemistry, the biosciences and the earth sciences as well as nuclear physics and engineering.

An exceptional centre of excellence and a fine example of successful cooperation in Europe ■

The Institute is now an exceptional centre of excellence and a fine example of successful cooperation in Europe, a prototype of the European Research Area. It operates the most intense neutron source in the world. About 1250 visiting scientists, performing a total of 800 experiments each year and the output in high impact journals, bear witness to the scientific success of the facility.



**We thank everyone
who contributed
to the production
of this report**

Editors:

Albert Wright, Katja Jenkins
and Andrew Harrison.

■ Contents

Design and Typesetting:

Synthèse ECA - Patrick Feuillye
Tel: +33(0)4 76 90 02 73
Fax: +33 (0)4 76 04 95 92

Photography:

by ILL and Artechnique
(artechnique@wanadoo.fr)

Printing:

Imprimerie Pont de Claix

Further copies can be
obtained from:

Institut Laue-Langevin
Scientific Coordination Office (SCO)
BP 156 - F-38042
Grenoble Cedex 9 (France)
Tel: +33 (0)4 76 20 72 40
Fax: +33 (0)4 76 48 39 06
email: sco@ill.eu - web: www.ill.eu





1	Director's foreword	6
2	What is the ILL ?	8
3	Scientific highlights	10
4	Millennium programme and technical developments	70
5	Experimental and user programme	90
6	Reactor operation	100
7	More than simply neutrons	104
8	Administrative matters	118
9	Facts and figures	120



1

Director's foreword

2008 may be regarded as a vital year for the ILL's long-term prospects and as a key milestone in shaping the future of the Institute. After eight years of hard and dedicated work, the first phase (M-0) of ILL's modernisation programme – the Millennium Programme – was successfully completed with the commissioning of 6 new instruments and 8 upgrades. In 2009 and beyond, ILL's ever expanding user communities will have access to an instrument suite with an overall average gain in data collection efficiency of ~ 17. In the year 2001 when the M-0 phase was launched, the objectives were defined as the '... systematic implementation of new inventions made at ILL in recent years... and to make ILL instruments, on average, 5 to 8 times more efficient.' This goal has certainly been more than reached for a total investment budget of just ~37 M€. A tribute must be paid to all our staff members who have contributed so imaginatively and admirably to this tremendous achievement.

The projects in the second phase (M-1) of the Millennium Programme have made good progress. Once they are completed in 2013, they will certainly help to ensure that for the next 20 years the ILL continues to be one of the world's leading neutron research facilities.

■ 2008 may be regarded as a vital year for the ILL's long-term prospects and as a key milestone in shaping the future of the Institute

Another key factor in the Institute's success is the safe and reliable operation of ILL's neutron source: the 200 days of beamtime delivered in 2008 according to schedule without the loss of a single day are an impressive demonstration of this and certainly contribute enormously to the persistently healthy demand for beamtime on ILL's instruments and the ILL's unrivalled scientific output in terms of peer-reviewed publications.

Until recently, the mandatory environmental monitoring operations in the vicinity of the ILL High-Flux Reactor were carried out by the CEA-Grenoble. As a result of the ongoing denuclearisation of the latter, ILL has had to create its own environmental monitoring service in order to comply with the nuclear safety regulations and thus to ensure the long-term operation of the Institute's neutron source.

At the end of the year, ILL Management and the Steering Committee had to take the difficult decision to abandon plans to renovate the Institute's detritiation facility, a project to which the Reactor Division had been strongly committed since 2005. This decision was forced upon us in the light of the high investment and operating costs anticipated for the project. To go ahead with the plans would have jeopardized most of the M-1 phase projects of our upgrade programme, projects which both Management and the Steering Committee consider to be more important for the ILL's long-term future.

Our Scientific Members contribute not only to the ILL's budget but also, and more significantly, to the scientific life and output of the Institute. This 2008 Annual Report highlights a large body of exciting science being conducted at the ILL by scientists from our Scientific Member countries. The negotiations on the renewal of the 8 Scientific Membership contracts due to expire at the end of 2008 have been brought to a successful conclusion. In addition, the ILL is pleased to welcome the Slovak Republic and Denmark as new partners of the Institute in 2009. This means that 94% of all European neutron scientists now belong to ILL's 14 partner countries. In this context another important highlight of the year for me was the ceremony held in November at the Paul Scherrer Institute in Villigen to celebrate 20 years of fruitful scientific cooperation between the ILL and Switzerland.

During the course of 2008 Russia expressed on several occasions its intention to renew its scientific membership of ILL, which expired in June 2007. However, the signature of the agreement is still pending. For this reason, all proposals submitted by Russian scientists have regrettably had to be put on hold until a new contract is signed.

2008 also saw a significant – and in my view overdue – strengthening of the ties between the Grenoble universities and the European Large-Scale Facilities in Grenoble, ILL and ESRF. On 22 October, ILL and ESRF signed an agreement with the Université Joseph Fourier (UJF) to foster links between research and education. The aim of the agreement is to establish two *Associate Professorship Chairs for Large-Scale Facilities* at UJF. These will be offered to internationally reputed scientists from ILL and ESRF, who will teach and train students and postdoctoral researchers to exploit neutron and synchrotron radiation for their present and future research. Hence, this win-win partnership will serve both sides – UJF and the Large-Scale Facilities – equally well in the future.

Indeed, 2008 has provided the ILL with a host of remarkable achievements and scientific results, many of which are described in this Annual Report. My warm thanks to everyone who has contributed to this success and to shaping the future of our Institute.

Richard Wagner
Director of the ILL

Why neutrons ?

Neutron beams have the power, when used as a probe of small samples of materials, to reveal what is invisible using other radiations. Neutrons can appear to behave either as particles or as waves or as microscopic magnetic dipoles and it is these specific properties which enable them to uncover information which is often impossible to access using other techniques.

Electrically Neutral

Neutrons are non-destructive and can penetrate deep into matter making them an ideal probe for e.g. engineering components and samples under extreme conditions of pressure, temperature, magnetic field or within chemical reaction vessels.

Microscopically Magnetic

They possess a magnetic dipole moment which makes them sensitive to magnetic fields generated by unpaired electrons in materials. Precise details of the magnetic behaviour of materials at the atomic level can be investigated. In addition, the scattering power of a neutron by an atomic nucleus depends on the orientation of the spin of both the neutron and the atomic nuclei in a sample thereby providing a powerful tool to detect the nuclear spin order.

Wavelengths of Ångströms

Their wavelengths range from 0.1 \AA (10^{-2} nm) to 1000 \AA making them an ideal probe of atomic and molecular structures ranging from those consisting of single atomic species to complex biopolymers.

Energies of millielectronvolts

Their energies are of the same magnitude as the diffusive motions of atoms and molecules in solids and liquids, the coherent waves in single crystals (phonons and magnons) and the vibrational modes in molecules. An energy exchange between the incoming neutron and the sample of between $1 \mu\text{eV}$ (even 1 neV with spin-echo) and 1 eV can readily be detected.

Randomly sensitive

The variation of scattering power from nucleus to nucleus in a sample varies in a quasi-random manner even in different isotopes of the same atom. This means that light atoms are visible in the presence of heavy atoms and atoms neighbouring in the periodic table may be distinguished from each other. In addition, isotopic substitution (for example D for H, or one nickel isotope for another) can allow contrast to be varied in certain samples thereby highlighting specific structural features. The neutron is particularly sensitive to hydrogen atoms and therefore is a powerful probe of hydrogen storage materials, organic molecular materials, and biomolecular samples or polymers.



2. What is the ILL?



Formally, ILL is a non profit-making French company under civil law, which is governed by an International Convention, signed at Foreign Ministry level by three countries – France, Germany and the United Kingdom. Our Associates – the CNRS and the CEA representing France, the FZ Jülich representing Germany and the STFC representing the United Kingdom – own and administer the Institute. They are also responsible for all liabilities and eventual decommissioning costs.

Whilst our Associates own the facility and contribute the largest amount to the almost 83M€ annual operating costs, the ILL also benefits from the scientific partnerships of nine other nations – Austria, Belgium, the Czech Republic, Hungary, Italy, Poland, Spain, Sweden and Switzerland – who together contributed in 2008 about 17% of the operational and investment costs of the Institute. All partner countries in addition can and do contribute to capital projects at the Institute, within the Institute's priorities but according to their own priorities also.

Our governing body is the Steering Committee, which meets twice-yearly and is made up of representatives of the Associates and the Scientific Partners together with Directors and Staff Representatives. Within the framework of the International Convention, the Steering Committee has the ultimate responsibility for determining operational and investment strategies for the Institute.

The Institute has a Director and two Associate Directors, representing each of the Associate countries, appointed on short-term contracts normally of five years. The Director's role is generally taken alternately by the German and British appointee. The two Associate Directors are responsible for the Science Division and the Projects and Techniques Division respectively. The Head of the Administration Division is also appointed on a short-term contract, whereas the Head of the Reactor Division is a permanent ILL employee. These five people together constitute the Management Board of the Institute and are responsible for its day-to-day operation.

The scientific life of the Institute is guided by the Directors, with input from the ILL's ten scientific colleges. A Scientific Council, comprising external scientists from the member countries, advises the Directors on scientific directions for the Institute, on the evolution of the instrument suite and technical infrastructure to best meet the needs of the user research programme, and to assess the scientific output of the Institute. It is helped in this process by the Instrument Sub-Committee and by the Chairmen of the nine Scientific Sub-Committees who twice-yearly peer review the experiment proposals.

The ILL is composed of four divisions, each with its distinct role and, it is true to say, its own culture.

The Science Division staffs the instruments and delivers the science; the Projects and Techniques Division designs and builds new instruments, develops new concepts

and maintains beamlines and instruments operational; the Reactor Division delivers the neutrons, operates and mans the reactor 24 hours during 4 cycles of 50 days each per year and has responsibility for all aspects of security; the Administration Division deals with personnel matters with particular responsibility for interactions with staff representative bodies, with purchasing, with finance and with site and building maintenance; and the Director's Services deal with radiological safety, with conventional safety, with health and working practices and with public relations.

The ILL's neutron source is the finest in the world, being based on a single element 58.3MW nuclear reactor designed for high brightness. The main moderator is the ambient D₂O coolant surrounding the core which delivers intense beams of thermal neutrons to 11 beamlines and to four neutron guides. A graphite hot source operating at 2400K delivers hot neutrons – energies up to 1 eV and wavelengths down to 0.3 Å – to 3 beamlines. Two liquid deuterium cold sources at 25K deliver cold neutrons with energies down to 200 µeV and wavelengths up to 20 Å to some 17 instruments. An ultra-cold neutron source fed from the top of one of the cold sources delivers neutrons vertically through the reactor pool to 5 instruments on the operational floor of the reactor.

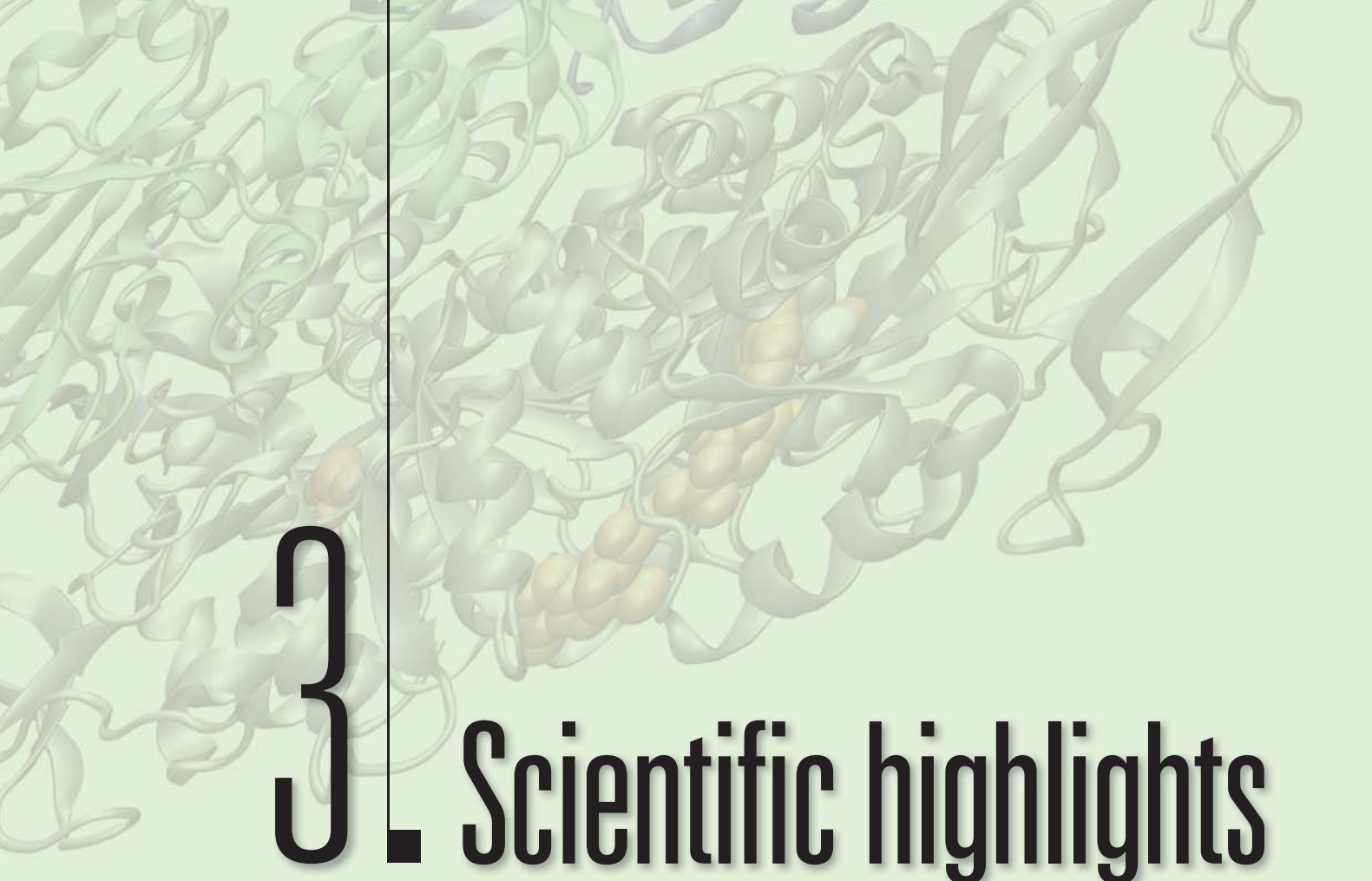
In all there are more than 50 measuring stations, 27 of which have full public access. In addition, the ILL provides a framework in which Collaborative Research Groups (CRGs) can build and manage instruments to carry out their own research programmes. At present there are ten CRGs at the ILL.

Our community of users is world-wide with scientists from non-partner nations also having a chance to apply for beamtime with outstanding research proposals. This broader community of users enriches the scientific life of the Institute.

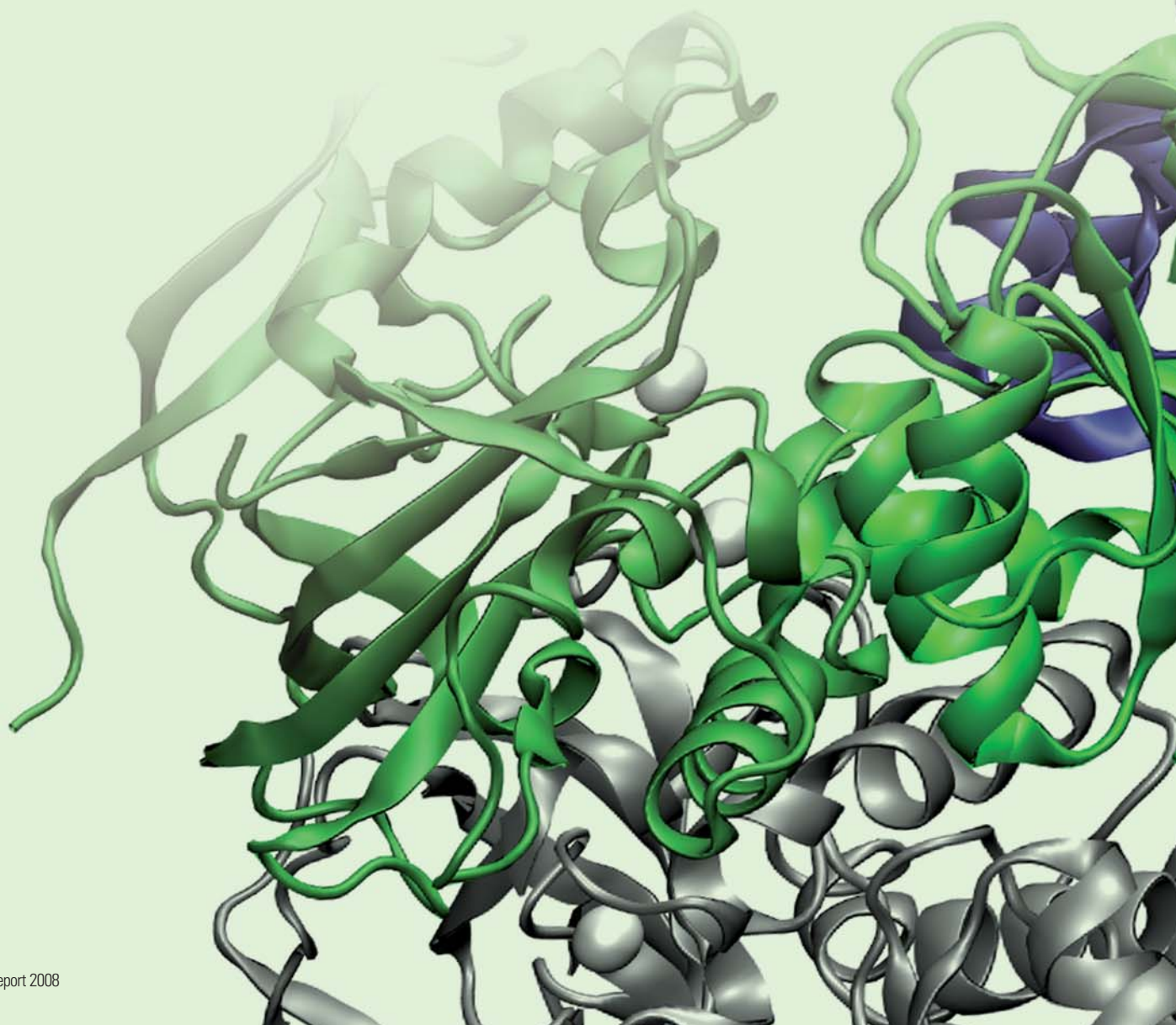
In 2000, the ILL launched an ambitious modernisation programme of instruments and infrastructure called the ILL Millennium Programme (Phase M-0: 2000-2008; Phase M-1: 2007-2013) whose aim is to optimise the ILL's instrument suite, and thereby maintaining the Institute's world-leading position for another 20 years.

The ILL monitors the papers published as a result of the use of our facilities. This gives a figure of almost 600 publications in peer-reviewed journals per year. With a total annual budget of about 83 M€, the cost per published paper is less than 140k€. We pay particular attention to papers published in high impact journals. Over 140 such papers per year are published from data taken on ILL instruments, which is greater than for any other neutron source in the world.

Beam days delivered for science during four reactor cycles amount to 6438 in 2008. The cost per beam day of science therefore stands at a very cost effective 12.8k€ per day.



3. Scientific highlights



Magnetism

Chemistry and crystallography

Materials

Soft matter

Liquids and glasses

Biology

Nuclear and particle physics

Spectroscopy, modelling and theory

■ We are most effective at facilitating science if we have a vibrant community of scientists and technicians at ILL.

2008 was a very stimulating year for science at the ILL, driven both by our users and our own staff. The highlights presented over the following pages illustrate the quality of the research we support, and also reflect the broadening of the scientific base as various initiatives to attract new users and enable new science to be explored by neutrons start to bear fruit. Arguably, the most striking development this year in the science we serve stems from the revelation of superconductivity at remarkably high temperatures in a family of pnictide materials. The small quantities of the first samples synthesised meant that our high flux was in great demand for these early studies, particularly for excitations. It also presented us with the (mostly) pleasant problem of coping with a deluge of requests for director's discretionary time.

Applications for beamtime through conventional applications were also extremely competitive, consistently 20% higher than five years ago. The increase in demand for biological science was particularly notable and our Partnership for Structural Biology (PSB) has doubtless played a significant role in this and looks set to become even stronger following the introduction of a new platform in small-angle X-ray and neutron scattering in partnership with the ESRF. The Partnership for Soft Condensed Matter has also matured, with the delivery of light-scattering and ellipsometry equipment, enabling users to perform better neutron experiments with the promise of more to come as the ESRF formally joined the initiative. 2008 also saw an increase in demand for industrial beamtime, for EASY access to beamtime for diffraction through mailed samples and for support by our Computing for Science Service. Our latest initiative is a Long-Term Proposal system, launched to encourage users to bring additional resources to ILL; modest amounts of beamtime may be offered over several years to enable the development of new equipment or techniques that are judged to be valuable for the wider community.

However, despite all these developments to broaden access, our core strength remains with the reactor – with essentially 100% delivery of four cycles this year – and with our high-performance instrument suite. Here, the Millennium Programme continues to deliver results, ensuring that an increasing fraction of neutrons produced are finally useful to our users; the average detected flux across our instrument suite has risen by a factor of more than 17 since 2000 – and this is set to rise further as we welcome IN5 and D11 back into the fold and release FIGARO for public use in 2009.

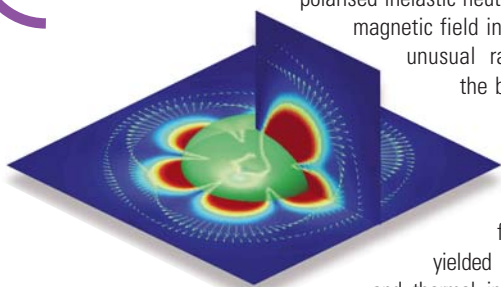
Finally, we believe that we are most effective at facilitating science if we have a vibrant community of scientists and technicians at ILL. Our student body has grown in strength and now numbers over 30 as increased funding for studentships has taken effect. We initiated or supported an unusual number of conferences and workshops this year and several of our staff won international prizes and recognition. The ILL is a great place to do science, and I am sure you will enjoy reading more about it over the next few pages.



Andrew Harrison
Associate Director

Magnetism

We often gain understanding of the true nature of unusual magnetic ground states only by admitting an ever increasing complexity. Nowhere is this more evident than in some of our 2008 highlights. Magnani *et al.* present an intriguing ground state, a triakontadipole, of the heavily studied neptunium dioxide. Magnetic order can exist due to the localised behaviour of the atomic magnetic field and as such is described by a dipole moment, a rank 1 tensor. However, a dipole is only a part of a multipole expansion leading to evermore complex magnetic field behaviours. It has been shown, using polarised inelastic neutron scattering on IN20, that the magnetic field in NpO_2 can be described by the unusual rank 5 tensor which displays the beautiful magnetic field pattern shown on the left.



Another thoroughly studied system, the heavy fermion compound URu_2Si_2 , has yielded information in the face of cold and thermal inelastic neutron scattering (INS), using IN12 and IN22, combined with the application of pressure. URu_2Si_2 has been the subject of intense debate for more than 15 years due to a region of the phase diagram in which the order is commonly known as 'hidden'. Villaume *et al.* performed simultaneously inelastic neutron scattering and thermal expansion measurements on a single crystal in a CuBe cell pressurised up to 0.67 GPa across 1.5 - 300 K. The group has found 2 inelastic peaks within the hidden order phase: one is interestingly found at the position which becomes the antiferromagnetic Bragg peak in the high pressure ordered phase and can be therefore looked upon as a signature of the 'hidden order'.

The third highlight presents a study of the dynamics of magnetic frustration in a rare earth kagome lattice. Simonet *et al.* have studied the kagome-like Nd-langasite compound using time of flight (IN4 and IN5) and neutron spin echo (IN11C) spectroscopy. These two techniques can probe overlapping but variable dynamic ranges to study dynamic magnetic order. This work reveals the importance of the crystal fields to model correctly the temperature dependence of the magnetisation. The magnetisation plateau originates from a single ion quantum process and thus diminishes the importance of collective processes and geometric frustration.

These highlights reveal the complexity of magnetic order and point to the need for continual upgrades of our instruments. In 2008 the greatest success story has been the upgrade of IN5. This time-of-flight spectrometer now features a 30 m² detection area with 100,000 cells in the 384 position-sensitive detector tubes. In addition to IN5, the development of a suite of new instruments, WASP, THALES and D33, are making progress. The prototype analyser bank for WASP has been successfully tested. D33 is entering into the detailed design phase and in early 2008 we launched the technical feasibility phase of THALES, the successor of IN14, which will ensure ILL's leadership in cold neutron three-axis spectroscopy over the next decades. Improvements for doing elastic magnetic scattering include the nearly routine use of the Paris-Edinburgh high-pressure cell and the replacement of the D3 base by a nonmagnetic one to improve the performance of the Cryopad.

2008 was the year of Fe based high Tc superconductors and as a consequence we have already experienced a flood of proposals to study their magnetic properties. Undoubtedly Fe based superconductors will feature among the 2009 highlights.

Pascale Deen, College 4 Secretary

Clemens Ritter, College 5b Secretary

<http://www.ill.eu/science-technology/science-at-ill/magnetism/>

Chemistry and structure

College 5a is dedicated to the study of nuclear structures using crystallographic methods. The knowledge of structure of crystalline matter is a key to chemical properties of a vast majority of solid materials. Elastic neutron diffraction techniques are frequently used in this field, with the neutron being an ideal probe for condensed matter: its zero-charge makes it interact only through short-ranged nuclear exchanges with low interaction probability, allowing for penetration of bulky samples and complex sample-environment as well as for distinction of isotopes and thus elements, in particular light atoms beside heavy ones.

The ILL instruments used in this area are mainly the single crystal diffractometers D9, D10, D19 and VIVALDI and the powder diffractometers D1A, D1B, D2B, D4 and D20. A new fast CCD neutron Laue detector, CYCLOPS, shows excellent results: a pattern of a standard ruby crystal can now be obtained in just 50 seconds. The combination of fast acquisition and readout will allow the development of thermo-diffractometry and *in-situ* experiments for the Laue technique on this facility.

In a workshop on powder diffraction with two-dimensional detectors, the equipment of existing and future powder diffractometers with large position-sensitive detectors was vigorously discussed. The first FullProf School was organised at ILL, focussing on its capabilities to analyse data from parametric powder diffraction experiments.

One ongoing trend is the growing number of high-pressure experiments, using the so-called Paris-Edinburgh press. These experiments are done mostly on D9 for single crystal diffraction (Loveday *et al.*) and D20 for powder diffraction (Klotz *et al.*), where one has the unique opportunity to cool the sample down to 3 K at a pressure of up to 10 GPa or even higher under special circumstances. A *première* was a first experiment with this press at elevated temperatures (Rouquette *et al.*), using a newly developed amorphous gasket enclosing a tiny vanadium furnace.

Another trend is the increasing interest in hydrogen. This defies the widespread assumption that neutron diffraction experiments need to be done at deuterated samples (Weller *et al.*). *In situ* experiments on phase transitions involving hydrogen (Kohlmann *et al.*) and in particular on the real-time behaviour of hydrogen-storage systems (Weidner *et al.*) increase in number and scope.

The contribution of College 5a to this Annual Report concerns the research on solid oxide fuel cells (SOFC): The structure of a new proton conducting oxide has been investigated to understand fully its properties, as this material is a promising candidate to lower the operation temperature of SOFCs.

Thomas Hansen, College 5a Secretary

<http://www.ill.eu/science-technology/science-at-ill/chemistry-crystallography/>

Materials science and engineering Soft matter



2007 proved to be an excellent year for applied sciences at ILL with nearly 50 high-quality experiments being performed. The breadth of the applications remains wide, ranging from geophysics to engineering via cultural heritage and biomaterials. A large proportion of experiments was in the field of engineering, in particular using the dedicated residual stress diffractometer SALSA. However, cultural heritage and materials science experiments still remain healthy and are spread over a wide suite of instruments. It is also important to recognise the important contribution of the ILL support laboratories, in particular the ILL chemistry laboratory and the materials science support laboratory.

It is only three years since SALSA came online for users, but the instrument has firmly established itself as world-class for the determination of bulk residual stresses. A group led by Davies have investigated the problem of how to manage the distortion in large steel plates used in the ship-building industry. The heat generated when welding causes local residual stress which can lead to distortion of the final product. This results in it being rejected and causes waste of materials, time and energy. Using SALSA, the group studied the relationship between weld filler material, residual stress and distortion. The results showed that it is possible to optimise the residual stress through the use of modified weld filler materials.

Significant research continues to be made into advanced superalloys for use in extreme environments (aircraft engines, power plants). Whilst scientists used SALSA to look at the macroscopic residual stress after manufacturing, other researchers looked at the underlying microstructure and its influence on component lifetime. Zickler *et al.* used D22 to study precipitation kinetics in new-generation nickel-based superalloys. With *in situ* techniques the group followed the kinetics of microstructural changes.

One of the biggest challenges facing libraries and museums worldwide is how to prevent degradation of historical paper documents. Mondelli *et al.* used IN13 and IN6 to attempt to understand the degradation process and identify the best conservation methods. Data from several ancient papers (XV-XVI centuries) showed that there are clear differences depending upon the state of degradation of the paper. The work is helping to provide a better understanding of the process of paper aging.

Darren Hughes, College 1 Secretary

<http://www.ill.eu/science-technology/science-at-ill/materials-science-engineering/>

This year was an exciting year for soft matter research at the ILL. The Partnership for Soft Condensed Matter (PSCM) progressed well. The ILL continued to complete the suite of the ancillary equipment, of which the biggest investment was a new light-scattering apparatus dedicated for the use of the ILL and ESRF soft matter community. This year the rebuilt D11 came online and will help to reduce the very high overload of small-angle scattering instruments. We now look forward to the start of the construction of D33, which will serve even more SANS users in the next decade. Since most beam time requests for reflectometers are submitted to college 9, we are delighted that FIGARO started operations at the end of the year. Additionally ADAM will be upgraded to Super-ADAM starting in 2009.

In anticipation of the large number of new users and great science that FIGARO will bring to ILL, we have two articles dealing with reflectometry in this year's Annual Report. Schollier and co-workers studied the absorption of globular proteins on poly-ethylene glycol (PEG) brushes. These PEG brushes are known to reduce clotting in blood-handling devices, yet the details of protein absorption on these surfaces were unknown. Neutron reflectometry uncovered the concentration profile of the proteins and the PEG brushes independently. The results showed that protein adsorption occurs in two modes, adsorption on the grafting surface and adsorption on the brushes themselves.

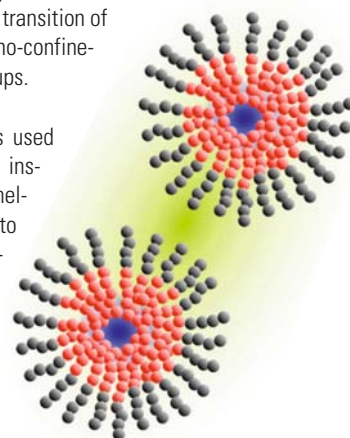
Zauscher *et al.* studied another polymer brush system also using neutron reflectometry. Poly N-isopropylacrylamide (NIPAAm) is known to have a reversible conformational collapse transition as a function of temperature or pH. The authors interpreted their results with two methods, using a conventional homogeneous layer model and a novel molecular level lattice mean-field theory. This new model greatly reduces the number of free fitting parameters, providing a powerful tool to analyze other polymeric systems undergoing a conformation change.

Arbe *et al.* studied polymer systems as well. Using selective deuteration and neutron spin-echo methods they were able to study the dynamics of the main chains and the side groups of poly(n-alkyl methacrylates) separately. Their data interpretation shows that the double glass transition of PnMAs can be ascribed to the separate nano-confinement of the main branch and the side groups.

Last but not least, Tabor and co-workers used the stopped flow technique on a SANS instrument to study the kinetics of a lamellar surfactant system transforming into a micro emulsion on dilution. They discovered two processes operating over very different timescales, a very fast swelling of the lamellar system followed by a slow dilution into a stable micro emulsion.

Péter Falus, College 9 Secretary

<http://www.ill.eu/science-technology/science-at-ill/soft-condensed-matter/>



Liquids and glasses

Among ILL's scientific topics in College 6, Dynamics and Structure of Liquids and Glasses, 2008 saw a gradual shift in terms of requested beamtime away from the more traditional fields of monoatomic liquids and gases and the glass transition. The emphasis now lies more on molecular liquids and gases, liquid alloys and molten salts as well as non-polymeric glasses and amorphous materials.

This year we have also detected an emerging field of science covering the physics of liquids and glasses to answer questions of importance to the environment. We have selected two highlights from College 6.

Programmable metallisation cells represent a radical departure from existing electronic memory technologies. They are silver-based chalcogenide glasses in which the silver ions are believed to play a key role. The electrical conductivity changes tremendously when a small voltage is applied. The mechanism for this is not well understood. Experiments by Piarristeguy *et al.* on D4 combined with *ab initio* molecular dynamics simulations have shed light on the coordination of the constituents of the Ag-Ge-Se system. The conductivity is tentatively correlated with the appearance of a second Ag-Ag peak in the radial distribution function. Thermodiffraction on D1B showed clearly the existence of a new metastable phase Ag_2GeSe_3 that transforms with increasing temperature to GeSe_2 and another new phase $\text{Ag}_{10}\text{Ge}_3\text{Se}_{11}$ that is stable at room temperature.



The other selected highlight concerns a study of the structure of the rare earth phosphate glass $\text{Sm}_2\text{O}_3 \cdot 4\text{P}_2\text{O}_5$ by Cole *et al.* They applied the neutron-diffraction anomalous-dispersion technique, which employs the wavelength dependence of the real and imaginary parts of the neutron scattering length close to the absorption resonance. Other resonance techniques have yielded the local structure up to about 4 Å, whereas the anomalous difference correlation function suggests that the average Sm^{3+} separation is 4.8 Å with distinct greater and smaller separations (4, 5.9 and 6.9 Å). The unraveling of the Sm-Sm distances by anomalous dispersion neutron diffraction using 4 wavelengths provides evidence of local clusters of Sm^{3+} ions within this glassy structure. This type of material is of great importance to the laser and optoelectronic industry.

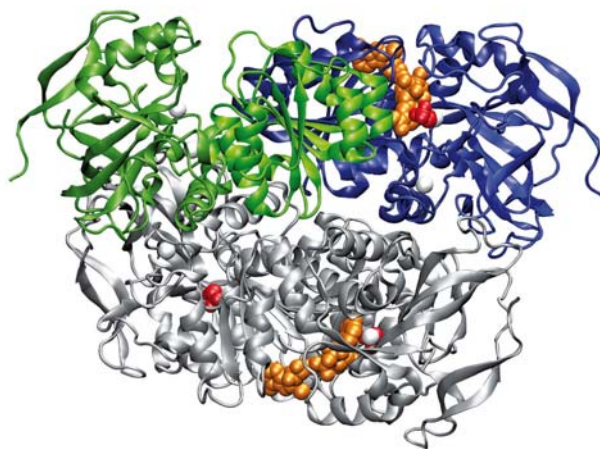
Lambert van Eijck, College 6 Secretary

<http://www.ill.eu/science-technology/science-at-ill/liquids-and-glasses/>

Biology

Biology at the ILL is more dynamic than ever! In this report we look into how structures can act together as a concerted system in highly-specialised biological environments and how interactions propagate in time and space. The Biology highlights reflect a revisited interest in systems that remain poorly understood despite their acknowledged importance in a wide range of fields: the complex environment of lipidic membranes and, inevitably, 'the liquid of life', water.

It cannot be said too often that biology at the ILL has been considerably strengthened through unique training opportunities available through the Partnership for Structural Biology. The door opens both ways, with ILL students and scientists taking advantage of the structural-biology expertise available at the PSB where, in turn, scientists have been brought closer to neutrons.



Within the PSB, the synergy between the Deuteration Laboratory and instrument developments continues to bear fruit. This is clearly shown for the case of LADI-III where, in one year only, the number of structures determined by neutron crystallography matched those studied over 10 years of operation of its predecessor LADI. In their studies on the collective dynamics of protein hydration water, Orecchini and co-workers comment on the advantages of having dedicated instruments – as opposed to more versatile, general purpose instruments – a recurrent argument all the more relevant at a time when new neutron sources are becoming available to biologists worldwide. It is therefore extremely timely that the upgraded D11 and the new reflectometer, FIGARO, are now available for users.

At the last proposal round, the Long-Term Proposal system was introduced. The LTPs are a unique opportunity for the users to have a direct contribution to the infrastructure and methodology at the ILL. The biological community is likely to respond to this new system with the same enthusiasm that welcomed the BAG proposals. After all, the ILL is also a vibrant, dynamic system where the biological scientific output is due to much more than simply neutrons.

Susana Teixeira, College 8 Secretary

<http://www.ill.eu/science-technology/science-at-ill/biology/>

Nuclear and particle physics

The NPP group organized two major scientific events in 2008. The 'workshop on spectroscopy of neutron-rich nuclei' documented the complementarity of in-flight and isotope separation facilities. In the former (like LOHENGRIN at ILL), the radioisotopes produced are mass-separated as 'fast' beams, enabling the spectroscopy of isotopes and isomers with lifetimes as short as hundreds of nanoseconds. ISOL facilities (like ISOLDE at CERN) produce intense 'slow' radioactive ion beams. Recently, the reacceleration of ISOL beams enabled fast beams with *high brightness* to be produced, essential for applications like the Coulomb excitation to excited nuclear states.

A separate conference was devoted to the 'most neutron-rich isotope' known: the neutron itself. Many contributions dealt with technical improvements to provide in future even more intense sources of ultracold neutrons (UCNs).

A powerful technique to produce UCNs is the down-scattering of cold neutrons in deuterium or helium kept at very low temperatures. The design of such an UCN source is very complex and the fundamental processes of down-scattering and UCN losses have to be studied individually. For liquid and solid deuterium, these processes were now studied in detail by TOF spectroscopy by Müller *et al.*

A more immediate gain in intensity of UCNs could come from improved VCN (very cold neutron) reflectors, e.g. by complementing ILL's vertical cold source to significantly improve the VCN intensity delivered to the UCN turbine of PF2. Nesvizhevsky *et al.* showed that diamond nanoparticle powder has the required properties for such a purpose and that even the long wavelength part ($> 10 \text{ \AA}$) of cold neutron beams would profit from such reflectors.

Future UCN sources are characterized by a very high phase-space density. If this could be preserved during acceleration to the regime of cold or thermal neutrons, one could generate short monochromatic neutron bunches with *high peak brightness*. Mayer *et al.* impressively demonstrated that this is indeed possible. Just as the reaccelerated ISOL-beams are a tool for science with radioactive ions, high brightness beams of reaccelerated UCNs could become a tool for specific applications of inelastic neutron scattering.



Usually the techniques and applications of UCNs were considered to have little in common with standard neutron scattering experiments. The traditional spatial separation at ILL (Level D versus Level C/ILL7/ILL22) amplified this impression. However, the present contributions on new technical developments show that strong synergies are now possible between neutron scattering and UCNs. Both fields should have a 'bright' future at the ILL.

Ulli Köster, College 3 Secretary

<http://www.ill.eu/science-technology/science-at-ill/nuclear-and-particle-physics/>

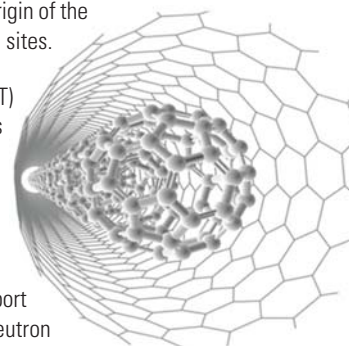
Spectroscopy, modelling and theory

The spectroscopy, modeling and theory section is naturally multidisciplinary and highlights the advantages of combining numerical methods and theory with spectroscopic techniques. It is composed of six articles covering the fields of superconductivity (Mittal *et al.*; Zbiri *et al.*), magnetism (Qureshi *et al.*), confinement (Rols *et al.*; Lauter *et al.*), biology (Bicout *et al.*) and quantum phase transition (Civelli *et al.*)

2008 marks the exciting discovery of a new family of AsFe-based high T_c superconductors known as pnictides. This has raised enormous attention in the worldwide scientific community, as there is the hope that these new materials will provide the key to understand the longstanding open problem of high T_c superconductivity. In this year's annual report two articles report on this subject, shedding light on the role played by phonons in the superconducting transition. In the first, Mittal and collaborators measured the phonon density of states of the parent and superconducting sample in a broad temperature range. In the second, Zbiri and collaborators performed a detailed *ab initio* study, which includes electron-phonon and spin-phonon coupling.

Ab initio calculations have also been used by Qureshi and collaborators to investigate magnetism in the Kagome staircase system Co₃V₂O₈. The calculations reveal that different populations of the t_{2g} and e_g levels are at the origin of the different magnetic moments on the two cobalt sites.

Filling in single wall carbon nanotubes (SWNT) with guest molecules provides physicists with a new molecular device for confinement studies. Rols and collaborators have measured a surprisingly high mobility of C₆₀ molecules confined on a 1D chain inside the SWNT.



In their article, Lauter and collaborators report a new quantum state of helium using neutron TOF spectroscopy. This new state is made of independent superfluid helium clusters confined in solid helium that was condensed into the open structure of aerogel by applying a pressure of 51 bars.

Bicout and Kats have developed a theoretical framework, which allows running simulations describing pore growth and the kinetics (and rupture) of membranes. Their study represents a working tool applicable to experiments, like e.g. on biological systems, where the closing and opening of membrane pores are fundamental processes.

The study by Civelli and collaborators focuses on heavy fermion compounds which can undergo a purely quantum phase transition. By using the 'cellular-dynamical mean-field theory' on a simple heavy fermion model, the authors have uncovered new aspects of the quantum phase transition.

Stéphane Rols, College 7 Secretary

<http://www.ill.eu/science-technology/science-at-ill/colleges/colleges/college7/home/>

Marcello Civelli, College 2 Secretary

<http://www.ill.eu/science-technology/science-at-ill/theory/>

Mark Johnson, Leader of Computing for Science

<http://www.ill.eu/computing-for-science/home/>

Authors

N. Magnani, R. Caciuffo, G. H. Lander and J. Rebizant (ITU Karlsruhe, Germany)

G. Amoretti, S. Carretta and P. Santini (University of Parma, Italy)

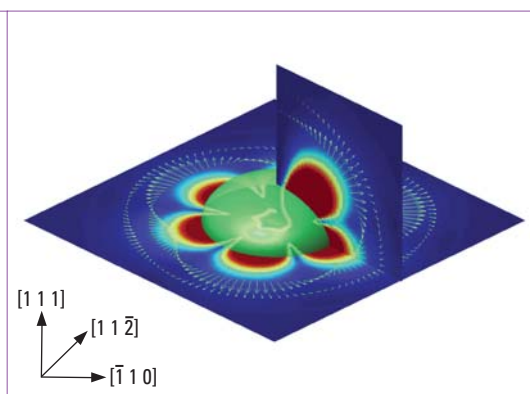
A. Hiess (ILL)

Higher-rank magnetic order parameter in NpO_2

The peculiar magnetic properties of the low-temperature phase in neptunium dioxide have been teasing scientists for five decades. Following recent theoretical work based on resonant X-ray scattering measurements, our inelastic neutron-scattering experiment has finally unveiled a clear signature of the high-rank primary order parameter in the low-energy dynamics.

Figure 1:

Intensity plot illustrating the magnetic field produced by a rank-5 component of the order parameter in two representative planes. The darkest red area corresponds to a field intensity larger than 5 T. The charge distribution of the ion at the centre has an electric quadrupole moment (illustrated by the central ellipsoid). Arrows show the magnetic field calculated at distances of 1 and 1.2 Å from the nucleus.



The first measurements in 1953 of the low-temperature specific heat on NpO_2 showed a clear phase transition at 25 K [1]. Half a century later this phase transition is still of major interest because intensive research has shown that it involves the ordering of high-order magnetic multipoles. Such higher-order multipole densities (deviations from spherical symmetry) appear in research areas as different as studies of nuclei deformations, molecular interactions, and phase transitions. They have been invoked to explain many unusual phenomena, but their experimental identification is always complex. Despite its exotic nature, the experimental situation in NpO_2 , which has the simple cubic fluorite structure, is now one of the clearest examples of this unusual ordering (figure 1), and the latest neutron experiments have added crucial experimental evidence to this long-running saga.

Initially thought to be a simple ordering of the magnetic moments (dipole order, rank-1), as in isostructural UO_2 , numerous neutron and Mössbauer experiments (1960s – 1980s) established the *absence* of any dipole magnetic moment. Sensitive muon experiments [2] revealed a weak signal suggesting that there must be ordering of a magnetic multipole (odd in rank to satisfy time reversal) [3], but could not identify the precise symmetry of that ordering.

A breakthrough occurred in 2002 using resonance X-ray scattering (at the ESRF) when an unambiguous signal was found identifying the ordering of the charge quadrupoles (invisible to neutrons and of rank-2) below 25 K [4]. NMR experiments confirmed the quadrupole ordering [5]. However, this cannot be the primary order parameter, as it must have odd rank to satisfy the muon experiments. Attempts to find the signature of the primary-order parameter were attempted by both resonant X-ray and NMR experiments, but were inconclusive.

A detailed theoretical analysis [6] then advanced our understanding by establishing that the difference between rank-3 and rank-5 ordering lay in the polarisability of the electronic states. Moreover, these calculations opened the way for a direct observation of the primary order parameter, by proving that the transitions between these levels are magnetic dipole

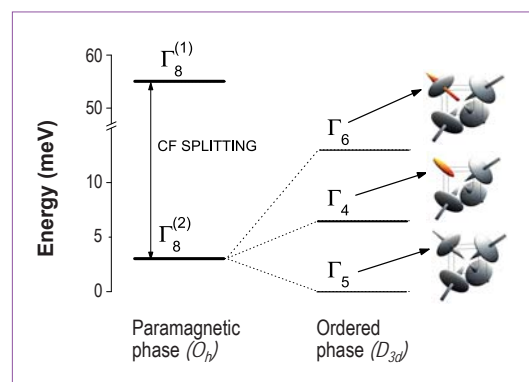


Figure 2: Crystal-field energy scheme for NpO_2 . The ground-state Γ_8 is separated from the next level by 55 meV. Below the phase transition at 25 K this quartet splits into a singlet-ground state (Γ_5), and excited states of a doublet (Γ_4) and a singlet (Γ_6). The doublet has a reversed quadrupole (shape of the charge density, rank-2) from the ground state and null magnetic triakontadipole, whereas the excited Γ_6 has a reversed rank-5 moment (orange arrow).

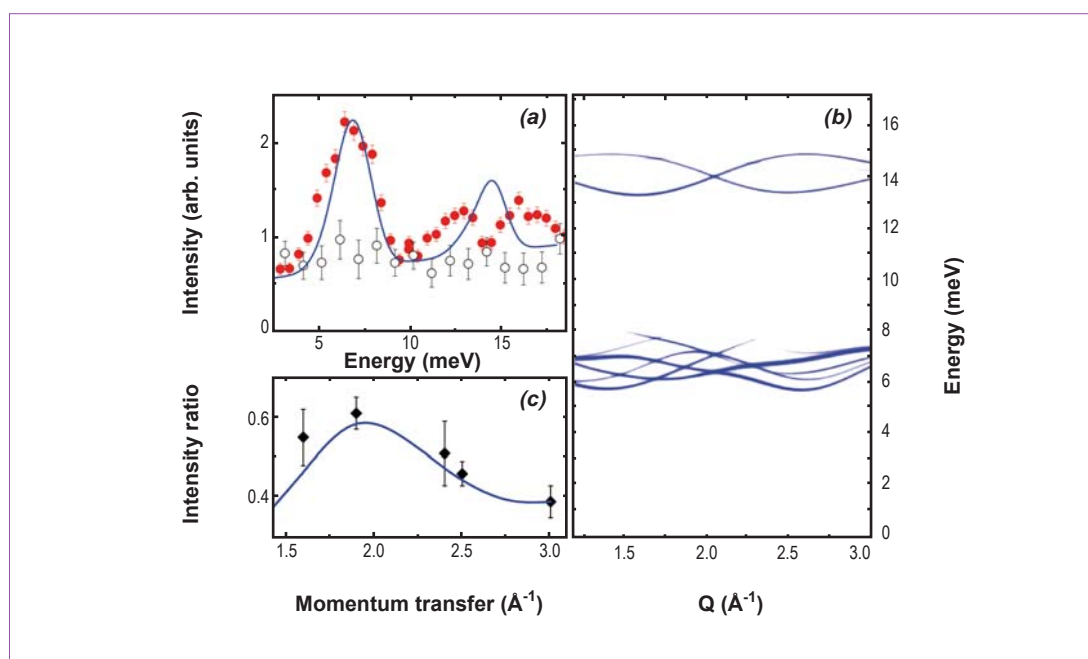


Figure 3: (a) Magnetic signal (red dots) and nonmagnetic background (open dots) measured on IN20 with polarised neutrons at $Q = 2.5 \text{ \AA}^{-1}$ and $T = 5 \text{ K}$. The first peak centred at $\sim 6 \text{ meV}$ shows the transitions from the ground-state singlet Γ_5 to the doublet Γ_4 , whereas the scattering at higher energy represents transitions to the Γ_6 excited singlet. (b) Intensity plot showing the calculated momentum and energy dependence of the neutron scattering function. (c) Experimental (diamonds) and calculated (line) momentum dependence of the ratio between the magnetic scattering intensity of the $\Gamma_5 \rightarrow \Gamma_6$ transition and that of the $\Gamma_5 \rightarrow \Gamma_4$ transition for a powder sample.

in character, and therefore observable by neutron scattering (figure 2). Detailed specific-heat measurements in a magnetic field further showed the absence of energy levels close to the ground state – again suggesting the need for neutrons.

Since only very small single crystals of NpO_2 exist, the experiments on IN20 were performed on a polycrystalline sample with full polarisation analysis. Consistent with the theoretical predictions, the observation of at least two inelastic peaks at energy transfers of up to 18 meV, together with their relative intensities, gives strong evidence (figure 3) that the primary order parameter is of rank-5 – the triakontadipole. These results rule out the possibility that only electric quadrupoles are involved in the phase transition, as in this case only one excitation peak would appear in the energy range explored.

Although some details remain to be resolved, the neutron experiments and accompanying theory have played a key role

in an extraordinary story extending back over half a century, and is still very relevant to our understanding of phase transitions in condensed matter.

References

- [1] D. W. Osborne and E. F. Westrum, *J. Chem. Phys.* 21 (1953) 1884
- [2] W. Kopmann et al., *J. Alloys Comp.* 271 (1998) 463
- [3] P. Santini and G. Amoretti, *Phys. Rev. Lett.* 85 (2000) 2188
- [4] J. A. Paixão et al., *Phys. Rev. Lett.* 89 (2002) 187202
- [5] Y. Tokunaga et al., *Phys. Rev. Lett.* 97 (2006) 257601
- [6] P. Santini et al., *Phys. Rev. Lett.* 97 (2006) 207203

Publication

N. Magnani et al., *Phys. Rev. B* 78 (2008) 104425

Authors

V. Simonet, R. Ballou, J. Robert, B. Canals, P. Bordet and P. Lejay (Institut Néel, CNRS/UJF, Grenoble, France)

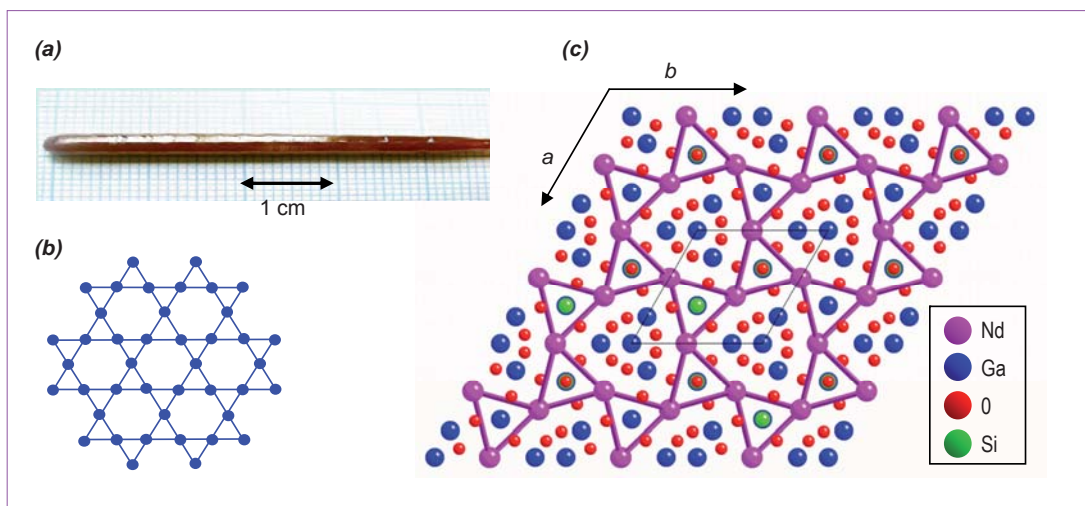
F. Hippert (LMGP, CNRS/Grenoble Institute of Technology, Grenoble, France)

P. Fouquet and J. Ollivier (ILL)

Hidden magnetic frustration by quantum relaxation in anisotropic Nd-langasite

Experimental investigations on $\text{Nd}_3\text{Ga}_5\text{SiO}_{14}$, the first example of a rare-earth kagome-type lattice, supported by analyses that take full account of the crystal electric field effects, have established a firm basis for a model of its magnetism and resolved previous inconsistencies. A novel finding is that the temperature-independent relaxation plateau of the moment dynamics observed below 10 K must originate from single-ion quantum processes and not from cooperative processes induced by geometrical frustration.

Figure 1:
(a) $\text{Nd}_3\text{Ga}_5\text{SiO}_{14}$ single crystal
(b) perfect kagome lattice
(c) structure of $\text{Nd}_3\text{Ga}_5\text{SiO}_{14}$ projected along the c axis with the lattice of magnetic Nd atoms in pink.



The kagome antiferromagnet is the prototype of geometrically frustrated 2-dimensional systems. It is predicted that in the classical case, its ground state remains disordered and is highly degenerate (spin liquid). In the few cases that magnetic kagome lattices have been experimentally observed, various secondary perturbations actually lead to long-range order (LRO) or spin glass phases. This however occurs at a temperature well below the onset of magnetic correlations and is often accompanied by a dynamical behaviour persisting below the transition temperature. These dynamics are characterized by a slowing down of the magnetic fluctuations which rounds off onto a relaxation plateau. Although rather generic, the origin of this peculiar relaxation is still being debated. In all the kagome compounds so far studied the magnetic entities that form the frustrated lattice of corner-sharing triangles are 3d transition metal ions with weak magneto-crystalline anisotropy. The recently discovered $\text{Nd}_3\text{Ga}_5\text{SiO}_{14}$ (NGS) langasite compound [1] provided us with the unique opportunity to study the role of a strong magneto-crystalline anisotropy in a geometrically frustrated 2-dimensional lattice. In this compound the rare-earth Nd^{3+} ions fully occupy a lattice showing the kagome connectivity

of corner-sharing triangles if only first neighbour interactions are taken into consideration. Powder and large single crystals of this material were synthesized for this purpose (figure 1).

Recent nuclear magnetic resonance and muon spectroscopy measurements [2], as well as neutron scattering [3] studies lead to contradictory conclusions concerning the static and dynamic magnetic behaviour in this compound, exclusively interpreted as a consequence of the geometrical frustration of the Nd^{3+} lattice. The influence of the crystal field was not taken into account. This aspect was emphasized in our recent reinvestigation of the NGS properties through neutron spectroscopy, macroscopic probes (magnetization and specific heat) and crystal field calculations [4].

Interesting information was obtained by time of flight (ToF) measurements on the IN5 and IN4 spectrometers and by neutron spin echo (NSE) on the IN11C spectrometer (see figure 2). The first two crystal field levels of the compound were determined through the ToF measurements. In addition, both techniques enabled the dynamics of the magnetic system to be investigated in overlapping time ranges. A slowing

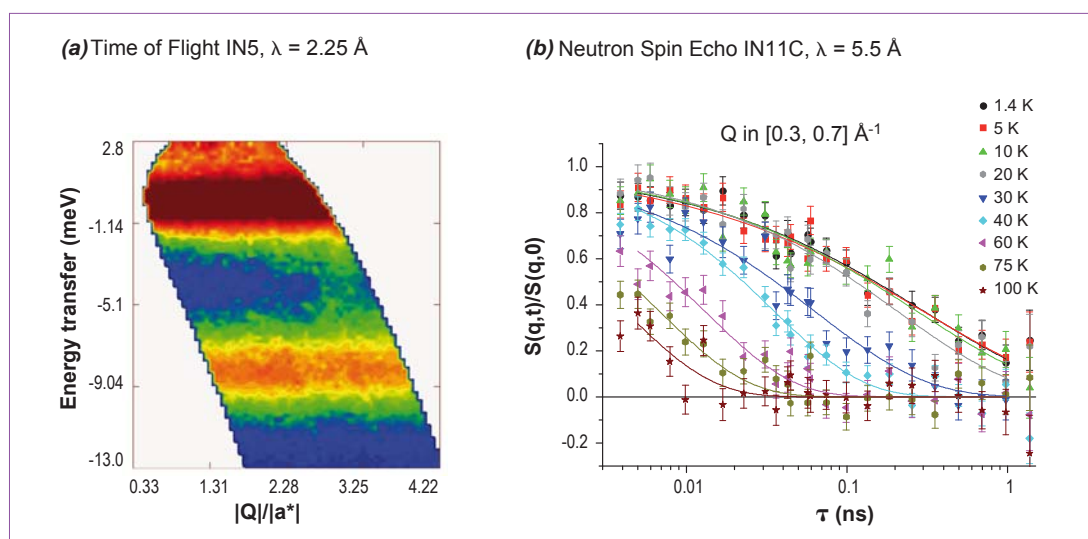


Figure 2:
(a) ToF results from IN5, $\lambda = 2.25 \text{ \AA}$, first crystal field level,
(b) NSE results from IN11C, $\lambda = 5.5 \text{ \AA}$: magnetic signal selected by XYZ polarization analysis; normalized intermediate functions fitted by stretched exponentials.

down of the magnetic dynamics was observed down to 10 K with a thermally activated behaviour above an energy barrier. Below 10 K, a plateau of relaxation is reached and the system fluctuates at a constant rate of $3 \times 10^{-9} \text{ s}^{-1}$ down to very low temperatures. This is at variance with the usual paramagnet with magnetic correlations where the magnetic slowing down leads to a LRO. The signal below 10 K was attributed to a single-ion process as indicated by the absence of spatial correlations revealed by the Q-independence of the NSE data. This suggested that the magnetic interactions were weak, in agreement with the fact that the magnetic behaviour of NGS mimics that of a sample where 99% of the magnetic Nd^{3+} was substituted by non magnetic La^{3+} . A quantitative multi-axial crystal field analysis (3 Nd^{3+} per unit cell in the ground multiplet $J = 9/2$) further showed that the experimentally observed signals at finite energy transfer should be ascribed to crystal field levels (see **figure 3**) and that this alone explains the shape and anisotropy of the single crystal magnetization versus temperature and the reduced value of the magnetization at low temperature. This calculation confirms the single-ion nature of the relaxation plateau, which is consequently not due to a cooperative process. Its temperature independence suggests a quantum origin, which still has to be clarified.

To summarize, our study has shown the importance of the crystal field effects on the rare earth in the kagome-like langasite compounds, and the essential information obtained by neutron scattering concerning both their dynamics and their static properties. More precisely, in the Nd-langasite the magnetic relaxation becomes constant at low temperature and is attributed to a single-ion quantum process. The effects of the geometrical frustration then would emerge only at very low temperatures.

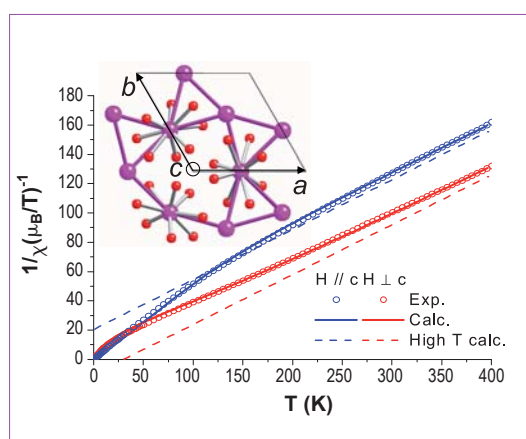


Figure 3: Full crystal field calculation of the inverse magnetic susceptibility $1/\chi$ compared to single-crystal measurements.

References

- [1] P. Bordet, I. Gelard, K. Marty, A. Ibanez, J. Robert, V. Simonet, B. Canals, R. Ballou, and P. Lejay, *J. Phys.: Condens. Matter* 18 (2006) 5147
- [2] H. D. Zhou, B. W. Vogt, J. A. Janik, Y.-J. Jo, L. Balicas, Y. Qiu, J. R. Copley, J. S. Gardner and C. R. Wiebe, *Phys. Rev. Lett.* 99 (2007) 236401
- [3] A. Zorko, F. Bert, P. Mendels, P. Bordet, P. Lejay and J. Robert, *Phys. Rev. Lett.* 100 (2008) 147201
- [4] V. Simonet, R. Ballou, J. Robert, B. Canals, F. Hippert, P. Fouquet, J. Ollivier, D. Braithwaite, P. Bordet and P. Lejay, *Phys. Rev. Lett.* 100 (2008) 237204, *idem*, in preparation

Authors

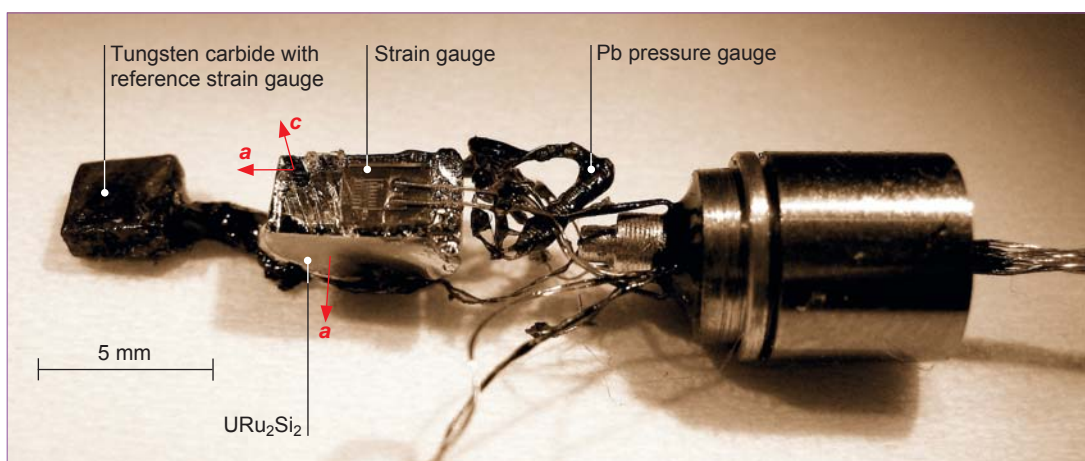
A. Villaume, F. Bourdarot, E. Hassinger, S. Raymond, V. Taufour,
D. Aoki and J. Flouquet (CEA-Grenoble, INAC/SPSMS, France)

Signature of 'hidden order' in heavy fermion superconductor URu_2Si_2 : Resonance at the wave vector $Q_0 = (1,0,0)$

For more than twenty years, URu_2Si_2 has been one of the most studied heavy-fermion compounds. Among strongly correlated electron systems, URu_2Si_2 presents a so-called 'hidden order' ground state which has so far not been resolved. This order, easily detected by many bulk measurements, has not been observed by any microscopic measurements. A new neutron-scattering experiment, performed under pressure on the cold and thermal triple-axis spectrometers IN12 and IN22 respectively, sheds light on the signature of this peculiar order.

Figure 1:

Experimental set-up of the sample and components installed in the pressure cell. A reference strain gauge is also glued to the tungsten carbide to compensate for thermal expansion. A Pb manometer is used to measure the pressure in the cell.



URu_2Si_2 belongs to the short list of rare compounds with an order parameter that has not yet been elucidated. Different proposals for this parameter have been debated as for example 'hidden orbital order', multipolar ordering or 'spin order accompanying loop current', but so far no evidence of any of these orders has been provided. To shed light on this mystery, we measured the dynamical magnetic response of URu_2Si_2 under a well selected pressure (0.67 GPa), for which the sample presents two different states on cooling: the 'hidden order' between ≈ 20 K and 12 K, and an antiferromagnetic order below 12 K named LMAF for Large Moment Antiferromagnetism (figure 2a). Knowing the order parameter, the symmetry, and the inelastic responses in this antiferromagnetic phase, we look at the differences between both phases.

A single crystal of URu_2Si_2 of size of $\sim 5 \times 4 \times 3 \text{ mm}^3$ was put in a specially designed CuBe pressure cell. The special features of this cell enable the simultaneous measurement of neutron scattering and thermal expansion during the experiment. To achieve this, a strain gauge, glued on a flat surface of the sample and a lead (Pb) manometer were installed in the pressure cell to measure the thermal expansion and the pressure

respectively. This set-up, which can be seen on figure 1, has been installed in the 5 mm diameter pressure cell. A pressure of 0.67 GPa was applied, and the pressure cell was cooled down for measurements between 1.5 K to 30 K.

The thermal expansion (figure 2b in red) measurement shows both transitions at $T_0 = 18.2$ K with a shape characteristic of the 'hidden order' transition, and a large anomaly in the lattice parameter at $T_x = 12$ K characteristic of a first order transition. At the same time, a large antiferromagnetic ordered moment appears below T_x (figure 2b in black). This magnetic phase corresponds to ferromagnetic sheets coupled antiferromagnetically along the tetragonal axis of URu_2Si_2 (Space group I_4/mmm) and with the moments along this same axis. At low temperature, the moment carried by the uranium atoms is about $0.4 \mu_B$. Between T_0 and T_x a small moment is detected, however it is attributed to inhomogeneities inside the sample as it is thought for ambient pressure.

The inelastic signals are known to appear in the 'hidden order' (HO) phase at two different positions of the Brillouin Zone. The first large signal appears at the position which becomes the antiferromagnetic Bragg peak in the high pressure

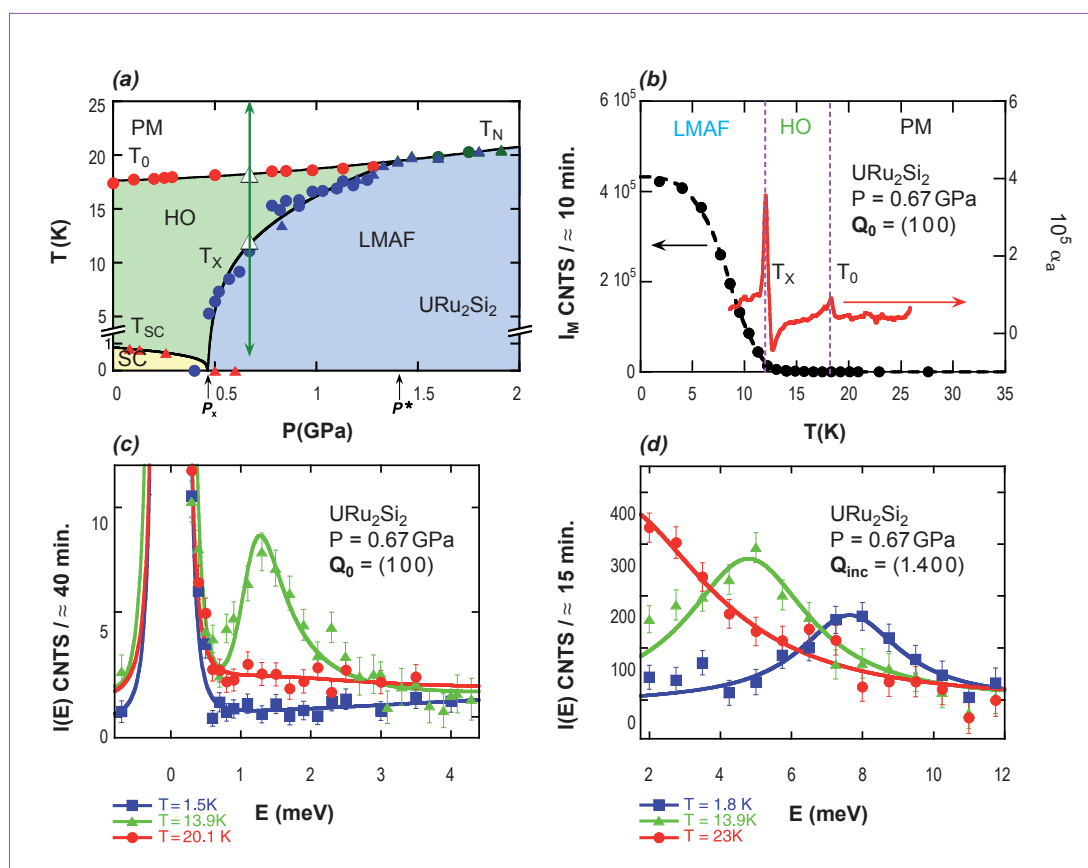


Figure 2
(a) Phase diagram of URu_2Si_2 from resistivity and ac calorimetry measurements.
(b) Intensity of Magnetic Bragg peak at $Q_0 = (1,0,0)$ and thermal expansion of URu_2Si_2 versus temperature. Data from IN12.
(c) Energy scan at $Q_0 = (1,0,0)$ of URu_2Si_2 . Data from IN12.
(d) Energy scan at $Q_{inc} = (1.4,0,0)$ of URu_2Si_2 . Data from IN22.

ordered phase ($Q_0 = (1,0,0)$). The second signal, as large as the first one, is at an incommensurate position on the edge of the nuclear Brillouin zone ($Q_{inc} = (1.4,0,0)$). At ambient pressure, these signals are really inelastic only in the 'hidden phase'; above T_0 the excitation at Q_0 vanishes quite quickly while at Q_{inc} the excitation becomes quasi-elastic and remains like that even up to a temperature two or three times T_0 .

In this experiment, at a pressure of 0.67 GPa in the HO phase between T_0 and T_x , the signals at Q_0 and Q_{inc} persist: a large inelastic signal is observed at ≈ 1.25 meV for Q_0 and at ≈ 5 meV for Q_{inc} . At lower temperature, on entering into the antiferromagnetic state, no more inelastic signal could be detected at the antiferromagnetic position while for Q_{inc} an inelastic signal could still be detected but shifted to ≈ 8 meV and with a smaller intensity (see **figures 2c/2d**).

To deduce the symmetry and the signature of the HO parameter, these results have to be analysed with bulk measurements, typically resistivity and specific heat. The shape of the curves and of the anomalies of the resistivity and of the specific heat measurements are very similar at low pressure when moving from the paramagnetic state

to the HO (T_0 transition line) or at high pressure when moving from the paramagnetic state to the antiferromagnetic state (T_N transition line). This similarity explains why the T_x transition line went undetected for more than 15 years. Clearly, we can deduce that the Fermi surface does not change in both states HO and LMAF. Therefore the symmetry is the same in both phases. Consequently, since Q_0 is the wavevector in the LMAF phase, it must also be the wavevector in the 'hidden order' state. Two signals (inelastic in this case) are detected in the HO, at Q_0 and Q_{inc} . The signal at Q_{inc} persists in the LMAF state: it is only shifted in energy. On the contrary, the signal at Q_0 exists only in the HO state and it is at the position of the wavevector of the order parameter.

We conclude that the inelastic signal at Q_0 is a resonant signature of the 'hidden order'. Despite the exclusion between 'hidden order' and antiferromagnetic order both phases have the same wavevector leading to the lattice doubling. Switching from body-centered tetragonal lattice to a simple tetragonal case leads to a complete Fermi surface reconstruction with a drop in electrical carriers and 'resurrection' of exotic 5f properties.

Authors

F. Moussa, M. Hennion, A. Gukasov and S. Petit (LLB, Saclay, France)

L. P. Regnault (CEA-Grenoble and ILL), A. Ivanov (ILL)

R. Suryanarayanan, M. Apostu and A. Revcolevschi (Université Paris-Sud, France)

Interlayer and intralayer exchange tuned by magnetic field in the bilayer manganite $(\text{La}_{0.4}\text{Pr}_{0.6})_{1.2}\text{Sr}_{1.8}\text{Mn}_2\text{O}_7$

The bilayer manganite $\text{La}_{1.2}\text{Sr}_{1.8}\text{Mn}_2\text{O}_7$ (LSMO) exhibits a phase transition from a paramagnetic insulating (PI) to a ferromagnetic metallic (FM) state with a colossal magnetoresistance effect (CMR). Upon 60% Pr substitution, this transition is suppressed. However, application of a magnetic field restores it with a CMR effect. Inelastic neutron scattering from a single crystal of $(\text{La}_{0.4}\text{Pr}_{0.6})_{1.2}\text{Sr}_{1.8}\text{Mn}_2\text{O}_7$ under a magnetic field reveals the in-plane exchange J_{ab} close to that of the Pr free compound LSMO although the interlayer exchange J_c is much smaller than that found in LSMO.

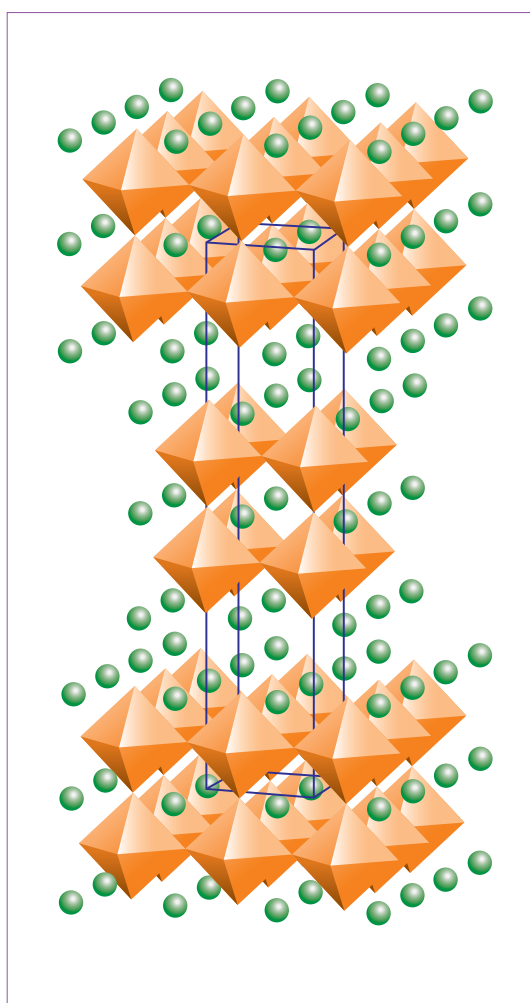


Figure 1a: Structure of the bilayer compound. Mn ions (not shown) are at the centre of MnO_6 octahedra. Green dots are (La, Pr, Sr) sites.

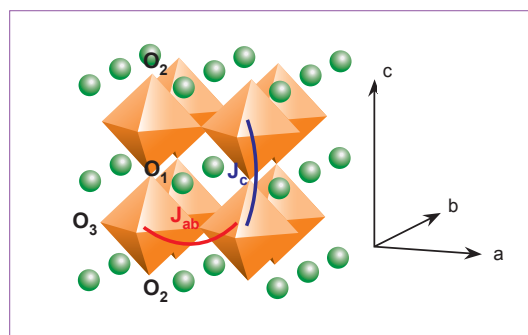


Figure 1b: Definition of intralayer J_{ab} and interlayer J_c couplings.

Systems showing a phase transition from a paramagnetic insulating (PI) to a ferromagnetic metallic (FM) state, tuned by magnetic field, have drawn considerable interest both from applications and fundamental points of view. The $(\text{La}_{0.4}\text{Pr}_{0.6})_{1.2}\text{Sr}_{1.8}\text{Mn}_2\text{O}_7$ (LPSMO) compound, discovered in the early 2000s [1], belongs to this category. It derives from the $n = 2$ member of the Ruddlesden-Popper series expressed generally as $(\text{La}_{1-x}\text{Sr}_x)_{n+1}\text{Mn}_n\text{O}_{3n+1}$. The bilayered compound with $n = 2$ and for the hole doping $x = 0.4$, shows a PI-FM transition at $T_c = 125$ K with a CMR ratio ~ 180 [2]. Keeping x constant at 0.4 but with an additional substitution of Pr on the La site, viz. $(\text{La}_{0.4}\text{Pr}_{0.6})_{1.2}\text{Sr}_{1.8}\text{Mn}_2\text{O}_7$, the material becomes a paramagnetic insulator at all temperatures. However an applied magnetic field induces a first-order PI to FM transition and a CMR effect. It seems interesting to measure the magnetic couplings in LPSMO: the in-plane exchange coupling J_{ab} and the interlayer exchange coupling J_c , see **figure 1a/1b**, (the magnetic coupling between neighbouring bilayers is very weak) and to compare them with these of LSMO.

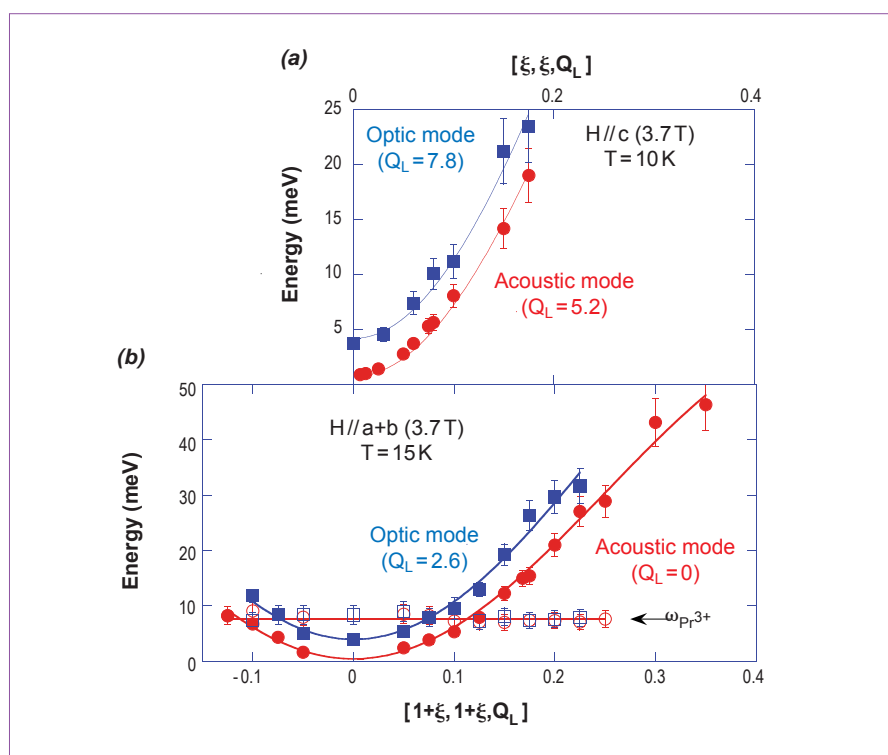


Figure 2: Dispersion of spin waves propagating along [110]. Acoustic branch: red solid dots; optic branch: blue solid squares. The solid lines represent the laws $\omega_{ac}(q)$ and $\omega_{opt}(q)$. **(a)** H//c; **(b)** H//a+b. The flat branch $\omega_{Pr^{3+}}$ represents the crystal field of the Pr^{3+} ion.

A straightforward way to measure such coupling constants is to determine the spin wave dispersion of the system and, for that, inelastic neutron scattering is a unique tool. Such measurements were achieved on the triple axis spectrometers IN22 and IN8 of the ILL with a magnetic field of 3.7 T applied along a+b or along c. The results are summarized in **figure 2**. One has analysed the data with the help of the Heisenberg ferromagnetic model. In that case two spin wave branches are found, an acoustic one $\omega_{ac}(q)$ and an optic one $\omega_{opt}(q)$ with $\omega_{ac}(q) = \omega_0 + 4SJ_{ab}[\sin^2(\pi q_x) + \sin^2(\pi q_y)]$ and $\omega_{opt}(q) = \omega_{ac}(q) + 2SJ_c$.

The main results are $SJ_{ab} \sim 8.6$ meV and $SJ_c = 1.7$ meV [3]. They are not very sensitive to the direction of the field. SJ_{ab} compares pretty well with SJ_{ab} of LSMO, while SJ_c is 1.7 times smaller than that of LSMO [4-6]. We explain these results by the strongly anisotropic distortions induced by the Pr ion. The Pr ion weakly distorts the robust structure of the ab plane, while its small size deeply modifies the O-Mn binds along the c axis.

References

- [1] M. Apostu, R. Suryanarayanan, A. Revcolevschi, H. Ogasawara, M. Matsukawa, M. Yoshizawa and N. Kobayashi Phys. Rev. B, 64 (2001) 012407
- [2] Y. Moritomo, A. Asimitsu and H. Kuwahara, Nature (London) 380 (1996) 141
- [3] F. Moussa, M. Hennion, F. Wang, A. Gukasov, R. Suryanarayanan, M. Apostu and A. Revcolevschi, Phys. Rev. Lett. 93 (2004) 107202; F. Moussa, M. Hennion, A. Gukasov, S. Petit, L.P. Regnault, A. Ivanov, R. Suryanarayanan, M. Apostu and A. Revcolevschi, Phys. Rev. B 78 (2008) 060406(R)
- [4] T. Chatterji, L.P. Regnault, P. Thalmeier, R. Suryanarayanan, G. Dhalenne and A. Revcolevschi, Phys. Rev. B 60 (1999) R6965
- [5] T. Chatterji, P. Thalmeier, G.J. McIntyre, R. Van de Kamp, R. Suryanarayanan, G. Dhalenne and A. Revcolevschi, Europhys. Lett. 46 (1999) 801
- [6] T.G. Perring, D.T. Adroja, G. Chaboussant, G. Aeppli, T. Kimura and Y. Tokura, Phys. Rev. Lett. 87 (2001) 217201

Authors

L. Malavasi and G. Chiodelli (INSTM and IENI-CNR, University of Pavia, Italy)
C. Ritter (ILL)

Correlation between thermal properties, electrical conductivity, and crystal structure in the $\text{BaCe}_{0.8}\text{Y}_{0.2}\text{O}_{2.9}$ proton conductor

The high-resolution neutron diffractometer D1A has been used to follow *in situ* the structural evolution at high temperature of a potential solid electrolyte material for protonic fuel cells, the Y-doped BaCeO_3 perovskite. The refinement of these high-quality data allowed us to define a precise evolution of the crystal structure from room temperature to 800 °C and to correlate the structural features with the behaviour of other physical properties such as the electrical conductivity.

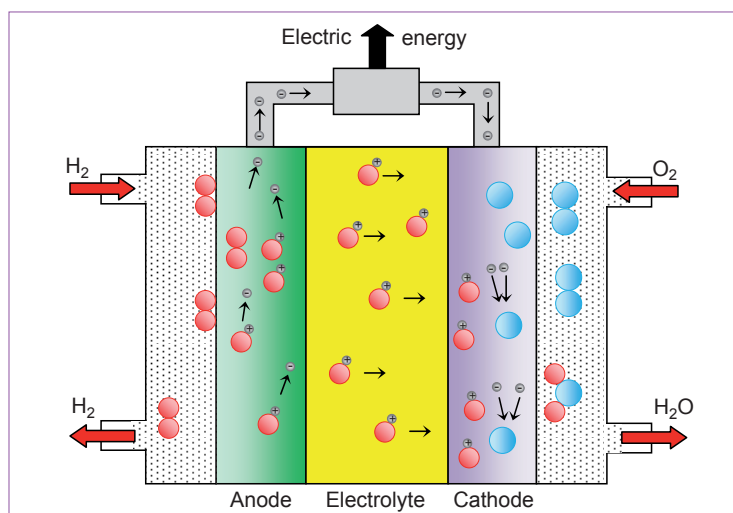


Figure 1:
Sketch of a
protonic fuel cell.

One of the most urgent challenges in material science research is the development of new power systems that could enable our dependency on fossil fuels for transport to be reduced. The most promising systems are based on fuel cell technology such as the solid oxide fuel cells (SOFC). The optimization of these systems requires, among other parameters, the reduction of their current operating temperature which is above 800°C if an oxide ion electrolyte is used (such as yttria-stabilized zirconia, YSZ). This requirement triggered the search for materials where the mobile species are protons instead of oxide ions which could lead to the reduction of the working temperature to an intermediate range, around 600°C (a schematic representation of a protonic fuel cell is displayed in **figure 1**) [1,2]. One of the prototype materials which showed very good conductivity performance is the doped barium cerate, BaCeO_3 [3]. Doping with Y or other aliovalent ions on the Ce-site is essential in order to create oxygen vacancies in the crystal structure which serve as preferential sites for water incorporation within the crystal lattice.

For any material to be implemented into a device, full knowledge of its structural behaviour in the temperature-range of use is desirable. In addition, this knowledge is essential in order to understand its behaviour related to other specific physical properties such as the electrical conductivity and the thermal stability.

Neutron diffraction is the technique of choice when the structural properties of an oxide have to be investigated due to the strong scattering power of oxygen which allows the oxygen atom positions and their occupancy to be precisely defined and to get valuable information related to the possible formation of superlattices.

In this experiment we collected neutron diffraction data on the Y-doped BaCeO_3 proton conductor $\text{BaCe}_{0.8}\text{Y}_{0.2}\text{O}_{2.9}$ as a function of temperature from room temperature to 800°C on the D1A instrument with an open furnace set-up [4]. The use of a quartz tube open to air to host the sample in the furnace allowed measurements to be made at ambient pressure, thus avoiding a possible reduction of the oxide sample at elevated temperatures within the more commonly used evacuated furnace. Neutron diffraction measurements were collected on the D1A instrument which is a very reliable instrument for standard crystallographic problems due to its high resolution and a near perfect Gaussian peak-shape.

Figure 2 shows the neutron diffraction patterns collected at different temperatures on $\text{BaCe}_{0.8}\text{Y}_{0.2}\text{O}_{2.9}$ under air while the inset shows a detailed view of the 2θ -range where the most intense peaks are present.

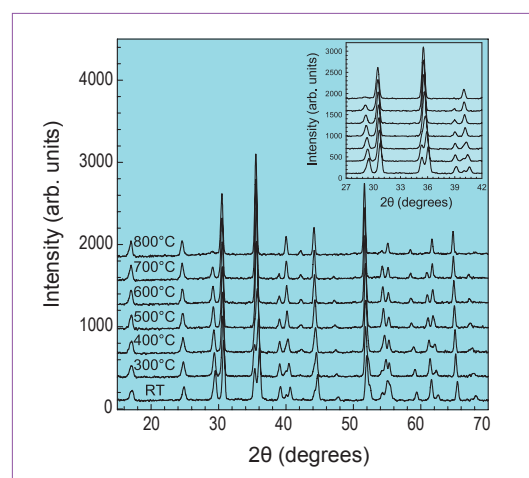
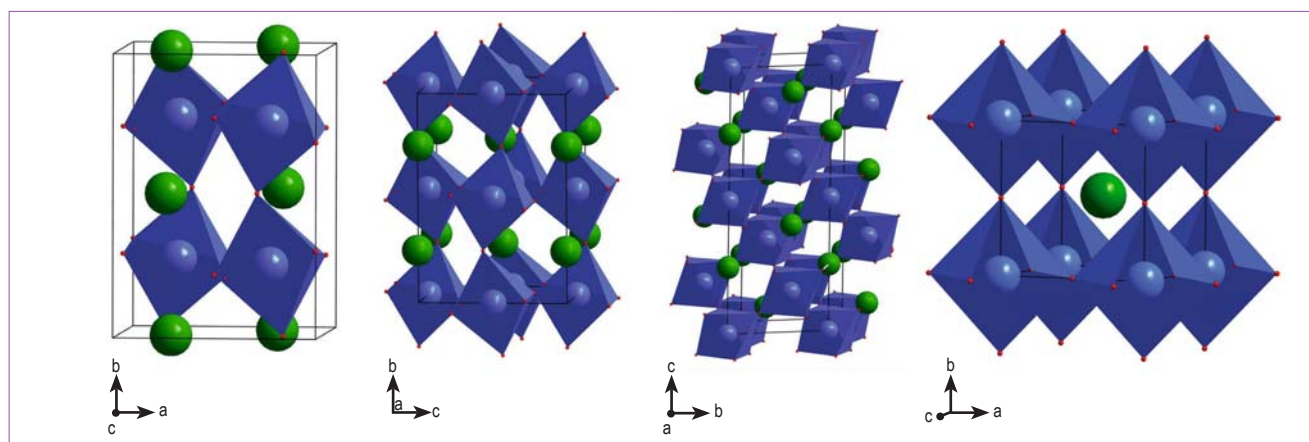


Figure 2: Neutron diffraction patterns of $\text{BaCe}_{0.8}\text{Y}_{0.2}\text{O}_{2.9}$ as a function of temperature. Inset: detailed view of the region where the most intense peaks are present.



the main peaks are located. A simple visual inspection of the pattern changes suggests an increase of symmetry with increasing temperature. The Rietveld refinement of the diffraction patterns was used to obtain useful information such as the crystal symmetry, the lattice parameters, the atomic positions and the oxygen atom occupancies. Regarding the structure, its evolution with temperature can be summarized as for follows:

- a)** from RT to 400 it is monoclinic with space group $I2/m$;
- b)** at 500°C it adopts the orthorhombic $Imma$ structure;
- c)** at 600 and 700°C it is rhombohedral ($R\bar{3}c$) and
- d)** finally at 800°C it becomes cubic ($Pm\bar{3}m$).

A sketch of the crystal structure evolution as a function of temperature is displayed in **figure 3**.

This progressive increase in the symmetry of the system is not accompanied by any first order phase transition. This was concluded from the thermal analysis carried out on the sample under the same conditions as the neutron diffraction acquisition and is supported by the absence of any relevant discontinuity in the cell volume evolution with temperature. A slight deviation of the cell volume at high temperature is most probably related to the variation of the oxygen content above 700°C which is presented in **figure 4** with a comparison between the oxygen content determined from the neutron diffraction data and that determined under the same experimental conditions, by means of thermogravimetry. These neutron diffraction data were also used to determine the location of the oxygen vacancies for the different crystal structures observed. This information is of great importance in unveiling the transport mechanism in these materials and can only satisfactorily be obtained from high-resolution, high-quality neutron diffraction data. Electrical conductivity measurements, again performed under the same experimental conditions of the neutron diffraction data collection, revealed a slope change at a temperature corresponding to the second order $Imma \rightarrow R\bar{3}c$ phase transition thus suggesting a direct correlation between structure change and transport properties.

In conclusion, these results provide direct evidence that the $BaCe_{0.80}Y_{0.20}O_{2.9}$ proton conducting oxide is a stable material without any volume discontinuity within the operational range of an intermediate fuel cell which is a fundamental pre-requisite for the incorporation of an electrolyte within a device. In addition, the experimental set-up employed the neutron diffraction measurements (which is the same as for the other techniques) enables a reliable structure-properties correlation to be defined.

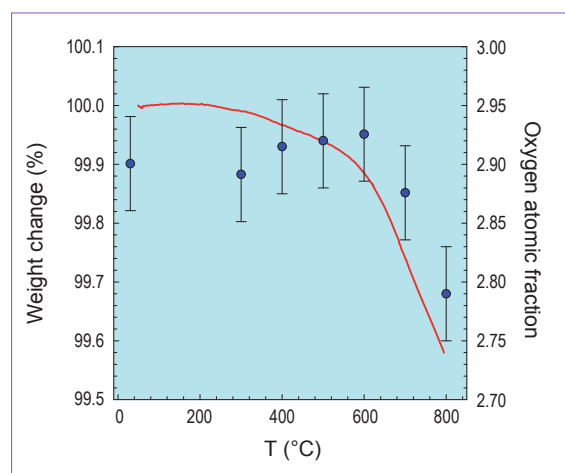


Figure 4: Weight change determined by TGA (red line) and oxygen content determined by neutron diffraction (blue points) as a function of temperature.

References

- [1] T. Hibino, A. Hashimoto, M. Suzuki, M. Sano, *J. Electrochem. Soc.* 149 (2002) A1503
- [2] A. Kruth, J.T.S. Irvine, *Solid State Ionics* 162-163 (2003) 83
- [3] N. Taniguchi, K. Haton, J. Niikura, T. Gamo, H. Iwahara, *Solid State Ionics* 53-56 (1992) 998
- [4] L. Malavasi, C. Ritter, G. Chiodelli, *Chem. Mater.* 20 (2008) 2343

Authors

C. M. Davies and K. M. Nikbin (Imperial College, London, UK)

R. C. Wimpory (Helmholtz-Zentrum Berlin, Germany)

M. Bérés and D. Dye (Imperial College, London, UK)

D. J. Hughes and E. Koukovini-Platia (ILL)

Managing weld distortion in thin steel plates

Distortion induced by welding residual stresses (RS) is particularly problematic for the assembly of thin structures and often requires costly reworking.

To understand the influence of process parameters on RS and distortion, RS measurements have been performed in 4 mm thick butt-welded and fillet-welded stiffened plates of a ferritic steel, using the strain scanner SALSA; the distortion has been quantified through surface profile measurements at the ILL. The influence of phase changes, plate and stiffener geometry, and welding parameters on the RS and distortion profiles has been determined.

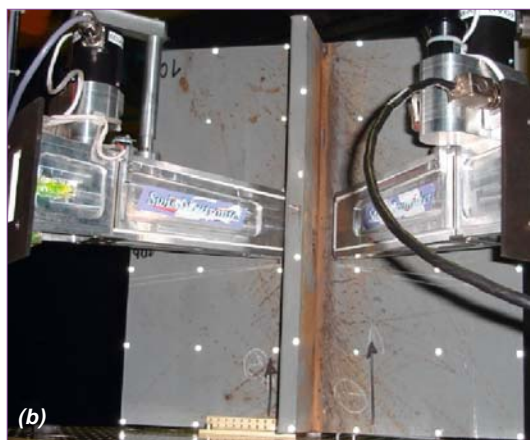
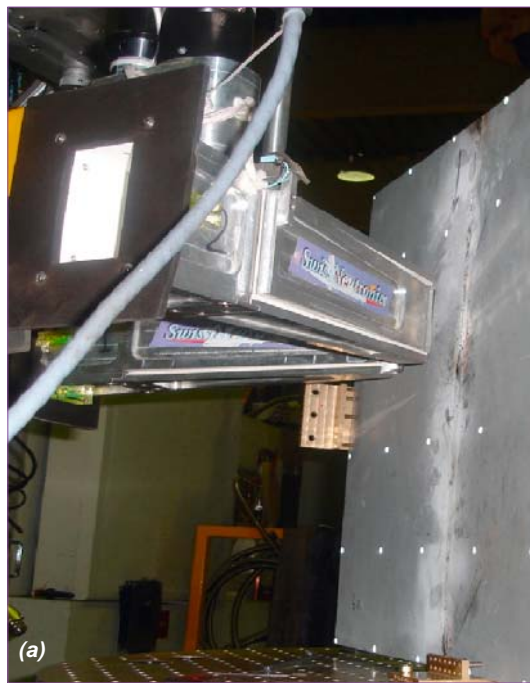


Figure 1:
Measurement of residual stress on
(a) butt-welded plate,

(b) fillet-welded stiffener on SALSA.

Steel structures are often fabricated through the assembly of welded plates. The residual stresses generated during the welding process and subsequent cool-down, can cause significant plate distortion. Weld distortion is particularly problematic for large thin structures. In the shipbuilding industry alone, over a third of the components must be reworked, at high cost, due to weld distortion [1]. Distortion rectification can amount to over half the original fabrication costs and consumes vast quantities of energy in the process.

Butt and fillet-welded stiffened plates of ferritic grade DH-36 steel (often used in ship construction), of dimensions $500 \times 500 \times 4 \text{ mm}^3$, were manufactured using the manual metal arc (MMA) process [2]. The residual stress states in these plates have been established using the strain scanner SALSA at the ILL (see **figure 1**). Measurements were made in three orthogonal directions; along the weld (longitudinal), transverse to the weld and normal to the plate surface. Small stress-relieved samples were machined in order to determine appropriate reference lattice parameters for the parent and filler materials.

The distortion was quantified through measurement of the surface profiles of the plates using the coordinate measurement machine (CMM) with the non-contact laser probe of the ILL-ESRF materials science support laboratory. An example of a plate's distortion profile is shown in **figure 2**.

The influence of plate and stiffener geometry, and welding parameters has been studied [3]. Symmetric stress profiles are effectively found (**figures 3, 4**) with a peak value at the interface of the heat affected zone and the parent material. A weld length/half-width of approximately 5 mm was observed. Stiffener thickness has relatively little influence on the stress distribution (see **figure 3**) as does weld speed. However, the increase in energy input due to lower weld speeds can influence the distortion profile.

Phase transformation effects, which were examined by changing the composition of the weld consumable (filler material), had a profound effect on the residual stress profiles. A peak tensile stress of yield magnitude is exhibited in the longitudinal direction using the standard weld consumable (see **figure 4**). Phase transformations that have specifically arisen using the alternative weld consumable induced significant compressive residual stresses within the weld. The weld consumable can therefore be customised to optimise the stress profiles and minimise distortion.

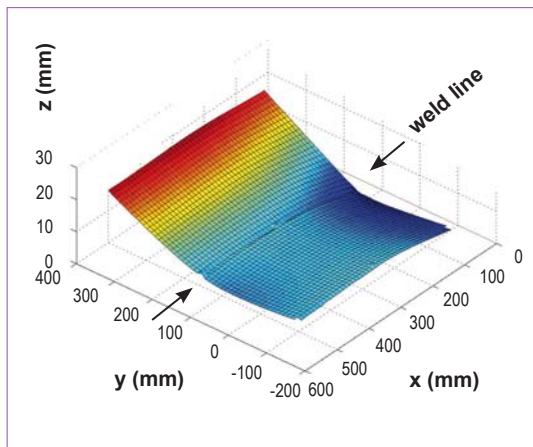


Figure 2: Distortion profile of a butt-welded plate.

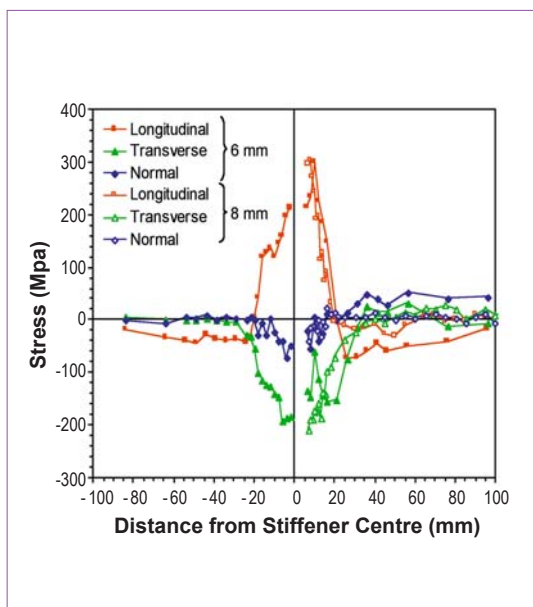


Figure 3: Comparison of residual stress distributions for 6 mm and 8 mm stiffener thickness.

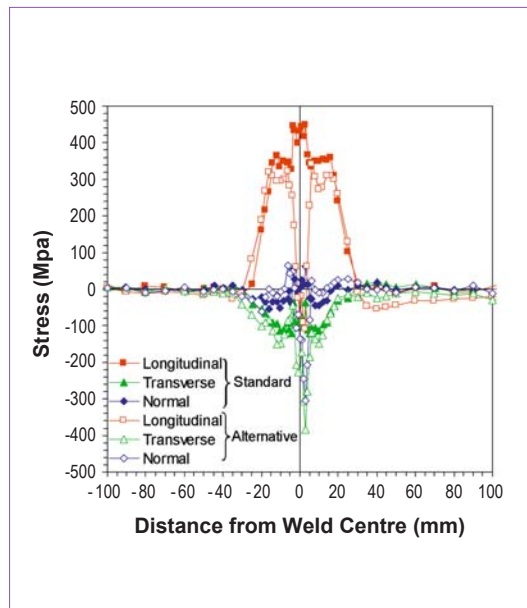


Figure 4: Comparison of the residual stress profiles measured in butt-welded plates using a standard and alternative weld consumable.

These measurements are being complemented by, and used to verify, finite element simulations of the welding procedure [4]. The optimal geometric and welding parameters may therefore be determined to enable the management of weld distortion.

References

- [1] J. Dydo, H. R. Castner and K. Koppenhoefer, *Guidelines for Control of Distortion in Thin Ship Structures*, Edison Welding Institute, Columbus, Ohio, Project No. 43272-GDE, October 1999
- [2] C. M. Davies, R. C. Wimpory, M. Béreš, M. P. Lightfoot, D. Dye, E. Oliver, N. P. O'Dowd and G. J. Bruce, *The Effect of Residual Stress and Microstructure on Distortion in Thin Welded Steel Plates in Proceedings of PVP2007 ASME Pressure Vessels and Piping Division Conference*, July 22–26, 2007, San Antonio, Texas, USA
- [3] C. M. Davies, R. C. Wimpory, D. Dye, and K. M. Nikbin, *The Effects of Plate Dimensions on Residual Stresses in Welded Thin Steel Plates*, in *Proceedings of PVP2008 ASME Pressure Vessels and Piping Division Conference*, July 27–31, 2008, Chicago, Illinois, USA
- [4] M. Tsunori, C. M. Davies, D. Dye and K. M. Nikbin, *Numerical Modelling of Residual Stress and Distortion in Thin Welded Steel Plates*, in *Proceedings of PVP2008 ASME Pressure Vessels and Piping Division Conference*, July 27–31, 2008, Chicago, Illinois, USA

Authors

A. Arbe and J. Colmenero (CFM, San Sebastián, Spain)

A. C. Genix (Université de Montpellier II, France)

D. Richter (IFF, Jülich, Germany)

P. Fouquet (ILL)

Nano-confinement through self-assembly: emergence of anomalous relaxation

We have exploited the selectivity of neutron scattering combined with isotopic substitution to study the structure and dynamics of poly(n-alkyl methacrylates). Our diffraction data nicely demonstrate the nanosegregation of main chains and side groups. Moreover, by NSE we have separately followed the structural relaxation of both subsystems. Contrary to the standard behaviour found at the main chain level, the correlations involving long side groups within the alkyl nanodomains relax through an exotic logarithmic decay - probably a signature of nano-confinement of the side-groups by the more rigid main chains.

Concepts such as self-assembly, confinement, nanophase separation and dynamic asymmetry are ubiquitous in multicomponent soft materials. However, these features are not exclusive for multicomponent systems but might also be present in some homopolymers, such as the family of poly(n-alkyl methacrylates) (PnMAs). In these polymers, the alkyl side groups of different monomers seem to self-assemble forming nanodomains (called polyethylene (PE)-like). Moreover, PnMAs show two glass-transitions which presumably correspond to the freezing of motions within the alkyl nanodomain and of the main-chain dynamics [1]. Until now, this scenario rests on results of techniques (calorimetry, dielectric and mechanical spectroscopy, X-rays) that cannot distinguish main-chain and side-group contributions. Neutron scattering combined with isotopic labelling is just the right tool to reveal the structure in PnMAs and selectively follow the collective dynamics of alkyl and main chain atoms. In addition to an unambiguous proof of the nanophase hypothesis, our study has revealed nearly perfect logarithmic decays for the structural relaxation within the side-group nanodomains - an anomalous and exciting behaviour!

Figure 1:
Chemical formulae of the polymers investigated together with the nanophase-separated structure suggested by the diffraction data.

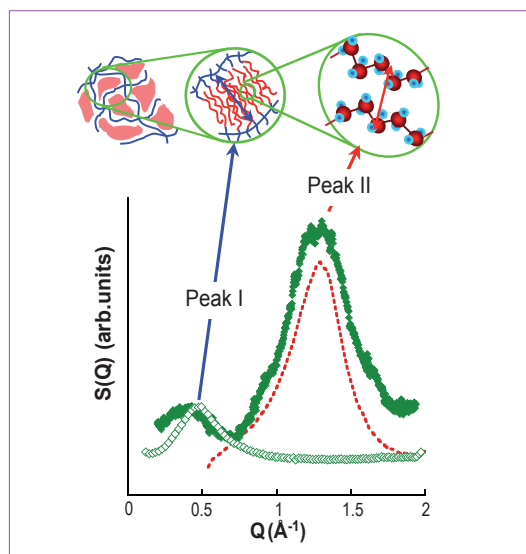
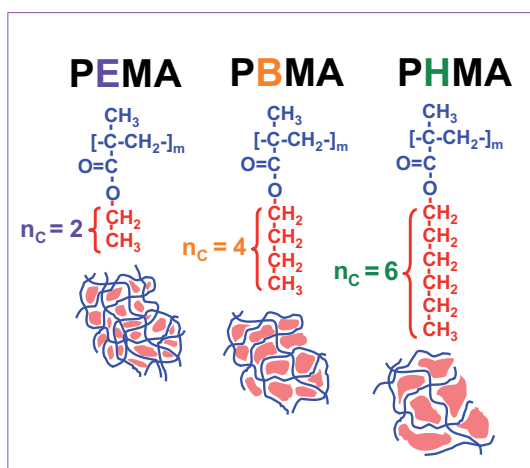


Figure 2: Neutron diffraction pattern of the fully deuterated PHMA ($n_c = 6$) sample (full symbols) and a PHMA sample deuterated only along the main-chain (empty diamonds). The dotted line shows the structure factor of bulk polyethylene. The cartoon shows the interpretation of the correlations giving rise to the two main peaks in the structure factor.

We have investigated PnMAs with different numbers of carbons in the side-group $n_c = 2, 4$ and 6 (figure 1). Diffraction on fully deuterated samples (reflecting all possible atomic pair correlations) reveals two peaks. Figure 2 shows the case of PHMA ($n_c = 6$). Peak I shifts to smaller Q-values with increasing side-group length, from 0.8 \AA^{-1} ($n_c = 2$) to 0.2 \AA^{-1} ($n_c = 6$). On the contrary, the position of Peak II, at about 1.3 \AA^{-1} , hardly depends on n_c . How can neutrons decipher the nature of the correlations giving rise to these two peaks? Let's 'hide' the side-groups through protonation! Then, Peak II completely disappears and only Peak I remains (figure 2).

In this way, we elegantly demonstrate that Peak I arises from correlations between main chains and Peak II reveals correlations between the side chains. A comparison with the static structure factor of pure PE in the melt reveals a strong similarity of Peak II with the amorphous halo of PE. Thus, the short-range order around the side-group atoms in PHMA is very close to that in pure PE. The side groups are in a PE-like environment, so they form domains. These are surrounded by the main chains, the average distance between which (and thereby the size of the domain) determines the position of Peak I. We deduce sizes of 10, 13 and 16 Å for PEMA, PBMA and PHMA respectively. Thus, we provide a clear-cut proof for the existence of PE-like nanodomains where size depends on the side-chain length (**figure 1**), supporting the nanophase hypothesis and pointing to a confined situation for the side-groups by the main-chains.

The clear separation of Peaks I and II in Q-space has facilitated the selective study by Neutron Spin Echo of the dynamics associated with each subsystem. At Peak I, the dynamics of the 'confining' main-chains shows the features of a completely standard α -relaxation (viscosity scaling and stretched exponential decay, i.e., $S(Q,t)/S(Q,0) \propto \exp[-(t/\tau)^\beta]$, with $\beta = 0.5$) [2]. This is also observed for the alkyl subsystem (Peak II) in PEMA (**figure 3**). However, the situation at Peak II dramatically changes for higher order members ($n_c = 4, 6$): surprisingly, we find nearly perfect logarithmic decays, strongly deviating from the typical expected stretched exponentials (**figure 3**). This novel effect arises when the confining subsystem relaxes much more slowly than the side-groups (i.e., high dynamic asymmetry).

What could be the origin of such anomalous dynamics? Logarithmic decays naturally emerge in the framework of a general kind of model based on hierarchically constrained dynamics so that the relaxation of the system involves a sequential, rather than parallel, series of correlated processes with an increasing characteristic time [3]. An alternative explanation can be based on analogies with some two-component miscible systems, e.g. dynamic asymmetric polymer blends, where the dynamics of the minority fast component is restricted ('confining') by the slow one. Such systems show a similar type of anomalous relaxation. An interpretation of that observation assumes the existence of two simultaneous arrest mechanisms for the fast component: bulk-like caging (by the neighbouring fast polymer) and a 'confinement effect' due to the slow component [4]. This interpretation suggests a high-order mode coupling theory (MCT) transition. We speculate whether similar mechanisms also exist in PnMAs and a MCT scenario can be applied. Obviously, the elucidation of the origin of the exotic dynamic behaviour reported here demands further experimental and theoretical efforts.

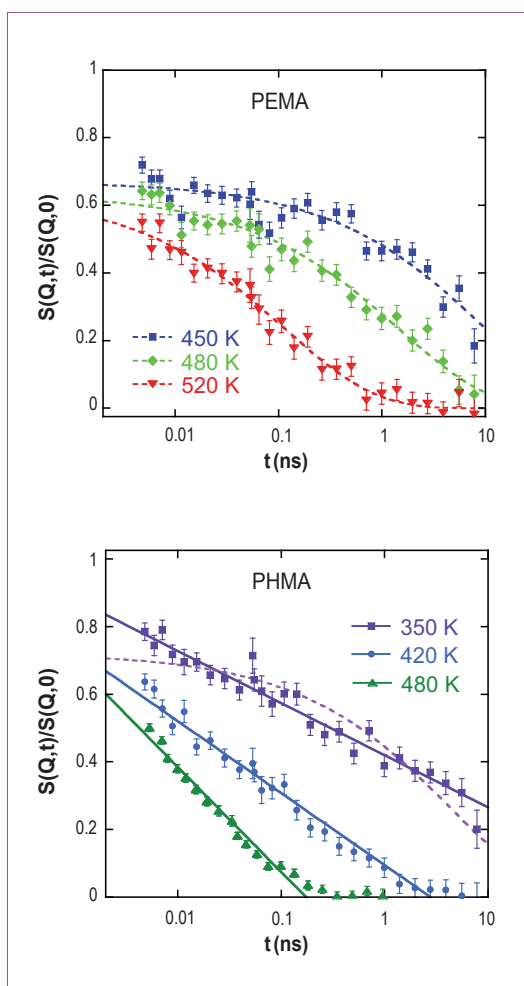


Figure 3: Dynamic structure factor at the second (nanodomain) peak ($Q = 1.3 \text{ \AA}^{-1}$) for PEMA ($n_c = 2$) and PHMA ($n_c = 6$) at the temperatures indicated. Dotted lines are fits to stretched exponentials with $\beta = 0.5$ and solid lines to a logarithmic expansion.

References

- [1] M. Beiner and H. Huth, *Nat. Mat.* 2 (2003) 595
- [2] A. Arbe, A.-C. Genix, J. Colmenero, D. Richter and P. Fouquet, *Soft Matter* 4 (2008) 1792
- [3] J. J. Brey and A. Prados, *Phys. Rev. E* 63 (2001) 021108
- [4] A. J. Moreno and J. Colmenero, *J. Chem. Phys.* 124 (2006) 184906

Authors

R. F. Tabor and J. Eastoe (University of Bristol, UK)
I. Grillo (ILL)

Time-resolved small-angle neutron scattering as a lamellar phase evolves into a microemulsion

Stopped-flow small-angle neutron scattering (SANS) was used to follow the formation of a microemulsion after dilution with toluene of a lamellar phase comprising the nonionic surfactant TX-100 and water. Initially after dilution, an oil-swollen lamellar phase was formed. Between 4 and 160 s, this evolved into a dense water-in-oil (w/o) microemulsion, during which the two phases co-existed. After 160 s, the system appeared to be a pure single-phase microemulsion.

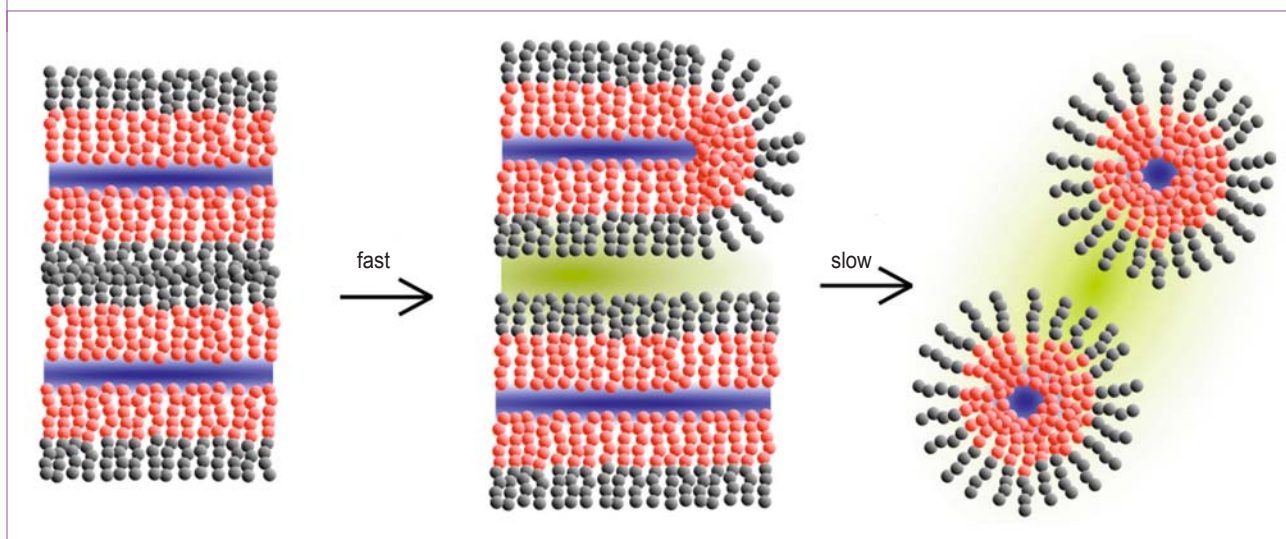
Colloidal and soft matter phase transition kinetics are experimentally challenging to study as they can occur on fast timescales (of the order of ms to s), although timescales tend to be highly dependent on the nature of the system [1]. Understanding the way in which such systems rearrange to give different phases (and how quickly this occurs) can provide insights into the fundamental nature of such processes, and help to improve formulation and application of soft colloids.

related systems, as substitution of H₂O by D₂O generates convenient contrast variation. One potential disadvantage of neutron scattering for time-resolved studies is the limitation of signal-to-noise, requiring long data acquisition times to achieve good statistics (typically 5-30 mins depending on the system of interest). However, the new generation of high-flux spectrometers, like D22 at the ILL, creates the possibility of real-time measurement with acquisitions of the order of 100 ms, coupled with histogramming memory data acquisition.

In this work, a lamellar phase (L_{α}) comprising the common non-ionic surfactant Triton X-100[®] (TX-100) and water was diluted with an equal volume of toluene, using a

Figure 1: Schematic representation of the oil-swelling of the lamellar phase and subsequent phase transition to a microemulsion.

Small-angle scattering represents the ideal tool for the equilibrium investigation of these soft-matter systems, as it can provide direct structural information. Neutron scattering is particularly suited to studying microemulsions and



stopped flow apparatus, and the growth of a nascent microemulsion phase (ME) was followed with time-resolved small-angle neutron scattering (TR-SANS). The results show that TR-SANS has great potential for following colloidal and surfactant phase transition kinetics. Previous work has demonstrated that the transition from an ME to an L_{α} phase can be effected by either temperature or pressure [2,3], and that at certain pressures and temperatures, both lamellar and microemulsion phases may coexist [3].

Analysis of the SANS profile of the initial (undiluted) TX-100/ D_2O lamellar phase with the appropriate model [4], suggests that the sheets are stacked with a separation of ~ 43 Å. Directly after mixing with toluene (before the first SANS measurement) a new phase had formed, with a membrane separation of around 50 Å. This suggests that the original TX-100/ D_2O L_{α} phase was swollen with some toluene on a very short timescale after the mixing (**figure 1**). This phase, however, was thermodynamically unstable with respect to a ME, this latter transformation taking much longer.

The timescale for the slow (swollen L_{α} -ME) phase transition is around 160 s (**figure 2**). After this time, the SANS data are consistent with a pure microemulsion. For times earlier than 160 s, the SANS data suggests contributions from varying amounts of L_{α} and ME phases, the populations of which evolve with time.

One possible explanation for the large difference between the timescales of the lamellar swelling and the subsequent swollen L_{α} -ME transition is a difference in energy demands. For swelling the L_{α} phase with toluene, the oil molecules must permeate between the tail-on interfaces of the membranes. As no new interface is created and the oil is entering a hydrocarbon environment, it is understandable that this could be both a low-energy and fast process. However, on evolution from the swollen L_{α} to a ME, the interface that now exists as a surfactant film layer (i.e. the lamellar membrane) must be broken up, in order to coat the interfaces of the nascent droplets. Overcoming the interfacial tension has a relatively high energy demand (activation barrier), and hence the process requires a longer time-scale. In addition, as the system is highly concentrated in surfactant (75% in L_{α} and 38% in ME), both phases are extremely viscous, hindering the diffusion required for the phase transition.

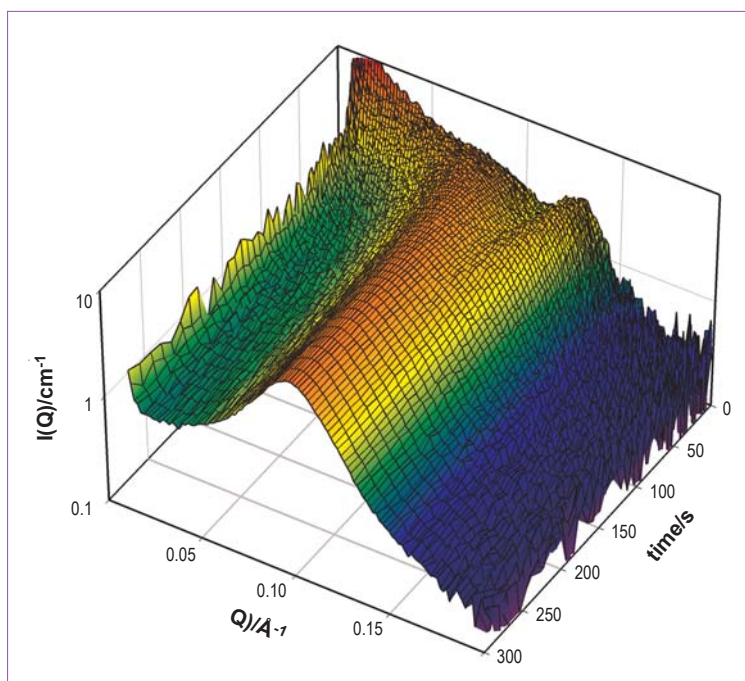


Figure 2: Time-resolved SANS data showing the gradual appearance of a low Q microemulsion profile, and disappearance of the high Q lamellar peak.

This work emphasizes the strength of SANS for determining structure, composition and phase transitions in soft colloidal systems. By use of a high intensity neutron source and data histogramming, short (20 ms) time-frames can be observed with high enough signal-to-noise for quantitative data analyses. Significantly, analysing structural information from such transformations gives insight into the nature of surfactant rearrangement in soft colloidal systems of interest.

References

- [1] M. Gradzielski, I. Grillo and T. Narayanan, *Prog. Colloid Polymer Sci.* 129 (2004) 32
- [2] M. Nagao, H. Seto, T. Takeda and Y. Kawabata, *J. Chem. Phys.* 115 (2001) 10036
- [3] M. Nagao and H. Seto, *Phys. Rev. E* 59 (1999) 3169
- [4] F. Nallet, D. Roux and S. T. Milner, *J. Phys.* 51 (1990) 2333

Authors

J. Zhang and S. Zauscher (Duke University, Durham, USA)

T. Nylander and P. Linse (Lund University, Sweden)

R. A. Campbell (ILL)

A. R. Rennie (Uppsala University, Sweden)

A novel evaluation method of neutron reflectivity data applied to stimulus-responsive polymer brushes

Neutron reflectivity (NR) measurements have been performed on stimulus-responsive polymer brushes containing N-isopropylacrylamide (NIPAAM) at different temperatures and in three isotopic solution contrasts.

The NR data were analysed using a novel method employing polymer density profiles predicted from lattice mean-field theory augmented with a model to describe polymer solubility that decreases with increasing temperature.

The predicted density profiles at the different temperatures are self-consistent with the experimentally observed profiles. The new evaluation approach derives from measured molecular physical properties and involves significantly fewer independent fitting parameters than conventional optical matrix fitting methods. Such model calculations provide a valuable tool to interpret results from NR experiments and to design experiments that optimise the use of beamtime.

Figure 1: Predicted reflectivity profiles $Q^4R(q)$ versus Q for small Q obtained in contrast-matched silicon at 293 K (blue curve), 303 K (green curve), 313 K (violet curve), and 328 K (red curve) using lattice mean-field theory. From ref [5].

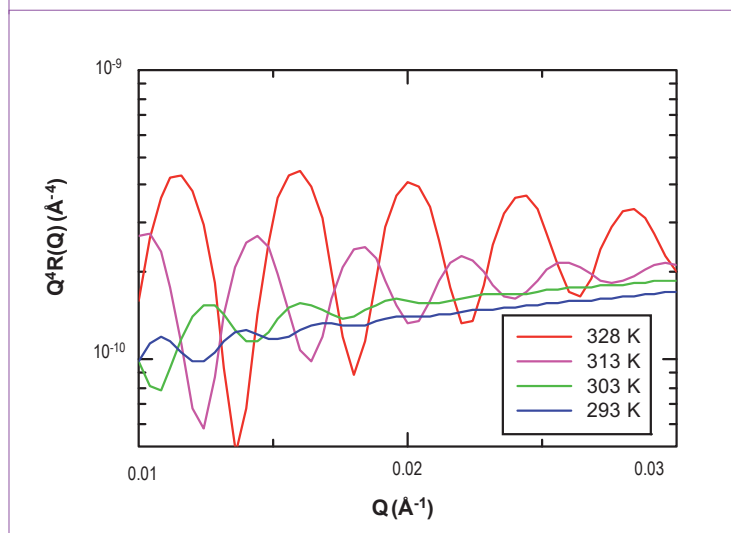
Stimulus-responsive polymers are macromolecules that undergo conformational changes in response to external stimuli such as changes in temperature, pH, or ionic strength. More specifically, poly(N-isopropylacrylamide) (pNIPAAM) brushes demonstrate significant and reversible conformational collapse in response to an increase in temperature [1]. Because of their unique thermo-responsive properties, these polymer brushes can be exploited in

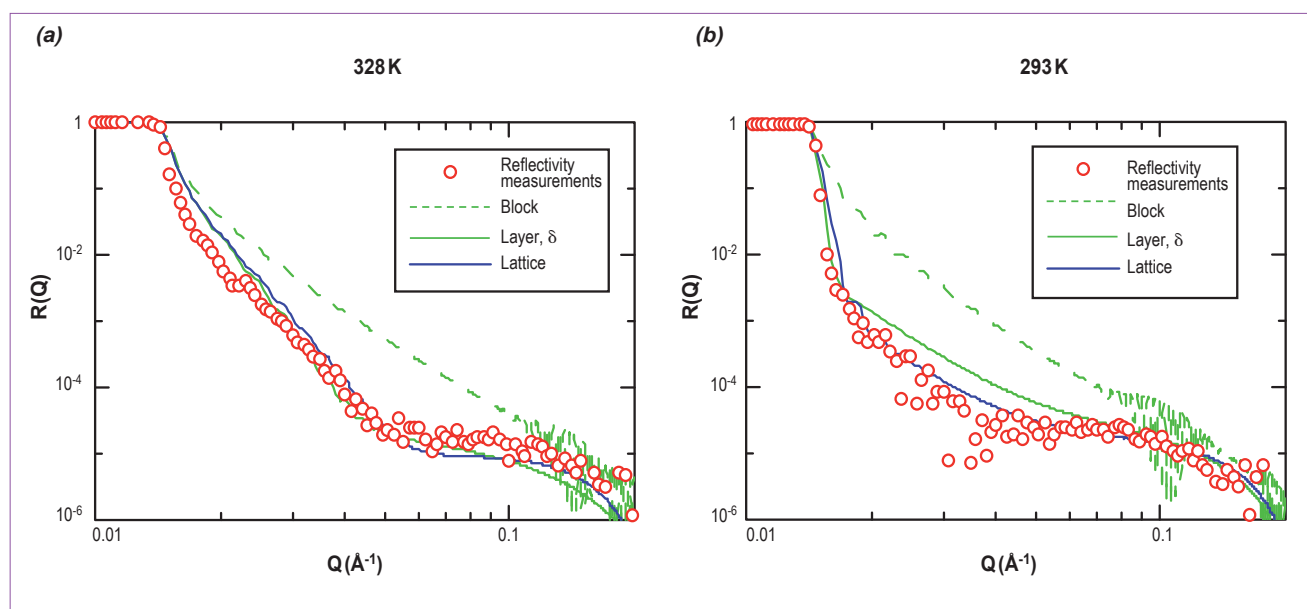
sensing and actuation devices on the nanoscale with potential applications from protein affinity separations [2] to tissue engineering [3].

A detailed understanding of the conformational change behaviour in these brushes is essential as it allows rational brush design and guides brush synthesis for optimising their performance for sensing and actuation applications. A thorough understanding of the change in conformation and hydration of pNIPAAM-containing polymer brushes on the sub-molecular level has, to date, not been achieved by common surface chemistry characterisation methods.

NR offers a powerful tool to determine the details of the segment density profiles perpendicular to the surface in grafted polymer layers and also in buried interfaces [4]. In the present project, we determined the structure of poly(N-isopropylacrylamide-co-acrylic acid) random copolymer brushes, using NR over the temperature range from 293 K to 333 K at pH 4.0 [5]. At 293 K the polymer brush is in a swollen state and at 333 K it is in a collapsed state.

The interpretation of the NR data was performed by using two different approaches: (i) a simple model using a single homogeneous layer and (ii) a novel approach utilising polymer brush theory [6]. In the second case, we have modelled





the segment density profiles using a molecular-based, lattice mean-field theory, augmented with an extension that enables a physical description of the reverse solubility displayed by pNIPAAAM. Necessary model parameters describing the copolymer-water interaction were determined from independently measured solubility data. The brush near the planar surface was divided into layers parallel to the surface, with a thickness for each layer corresponding to the size of a polymer segment. The equilibrium distributions of the polymer segments in the layers and of the internal states of the polymer segments were obtained by minimisation of the free energy of the system. From the segment density profiles and contrast conditions, the NR profiles were computed.

As an illustration of pNIPAAAM brushes, **figure 1** shows predicted reflectivity profiles at low Q range, where the increase in fringe amplitude and the concomitant increase in the number of fringes with increasing temperature is consistent with a conformational collapse of the pNIPAAAM brush at high temperatures.

Experimental and fitted reflectivity profiles in D_2O are shown in **figure 2**. NR profiles predicted by polymer theory provide an improved fitting over that of a conventional layer model of the NR data of pNIPAAAM copolymer brushes in both D_2O and contrast-matched silicon (cmSi) at two

different temperatures. Moreover, this new evaluation approach involved significantly fewer independent fitting parameters than methods involving layers of uniform density. Our approach can straightforwardly be extended to analyse neutron reflectivity data of grafted, weakly charged responsive polymers. Furthermore, it provides a powerful tool for the interpretation of NR data from polymeric systems that undergo conformational change. This development has potential to aid the design of novel smart surfaces that respond or adapt to their environment.

References

- [1] M. Kaholek, W. K. Lee, S. J. Ahn, H. W. Ma, K. C. Caster, B. LaMattina and S. Zauscher, *Chem Mater* 16 (2004) 3688
- [2] N. Nath and A. Chilkoti, *J Am Chem Soc* 123 (2001) 8197
- [3] T. O. Noriko Yamada, Hideaki Sakai, Fumiko Karikusa, Yoshio Sawasaki, Yasuhisa Sakurai, *Makro. Chem.Rapid. Commu.* 11 (1990) 571
- [4] T. P. Russell, *Annu Rev Mater Sci* 21 (1991) 249
- [5] J. M. Zhang, T. Nylander, R. A. Campbell, A. R. Rennie, S. Zauscher and P. Linse, *Soft Matter* 4 (2008) 500
- [6] P. Linse and M. Björling, *Macromolecules* 24 (1991) 6700

Figure 2. Experimental reflectivity profiles (red circles) taken at (a) 328 K and (b) 293 K.

The green lines refer to the fitted reflectivity for a single polymer layer with zero roughness (green dashed line) or optimal roughness (green solid line). The blue line is the fit for lattice mean-field theory. All profiles were collected in D_2O . From ref [5].

■ Authors

A. Schollier (ILL and ULB, Brussels, Belgium), **G. Fragneto** (ILL)
M. Sferazza (ULB, Brussels, Belgium), **A. Halperin** (UJF, Grenoble, France)
D. Clément (ILL and University of Waikato, Hamilton, New Zealand)

Protein adsorption on PEG brushes studied by neutron reflectivity

Poly(ethylene glycol) (PEG) brushes are known for their anti-fouling properties. Understanding the mechanism of interaction between such brushes and proteins can lead to improvements in the design of anti-fouling materials. Neutron reflectivity, combined with the use of deuterated proteins, is an ideal technique to obtain this information. Experiments have been performed on the D17 reflectometer at the ILL, showing the feasibility of such a study.

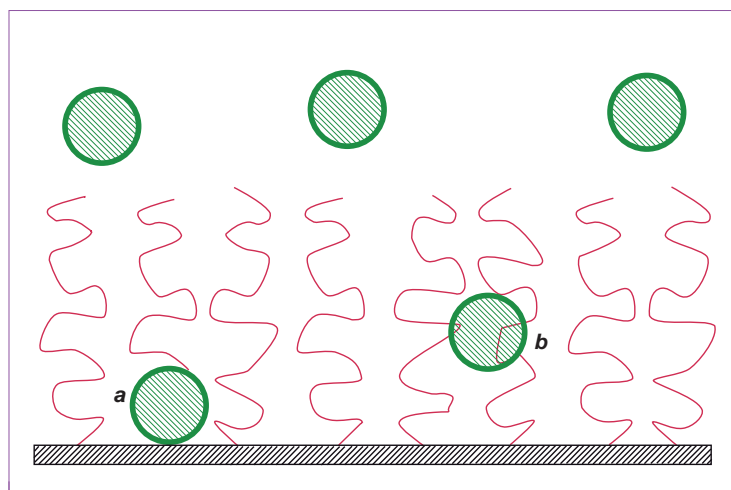


Figure 1:

The PEG brush is immersed in a diluted globular protein solution, and two adsorption modes can take place:

(a) primary adsorption, at the grafting surface and

(b) ternary adsorption, within the brush itself.

Materials used in medical devices that come into contact with biological fluids suffer from fouling problems due to the adsorption of proteins onto their surfaces. Examples of such unwanted effects include clotting in the case of blood-contacting devices, fouling of contact lenses, or reduction of circulation time of therapeutic proteins and drug-bearing liposomes in the body.

Coating the surface of a device with brushes of the polymer poly(ethylene glycol), or PEG, is known to reduce protein adsorption. PEG is a neutral water-soluble polymer which can be deployed in a brush form. A polymer brush is a layer of polymers attached by one end to a surface - either chemically or by adsorption - with a high density of grafted chains.

We have recently published a theoretical model [1], assuming that two types of adsorption on to polymer brushes can simultaneously take place for globular proteins: **(a)** primary adsorption, at the grafting surface, due to attractive interactions between the protein and

the surface, and **(b)** ternary adsorption, within the brush itself, due to a weak PEG-protein attraction (**figure 1**). A third mode is known: secondary adsorption, at the outer edge of the brush, due to van der Waals interactions between the proteins and the external surface of the brush. This last mode occurs only in the case of long cylindrical proteins. Here we focus on primary and ternary adsorption of globular proteins.

The model suggests that both primary and ternary adsorptions are repressed by increasing the grafting density of the brush. Increasing the chain length however favours ternary adsorption. The interplay of these factors determines the efficiency of the brush in repressing protein adsorption. In order to illustrate this experimentally, we have to know the structure of the PEG layer, together with the protein concentration profile within the brush.

The parameters characterising the PEG brush are then the chain length and the grafting density. For the experiments described here, the brush was adsorbed on a polystyrene (PS) sublayer using the Langmuir-Schaefer technique: a solution of PS-PEG diblock copolymers was spread at the air/water interface of a Langmuir trough, the film was compressed to the desired grafting density and then transferred to a silicon substrate, previously coated with PS [2,3].

Because the concentration profiles of the proteins and the PEG monomers must be obtained separately, it is difficult to use traditional methods - they are usually sensitive to mass changes at the surface but cannot provide information about the location of the different components. On the other hand, neutron reflectivity, combined with the use of deuterated proteins, can give the required information.

This technique gives access to the structure and composition of layers at buried interfaces with the resolution of a fraction of a nanometre. Because neutrons are scattered very differently by hydrogen and deuterium, if a deuterated protein

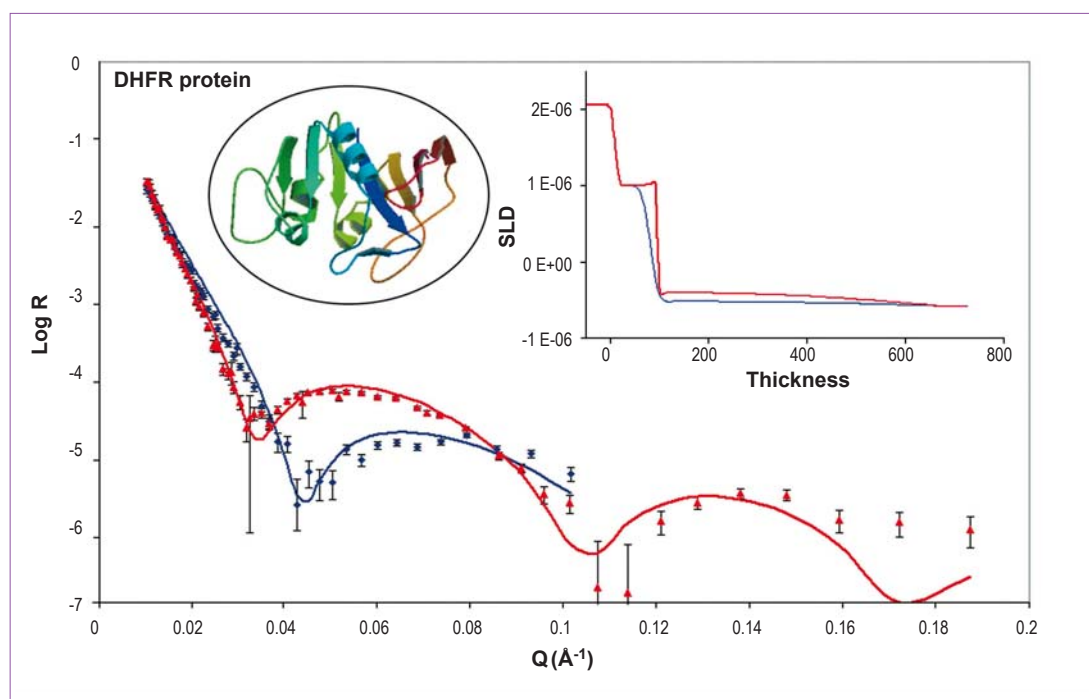


Figure 2: Neutron reflectivity data and scattering length density (SLD) of the adsorption of deuterated dihydrofolate reductase on a PEG brush formed of chains of 770 monomers, with a grafting density of 1000 Å²/mol. Blue data and lines refer to the PEG brush alone, while red data and lines refer to the system after adsorption of the protein. Simultaneous primary and ternary adsorptions are observed, as predicted by the theory.

inserts into a non-deuterated PEG layer on a surface, it becomes visible, and its amount can be quantified and localised inside the brush.

We carried out neutron reflectivity measurements (**figure 2**) on PEG brushes formed of chains of 770 monomers deposited at grafting densities ranging from 500 Å²/mol to 1250 Å²/mol. The system was first characterised before adsorption of the protein, with several contrasts. This technique, known as the contrast variation technique, consists in using water of different scattering-length densities by mixing H₂O and D₂O, allowing us to enhance certain components of the system. The protein solution, at a concentration of 0.5 mg/ml, was then injected in the cell containing the sample. The protein, supplied by D. Clément and the ILL Deuteration Laboratory, is a small enzyme called dihydrofolate reductase (DHFR), playing a role in the replication of DNA. Its molecular weight is about 20 kDa, with an 80 % deuteration level. The system was finally characterised after protein adsorption, using several contrast levels.

The data analysis was performed thanks to a program developed by A. Rennie (Uppsala University, Sweden) and R. Ghosh (ILL). Before protein adsorption, the system was modelled by

successive layers: the silicon oxide and the PS layers were modelled as boxes of constant thickness, roughness and scattering length density, while the PEG brush was modelled with a parabolic scattering length density profile. The effect of the protein has been fitted assuming that it did not perturb the structure of the brush. A layer, composed of proteins and PEG, was added above the PS layer for primary adsorption, while ternary adsorption was also modelled with a parabolic profile, superposed to that of the PEG.

Our results confirm the theoretical predictions that adsorption of a globular protein within a PEG brush occurs in the two stages: a layer on the grafting surface (primary adsorption), and proteins adsorbed within the brush (ternary adsorption). The results are in qualitative agreement with the theory.

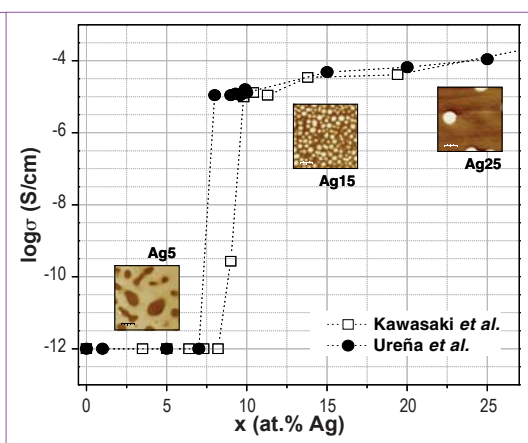
References

- [1] A. Halperin, G. Fragneto, A. Schollier and M. Sferrazza, *Langmuir* 23 (2007) 10603
- [2] W. T. E. Bosker, P. A. Iakovlev, W. Norde and M. A. Cohen Stuart, *J. Colloid Interface Sci.* 286 (2005) 496
- [3] W. Norde and D. Gage, *Langmuir* 20 (2004) 4162

Silver-conducting chalcogenide glasses: application in programmable metallization cells

AgGeSe glasses have aroused a strong interest in recent years because of their potential application as components of memory devices. Neutron diffraction experiments, combined with *ab initio* molecular dynamics simulation, were carried out in order to find differences in the network structural organisation associated with two different regions of the Ag-Ge-Se system, namely those before and after the percolation threshold of conductivity. It was observed that the silver environment depended very much on the silver content in the glasses. The dynamical process of re-crystallisation was also studied. This experiment revealed the appearance of a new phase, Ag_2GeSe_3 , at high temperature which partially decomposed with time or when the temperature increased into GeSe_2 and a new phase $\text{Ag}_{10}\text{Ge}_3\text{Se}_{11}$.

Figure 1: Variation of the conductivity at room temperature (in at. %) for $\text{Ag}_x(\text{Ge}_{0.25}\text{Se}_{0.75})_{100-x}$ glasses and EFM micrographs of the glasses with $x = 5, 15$ and 25 at. % Ag.



Recent developments in multimedia applications as well as the nature of the internet have led to massive and ever increasing storage needs. A new boost in the development of electrical memories has been given recently with the finding of new chalcogenide-based cells, which represent very strong competition for existing techniques. This application is possible thanks to the property known as photodiffusion present in Ge-Se(S) glasses and the ionic conductivity observed in Ag-Ge-Se(S) glasses. However, the working mechanism of the Programmable Metallisation Cells (PMC, as this approach is called) is still unclear.

A PMC memory typically comprises a silver-photodoped glassy thin film of composition $\sim \text{Ge}_{0.25}\text{Se}_{0.75}$ placed between two electrodes, a silver one and a nickel one, for example. The conductivity of the film is reversibly changed by several orders of magnitude when a weak voltage is applied ($\sim 0.3\text{V}$). When applied to nanometric devices (where the thickness of the glassy film is typically 20–30 nm), the phenomenon is characterised by a very short time for commutation

($\approx 10\text{ ns}$) and a very high cyclability ($>10^6$ cycles). The presence of silver-rich domains in the film was proposed to explain the phenomenon [1].

At a first stage, a series of experiments were carried out on bulk $\text{Ag}_x(\text{Ge}_{0.25}\text{Se}_{0.75})_{100-x}$ glasses with $1 < x < 30$ at.%. The combined investigation of electrical conductivity by complex impedance spectroscopy and microstructure by Field Emission Scanning Electron Microscopy and Electric Force Microscopy (EFM) helped in understanding the difference of 7–8 orders of magnitude in the conductivity of the system: the glasses were phase-separated and the percolation of the Ag-rich phase was at the origin of a sudden jump in conductivity [2, 3] (figure 1).

Combining neutron diffraction experiments (on the D4 diffractometer at ILL) with *ab initio* molecular dynamics simulation helped in studying the differences in the network structural organisation associated with the two different regions of the conductivity. For all glasses, we could show the presence of both Se-Se and Ge-Se correlations in the first peak of the Radial Distribution Function, a kind of probability of finding two particles at a given distance. These results are consistent with a structure containing both $\text{GeSe}_{4/2}$ tetrahedra and Se-Se bonds [6]. In contrast, the simulations showed very different Ag-Ag correlations for glassy compositions situated before or after the percolation threshold. While the glass with the lowest silver content ($x=5$) presented only one correlation peak at 4.4 Å, the Ag-rich glasses ($x=15$ and $x=25$) presented two peaks: a main peak at 3 Å and a less intense peak at 4.4 Å. This result can tentatively be related to the conductivity of the materials, namely a very low conductivity for the Ag_5 sample and a fast Ag^+ conductivity for the samples Ag_{15} and Ag_{25} .

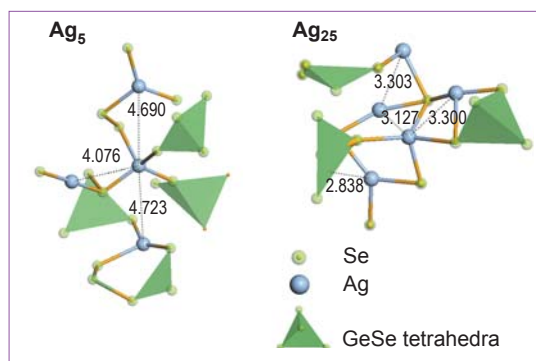


Figure 2: Representations of the glass structures for the $Ag_x(Ge_{0.25}Se_{0.75})_{100-x}$ system: $x=5$ (left) and $x=25$ (right). Several characteristic bond distances are also shown.

Figure 2 shows representations of the glass structures as determined from molecular dynamics simulation. These images can be used to visualize the most important bonds present in the $Ag_x(Ge_{0.25}Se_{0.75})_{100-x}$ glasses and obtain a better understanding of the changes induced when the silver atom is introduced in the $Ge_{25}Se_{75}$ matrix. For high silver concentrations ($x=25$), the Ag atoms can freely diffuse forming the conductivity pathways.

The functioning of a PMC device implies a dynamic process with an applied voltage on a miniaturised component and therefore some energy transfer to the glassy Ag–Ge–Se film. Therefore, a complementary investigation of the bulk glasses under dynamic conditions was thought pertinent to bring additional information to understand the phenomena underlying the functioning of PMC. At this point we chose the temperature as the parameter to study the glasses under dynamic conditions and, more precisely, the crystallisation process of the $Ag_x(Ge_{0.25}Se_{0.75})_{100-x}$ glasses by *in situ* neutron thermodiffraction investigation using the D1B diffractometer. Two stable crystalline phases formed during the heating process were clearly identified: first Ag_8GeSe_6 and then $GeSe_2$. Surprisingly, the experiment showed the existence of a new phase Ag_2GeSe_3 at high temperature. This phase partially decomposes with time or when the temperature increases, and gives $GeSe_2$ and a new $Ag_{10}Ge_3Se_{11}$ phase that has also been found at room temperature [7] (**figure 3**).

The PMC memory represents a radical departure from all existing memory technologies, including those currently in development. PMC memory utilizes solid-state electrochemistry to attain easily detectable non-volatile changes in a simple, highly scalable structure at hitherto unattainably low voltage and energy. The fundamental mechanism at the basis of the switching is unclear even though the presence of silver-rich domains was proposed to explain it. Our work indeed pointed out that electrical heterogeneities explain

a conductivity percolation threshold in related Ag-Ge-Se glasses with different Ag-Ag correlations in the materials before and after the threshold. The thermodiffraction experiment also showed clearly the strong metastability of these materials with appearance of unstable phases when (thermal) energy was brought to the glasses.

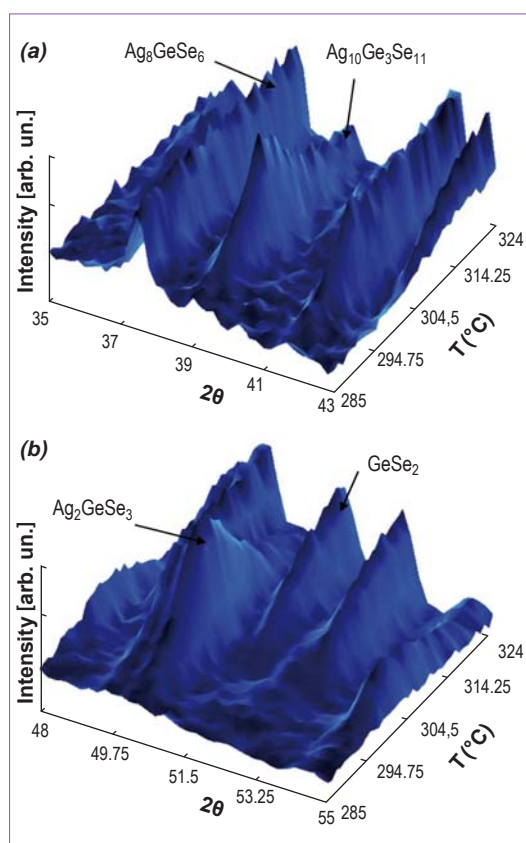


Figure 3: Neutron thermodiffraction for $Ag_{25}(Ge_{0.25}Se_{0.75})_{75}$ during a heating ramp from 285°C to 324°C. The graphs specifically show the peaks at: (a) $2\theta = 39^\circ$, which started decreasing above 320°C and finally remained constant for the remaining part of the heating process, and at: (b) $2\theta = 50.2^\circ$, that started decreasing in intensity at 300°C to disappear completely at about 315°C.

References

- [1] M. N. Kozicki, M. Mitkova, M. Park, M. Balakrishnan, C. Gopalan, *Superlatt. Microstruct.* 34 (2003) 459
- [2] V. Balan, A. A. Piarristeguy, M. Ramonda, A. Pradel, M. Ribes, *Journal Optoelectronics and Advanced Materials* Vol.8 ISS.6 (2006) 2112
- [3] A. A. Piarristeguy, M. Ramonda, M. A. Ureña, A. Pradel, M. Ribes, *Journal of Non-Crystalline Solids* 353 (2007) 1261
- [4] M. A. Ureña, A. A. Piarristeguy, M. Fontana, B. Arcondo, *Solid State Ionics* 176 (2005) 505
- [5] M. Kawasaki, J. Kawamura, Y. Nakamura, M. Aniya, *Solid State Ionics* 123 (1999) 259
- [6] G.J. Cuello, A.A. Piarristeguy, A. Fernández-Martínez, M. Fontana, A. Pradel, *Journal of Non-Crystalline Solids* 353 (2007) 729
- [7] A. A. Piarristeguy, G. J. Cuello, P. Yot, A. Pradel, M. Ribes, *Journal of Physics: Condensed Matter* 20 (2008) 155106

Authors

J. M. Cole and **S. J. Clarke** (University of Cambridge, UK)

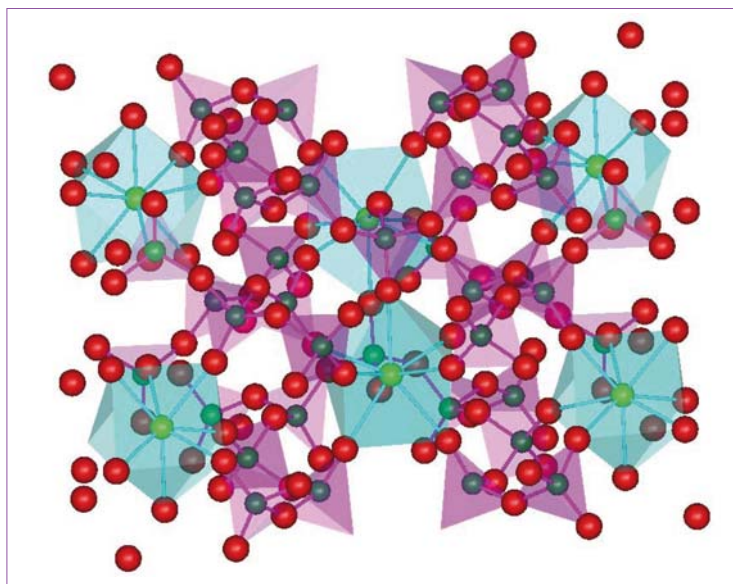
A. C. Wright and **R. N. Sinclair** (University of Reading, UK)

R. J. Newport (University of Kent, UK), **C. E. Fisher** and **R. A. Martin** (University of Bath, UK)

G. J. Cuello and **H. E. Fischer** (ILL)

Structure of rare-earth phosphate glass studied by anomalous dispersion neutron diffraction

Rare-earth (R) phosphate glasses $(R_2O_3)_x \cdot (P_2O_5)_{1-x}$ where $x=1/4$ or $1/6$ have shown great promise in the laser and optoelectronics industry. This is because the rare-earth ions possess the required energy levels for achieving successful population inversion and the non-linear refractive index is large enough to exhibit the desired optical effects without causing beam breakup and damage. Moreover, the particularly high concentration of rare-earth ions present in these materials results in a myriad of exotic physical properties at low temperatures: negative thermal expansion, negative pressure dependence of bulk moduli and unprecedented magnetic, magneto-optical and opto-acoustic phenomena [1].



The structural nature of these glasses dictates their physical properties, especially the closest R...R approach, since too close a separation impairs their optical and magnetic phenomena. Conventional X-ray [4-8] and neutron diffraction, X-ray absorption spectroscopy, and solid-state NMR studies have, in combination, been able to piece together a model of the local structure of these glasses, out to an interatomic distance, r , of about 4 Å (see **figure 1**). However, the R...R separation is not part of this defined local structure, and beyond this ~ 4 Å radial limit conventional characterisation techniques are uninformative owing to (i) increasing numbers of overlapping pair-wise correlations in conventional diffraction; (ii) the progressively damped signal, and obscu-

ring multiple scattering effects in X-ray absorption spectroscopy; (iii) the inherent short-range J-J coupling effects in NMR, and heavily broadened signal due to the paramagnetic nature of rare-earth ions.

One must therefore turn to non-conventional diffraction techniques to determine the nearest R...R separation. Samarium has a physical characteristic, unique to all rare earths, that makes it ideal for use in such a non-conventional diffraction experiment, which yields R...R correlations exclusively in one part, and R...X and X...X correlations (X is any element that is not R) in another part. This is the anomalous neutron dispersion effect associated with the ^{149}Sm isotope, which is 14% naturally abundant in samarium. It is this physical characteristic that we exploit here in performing an anomalous dispersion neutron diffraction experiment on vitreous $\text{Sm}_2\text{O}_3 \cdot 4\text{P}_2\text{O}_5$ [2].

The anomalous dispersion technique is employed successfully with X-rays at synchrotron radiation sources, which provide the required incident intensity and sufficiently dynamic energy spectrum that encompasses the required absorption edge as well as an energy void of all resonant effects. The equivalent neutron technique involves the variation in the neutron scattering length with wavelength around an absorption resonance, $b = b^0 + b'(\lambda) + i b''(\lambda)$, $b'(\lambda)$ and $b''(\lambda)$ being the wavelength-dependent real and imaginary parts of the scattering length, usually arising from a single isotope of the element in question; b^0 is the wavelength-independent contribution to the scattering length from all of the isotopes present. The relative change in the scattering length for neutrons is very much larger than that in the atomic form factor for x-rays. This, together with the greatly enhanced

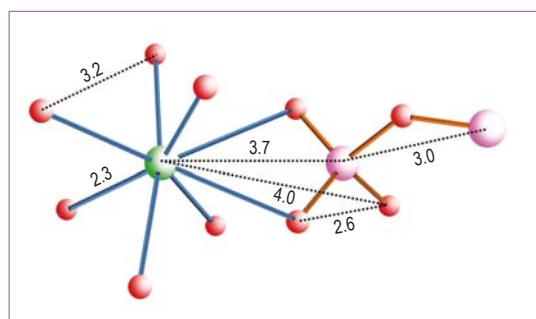


Figure 1: A model of rare-earth meta-phosphate glass. Green, red, and purple spheres represent the rare-earth, oxygen and phosphorus atoms, respectively. The dashed lines represent possible coordination levels since that of the rare-earth varies from 6 to 8 depending on the glass stoichiometry. The numbers represent interatomic distances in Å.

cross-section in the region of the absorption resonance, means that it is possible to perform measurements at the peak of the resonance.

The judicious choice of four wavelength measurements allows one to exploit both the real and imaginary components of b_{Sm} in an anomalous dispersion neutron diffraction experiment, such that one can obtain not only a spectrum comprising the Sm...Sm and Sm...X components, but also one comprising the Sm...Sm correlations exclusively. Due to the highly involved technical and analytical nature of this investigation, further technical details of this study are presented in [3].

Results show (**figure 2**) that vitreous $Sm_2O_3 \cdot 4P_2O_5$ comprises a mixed network of SmO_n polyhedra and PO_4 tetrahedra. The Sm^{3+} ions have an average co-ordination number of 7, which corroborates prior complementary X-ray diffraction, L-edge and K-edge EXAFS results. This confirms our previously held knowledge about the basic phosphate network and rare-earth environment; such corroboration is extremely useful for the verification of this study given its complexity. The mean Sm–O bond length is 2.375(5) Å. The ability to draw out Sm...X + Sm...Sm correlations exclusively via the first-order difference, $\Delta T'(r)$ affords excellent accuracy in the determination of these Sm–O correlation parameters; in conventional diffraction, Sm–O and O–(P)–O correlations overlap. The anomalous difference correlation function, $\Delta T''(r)$, suggests that most of the Sm^{3+} ions are separated from each other on average 4.8 Å apart. By calculations based on the R–O correlation, we have shown that the $\Delta T'(r)$ and $\Delta T''(r)$

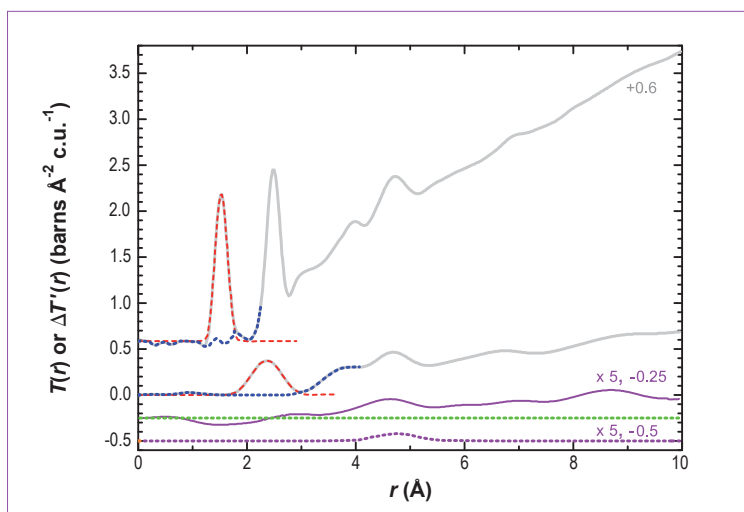


Figure 2: $T(r)$ for the 0.45 Å data, together with the fit to the first (P–O) peak (top curves shifted by +0.6); $\Delta T'(r)$ plus the fit to the Sm–O peak (middle curves); (gray curves: data; red curves: fit; blue curves: residuals). $\Delta T''(r)$ together with the simulated peak for Sm...Sm pairs based on a linear Sm–O–Sm arrangement (orange curves). The bottom mauve curves are calculated using a Q_{max} of 7 \AA^{-1} and are scaled by a factor of five and shifted by -0.25 and -0.5; the dotted green line is zero.

results, which yield the main R...R peak, are mutually consistent. There is evidence of a closer Sm...Sm separation nearer to 4 Å, and other Sm...Sm correlations at around 5.9 and 6.9 Å. A peak with a very wide distribution (of nearly 2 Å) is centred at 8.8 Å. The fact that there is clear evidence for Sm...Sm correlations below those anticipated for a random distribution of Sm^{3+} ions means that local clusters of Sm^{3+} ions must be present in the structure. This information will help in producing more comprehensive structural models so that one can relate better to the optical and magnetic properties of these materials.

References

- [1] J. M. Cole *et al.*, *J. Phys.: Condens. Matter* 11 (1999) 9165; *ibid.* 13 (2001) 6659
- [2] J. M. Cole *et al.*, *J. Phys.: Condens. Matter* 19 (2007) 056002
- [3] A. C. Wright *et al.*, *Nucl. Instr. Meth. A* 571 (2007) 622

Authors

M. C. Rheinstädter, J. Das, E. J. Flenner and I. Kosztin (University of Missouri-Columbia, USA)

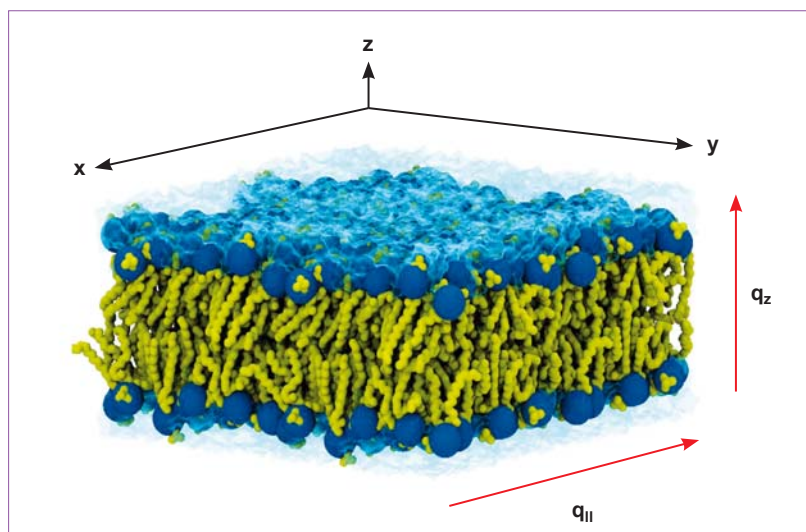
T. Seydel (ILL)

B. Brüning (Institut für Röntgenphysik, Göttingen, Germany)

Motional coherence in fluid phospholipid membranes

Atomic and molecular motions in regions of biomolecular systems with strong local interactions are highly correlated on a certain range of time and length scales. In proteins, intra-protein correlations are believed to be essential for their biological functioning, such as protein folding, domain motion and conformational changes. Very recently, intra [1] and inter-protein correlations in protein crystals and also membranes have been reported from experiment and simulation [2, 3]. By employing high energy-resolution neutron backscattering, combined with *in situ* diffraction, we have investigated slow molecular motions on nanosecond time scales in the fluid phase of phospholipid model membranes of 1,2-dimyristoyl-sn-glycero-3-phosphatidylcholine (DMPC) [4]. We found that correlated dynamics in lipid membranes occurs over several lipid distances, spanning a time interval from pico- to nanoseconds.

Figure 1: Molecular dynamics simulation of a phospholipid model membrane (DMPC). The system contained 128 lipid molecules, hydrated by 2577 water molecules to guarantee full hydration of the bilayer. An all-atom Molecular Dynamics simulation was then run for 0.1 microseconds.



We studied dynamical modes at nearest neighbour distances of the lipid molecules in the fluid phase of the bilayers (**figure 1**). Selective deuteration of the lipids (hydrogenated DMPC-h and chain deuterated DMPC-d54) was used to discriminate relaxations due to collective molecular motions from relaxations arising from localized, single molecule excitations. The experiments were carried out at the cold neutron backscattering spectrometer IN16, accessing time scales of $0.28 \text{ ns} < t < 4.6 \text{ ns}$ and length scales of $3.2 \text{ \AA} < d < 14.6 \text{ \AA}$. A separate line of diffraction detectors was used to determine the bilayer structure *in situ*. Neutrons are scattered by the atomic nuclei, and each element intrinsically has non zero coherent and incoherent scattering cross sections. In experiments the different contributions can be enhanced with respect to each other, by, e.g., using different isotopes or selective deuteration. While in protonated samples the incoherent scattering is dominant and the time-autocorrelation

function of individual scatterers is accessed, partial deuteration emphasizes the coherent scattering and probes the pair correlation function. Four different samples (referred to as S1, S2, S3, and S4) were prepared: DMPC-d54 hydrated by D_2O (S1), DMPC-d54 hydrated by H_2O (S2), DMPC-h hydrated by D_2O (S3), and DMPC-h hydrated by H_2O (S4). By careful analysis of the scattering of all samples S1 to S4, it was possible to distinguish between the collective and self motions in the underlying dynamics.

Figure 2(a) depicts in-plane diffraction patterns. Subtracting the static structure factor $S(q_{||})$ for samples S3 and S1 emphasizes the coherent scattering of the lipid acyl chains. There are two peaks in $S(q_{||})$ of the lipid chains around $q_{||} = 0.7 \text{ \AA}^{-1}$ and 1.4 \AA^{-1} , which correspond to the nearest neighbour distances of phospholipid head groups and the acyl chains in DMPC, respectively.

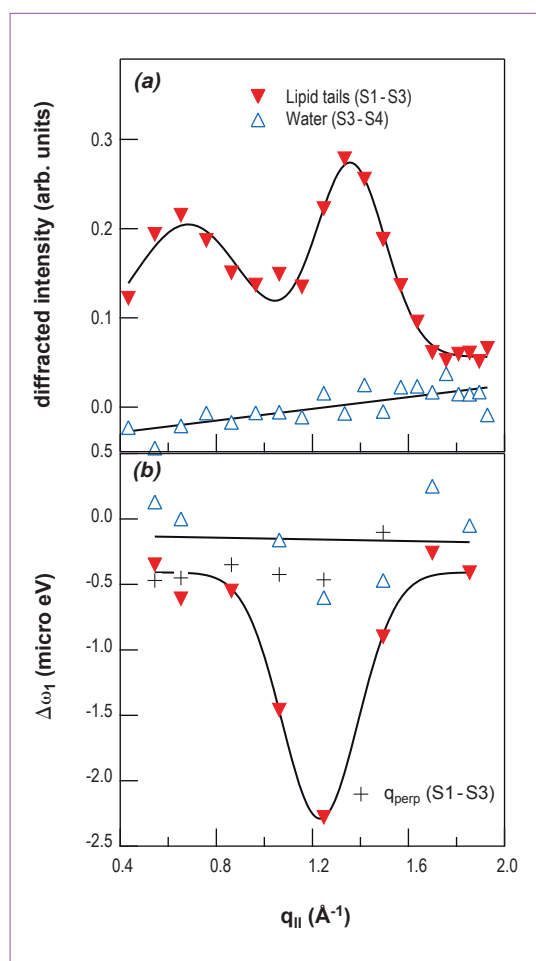
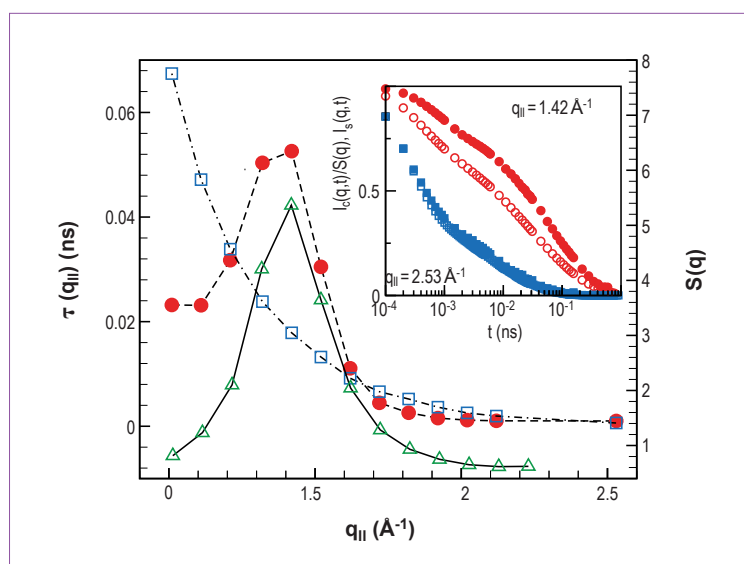


Figure 2: (a) Diffraction patterns generated by subtraction of $S(q_{||})$ for pairs of samples S1, ..., S4, which emphasize contributions from collective molecular motions of the lipid acyl chains (\blacktriangledown), and the water molecules (\triangle). (b) $\Delta\omega_1$ for the lipid acyl chains (\blacktriangledown) and the membrane hydration water (\triangle). For the water, the difference of $\Delta\omega_1$ of samples S1 and S2 was taken. Peaks and minimum were fitted using Gaussian line shapes to determine position and width.

Figure 2(b) shows the difference in the quasi-elastic width $\omega_1(q_{||})$. As with the diffraction data discussed above, subtracting the widths of spectra S1-S3 emphasizes the coherent lipid tail dynamics. $\Delta\omega_1(q_{||})$ shows a pronounced minimum around $q_{||} = 1.22 \text{ \AA}^{-1}$ and qualitatively reproduces the behavior of $S(q_{||})$ in **figure 2(a)**. This points to a strong coupling of dynamical properties to the static structure of the system and to a softening of the coherent relaxation rate around the maximum of the static structure factor $S(q_{||})$. The slowing down of the decay of the density autocorrelation function for distances corresponding to nearest neighbours is well known as ‘de Gennes narrowing’.



The in-plane incoherent (self) $I_s(q_{||}, t)$ and the coherent $I_c(q_{||}, t)$ intermediate scattering functions were calculated from a 0.1 microsecond all atom molecular dynamics simulation. We used a pre-equilibrated DMPC bilayer containing 128 lipid and 2577 water molecules. Shown in **figure 3** are the corresponding $\tau_s(q_{||})$ and $\tau_c(q_{||})$, as determined from fits to the scattering functions. Also shown is the calculated $S(q_{||})$. The non-monotonic behaviour of $\tau_c(q_{||})$ yields a minimum in the difference $\tau_s - \tau_c$ around the peak of $S(q_{||})$. Thus, the simulation results are in qualitative agreement with those from the experiment and reinforce the conclusion that the difference of the quasi elastic widths $\Delta\omega_1(q_{||})$ is due to correlated dynamics of the lipid acyl chains. Further investigation shows that the displacements of the lipid acyl tails are correlated for times from around 1 picosecond to 10 nanoseconds, i.e., for much longer than the microscopic collision time but shorter than the time needed for a molecule to diffuse one lipid diameter. The correlation does not decay to zero until around 30 \AA , for at least four lipid diameters. A possible implication of this motional coherence of the lipid acyl chains is, e.g., that information about a local structural perturbation of the lipids can propagate in the bilayer. This might be relevant for understanding processes and functions involving collective structural changes.

Figure 3: Relaxation times τ_c (\bullet) and τ_s (\square) as obtained from MD simulation as a function of wave-vector $q_{||}$. Also shown is the static structure factor $S(q_{||})$ (\triangle). Inset: $I_s(q, t)$ (open symbols \square \circ) and $I_c(q, t)$ (filled symbols \blacksquare \bullet) for two different $q_{||}$ values.

References

- [1] Dazhi Liu *et al.*, Phys. Rev. Lett. 101 (2008) 135501
- [2] V. Kurkal-Siebert, R. Agarwal and J. C. Smith, Phys. Rev. Lett. 100 (2008) 138102
- [3] M. C. Rheinstädter, K. Schmalzl, K. Wood and D. Strauch, <http://arxiv.org/abs/0803.0959>
- [4] M. C. Rheinstädter, J. Das, E. J. Flenner, B. Brüning, T. Seydel and I. Kosztin, Phys. Rev. Lett. 101, 248106 (2008)

Authors

A. Orecchini, A. Paciaroni, C. Petrillo and F. Sacchetti (Univ. Perugia and INFN-CNR CRS Soft, Roma, Italy)
A. De Francesco (INFN-CNR, CRS Soft at ILL)

Collective dynamics of protein hydration water

Water is a fascinating liquid, both because of its peculiar physical properties and because it is the liquid of life. In particular the microscopic dynamics of protein hydration water can determine the biological functionality of living biomolecules. In close interaction with the protein surface, hydration water also provides an original system for studying the dynamics of liquids in 2D-confinement. The new spectrometer BRISP enabled us to detect the propagation of high-frequency density fluctuations within the hydration shell of the RNase protein. The behaviour of such collective modes recalls those of vitreous systems and is interpreted as the dynamic signature of a glass-like character of hydration water.

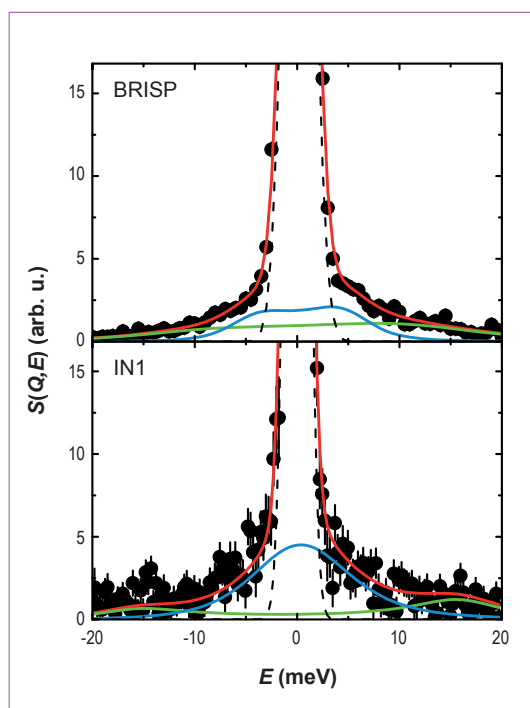
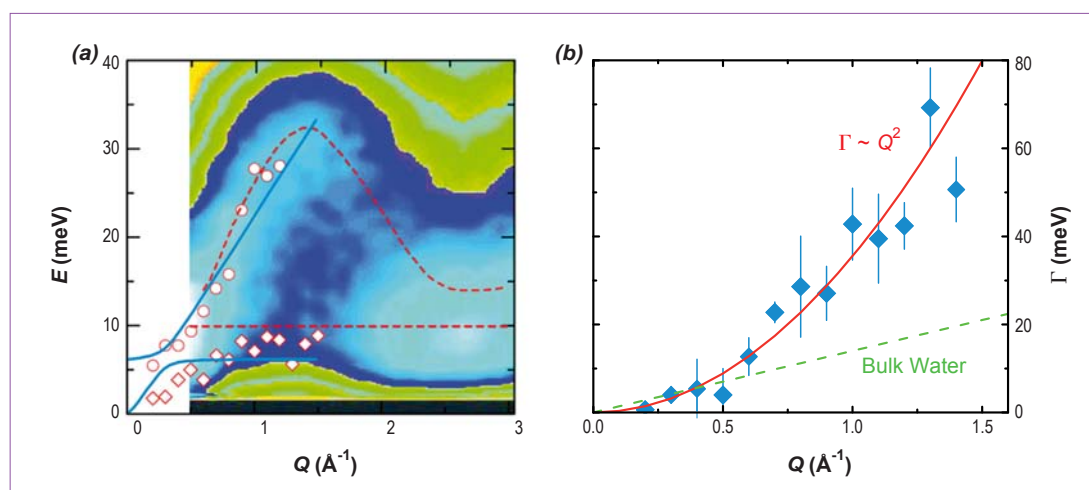


Figure 1: Dynamic structure factor of RNase hydration water, measured at $Q = 0.8 \text{ \AA}^{-1}$ on BRISP and IN1. The best-fitting function (red line), composed of two damped harmonic oscillator components (green and blue lines), is compared with the experimental data and the instrumental resolution function (dashed line).

The microscopic dynamics of protein hydration water has, for many years, been the subject of continuous and wide-ranging investigations by a broad range of experimental and numerical techniques. Huge amounts of information about diffusive and relaxational dynamics exist to date but few studies about *propagating collective excitations* have been made. Recently, coherent density fluctuations in the hydration shell of the RNase protein were investigated by molecular dynamics simulations [1], which predicted that such collective excitations exist, propagate with thermal energies (THz frequencies) and exhibit two modes, similar to previous observations in pure water [2]. Nonetheless, the collective dynamics of the sole hydration water remained until now experimentally unexplored, mainly due to severe instrumental limitations and intrinsic experimental difficulties connected with the problem of isolating the signal of hydration water alone.

The recently-built CRG spectrometer BRISP, conceived for optimised access to the region of thermal energies and low-wavevector transfers, is particularly well suited to investigate collective THz dynamics of hydration water. Aiming at the coherent signal of the sole hydration water, we measured at 300 K a dry reference sample of RNase protein powder, and a wet one hydrated with D_2O . The optimised design of BRISP enabled data of unprecedented statistical quality to be collected, significantly better than those collected on the triple axis spectrometer IN1 under similar conditions (**figure 1**). While triple axis spectrometers remain unequalled for detailed studies of a specific dynamic region, they would appear to be less suited than a dedicated



instrument for wider surveys on amorphous and isotropic systems. The good performance of the BRISP spectrometer and a rigorous data reduction procedure [3] enabled us to extract the coherent inelastic signal of the hydration shell alone.

To interpret the data, we used the double-mode model commonly used for bulk water and later proposed, on the basis of simulation results, for hydration water as well. With this picture in mind, the inelastic spectrum of the RNase hydration shell was fitted with the combination of two damped harmonic oscillators convoluted with the instrumental energy resolution, as shown in **figure 1**. Trials with a simplified model function containing a single inelastic mode resulted in an overall worsening of the fit quality. As a final result, we could ascertain the existence of two coherent collective modes in the RNase hydration shell and determine their dispersion curves. The high-frequency mode disperses and propagates with a speed of about 3300 m/s, whereas the low-frequency mode is characterised by a constant energy of about 6-7 meV.

As demonstrated in **figure 2a**, the consistency with simulation results is remarkable, while the agreement with the behaviour of pure water is even more impressive. Contrary to what is observed for diffusive and relaxational movements, which are significantly slowed down, the characteristic energies and speed of collective modes in water seem unaffected by the interaction with the protein surface. This suggests that the biological processes, possibly driven by collective modes are governed by the protein environment, i.e. the hydration shell, rather than by the protein itself.

An interesting novel element is provided by the wave-vector dependence of the damping factors of the observed collective modes. In **figure 2b**, we show how the hydration water damping factors increase rapidly with a peculiar Q^2 -dependence, whereas the growth is only linear in pure water. Interestingly enough, such a quadratic increase, which is uncommon for complex liquids at THz frequencies, is systematically observed in amorphous solids. The strong increase with Q of the damping factor, reflecting a shorter lifetime of the relevant collective excitations, can be ascribed to the disordering effect that the interaction with the protein surface induces on the otherwise locally-ordered hydrogen-bonded structure of water.

Such novel experimental findings suggest that despite the propagation speed and energies being unaffected by the presence of the protein, the dynamical coupling between protein and water confers on the latter a peculiar and intriguing glass-like character.

References

- [1] M. Tarek and D. Tobias, *Phys. Rev. Lett.* 89 (2002) 275501
- [2] F. Sacchetti, J. B. Suck, C. Petrillo and B. Dörner, *Phys. Rev. E* 69 (2004) 061203
- [3] A. Orecchini, A. Paciaroni, A. De Francesco, L. Sani, M. Marconi, A. Laloni, E. Guarini, F. Formisano, C. Petrillo and F. Sacchetti, *Meas. Sci. Technol.* 19 034026 (2008); A. Orecchini, A. Paciaroni, A. De Francesco, C. Petrillo and F. Sacchetti, *JACS* in press (2009).

Figure 2:
(a) The experimental dispersion curves of RNase hydration water (empty circles and diamonds) are compared with the results obtained by molecular dynamics simulations (red dashed lines) and with the behaviour observed in bulk liquid water (blue lines).

(b) Damping factors of RNase hydration water (blue diamonds). The rapid Q^2 increase is compared with the linear behaviour observed in bulk water.

■ Authors

R. Biehl, M. Monkenbusch and **D. Richter** (IFF Jülich, Germany)

B. Hoffmann and **R. Merkel** (IBN, Jülich, Germany)

P. Falus (ILL)

S. Prévost (HMI, Berlin, Germany)

NSE reveals protein domain motions in space and time

Proteins are part of the molecular machinery of life. They are tirelessly active, transporting, synthesizing, dividing and transforming substances in every living cell. Many transformation processes take place in characteristic shaped pockets, into which only certain substances can fit, as a key fits in a lock. The shape of these pockets can change according to the sequence and three-dimensional arrangement of amino acids. Neutron scattering can be used to investigate the timescale of these large-scale movements in biomolecules. It provides information on the location and movement of atoms, without destroying the sample.

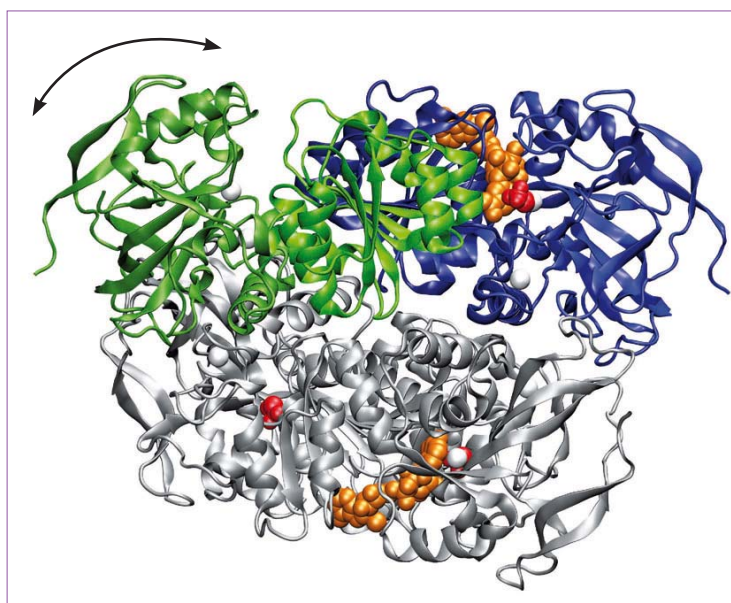


Figure 1: Tetrameric Alcohol Dehydrogenase of yeast is built up from two dimers (green-blue and gray). The blue monomer is in the closed conformation with a NAD cofactor (orange) and an ethanol molecule (red) in the cleft between the binding domain and the active domain. In the cleft between both domains of the open configuration (green monomer) the catalytic Zinc atom at the catalytic centre is visible. The second dimer (gray) is bound at the back of the first dimer. The arrow indicates schematically the movement of the active domain.

To bind a cofactor to the active center of a protein sometimes requires structural change of the host. This “induced fit” may involve small changes of single bonds but also the reorganization of large domains to create the active structural configuration. Here we have used neutron spin echo spectroscopy to observe the domain dynamics of the protein alcohol dehydrogenase [1]. The collective motion of domains as revealed by their coherent form factor relates to the cleft-opening dynamics between the binding and the catalytic domains enabling binding and release of the cofactor to the active center.

This effect has mostly been revealed through structural studies of crystallized proteins, which represent snapshots of different configurations. Internal movements may also be observed by fluorescent labelling of two points on a protein with molecular biological methods to track distance changes [2]. Further information can be also obtained by computer simulations.

One of the most studied proteins and one of the key enzymes is Alcohol Dehydrogenase (ADH, **figure 1**). It produces ethanol in yeast or converts it back to acetaldehyde in the human liver. A functionally important molecule (cofactor) Nicotinamide Adenine Dinucleotide (NAD) and a substrate molecule (ethanol or acetaldehyde) bind to the binding domain in a cleft between active and binding domains.

The active domain, with a catalytic Zinc atom in its centre, opens and closes the cleft by thermal movements. The closing action places the active centre in the right position for the transfer of a hydrogen atom between the substrate and cofactor molecule and another hydrogen atom is released. When it opens, the cofactor and the product of the reaction are released. The measurements were done in dilute D₂O buffer solutions, close to the natural environment of the protein.

Scattering at the atomic nuclei of the protein produces a characteristic interference pattern. Movements of the atoms during the scattering process change the speed of the neutrons in the scattered beam. The change in speed for the scattered neutrons is very small. In order to detect it, neutron spin echo spectroscopy uses the Larmor precession of the neutron spins in a magnetic field as a stopwatch.

The result is a length-scale dependent flexibility, which differs from the expected motion of a rigid protein, only showing translation and rotation movements of diffusion. These length scale variations reflect the pattern of the movements due to the underlying dynamics.

NSE spectroscopy always measures the collective movement of all protein atoms (see **figure 2**), so in the evaluation, the contribution of diffusion to the observed scattering has to be separated from the internal dynamics.

We found in our studies at the IN15 spectrometer that the patterns of the movements observed are mainly due to the movement of the active domain relative to the binding domain at a time-scale of 30 ns.

Figure 1 illustrates schematically the movement of the active domain, leading to the opening of the gap. If the cofactor binds, it stiffens the protein and the domain movement is significantly reduced. In ADH, we find an average amplitude of about 0.8 nm for the extent of the spatial movements between the two domains. We also determined a spring constant of about 5 pN/nm for the stiffness of the cleft opening.

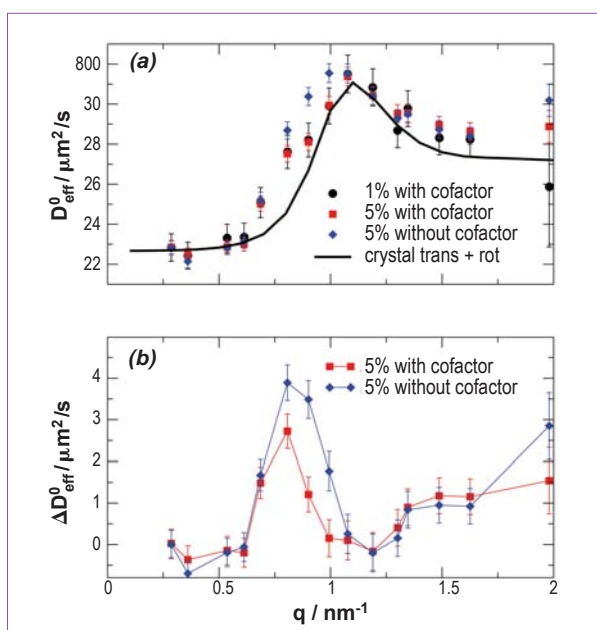


Figure 2:

(a) Single tetramer diffusion coefficient D_{eff}^0 after corrections, measured at IN15 with and without the bound cofactor.

The black solid line represents the calculated effective diffusion coefficients or the ADH crystal structure, including translational and rotational diffusion of the stiff protein.

(b) Difference of the corrected diffusion coefficients and the calculated translational/rotational diffusion coefficient, reflecting the internal dynamics.

References

- [1] R. Biehl, B. Hoffmann, M. Monkenbusch, P. Falus, S. Prévost, R. Merkel and D. Richter
Phys. Rev. Lett. 101 (2008) 138102
- [2] D. W. Pistona, G.-J. Kremers, Trends in Biochemical Sciences, 32 (2007) 407

Authors

A. Paciaroni, A. Orecchini, E. Cornicchi, M. Marconi, C. Petrillo and F. Sacchetti (Università di Perugia and CNR-INFM CRS SOFT, Roma, Italy)

M. Haertlein, M. Moulin and H. Schober (ILL)

M. Tarek (UMR, Nancy-University, CNRS, France)

Similar vibrational behaviour of protein hydration water and amorphous ice in the meV domain

Proteins perform a plethora of essential functions in living systems.

The early view of proteins as relatively rigid structures has been gradually replaced by dynamic models where internal motions are key players in building up specific protein functions. It is a crucial step to completely understand how these motions result from the interplay between the biomolecule and its solvent.

Here we shed some light on the vibrational behaviour of the hydration water surrounding the proteins and we show that it is quite similar to that of amorphous ice [1].

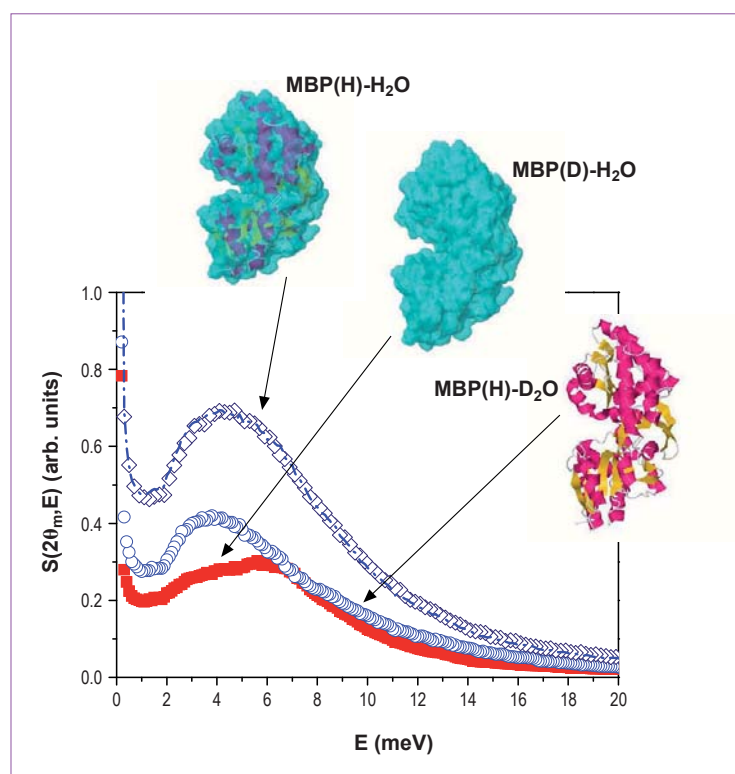


Figure 1: Normalised spectra of MBP(D)-H₂O (red closed squares), MBP(H)-D₂O (open circles), MBP(H)-H₂O (open lozenge) hydrated powders (hydration degree 0.4 grams of water/grams of protein). All curves are the average of the measured spectra for $2\theta=65^\circ$. For comparison, the sum of MBP(D)-H₂O and MBP(H)-D₂O is plotted as the dash-dot line.

Protein motions are not simply the inherent property of molecules held together by relatively weak interactions, but rather evolve along paths that enhance the protein biological effectiveness. This is why it is necessary to have an exhaustive picture of the complex dynamical scenario that can be observed in biomolecules. Whether their nature is vibrational or diffusive, protein motions intimately depend on the presence of the solvent surrounding the protein surface. Structural and dynamical features of protein hydration water (water within a few Å from the protein surface) are significantly altered with respect to the bulk, as they are affected by the local topography and specific interactions with the protein.

On these grounds it is important to understand if the heterogeneous structural character of water at the interface with the protein is related to peculiar vibrational features in the THz window where collective phonon-like modes are found. We used inelastic neutron scattering to study such features, which may be crucial to biological activity [2].

The investigated system is the maltose binding protein (MBP), a biomolecule which is widely considered as a prototype for biosensing platforms [3]. The ILL-EMBL Deuteration Laboratory in Grenoble has developed a high-yield expression protocol to make available significant amounts of hydrogenated and fully deuterated MBP powder.

Due to the high incoherent cross section of the hydrogen atom, the neutron scattering spectra from the fully deuterated protein hydrated with H₂O, hydrogenated protein

hydrated with D_2O and hydrogenated protein hydrated with H_2O , will give information on respectively hydration water, hydrated protein and both protein and water. The availability of fully deuterated samples, together with the high flux at the IN5 spectrometer, enabled us to investigate the hydration water vibrational dynamics with unprecedented accuracy.

In **figure 1** we show the spectra measured at 100K. The signal of the hydrogenated protein plus D_2O shows a clearly visible bump at ~ 3.5 meV, which originates from the dynamical features of non-exchangeable protein hydrogen atoms. This bump, also called a boson peak, is also observed in glasses. A rather different shape is exhibited by the spectrum of deuterated MBP hydrated with H_2O , where the main contribution comes from the solvent. We note a distinctive mode at ~ 6 meV and a shoulder between 2 and 5 meV, *i.e.* in the region of the protein boson peak. The bump appearing at ~ 6 meV is reminiscent of the collective transverse acoustic mode TA1 of the hydrogen bond network in ice [4].

To discuss non-diffusive dynamics of hydration water molecules, we calculated their vibrational density of states, *i.e.* the number of modes per energy unit. In **figure 2a** we show that the low-energy translational range of the hydration water density of states is clearly different from that of simple crystalline ice phases, *i.e.* hexagonal and cubic ice. On the other hand, the density of states of the protein hydration water lies just between those of low- and high-density amorphous ice (see **figure 2b**). It is well known that in the glassy state, water shows polyamorphism, *i.e.* the presence of more than one amorphous state [5]. The fact that the density of states of hydration water is very well reproduced by a linear combination with approximately equal weights of low- and high-density amorphous ice strongly supports its glassy character and, at the same time, suggests that protein hydration water is able to sample many amorphous states.

Interestingly enough, the average mass density of a mixture of high-density and low-density amorphous ice with the same weights would be $\sim 5\%$ larger than bulk water density, which is in nice agreement with the estimates from molecular dynamics simulations [6]. The similarity between low-temperature protein hydration water and amorphous ice can be related as

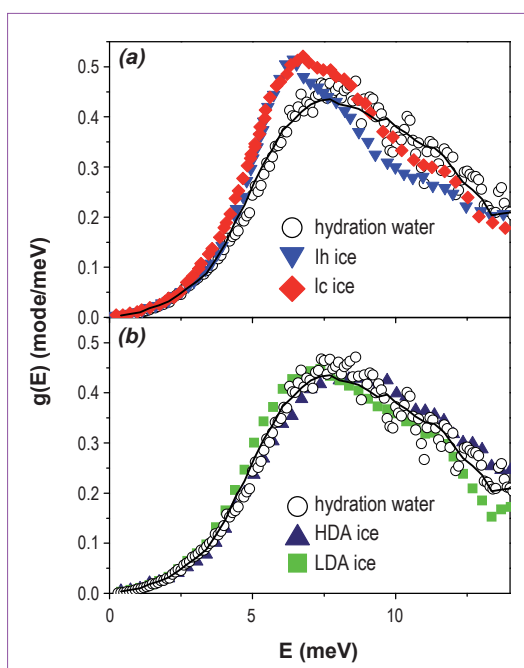


Figure 2:
(a) Density of states of the protein hydration water at 100 K, hexagonal (lh) ice at 37 K, cubic (lc) ice at 160 K.
(b) Density of states of the protein hydration water at 100 K, high-density amorphous (HDA) ice at 75 K, and low-density amorphous (LDA) ice at 75 K. The line is the weighted sum of low- and high-density amorphous ice contributions.

well to some physical aspects of cryopreservation. It may be supposed that biological specimens are not damaged when they are embedded in amorphous ice environments, because these environments just resemble the structure of naturally-formed protein hydration water.

References

- [1] A. Paciaroni *et al.*, Phys. Rev. Lett. 101 (2008) 148104
- [2] P. W. Fenimore *et al.*, Proc. Natl. Acad. Sci. U.S.A. 101 (2004) 14408
- [3] I. L. Medintz and J. R. Deschamps, Curr. Opin. Biotech. 17 (2006) 17
- [4] M. Tarek and D.J. Tobias, Phys. Rev. Lett. 89 (2002) 275501
- [5] C.A. Angell, Science 319 (2008) 582
- [6] F. Merzel, and J. C. Smith, Proc. Natl. Acad. Sci. U.S.A. 99 (2002) 5378

Authors

J. Pieper (TU Berlin, Germany), A. Buchsteiner (Helmholtz - Zentrum Berlin, Germany)

J. Ollivier (ILL)

N. A. Dencher and R. E. Lechner (TU Darmstadt, Germany)

T. Hauß (HMI, Berlin and TU Darmstadt, Germany)

Light-induced modulation of protein dynamics monitored in real time

Protein functionality is often dependent on the internal flexibility of the macromolecule represented by random structural fluctuations of small protein subgroups on the picosecond time scale. Consequently, knowledge about the dynamical properties of proteins is essential for understanding the structure-dynamics-function relationship at the atomic level. Here we describe a novel type of (laser-neutron) pump-probe experiment, which combines *in situ* optical activation of the biological function of the light-driven proton pump bacteriorhodopsin, with a time-resolved observation of internal protein dynamics using quasielastic neutron scattering on the time-of-flight spectrometer IN5.

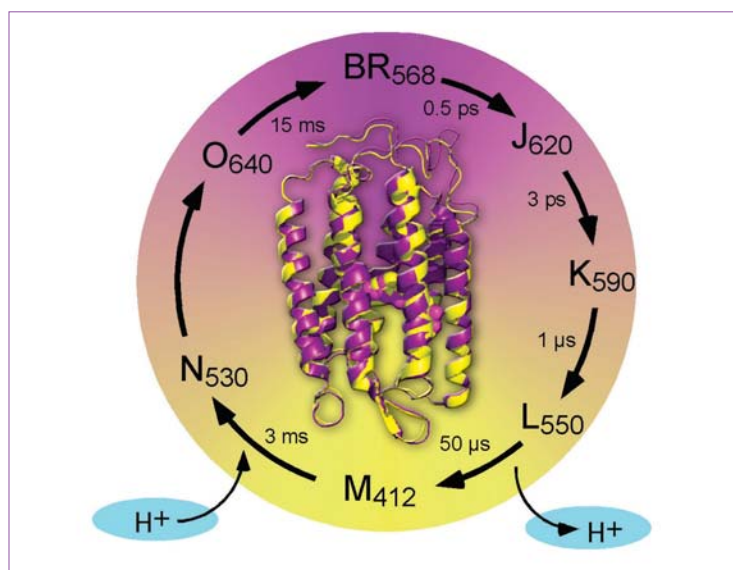


Figure 1: Photocycle and structural changes induced by laser excitation:
- the light-induced BR photocycle with its intermediates characterized by their absorption maxima and decay times,
- the structures of a BR monomer in the ground state BR₅₆₈ (purple) and in the M-intermediate (yellow), respectively, according to Sass et al.[2].

The correlation between internal protein dynamics and functionality has previously only been studied indirectly in steady-state experiments by varying external parameters like temperature and hydration. A potential model system for biological mechanics is the light-driven proton pump bacteriorhodopsin (BR) embedded in the purple membrane (PM) of *Halobacterium salinarum*. BR binds the photoactive chromophore retinal and functions as a light-driven proton pump, which enables the bacterium to create a proton gradient over the cell membrane. This process is an important step in the photosynthetic transformation of light energy into storable chemical energy.

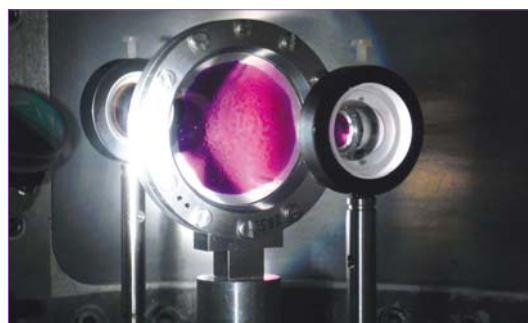


Figure 2: The purple membrane sample in the sample cell inside the IN5 sample chamber.

In the experiment described here, the biological function of BR was initiated by a laser flash and, subsequently, the related protein dynamics was observed in real time using quasielastic neutron scattering on the time-of-flight spectrometer IN5. The purpose of the experiment was to isolate the protein dynamics of intermediate states of BR in corresponding time intervals during the temporal evolution of the photocycle at room temperature.

In more detail, absorption of a light quantum in BR initiates the so-called photocycle, which is a sequence of intermediate protein-chromophore conformations [1]. The photocycle intermediates are characterized by specific absorption maxima and decay times ranging from 500 fs to about 15 ms in aqueous solution (figure 1). A large-scale structural alteration (figure 1) has been observed in the M-intermediate (M412) of BR by protein crystallography [2], which is a prerequisite for the vectorial character of the proton transport. The characteristic temperature and hydration dependence of the decay time of M412 and of the proton transport itself indicates a crucial role of internal protein dynamics for the large-scale structural changes within M and, thus, for BR functionality.

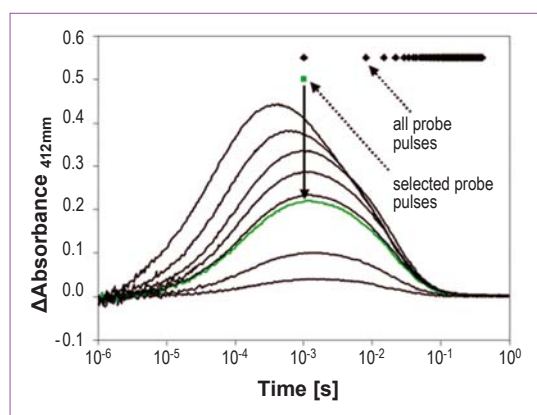


Figure 3: Definition of laser excitation conditions and temporal synchronization of the QENS experiment on IN5 by measurement of absorbance changes of BR at 412 nm at room temperature. Absorbance changes were induced by laser excitation at 532 nm and $t = 0$ with pulse energies varying from 1.4 to 70 mJ/cm² (from bottom to top curve). The green curve represents the optimum conditions of the QENS experiment with a laser pulse energy of 8 mJ/cm² and a laser pulse repetition time of 400 ms. Black diamonds indicate the arrival times of the neutron pulses at the sample relative to the laser pulse at $t = 0$, while the green square symbolizes the neutron probe pulse within the M-intermediate.

Two pulsed high-intensity Nd-YAG lasers with a combined pulse intensity of ~500 mJ/pulse in 5 ns were used to excite the BR-molecules in the PM sample. The neutron probe pulses were synchronized with the light excitation pulses and sent to the sample with well-chosen delays to study the PM dynamics in selected time intervals of the photocycle. In **figure 2** the PM sample is shown in its sapphire cell together with a part of the optical setup used to homogeneously illuminate the 50 mm diameter sample container inside the IN5 sample chamber. The laser light is guided into the sample chamber by a special system of laser mirrors. Careful optical characterization of the sample prior to the experiment revealed the optimal excitation conditions which ensured a 20% conversion for each laser pulse and prevented photodestruction (**figure 3**).

An essential contribution to this experiment was a special "ToF-Movie" mode for the data acquisition system NOMAD developed by the Instrument Control Service (SCI), which was necessary for the synchronisation of the laser and the data acquisition system with the IN5 chopper pickup reference. As a result, QENS spectra of each neutron probe pulse could be recorded independently and accumulated for each laser period. Therefore, this experiment

was only possible due to the high commitment of all the people of the SCI involved in the development of the ToF-Movie Mode.

Taking advantage of the high flux of IN5, several time delays between laser excitation and neutron probe pulses were studied in the μ s to ms range, which revealed a light induced protein softening within the M-intermediate of BR [3] and its complete time evolution. Typical QENS spectra are shown in **figure 4**. The decay of the protein softening appears to be strictly correlated with the large-scale structural change in the M-intermediate of BR [4]. This observation is direct proof of the significance of protein structural flexibility. We thus anticipate that functionally-important modulations of protein dynamics are of relevance for most other proteins exhibiting conformational transitions.

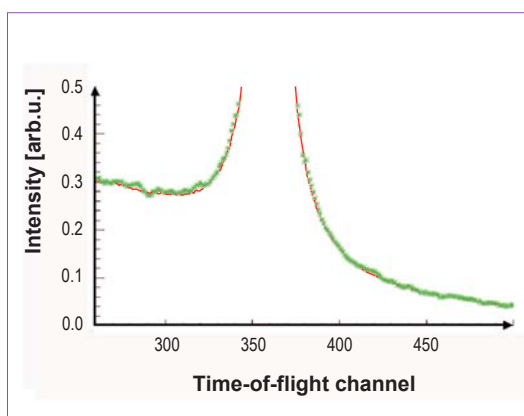


Figure 4: Laser-induced IN5-QENS spectra measured selectively within the M-intermediate (green) and averaged over all neutron probe pulses within the photocycle (red line). The data show a small, but statistically significant difference within the quasielastic range.

References

- [1] J. K. Lanyi, J. Phys. Chem. B 104 (2000) 11441
- [2] H. J. Sass, G. Büldt, R. Gessenich, D. Hehn, D. Neff, R. Schlesinger, J. Berendzen and P. Ormos Nature 406 (2000) 649
- [3] J. Pieper, A. Buchsteiner, N. A. Dencher, R. E. Lechner and T. Hauß, Phys.Rev.Lett. 100 (2008) 228103
- [4] J. Pieper, A. Buchsteiner, J. Ollivier, N. A. Dencher, R. E. Lechner and T. Hauß, in preparation

Authors

V. V. Nesvizhevsky (ILL)

E. V. Lychagin, A. Y. Muzychka and A. V. Strelkov (JINR, Dubna, Russia)

G. Pignol and K. V. Protasov (LPSC, Grenoble, France)

The reflection of very cold neutrons from diamond nanoparticle powder

We predicted and observed extremely intense scattering of very cold neutrons from thin samples of diamond nanoparticle powder. We show that this intense scattering would allow us to use nanoparticle powders very efficiently as the first reflector for neutrons with velocities within a complete range of very cold neutrons up to a few hundred m/s, thus bridging the energy gap between efficient reactor reflectors for thermal and cold neutrons and the Fermi potential for ultracold neutrons.

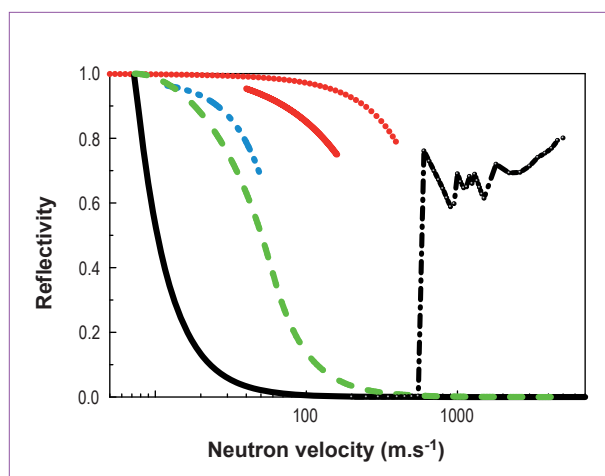


Figure 1: The neutron reflectivity as a function of neutron velocity for various reflectors; for isotropic angular distribution. Left full black line: Fermi potential of diamond; right dashed black line: graphite reflector for thermal neutrons; green line: supermirror reflectors; blue line: early data on VCN reflection from nano-structured materials; full red line: VCN reflection from diamond nanoparticles; dotted red line: estimated upper limit of an optimized diamond nanoparticle reflector.

It is well known that ultracold neutrons (UCN) are ~100% reflected by the Fermi potential of most materials (thin black line on the left of **figure 1** for the best diamond-like coating). At the other extreme, thermal neutrons are reflected rather efficiently, without gaining energy, by graphite reactor reflectors (dashed black line on the right of **figure 1**). In order to decrease the energy gap between these two limiting cases super-mirrors consisting of many thin layers with contrasting reflective indices are used for example in certain neutron guides (green dashed line in **figure 1**).

We describe here another approach, particularly suitable for very cold neutrons (VCNs): multiple scattering of neutrons from diamond nanoparticle powders [1]. The use of nanoparticles provides a sufficiently large cross section of coherent interaction and inhomogeneity of the reflector density on a spatial scale approximating to the neutron wavelength. Nevertheless, many neutron–nanoparticle collisions are needed for good VCN reflection since they scatter preferably in the forward direction. This requirement constrains the choice of materials to low-absorbing materials with a high effective Fermi potential. Diamond nanoparticles are therefore an obvious choice for a VCN reflector.

Early experiments on the reflection of VCNs from nano-structured materials as well as on VCN storage were carried out in the seventies (blue dashed line in **figure 1**) [2]. More recently we have extended the energy range and the efficiency of VCN reflection by exploiting diamond nanoparticles. A reflector of this type would be particularly useful for both UCN sources using nanoparticles at extremely low temperatures (a few mK) [3] and for VCN sources.

The measurement was carried out at the VCN PF2 beam position, providing access to neutrons with a velocity in the range of 30–160 m.s⁻¹. In contrast to experiments with cold and thermal neutrons, for which standard instruments exist, we had to build a dedicated instrument for VCNs.

First, we studied the reflection of neutrons from and transmission through thin layers of diamond nanopowder. Our sample was a powder of diamond nanoparticles with diameters in the range of 2–5 nm and a known size distribution. The powder was placed between two thin sapphire plates. We prepared four samples with nanoparticle thicknesses of 0.2, 0.4, 2 and 6 mm. We used the thinner samples to explore neutron–nanoparticle interactions and the thicker samples to assess the feasibility of using nanopowder as reflectors. The sample was placed at the centre of 11 neutron counters measuring the neutrons scattered by the sample (**figure 2**).

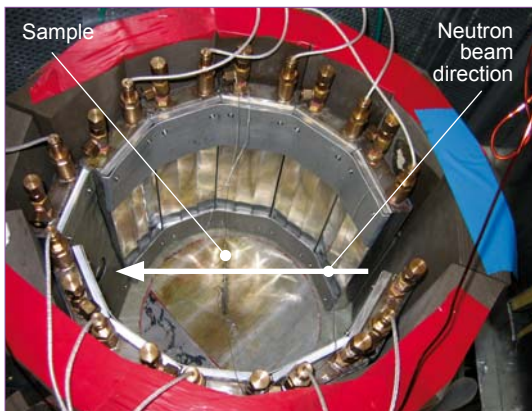


Figure 2: Diamond nanoparticle reflector sample mounted at the centre of 11 neutron detectors. The neutron beam is horizontal and the diamond nanoparticle reflector is mounted vertically. The sample thickness was varied from 0.2 to 6 mm.

Since a precise measurement of the reflectivity can only be made after multiple consecutive reflections, we extended our study by building a VCN storage trap (**figure 3**). The 2 cm-thick walls of the trap were made from a very thin aluminium envelope filled with diamond nanoparticle powder. After entering the trap, the VCNs are reflected many times from the walls before being detected at the trap exit. The reflectivity results as a function of VCN velocity are presented in **figure 1** as the full red line.

The maximum energy of the reflected VCNs and the reflection probability far exceed the corresponding values for the best super-mirrors available [5] (green dashed line in **figure 1**), even though the reflection is not specular at the nanopowder reflector. If we eliminate any additional losses, due in particular to hydrogen-containing impurities, the reflection probability from an infinite nanopowder reflector could be as high as the red dotted line shown in **figure 1**. Such a reflector could play an important role in the storage of VCNs for use in future devices and instrumentation.

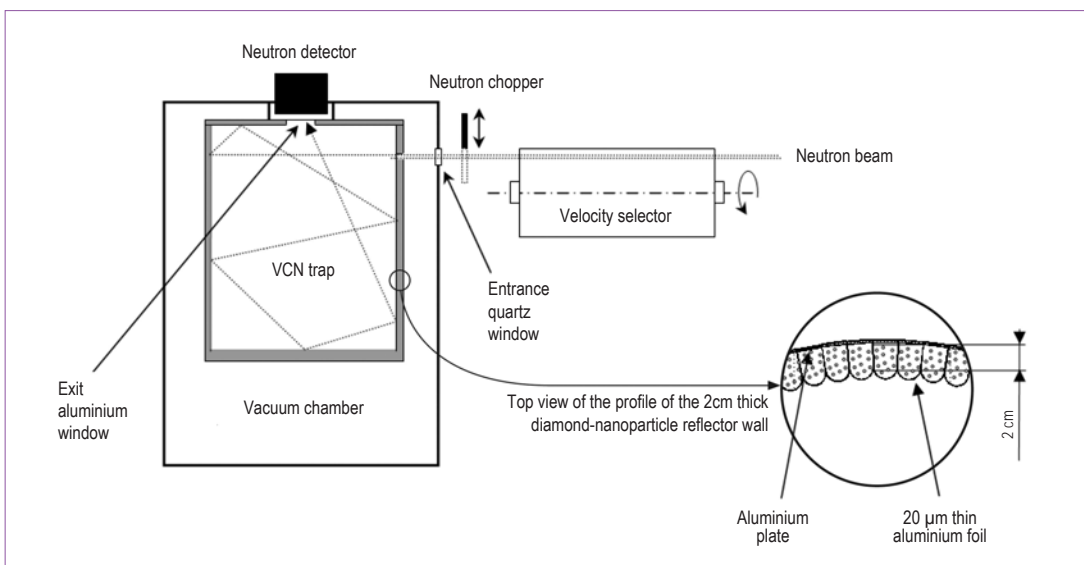


Figure 3: Diagram of the VCN trap enclosed by a 2 cm diamond nanoparticle reflector used to obtain precise measurements of the VCN reflectivity at different velocities.

To analyze the data we developed a Monte-Carlo model of the experiment. The interaction of the neutrons with a nanoparticle powder can be described using the simple approach proposed in ref. [4]. In the broad range of VCN velocities and sample thicknesses, good qualitative agreement was obtained between the probability and the angular distribution of scattered neutrons, and the predictions of the model of independent nanoparticles at rest [1]. In particular, the probability of the reflection of the VCNs with the smallest velocities is in agreement with 100% diffuse reflection, given the value of the solid angle from the sample to the counter assembly.

References

- [1] V. V. Nesvizhevsky *et al*, Nucl. Instr. Meth. A 595 (2008) 631
- [2] A. Steyerl and W. D. Trüstedt, Z. Physik 267 (1974) 379
- [3] V. V. Nesvizhevsky, Phys. At. Nucl. 65 (2002) 400
- [4] V. V. Nesvizhevsky, G. Pignol and K.V. Protasov, Int J. Nanoscience 6 (2007) 485
- [5] R. Maruyama *et al*, Thin Solid Films 515 (2007) 5704

Authors

S. Mayer (ILL and TU-Vienna, Austria), H. Rauch (TU-Vienna, Austria)
P. Geltenbort (ILL), G. Zsigmond (PSI, Switzerland)

High-brightness pulsed beams produced by ultra-cold neutron up-scattering

Because neutron scattering research is an intensity-limited technique, many attempts have been made to increase beam intensities and efficiencies. In particular, for TOF instruments it is the neutron beam intensity in the pulse that matters, i.e. the intensity in a narrow angular range, a small wavelength range and a short time interval. We demonstrate here a new method for the production of high-brightness pulsed beams in which ultra-cold neutrons (UCN) are up-scattered by Bragg diffraction from a fast moving crystal to higher energies while preserving their high phase-space density. Intense monochromatic pulsed beams can thus be produced with intensities that overcome the limitations of the neutron source.

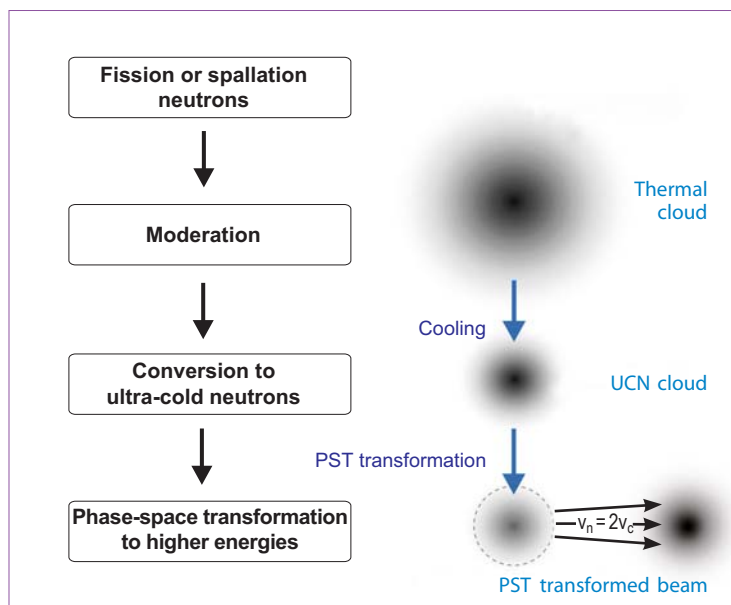


Figure 1:
The phase-space transformer (PST) principle.

Powerful new methods for the production of ultra-cold neutrons due to down-scattering in super-fluid ^4He and in ortho-deuterium have been reported in the literature [1,2]. Intensity gain factors of 100 to 1000 are anticipated. Such phase-space densities can be achieved by non-Liouville interactions, e.g. by spectrum cooling or advanced down-scattering techniques. Their high densities can then be shifted to higher energies by means of a proper phase-space transformer (PST - shown schematically in **figure 1**). An isotropic gas is shifted towards one direction with a divergence and momentum resolution given by the UCN-gas.

Up-scattering can be achieved by inverse Bragg diffraction from a fast moving single crystal. When backscattering

is considered the following relation between the velocity of the reflecting crystal (v_c) and the lattice constant (d) has to be fulfilled:

$$v_c = h/md_{h,k,l} \quad \text{or} \quad v_c [\text{m/s}] = 1978/d_{h,k,l} [\text{\AA}]$$

The related neutron velocity becomes $v_n = 2v_c$. High linear velocities are rather difficult to achieve and therefore the first measurements used fast rotating crystals where the condition mentioned above can only be fulfilled for one distance from the centre because the crystal velocity depends on the radius. Due to the different orientations the beam becomes deflected into a broader angular range. In order to keep the mechanical velocities within reasonable limits we used intercalated graphite (i-HOPG) with a lattice constant of 8.74 Å and a mosaic spread of about 5.5 degrees.

This requires a crystal velocity of 226.3 m/s and produces cold neutrons with a wavelength of 8.73 Å. The experiments have been performed at the ultra-cold neutron facility PF2.



Figure 2: Simon Mayer (left) and Peter Geltenbort (right) with the raised PST rotor.

A centrifuge device from Schenck RoTec (Darmstadt/Germany) was adapted to upscatter UCN leaving the guide tube (**figure 2**).

Typical results are shown in **figure 3**. The four peaks relate to the four crystals mounted at the rotor. The rather high counting rate and the pulsed structure of the beam are visible. The slight intensity differences result from the different reflectivities of the crystals. The monochromaticity of the beams is determined by the UCN cloud and amounts to $\Delta\lambda/\lambda = 0.34\%$. A position-sensitive detector (PSD) has been used to register the spatial and angular structure of the beam (**figure 4**).

From these results a time-averaged intensity in the centre of the beam of about $350 \text{ cm}^{-2}\text{s}^{-1}$ can be extracted. A comparison with the intensity of UCN at the entrance gives an efficiency of about 7%. Monte-Carlo calculations [3] support these estimates. Various improvements should be taken into account when discussing this new method for future advanced neutron beam tailoring:

- A fast translational motion can be achieved by means of a double arm rotor. In this case the Bragg condition can be fulfilled for the whole reflecting crystal. This will result in an intensity gain by a factor of 4.
- A translational motion would scatter the neutrons into a smaller angular range which results in a gain factor of at least 5.
- Only a small proportion of the UCN is hit by the crystal, the rest are lost between the crystal paddles. By means of a back-reflecting plate these UCN can be up-scattered by one of the next crystals (gain factor of about 10).
- New UCN sources may have a 100 times higher intensity than PF2, which gives also a corresponding gain factor. These estimates show that intensities of a highly monochromatic and pulsed beam of $7 \times 10^6 \text{ cm}^{-2}\text{s}^{-1}$ can be achieved from a dense UCN gas. This value could be significantly above the intensities of IN5 at ILL ($2 \times 10^5 \text{ cm}^{-2}\text{s}^{-1}$ at 8.7 Å), TOFTOF at FRM II and CNCS at SNS.

Using this technique, the most brilliant pulsed cold neutron beams could be produced at a stationary neutron source such as ILL.

PST (NMI3-NO-PST) is supported by the European Commission under the 6th FP Contract no: RII3-CT-2003-505925 and the Austrian Science Foundation FWF (project F 1514).

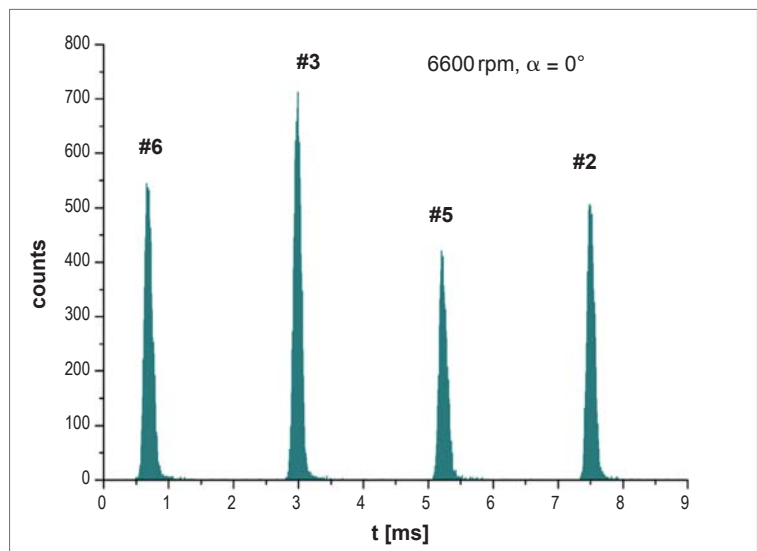


Figure 3: Peak structure of the time-resolved measurement of the beam (# crystal number).

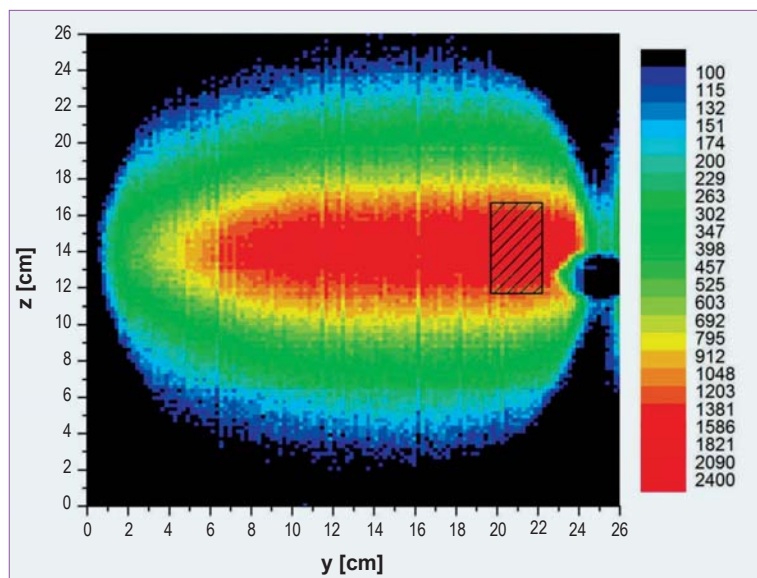


Figure 4: Beam profile measured with a position sensitive detector. The shaded area represents the size of the crystal.

References

- [1] O. Zimmer et al., Phys. Rev. Lett. 99 (2007) 104801
- [2] F. Atchison et al., 2007 Phys.Rev. Lett. 99 (2007) 262502
- [3] S. Mayer, G. Zsigmond and P. Allenspach, Nucl. Instr. and Meth. A 586 (2008) 110-115
- [4] S. Mayer, H. Rauch, P. Geltenbort, P. Allenspach, G. Zsigmond, Science (submitted)

Authors

A. R. Müller, E. Gutmiedl, M. Urban and S. Paul (TU München, Garching, Germany)

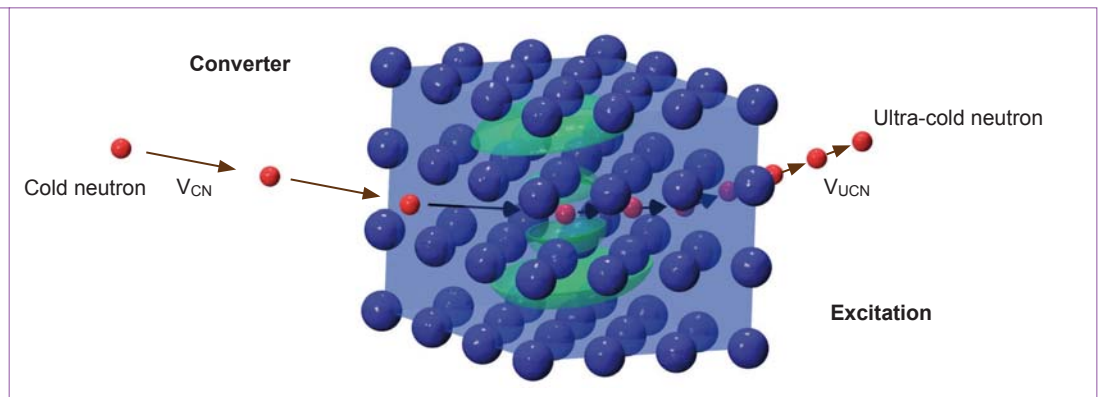
T. Unruh and Ch. Morkel (FRM-II, Garching, Germany)

H. Schober and S. Rols (ILL)

Characterising ultra-cold neutron converter materials with time-of-flight spectroscopy

Ultra-cold neutrons (UCNs) are ideal candidates for investigating many questions related to fundamental interactions in physics. There are currently many projects that aim to achieve large gains in UCN density. They all rely on slowing-down cold neutrons via energy exchange with a scattering medium. Using neutron spectroscopy we can determine the probability with which a neutron is brought close to a stop by a scattering event or vice versa. This enables UCN production and loss mechanisms to be studied. The method was successfully employed on the instrument IN4 at the ILL and on TOFTOF at FRM-II for liquid and solid deuterium D_2 in the technically relevant temperature range of 4 to 20 K.

Figure 1: Diagram of the down-scattering process used inside a super-thermal source to produce ultra-cold neutrons (UCNs) from a cold neutron beam via the creation of an excitation.



Neutrons with kinetic energies below ≈ 200 neV (corresponding to temperatures of about 2 mK) are called ultra-cold neutrons (UCNs). They are totally reflected under any incident angle by the Fermi potential of suitable materials, or by magnetic fields of about 1 T. This provides a means of confining UCNs for hundreds of seconds, enabling them to be stored and manipulated. The resulting trapped UCNs, acting like a highly diluted neutron gas, are used to address fundamental questions in physics including quantum levels in the gravitational field, the baryon asymmetry in the universe and precision tests of the standard model of particle physics.

For all these experiments an UCN density orders of magnitude higher than that currently available at the UCN turbine of the ILL is desirable. This should be achievable using super-thermal processes as schematically shown in **figure 1**. The principle of such a source relies on the fact that a neutron can be brought close to a stop when it has the chance to exchange its energy and momentum with a converter material in a scattering event. Thermodynamic equilibrium between the converter and the UCN gas is avoided with this super-thermal source concept. Apart from giving a high production rate the converter has to be chosen such as to provide a sufficient chance for the UCNs to escape before

they are absorbed or back converted. Due to its large scattering cross section, solid deuterium at temperatures of 4.5 K is one good candidate for UCN conversion.

The probability that a neutron will exchange a certain amount of energy and momentum with a sample can be directly measured in an inelastic neutron scattering experiment. The corresponding probability as a function of momentum and energy is called the dynamic structure factor $S(Q, \omega)$. **Figure 2** shows $S(Q, \omega)$ for solid deuterium at 4.5 K as measured on the time-of-flight spectrometer IN4 of the ILL. For our purpose we can divide the landscape plot into three regions of interest:

1) First of all we consider the intensity along the elastic line, i.e. the probability of zero energy transfer. From the position of the peaks we get structural information including the texture of the potential converter material as a function of its preparation conditions. Structure may affect the extraction probability of UCNs from the source.

2) Focusing on the neutron-energy loss side, we enter the region of UCN production. As usual, energy and momentum have to be conserved for all scattering processes, but in the case of UCN production we can put the final energy to zero. Thus the relevant area is reduced to a narrow strip centered on the free neutron parabola E_f [meV] = 2.077 q^2 (q in \AA^{-1}). By integrating the measured scattering probability along this line it is possible to extract the UCN production cross section as a function of incident neutron energy. This result can be used for efficient prediction of UCN source performance including the optimal incident neutron spectrum.

3) On the neutron energy gain side we measure the UCN loss channels. Due to the low temperature and the principle of the super-thermal production we would expect just small contributions. There should be no excitations capable of transmitting energy to the neutrons. The exception shown in the figure has to be attributed to the spin flip probability at 7.5 meV, a well-known loss channel for deuterium in the para spin state. The relaxation of the para spin state is slow in deuterium at low temperatures maintaining the sample in a non-equilibrium state - unless a suitable converter catalyses spin conversion. In the present case the para concentration was 33 %, whereas

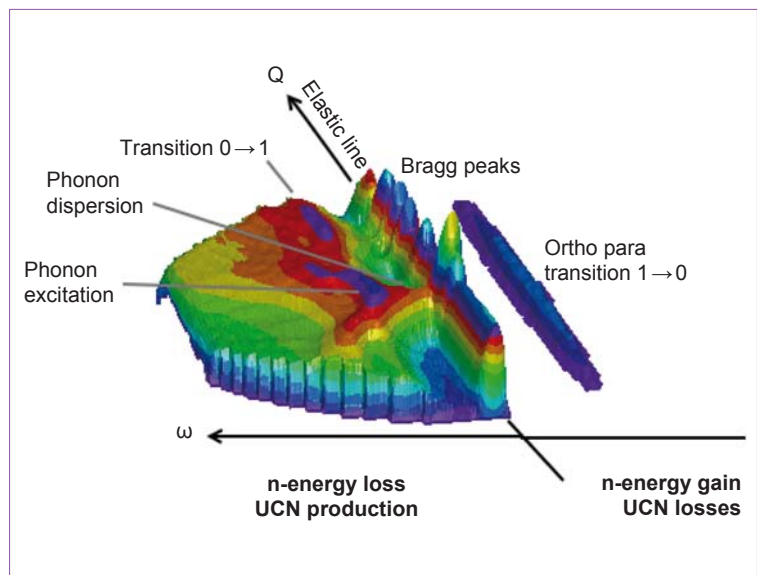


Figure 2: Dynamic structure factor $S(q, \omega)$ for solid deuterium at 4.5 K. From this measured scattering probability it is possible to predict the production rate of UCNs as well as the efficiency of certain UCN loss processes.

this concentration will be reduced below 2 % if the deuterium is used as a UCN converter. Together with the known spin concentration and the para \rightarrow ortho scattering cross section we can make reliable predictions of the necessary corrections of the achievable UCN density due to additional loss channels.

In summary, from the dynamic structure factor it is possible to characterise possible converter materials for the production of ultra-cold neutrons with regard to structure, production and loss probabilities. This opens up the possibility to compare new converter materials with much less effort than by building test sources. Due to the rather short measuring times it has the potential for systematic studies of the parameters of the chosen materials.

Authors

R. Mittal (JCNS, Garching, Germany and BARC, Trombay, India), **Y. Su** (JCNS, Garching, Germany), **S. Rols, H. Schober** (ILL)
S. L. Chaplot (BARC, Trombay, India), **T. Chatterji** (JCNS and ILL), **M. Tegel, M. Rotter** and **D. Johrendt** (LMU, Munich, Germany)
Th. Brückel (JCNS, Garching and Jülich Germany)

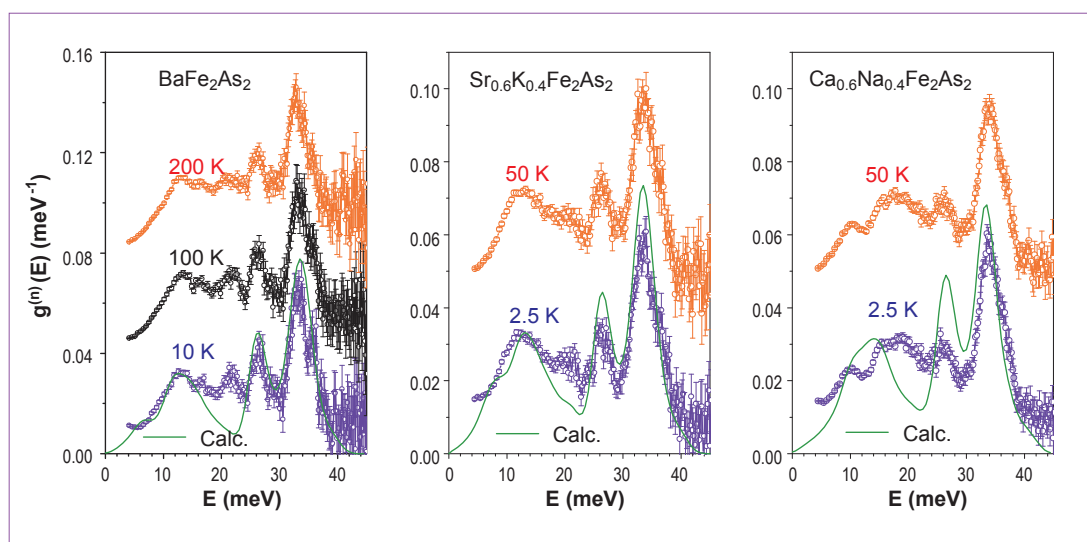
Phonon dynamics in parent and superconducting FeAs compounds

The discovery [1, 2] of high transition temperature (T_c) superconductivity in K-doped BaFe_2As_2 has attracted immense attention. It is important to note that these compounds have high T_c without requiring the presence of copper oxide layers. The role of lattice dynamics in the mechanism of superconductivity in these newly discovered doped materials is still to be settled.

The parent compounds, MFe_2As_2 (where $M = \text{Ba, Sr, Eu, Ca}$) also show pressure-induced superconductivity. Therefore it is important to study the phonons in these compounds carefully as a function of pressure and temperature.

Figure 1:

Comparison between the calculated and experimental phonon spectra of parent BaFe_2As_2 and superconducting $\text{Sr}_{0.6}\text{K}_{0.4}\text{Fe}_2\text{As}_2$ and $\text{Ca}_{0.6}\text{Na}_{0.4}\text{Fe}_2\text{As}_2$ compounds. The measurements are carried out with an incident neutron wavelength of 1.18 \AA (58.8 meV) using the IN4C spectrometer at ILL.



We have measured (figures 1, 2) the temperature dependence of the phonon density-of-states in the parent BaFe_2As_2 [3] and superconducting $\text{Sr}_{0.6}\text{K}_{0.4}\text{Fe}_2\text{As}_2$ ($T_c = 32 \text{ K}$) and $\text{Ca}_{0.6}\text{Na}_{0.4}\text{Fe}_2\text{As}_2$ ($T_c = 21 \text{ K}$) compounds [4] using the IN4C and IN6 spectrometers at the ILL on polycrystalline samples. The temperature dependence of the phonon density of states for the superconducting compounds shows a strong similarity (figure 1) for the measurements carried out above and below the superconducting transition temperature. This suggests that the formation of Cooper pairs have only a very minor influence on the overall vibration spectrum.

By comparing the experimental phonon spectra with the calculated neutron-weighted density of states

obtained from a lattice-dynamical model, the dynamical contribution from various atoms has been identified.

In comparison of the parent compound BaFe_2As_2 , the phonon spectra of $\text{Sr}_{0.6}\text{K}_{0.4}\text{Fe}_2\text{As}_2$ and $\text{Ca}_{0.6}\text{Na}_{0.4}\text{Fe}_2\text{As}_2$ show (figure 2b) a very strong renormalization in the lower and intermediate frequency part of the vibrations. The high-frequency band reacts moderately to the doping. Mass effects and lattice contraction in the CaNa compound cannot explain these changes alone. Therefore, the type of buffer ion influences the bonding in the Fe-As layers. The buffers thus cannot be considered a mere charge reservoir.

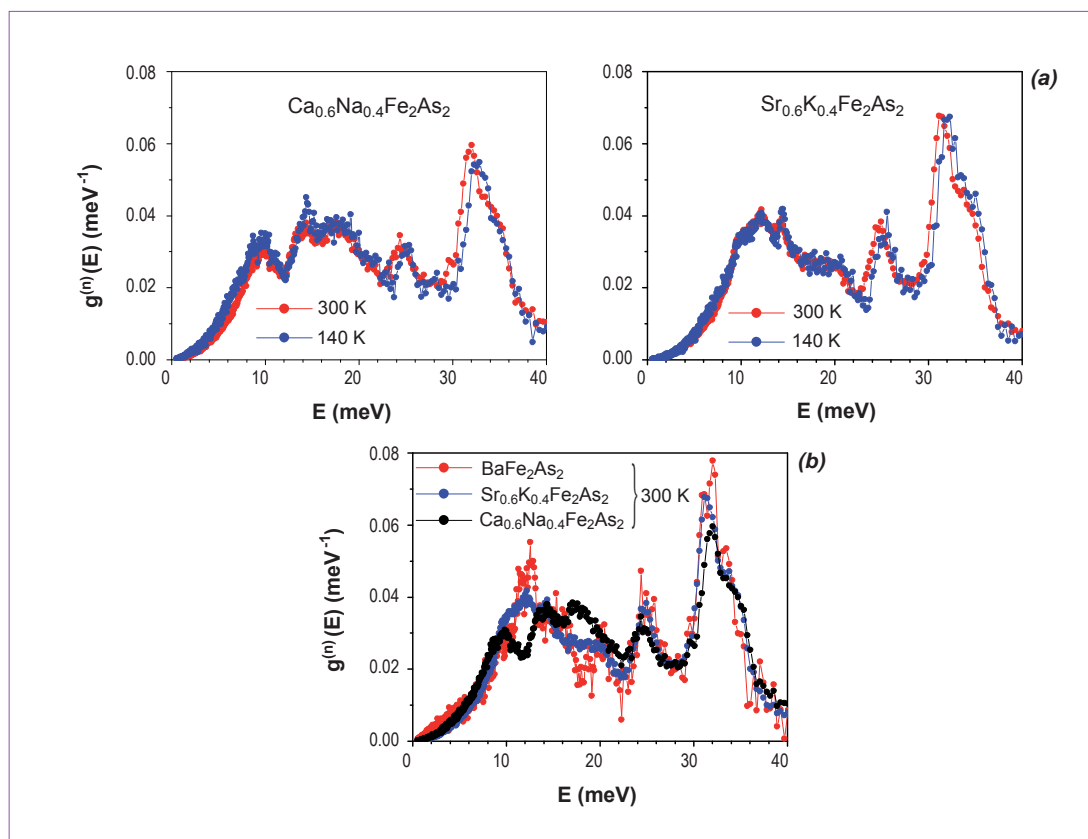


Figure 2
(a) The experimental phonon spectra of $\text{Sr}_{0.6}\text{K}_{0.4}\text{Fe}_2\text{As}_2$ and $\text{Ca}_{0.6}\text{Na}_{0.4}\text{Fe}_2\text{As}_2$ measured with incident neutron wavelength of 5.1 Å (3.12 meV) using the IN6 spectrometer at ILL.
(b) Comparison of the experimental phonon spectra of BaFe_2As_2 , $\text{Ca}_{0.6}\text{Na}_{0.4}\text{Fe}_2\text{As}_2$ and $\text{Sr}_{0.6}\text{K}_{0.4}\text{Fe}_2\text{As}_2$.

The high resolution data collected using the IN6 spectrometer show softening of phonon modes (**figure 2a**) below 10 meV as we decrease the temperature from 300 K to 140 K. Softening of low energy phonons is larger for the Ca compound (about 1 meV) in comparison to that in the Sr compound (about 0.5 meV). These phonon modes below 10 meV arise from the atomic vibrations of Ca/Na or Sr/K atoms.

The higher softening in the CaNa compound may indicate that electron-phonon coupling is stronger than for SrK. Since the phonon softening is observed only in the normal state of both superconducting samples, it is unlikely that it is directly associated to superconductivity, and this despite the isotope effect observed in pnictide superconductors. As the tetragonal to orthorhombic phase transition is suppressed in the superconducting compounds, the structure phase transition also appears not relevant to the observed phonon softening. No anomalous effects are observed in the phonon spectra

when passing the superconducting transition temperature. All this indicates that while electron-phonon coupling is present it cannot be solely responsible for the electron pairing.

References

- [1] Y. Kamihara, T. Watanabe, M. Hirano and H. Hosono, *J. Am. Chem. Soc.* 130 (2008) 3296
- [2] M. Rotter, M. Tegel and D. Johrendt, *Phys. Rev. Lett.* 101 (2008) 107006
- [3] R. Mittal, Y. Su, S. Rols, T. Chatterji, S. L. Chaplot, H. Schober, M. Rotter, D. Johrendt and Th. Brueckel, *Phys. Rev. B* 78 (2008) 104514
- [4] R. Mittal, Y. Su, S. Rols, M. Tegel, S. L. Chaplot, H. Schober, T. Chatterji, D. Johrendt and Th. Brueckel, *Phys. Rev. B* 78 (2008) 224518

Authors

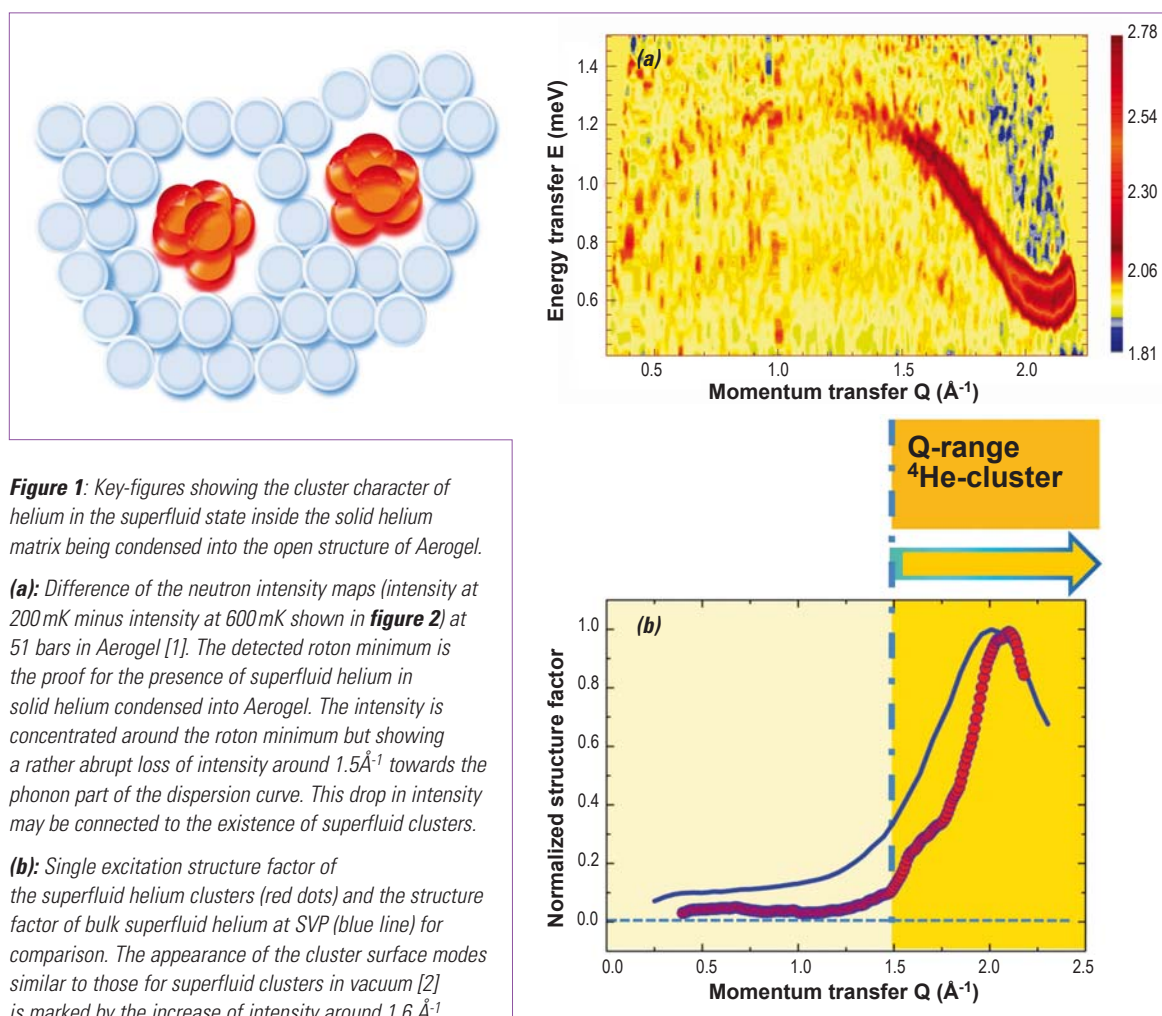
A. Puchkov and I. Kalinin (IPPE, Obninsk, Russia)

E. Kats, M. Koza, X. Tonon and H. Lauter (ILL)

V. Lauter (ORNL, Oak Ridge, USA)

Superfluid helium clusters in solid helium in Aerogel

Superfluid helium clusters have been detected in solid helium condensed at 51 bars into the open structure of Aerogel. Neutron scattering data obtained on the IN6 instrument are consistent with the existence of helium clusters in a superfluid state in a restricted geometry, thus forming a new quantum state with localized character.



The presence of helium clusters is suggested by the observation of a truncated intensity along the excitation curve with a roton minimum, typical for a superfluid state (figures 1a and 2a). The solid helium hosting the helium clusters exhibits Bragg peaks indicating the coexistence of hcp and bcc structures (figure 2). Three experimental observations support the model of superfluid clusters in the matrix of solid helium:

- The exceptional event along the dispersion curve (figure 1a) is the almost total absence of long-wavelength phonons, which characterizes the existence of a restricted geometry such as clusters. A further notable feature is the exceptionally low energy gap of the roton minimum which is not found in bulk liquid helium under pressure. The superfluid state is consistent with the absence of diffuse scattering around the dispersion curve.

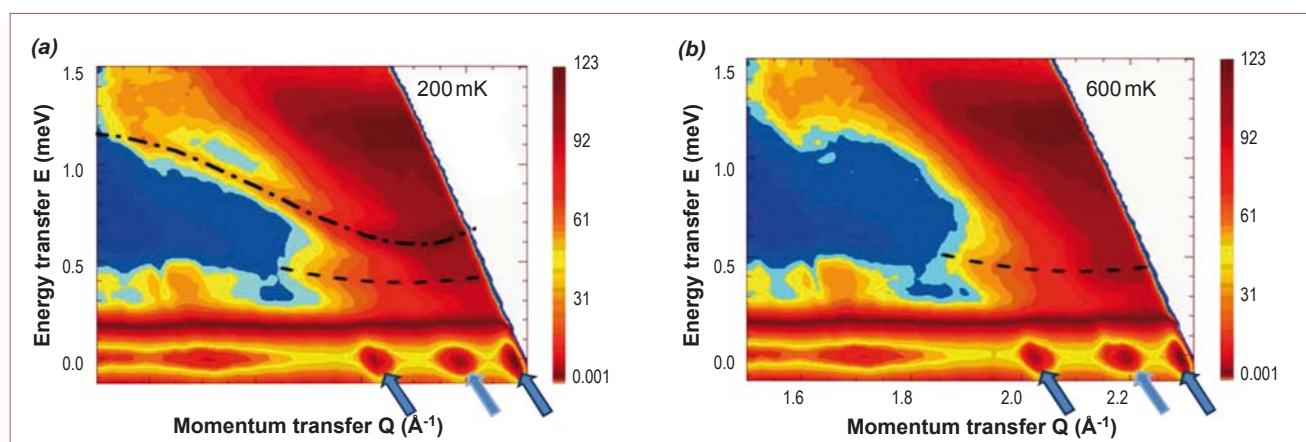


Figure 2: Phase transition of the superfluid clusters in the solid helium matrix.

Neutron intensity maps as a function of energy transfer E and momentum transfer Q in solid helium of a pressure of 51 bars in Aerogel at 200 mK **(a)** and 600 mK **(b)**. hcp Bragg-peaks are marked by dark blue arrows. (A bcc-peak stabilized by the Aerogel surface potential is marked with a light blue arrow). The dash-dotted line marks the dispersion of the superfluid clusters, which disappeared after re-cooling from a temperature of 1.6 K to 600 mK. The dispersion of the superfluid interface mode (dashed line) at the helium-substrate interface, characterizing another superfluid phase, persists after re-cooling to 600 mK. The dark red region shows phonons of the solid helium.

- Further proof of superfluid helium clusters is obtained from the single excitation structure factor (**figure 1b**). The maximum intensity at the momentum transfer of the roton represents the nearest neighbour interaction in the cluster. A normalized structure factor of bulk liquid helium compared to that for helium in Aerogel shows the different nature of the helium contained in the latter. The supplementary intensity around 1.6 \AA^{-1} may indicate superfluid surface modes of the clusters similar to those for superfluid clusters in vacuum [2]. In any case the limit of the spatial range of the clusters is marked by this event (**figure 1b**).

- A phase transition occurs when the sample temperature is raised to just above 1.6 K, a temperature still within the bulk solid helium phase. The transition is marked by the disappearance of the intensity of the roton, which is visible in **figure 2a** at 200 mK. Subsequent re-cooling to 600 mK does not lead to the reappearance of the dispersion curve of the helium clusters (**figure 2b**). A new phase without clusters is created showing that the phase containing superfluid helium is a metastable phase. The Bragg peaks of the solid helium are slightly influenced by this transition. The peak intensity is slightly increased and the width of the peaks is slightly reduced. As these effects also occur for the bcc and hcp Bragg peaks, it can be assumed that the superfluid helium clusters are localized at the interfaces between the two structures. This model is consistent with the fact that a second excitation which survives the phase transition

described above (**figure 2b**), is detected below the energy of the cluster roton (**figure 2a**). This excitation is due to the similarity to the layer-roton in helium films [3], an interface-roton at the solid-helium substrate interface. It is the high substrate potential which lowers the energy of the interface roton. Thus the cluster roton cannot be localized at the solid helium substrate interface, but is localized at solid helium interfaces due to its higher energy at the roton minimum.

In conclusion we have detected a superfluid phase of ^4He in a restricted geometry which we interpret as clusters at the internal interfaces of solid helium under high pressure being condensed into Aerogel. In addition another superfluid phase appeared at the solid helium substrate interface.

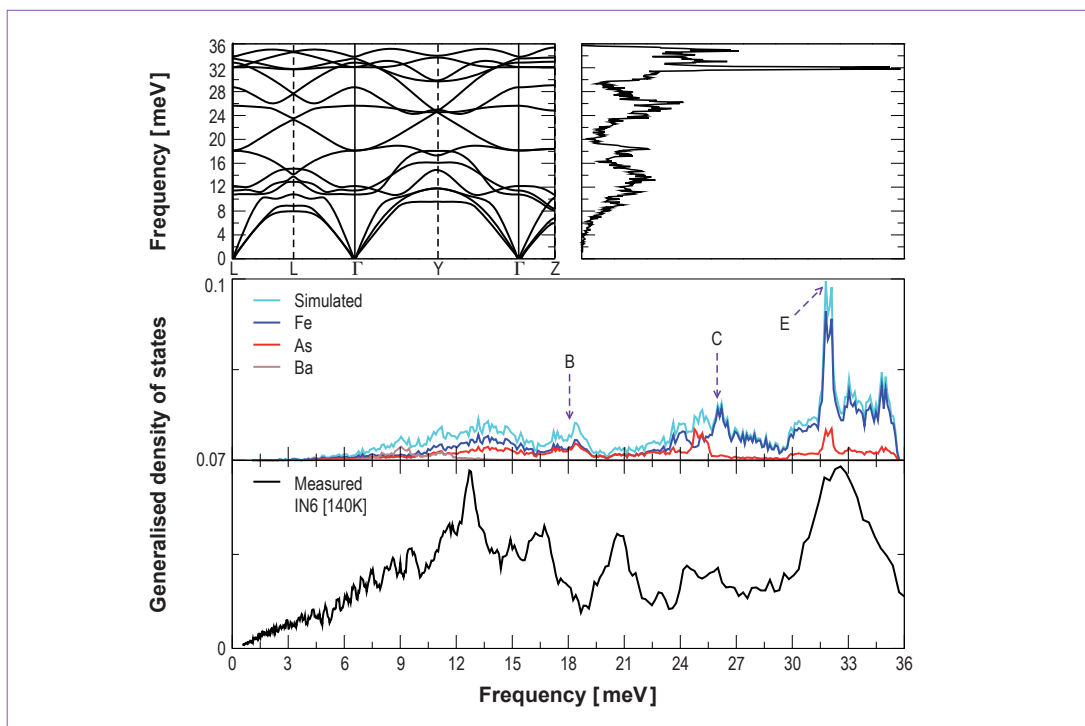
References

- [1] I. Kalinin, E. Kats, M. Koza, V. Lauter, H. Lauter, A. Puchkov, JEPT Lett. 87 (2008) 743
- [2] S. A. Chin, E. Krotschek, Structure and collective excitations of ^4He clusters. Phys. Rev. B 45 (1992) 852-874
- [3] B. E. Clements, H. Godfrin, E. Krotschek, H. Lauter, P. Leiderer, V. Passiuk, C. J. Tymczak, Excitations in a thin liquid ^4He film from inelastic neutron scattering, Phys. Rev. B 53 (1996) 12242-12252

First-principle calculations reveal how in BaFe_2As_2 electrons interact with phonons through their spin

In 2008 several families of new superconductors all based on Fe-As layers were discovered. Due to their high transition temperatures they immediately occupied a central position on the stage of solid-state physics research, driven by the hope that they might provide a better understanding of high- T_c superconductivity in general. The parent compounds, i.e. the materials from which the superconductors are derived via selective doping, possess a rather simple structure and are thus amenable to detailed first-principle calculations. We have performed such calculations on BaFe_2As_2 and show that phonons interact with electrons by influencing the spin states. The combined evidence for phonon influence on the electron system is of considerable importance to understanding the conduction and superconduction processes in BaFe_2As_2 .

Figure 1: Measured and simulated generalised density of states together with the calculated dispersion relations.



The recent discovery of superconductivity in Fe-As based materials [1,2] has opened a new door to an improved understanding of the phenomenon of high-temperature superconductivity. The fundamental question to answer is how the electrons couple to form pairs. A possible mechanism could concern phonons. However, it quickly became clear that simple electron-phonon coupling would not do the job. In this context we have investigated the phonon and electronic structure of BaFe_2As_2 with special attention to the electron spin system. BaFe_2As_2 is one of the parent

compounds to the Fe-As based superconductors [3] and particularly useful for this kind of study due to its rather simple structure. It is found that: (i) phonons are correctly described when magnetic ordering of Fe cations is considered; (ii) the position of As along the C-axis considerably affects both vibrational and electronic spectra, and; (iii) due to some specific phonons the magnetization density of Fe changes considerably through an up/down spin-rocking with a corresponding, significant change of the electronic distribution around the Fermi level.

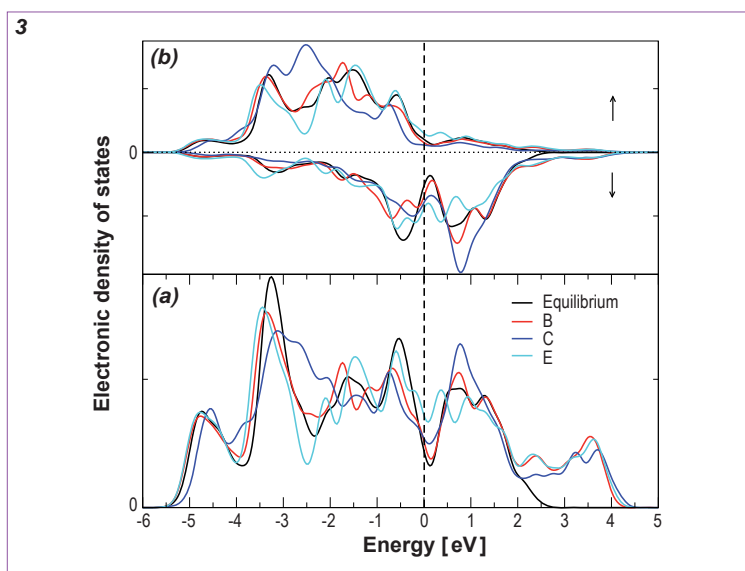
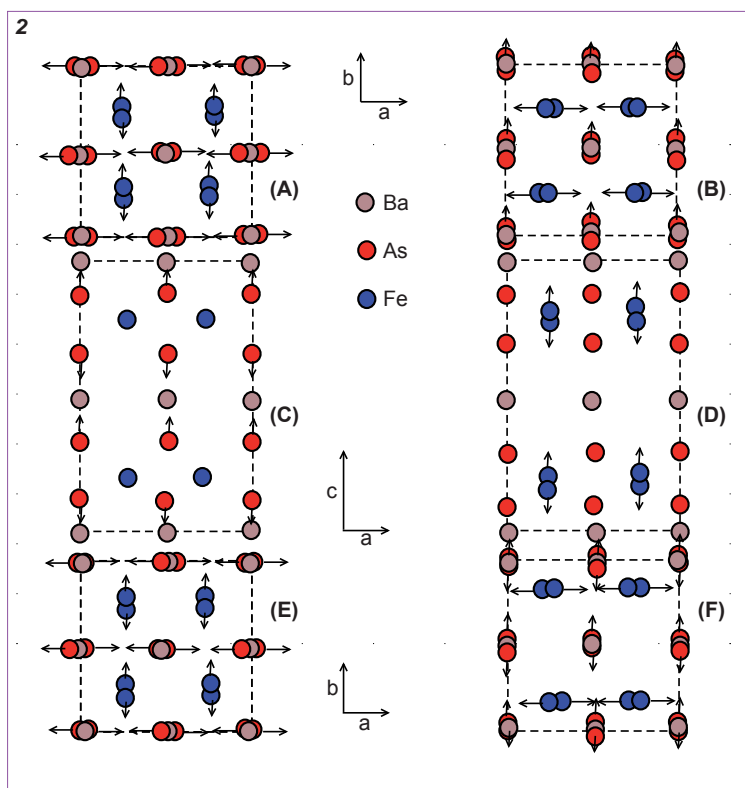
Figure 1 shows the calculated dispersion curves and generalized density of states (full and partial GDOS) for the orthorhombic phase. Simulations were carried out using the direct method with density functional theory. The comparison with the spectra measured on IN6 [3] is generally good and thus validates the calculations. From *ab initio* lattice dynamical calculations, the Raman active modes are also extracted (there are six active modes under the space group F_{mmm}). The corresponding displacement patterns are shown in **figure 2**.

To gain insight into the effect of phonons on the electronic structure, the electronic density of states (eDOS) for the six frozen phonon patterns of the Raman active modes as well as for the reference unperturbed (equilibrium) structure were calculated [3]. The results are shown in **figure 3** for the three Gamma point modes (B, C and E) that most strongly perturb the equilibrium electronic structure. The electronic bands close to the Fermi level and in particular the eDOS at the Fermi level depend strongly on the phonon distortion via the d-bands of Fe. As the Fermi level of the equilibrium structure is found at the minimum of a rather steep-walled valley of the eDOS, phonon modes that displace the Fermi level only slightly, create a large fluctuation of the electron density at the Fermi-level.

In view of the importance of magnetic ordering on the equilibrium structure of $BaFe_2As_2$, we have also investigated the spin-resolved eDOS of the d-electrons of the Fe cation. It is seen that modes B and C cause a decrease in the spin-down population and an increase in the spin-up population and, therefore, an increase in the magnetic moment. On the other hand, mode E causes a rocking of the spin population from the majority up-channel to the minority down-channel, decreasing the magnetic moment. Mode E tends to reduce the magnetic ordering. For all 3 modes, the Fermi level changes by less than 0.5%. Phonon modes that modulate the Fe-As layer cause the most significant changes in the eDOS at the Fermi level, which indicates the extent of electron-phonon coupling. In addition the magnetic moment and spin-resolved eDOS of the Fe cation vary significantly with the phonon displacements, demonstrating spin-phonon coupling, which is relevant to the search for a composite mechanism for high temperature superconductivity that goes beyond simple, electron-phonon coupling.

Figure 2: Displacement patterns of simulated Raman active modes in $BaFe_2As_2$ (**A**: 18 meV, **B**: 18 meV, **C**: 26 meV, **D**: 29 meV, **E**: 32 meV and **F**: 34 meV).

Figure 3: (a) Total eDOS of the unperturbed (Equilibrium) structure and the frozen phonon patterns in $BaFe_2As_2$. (b) The corresponding spin-resolved eDOS of the d-electrons per Fe cation.



References

- [1] Y. Kamihara *et al.*, JACS. 128 (2006) 10012
- [2] C. Y. Liang *et al.*, SST. 20 (2007) 687
- [3] M. Zbiri, H. Schober, M. R. Johnson, S. Rols, *et al.*, Phys. Rev. B (in press)

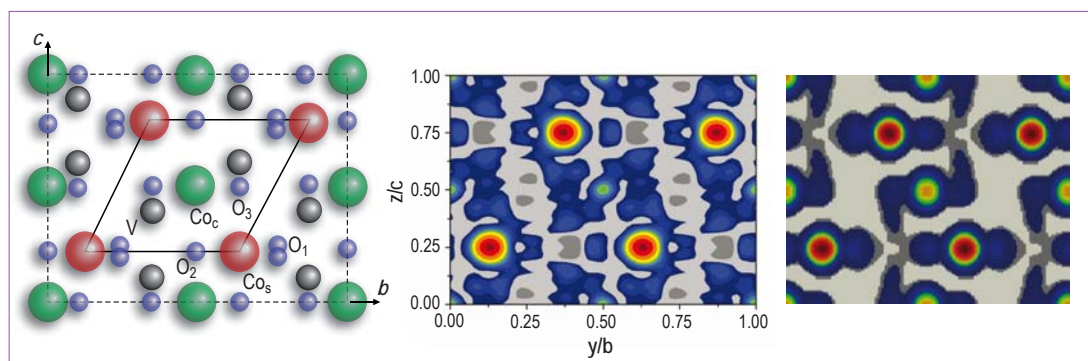


Figure 2: Crystal structure of $\text{Co}_3\text{V}_2\text{O}_8$ viewed along the a axis (left), observed (centre) and simulated (right) spin density maps in real space.

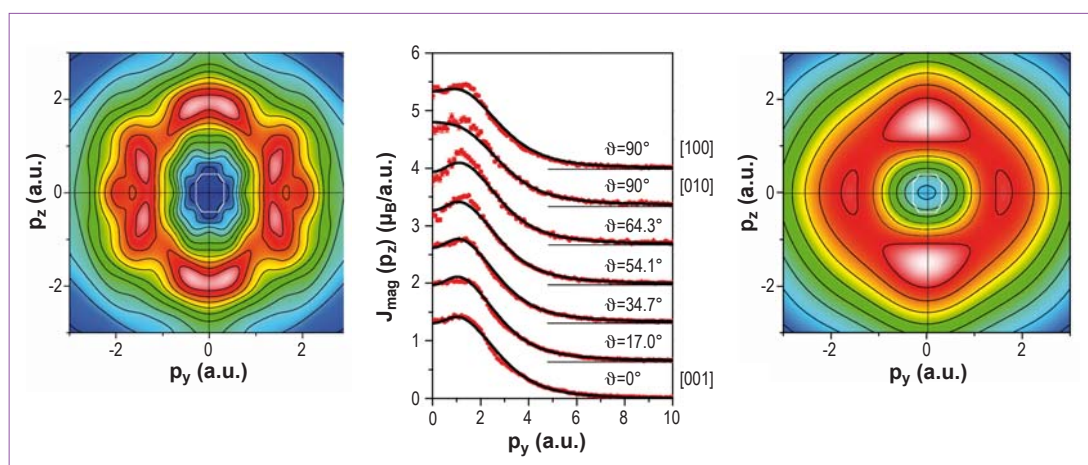


Figure 3: Reconstructed, experimental (left) and modelled (right) spin density in momentum space. The middle panel compares the corresponding observed (dots) and simulated (solid curves) magnetic Compton profiles.

Their contributions to the real and momentum space densities were refined using one and the same model of an unpaired electron distribution.

Periodic solid-state modelling was used to simulate the spin density map of the material and to obtain the magnetically projected electronic structure, which allows the induced magnetization on O and V sites to be estimated. The nuclear structure factors, deduced from the unpolarized neutron experiments, have been used to derive the magnetic structure factors from the observed flipping ratios. As the crystal structure is centrosymmetric the experimental magnetization density can be directly reconstructed by Fourier synthesis.

Figure 2 demonstrates the good agreement between observed and simulated magnetization density, in real space, projected onto the b - c plane. Despite the fact that a field of 2 T has been applied along the easy axis a for the flipping ratio measurement, the magnetic moments of Co_s and Co_c are still significantly different. Furthermore, remarkable induced magnetization can be observed experimentally and computationally on the V and O sites.

The real space quantities have simultaneously been refined with the momentum space quantities as the spin-orbitals contribute to both densities in the same way. Magnetic Compton profiles provide the one-dimensional projection of the momentum spin

density, as shown in **figure 3**, and the shape of these profiles makes it possible to determine the population of each orbital. In real space this is represented by the magnetic form factor. The correlated refinement yielded stable and reliable results. The sum of the individual magnetic moments in the different metal and oxygen ions (defined in **figure 2**) [$\mu(\text{Co}_c)=1.54 \mu_B$, $\mu(\text{Co}_s)=2.87 \mu_B$, $\mu(\text{V})=0.41 \mu_B$, $\mu(\text{O}_1)=0.05 \mu_B$, $\mu(\text{O}_2)=0.35 \mu_B$, $\mu(\text{O}_3)=0.36 \mu_B$] with respect to their site multiplicity leads to a value of $3.52 \mu_B$, which is in good agreement with macroscopic measurements [4], where the magnetic moment has only been attributed to the Co cations [3].

Our study, however, shows that spin populations are equally distributed over the t_{2g} and e_g levels for Co_s , but that only 30% of the magnetic signal stems from the e_g orbitals for Co_c . Covalency is therefore at the origin of this reduced value with the relatively large induced moments on the oxygen anions, marked O_2 and O_3 anions surrounding Co_c .

References

- [1] H. Fuess *et al.*, Acta. Crystallogr. Sect. B: Struct. Sci B 26 (1970) 2036
- [2] Y. Chen *et al.*, Phys. Rev. B 74 (2006) 014430
- [3] N. R. Wilson *et al.*, J. Phys. Condens. Matter 19 (2007) 145257
- [4] N. Qureshi, M. Zbiri *et al.*, Phys. Rev. B. (Accepted)

Authors

S. Rols, H. Schober, A. Ivanov and M. Johnson (ILL)
J. Cambedouzou, M. Chorro and P. Launois (LPS, Orsay, France)
H. Kataura (AIST, Tsukuba, Japan)
L. Alvarez and J. L. Sauvajol (LCVN, Montpellier, France)

How confinement affects the dynamics of C_{60} in carbon nano-peapods... "And yet they do move"

The empty hollow core of single-walled carbon nanotubes (SWNT) represents a unique environment in which new one-dimensional molecular phases can be designed. In this space confined to the nanometer scale, the physical properties of the encapsulated molecules differ strikingly from that of bulk material. We have measured the dynamics of C_{60} fullerenes encapsulated inside nanotubes, (forming a 'peapod' like structure) using the IN1 BeF and IN4C spectrometers. We found that the encapsulated molecules show an unexpectedly high rotational mobility down to relatively low temperatures.

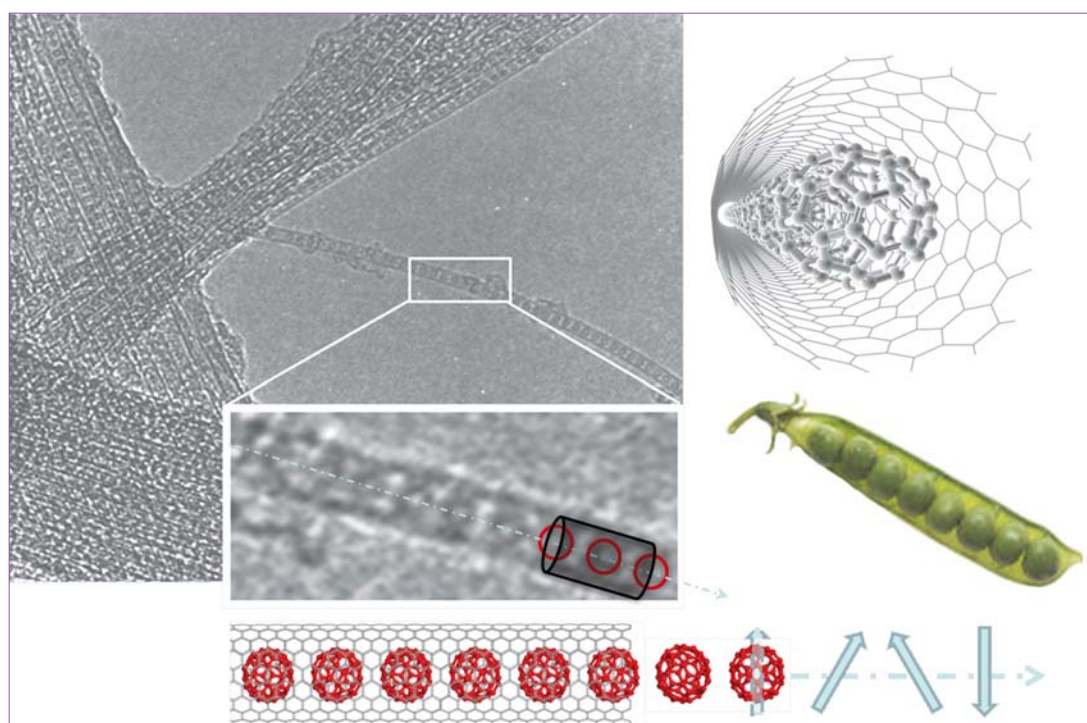


Figure 1: Electron micrograph of C_{60} fullerenes inside carbon nanotubes forming carbon nano-peapods.

Discovered in 1985, C_{60} fullerenes form plastic crystals in their bulk phase. Each C_{60} molecule rotates almost freely around its center of mass for temperatures greater than 260 K (-13°C). Below this temperature, C_{60} fullerenes lose their isotropic rotational motion and undergo a dynamic disorder/order transition. Since 1998, it has been possible to insert C_{60} molecules inside single-walled carbon nanotubes in order to form a structure called 'peapods' [1] (**figure 1**). C_{60} fullerenes form long one-dimensional (1D) chains inside nanotubes that are not observed elsewhere.

We have studied the dynamics of these confined 1D phases of C_{60} molecules using inelastic neutron scattering on the IN4C time-of-flight spectrometer and the IN1 BeF spectrometer [2]. Great advantage can be taken from the complementary energy range and resolution of these techniques. **Figure 2** shows the extensive generalized phonon density of states of a peapod sample and of an empty nanotube sample at low temperature (10 K), as it can be displayed by merging results obtained with each technique. The comparison between these curves allows C_{60} intra-molecular vibration modes

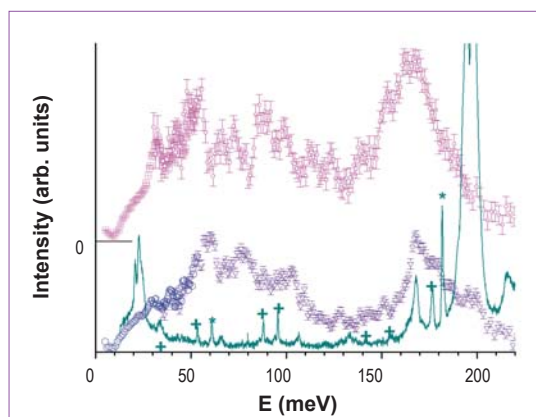


Figure 2: Generalized density of states of peapods (top; squares: IN4, circles: IN1) and empty nanotubes (middle; hexagons: IN4, triangles: IN1). The Raman spectrum of peapods is also shown (bottom), with C_{60} Ag and Hg modes denoted by stars and crosses, respectively.

to be resolved from the nanotube density of states. Some of these modes are C_{60} Raman active modes (**figure 2**).

After having checked that the nanotube guest structure did not strongly affect the intra-molecular vibrations of C_{60} molecules, we focused on the low-energy inter-molecular modes and on diffusion motions that can be extracted from IN4C data. The bottom part of **figure 3** shows the scattering function $S(Q, \omega)$ of the peapod sample at 280 K. A remarkable feature in these data is the strong quasi-elastic signal, whose intensity versus scattering vector Q is in good agreement with that of a coherent signal from a free rotation model. This quasi-elastic signal can be observed down to temperatures lower than 200 K, i.e. at much lower temperature than in the bulk C_{60} phase. Whereas one could have expected that the geometrical confinement exerted by the nanotube wall on C_{60} molecules would have reduced their mobility, our experiments prove that, on the contrary, C_{60} fullerenes keep a greater mobility at low temperature in peapods. Another remarkable result stands in the absence of a well-defined libration excitation even down to low temperature (10 K). This suggests that no ordering of the C_{60} pods is achieved at these temperatures, i.e. confinement suppresses the first order-disorder transition observed at 260 K in the bulk phase.

A possible interpretation can be found in the fact that the SWNT wall forces C_{60} molecules to align along the tube axis forming 1D chains, but that it does not impose a strong influence on the relative orientation of the C_{60} molecules with

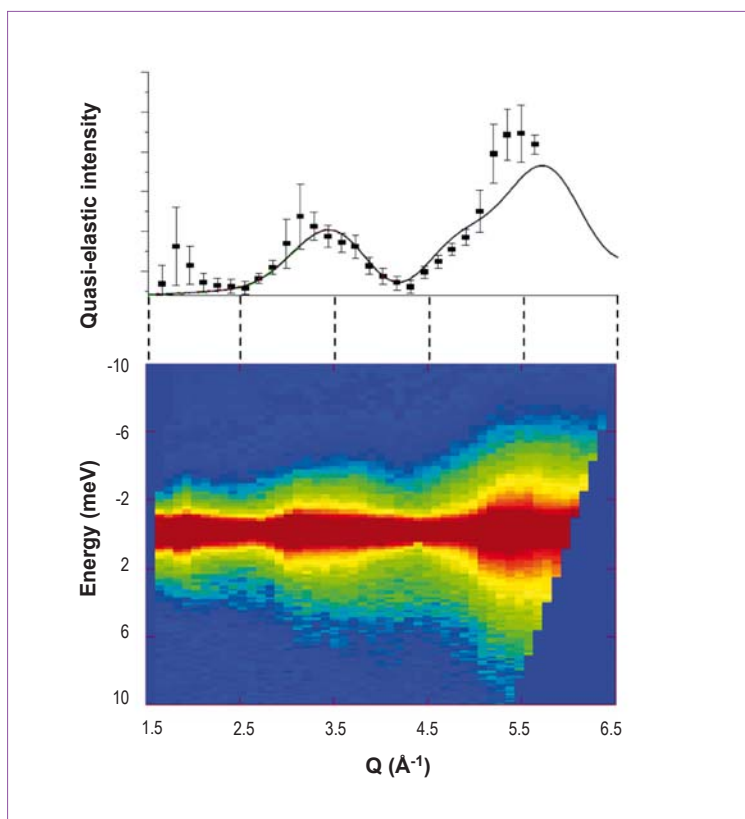


Figure 3: Scattering function $S(Q, \omega)$ of a peapod sample at 280 K (bottom), measured intensity of the quasi-elastic signal (top squares), and calculated quasi-elastic intensity for a free rotational diffusion (top full line).

regard to the nanotube [3]. The prevailing 1D character of the C_{60} chain allows a parallel with a 1D Ising model, in which no order/disorder transition is expected at finite temperature. Taking this point of view, the absence of long-range orientation of the C_{60} in SWNT and their high mobility stands as a textbook example of a 1D Ising model.

References

- [1] B.W. Smith, M. Monthieux and D.E. Luzzi, Nature 396 (1998) 323
- [2] S. Rols, J. Cambedouzou, M. Chorro, H. Schober, V. Agafonov, P. Launois, V. Davydov, A.V. Rakhmanina, H. Kataura and J.L. Sauvajol, Phys. Rev. Lett. 101 (2008) 065507
- [3] K.H. Michel, B. Verberck and A.V. Nikolaev, Phys. Rev. Lett. 95 (2005) 185506

Authors

L. De Leo (Ecole Polytechnique, CNRS, Palaiseau, France)

M. Civelli (ILL)

G. Kotliar (Rutgers University, USA)

The $T = 0$ heavy fermion quantum critical point as an orbital selective Mott transition

We establish a link between the quantum critical phase transition in heavy fermion materials and the so-called orbital selective Mott transition [1]. Heavy fermion materials are metallic compounds (for example CeCu_6 , URu_2Si_2 , CeAl_3 and CeCu_2Si_2) containing heavy electrons (effective mass 1000 times the free electron mass) in open 4f or 5f shells and light electrons in broad spd bands [2]. These materials display a $T = 0$ phase transition, which is a purely quantum phenomenon associated with Heisenberg's uncertainty principle. Its understanding represents one of the most outstanding open questions in condensed matter physics.

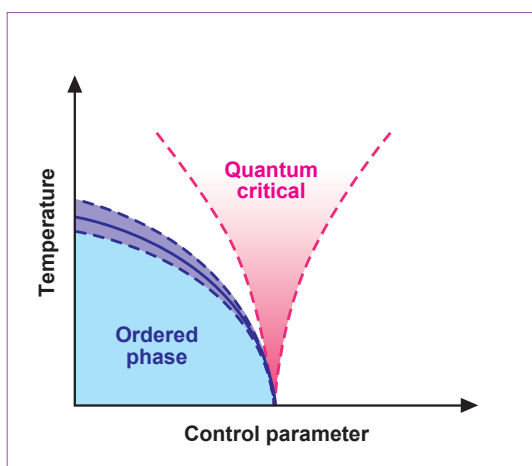


Figure 1:
The quantum critical phase diagram in heavy fermion materials.

Typically in heavy fermion materials, a quantum phase transition between a paramagnetic phase and a magnetically ordered phase can be driven by tuning an external control parameter, such as the pressure, the external magnetic field or doping (see **figure 1**). We describe the $T = 0$ quantum phase transition in heavy fermion systems as an orbital selective Mott transition, using one of the state-of-the-art methods in strongly correlated electron systems, the Cellular Dynamical Mean Field Theory (CDMFT)[3]. We show that this transition is characterized by the emergence of a new intermediate energy scale, corresponding to the opening of a pseudogap in the one-particle spectra of the f-electrons and the vanishing of the low-energy hybridization between the light spd and heavy f-bands. We interpret these phenomena in terms of a Mott localization of particles in the f sub-band and derive particle spectra (**figures 2 and 3**), which can be compared with experimental results from photo-emission experiments.

In **figure 2** we show the evolution of the low-energy local density of states, *f* cluster, as a function of an external tuning parameter V (which represents the external pres-

sure in experiments). The line labelled *f* periodized is the same quantity obtained after introducing a 'periodization' procedure in momentum space, which allows us to extract information that we present in the following. The good agreement between the two curves validates our procedure. We show then the density of states for the spd-electrons (green dashed-dot line) and the effective hybridization (bottom panels, labelled f-spd), expressing the probability for an electron to jump between f and spd bands. These quantities demonstrate that, as a function of V , the system undergoes a phase transition. For $V > V^* \approx 0.58 W$ (where $W \sim 1-2$ eV is the half electronic bandwidth in heavy fermion materials) the system is in the heavy-fermion phase where the f-electrons present a Kondo peak at the Fermi level $\omega = 0$ and take an active part in the conduction. The strong hybridization with the spd-electrons is evident in the suppression of the spd density of states and in the non-zero value of the effective f-spd hybridization close to $\omega = 0$. The intensity of the f-peak is reduced approaching V^* , while at the same time the spd spectral weight enhances. For $V < V^*$ the system is in an f-orbital selective Mott state.

The f-electron spectral weight is not completely transferred from low energy to the Hubbard bands (placed around $\omega \approx \pm 5W$, not shown in the picture) but rather to a new intermediate energy scale, giving rise to a pseudogap. Within this pseudogap the spd-electrons recover the free band density of states and the effective f-spd hybridization is zero. This shows that the spd-band at low energy is completely decoupled from the f-band, but the f-spd hybridization remains active at a finite intermediate energy scale.

We can now display the quasiparticle bands along some specific cuts in the ω - k space, as shown in **figure 3**. We display the f (top row) and spd (bottom row) spectral functions in the path $X = (\pi, 0, \pi) \rightarrow \Gamma = (0, 0, 0) \rightarrow \Pi = (\pi, \pi, \pi)$ of momentum space, for varying hybridization-parameter V (from left to right). The spectral-

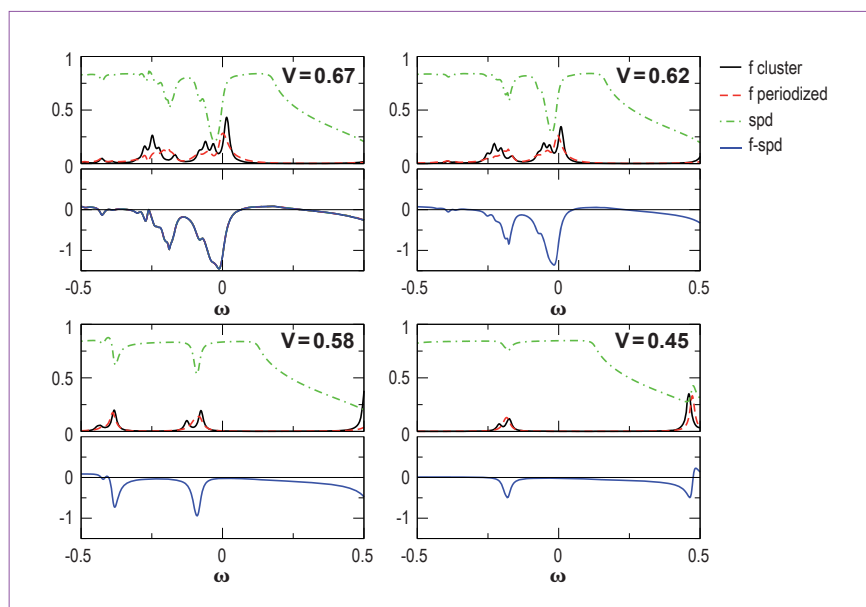


Figure 2: The local density of states as a function of the control parameter V in a low energy window around the chemical potential. Black continuous and red dashed lines are the f -electrons, green dot-dashed lines are the spd -electrons, the blue continuous line the effective f - spd hybridization.

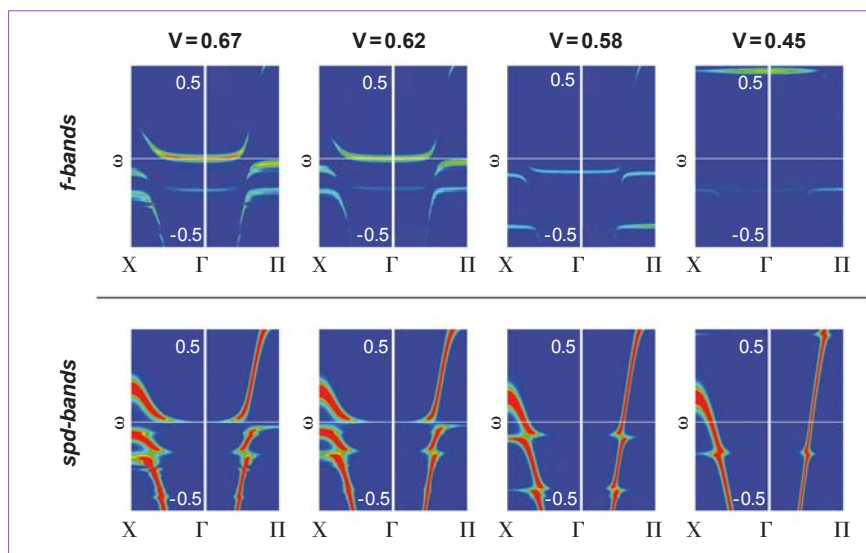


Figure 3: Evolution across the transition point $V^* \approx 0.58$ W of the f (top row) and spd (bottom row) electron spectral functions in momentum space, measurable in photo-emission experiments.

weight contribution to the electronic bands from f - and spd -electrons is very different. For $V = 0.67$ $W > V^*$ the band crossing the Fermi level has predominantly f character at low energy and a strongly renormalized effective mass. On approaching the transition point the f -electron contribution quickly decreases, disappearing completely at the Fermi level for $V \approx 0.58$ $W = V^*$. In addition, beyond the transition the f -band shifts to negative energies. In describing the localization of the f -electrons therefore, the double effect of suppression and translation of the f -band has to be taken into account. At the same time, in crossing the transition, the effective mass of the spd -electrons approaches

the non-interacting value. Our result is a prediction that can be observed in photo-emission experiments.

References

- [1] L. De Leo, M. Civelli and G. Kotliar, Phys. Rev. Lett. 101 (2008) 256404
- [2] H. V. Löhneysen, A. Rosch, M. Vojta and P. Wölfle, Rev. Mod. Phys. 79 (2007) 1015
- [3] G. Kotliar, S. Y. Savrasov, K. Haule, V. S. Oudovenko, O. Parcollet and C. A. Marianetti, Rev. Mod. Phys. 78 (2006) 865

Simulating the rupture of a biomembrane under dynamic surface tension

How long can a fluid membrane vesicle resist rupture when stressed under steadily increasing tension? This article is about developing a theoretical framework that simulates Dynamic Tension Spectroscopy experiments. Using simulations, we have studied the membrane lifetime and distribution of membrane surface tension at rupture as a function of membrane characteristics (energy barrier to failure) and tension loading rate.

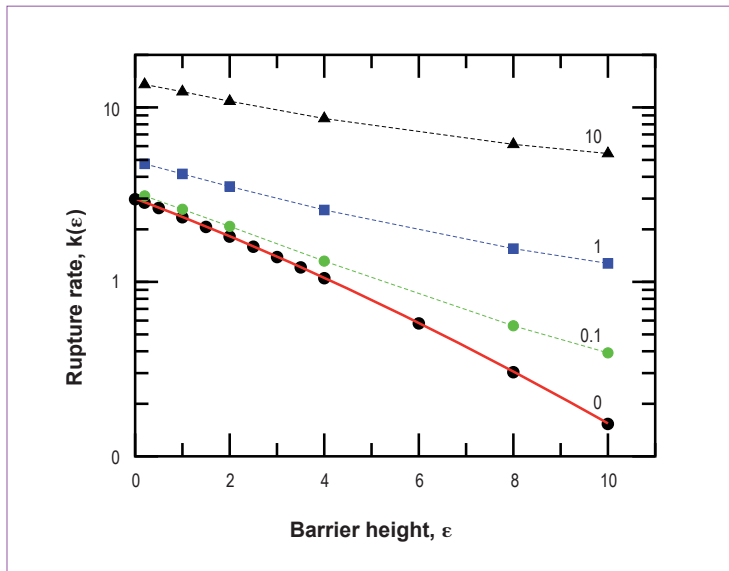


Figure 1: Rupture rate $k(\epsilon)$ as a function of the barrier height ϵ for various reduced loading rates v (quoted numbers). Filled symbols correspond to simulations; dashed lines are guides to the eye, and the solid line through the data relates to an analytical expression.

There are several reasons underlying the general interest in membrane pore formation and dynamics, reflecting both its practical importance and the associated theoretical challenges. A closed vesicle without pores can survive for a very long period of time. Pores can form and grow in the fluid lipid membrane in response to thermal fluctuations and external influences. Several innovative techniques are available for observing transient permeation and opening of pores. These include mechanical stress, strong electric fields (electroporation), optical tweezers, imploding bubbles, adhesion at a substrate, and puncturing by a sharp point. In all instances, the resulting transient pore is usually unstable and leads to membrane rupture for some level of the surface tension. Using the rupturing of biomembranes under ramps of surface tension, the challenge of dynamic tension spectroscopy (DTS) is to identify and quantify the relevant parameters that govern the dynamics of membrane rupture and thereby characterize the mechanical strength of the membrane. Motivated by these experimental investigations and findings, our objective in this work is to develop a theoretical framework of DTS to describing the kinetic process of membrane rupture.

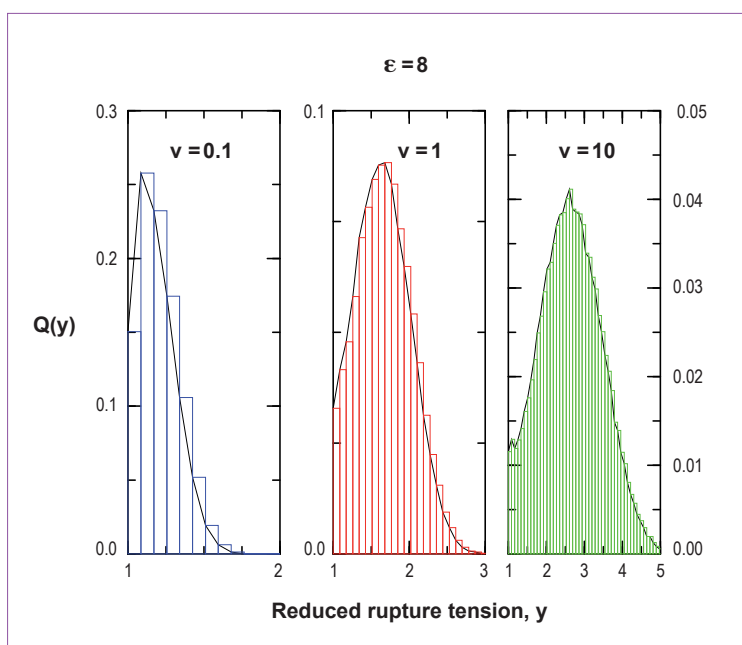
In our description, we treat the membrane as a two-dimensional elastic continuum medium. The net energy $V(r)$ of such a membrane with a circular pore of radius r

consists of two opposing terms: the surface tension $\sigma > 0$, favouring the expansion, and the energy cost $\gamma > 0$ of forming a pore edge (line tension), favouring the closure: $V(r) = 2\pi\gamma r - \pi\sigma r^2$. In DTS experiments [1], the membrane is stressed such that (provided that γ remains constant) the surface tension grows linearly with time as, $\sigma = \sigma_0 + vt$, where σ_0 is the unstressed membrane surface tension and v the dimensionless loading rate constant.

Based on the general framework of Kramers reaction rate theory, we have developed a theoretical framework for DTS to describe the pore growth and membrane rupture dynamics as a Markovian stochastic process crossing a time-dependent energy barrier. The set of stochastic and dynamical equations obtained was used for simulations of the kinetics of the membrane rupture [2].

Simulation results are summarized by the following illustrations. **Figure 1** displays the rupture rate (or the reverse of membrane mean lifetime) as a function of the energy barrier $\varepsilon = \gamma^2/[\sigma_0 k_B T]$ (where $k_B T$ is the thermal energy) and loading tension rate v , and **figure 2** reports the distribution $Q(y)$ of dimensionless tensions y at rupture. As can be seen in **figure 1** the rupture rate (or inversely the mean lifetime) increases (decreases) with loading rate v and decreases (increases) when ε gets larger. Accordingly, the distributions of tensions at rupture depart from a delta function and become wider when both v and ε increase (**figure 2**).

The simulated histograms reproduce already several features observed in DTS experiments in [1]. This is very promising. Note also that dynamic properties are especially important for biological systems since their static characteristics describe mainly a dead structure. Life and biological functions are associated with molecular motions and




the formulation developed in this work can be applied as a working tool to describe, for instance, the opening and closing processes of the membrane pores, or double strand DNA splitting and replication.

Figure 2: Simulated distribution, $Q(y)$, of reduced rupture tensions, y for various values of the dimensionless energy barrier, ε and reduced loading rate, v .

References

- [1] E. Evans, V. Heinrich, F. Ludwig and W. Rawicz, *Biophys. J.* 85 (2003) 2342
- [2] D. J. Bicout and E. Kats, *Phys. Rev. E* (2008) submitted



4 Millennium programme and technical developments

Millennium programme

Technical developments

- 2008 marks the end of the first phase of the Millennium Programme in which we designed and built 6 new instruments and upgraded another 8.

The year 2008 culminated in the commissioning of three of our Millennium Programme instruments, IN5B, FIGARO and D11, an excellent performance by our scientific and technical services. The end of the year saw the official end of the initial phase (phase M-0) of the Millennium Programme, a phase of intense and fruitful activity, in which we designed and built 6 new instruments (BRISP, FIGARO, Lohengrin/MiniBall, SALSA, FLATCONE and VIVALDI) and upgraded another 8 (SuperD2B, D3C, D7, D11, D19, IN5B, IN20 and D22). The M-0 phase also delivered major improvements in the ILL's neutron delivery lines, with major work accomplished on guides H1/H2, H17 and H22.

The effort invested over previous years have brought their rewards; we can be proud of the results now achieved, a factor of 17 improvement in the overall performance of the ILL suite of instruments. This is particularly exciting in terms of new research potential, not to mention the time gains being recorded on standard measurements.

The Millennium Programme, although clearly exhausting, does not drain all the energy of our scientific and technical staff. Normal support services continue to be delivered to the instruments, apparently with great efficiency if the low failure rate is anything to go by. The staff remains motivated and continues to generate new ideas for technical development. Recent work on detector design is a good example: the ILL's new designs are extending the limits of the technology available and the detectors recently built at ILL are helping our instruments deliver what cannot be envisaged elsewhere.

Progress is also being made thanks to the advances being made in scientific computing. The art of computer simulation has been limited in the past by the computing resources available and software difficulties. Simulations remained restricted in scope and value, despite long calculation times. Now, however, with the advent of new techniques and algorithms it is possible to simulate the behaviour of a complete neutron instrument, from source to detector. This has become an essential component in the design of new instruments and their associated support systems (guides, filters, collimating optics,...). Modern simulations offer our development teams a more reliable image of the system in gestation and the balance to be achieved between its constituent parts. This is more than a short-term investment, for the simulation techniques being developed can often be redeployed to serve on very different platforms.

If the health of a research facility can be judged on its technical activity and its capacity to generate energy and ideas, the ILL has passed its test in 2008 - we are fit and ready for the challenges to come.



José Luis Martínez
Associate Director

Millennium programme 2008

In 2008, the first phase (M-0) of the Millennium Programme came to a close with the commissioning of the last three instruments: IN5B, FIGARO and D11. This important milestone represents the culmination of work carried out over the last nine years (2000-2008) by the various teams of scientists and the related technical services of the ILL.

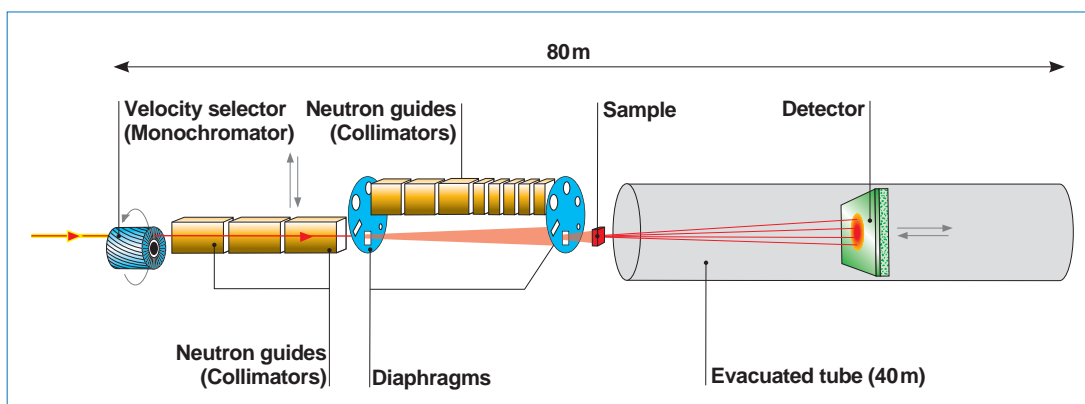
IN5B completed its commissioning phase and was incorporated into the normal scientific programme in November 2008. Its new performance levels clearly make it the most efficient time-of-flight (TOF) instrument in its energy range in the world. The performance increase (global gain factor) with respect to the previous IN5 is of the order of 60, with an optimised energy resolution and acquisition time. One fundamental part of the instrument is the new PSD detector, which covers an angle of 150 degrees, a height of over 3m and a total surface area of 30m² around the sample, with a spatial resolution better than 25 x 30mm². The first experiment runs performed on IN5B have already demonstrated its impressive energy resolution, very low background, excellent differentiation from the direct beam and fast collection time per spectrum. All these improvements will allow the IN5B user community to explore and meet new scientific challenges.

FIGARO, a horizontal reflectometer for the study of fluid interfaces, was also completed in 2008. Initial commissioning with neutrons began in December 2008 and will continue during the first half of the first reactor cycle in 2009. The first neutron reflection and refraction image from a liquid surface (liquid D₂O) was obtained on the last day of the last reactor cycle in 2008. The final alignment of the various optical and mechanical components was achieved without difficulty. The new detector, based on the Aluminium Monoblock Multitube technology, has also proved its worth, demonstrating a resolution better than 2mm in the vertical

direction and a very high dynamic response. Work on finalising the set-up of the sample area and the associated sample environment equipment is under way, in order to be able to start the scientific users programme as of the second half of the first reactor cycle in 2009, i.e. around mid-April 2009.

D11, the Small-Angle Neutron Spectrometer (SANS), has undergone a continuous upgrade programme, which was divided into 3 phases. The first phase involved upgrading the mechanical collimation system, including the diaphragms (2001-2004). During the second phase (2005-2008) the detector vacuum tube and the detector itself were replaced. The new D11 detector is the refurbished D22 detector, with redesigned electronics to achieve very high counting rates at high clock frequencies. The 40m vacuum tank was completely replaced; it is made of aluminium in order to avoid any magnetic interference. Its diameter is 2.2m in order to house the new detector, which is bigger than the previous one. All these improvements were included in phase M-0 of the Millennium Programme. Finally in a third phase (2007-2008), the collimation neutron guides were replaced with new guides made of uncoated Borofloat glass. This final phase is formally part of phase M-1 of the Millennium Programme and is therefore officially the first M-1 project to be completed. D11 began its neutron commissioning phase in December 2008. During the last few days of the last reactor cycle in 2008 many tests were carried out with the new detector in order to fine tune the electronics at very high counting rates and very short sampling times. These tests suggest that the performance of D11 has been greatly improved, both from the Q range obtained as well as from the significant increase in the flux recorded at the sample position. The scientific users programme will begin during the first reactor cycle of 2009 and we anticipate new and exciting scientific results following the renaissance of D11.

Figure 1:
Schematic diagram
of the upgraded
small-angle
scattering
instrument D11.



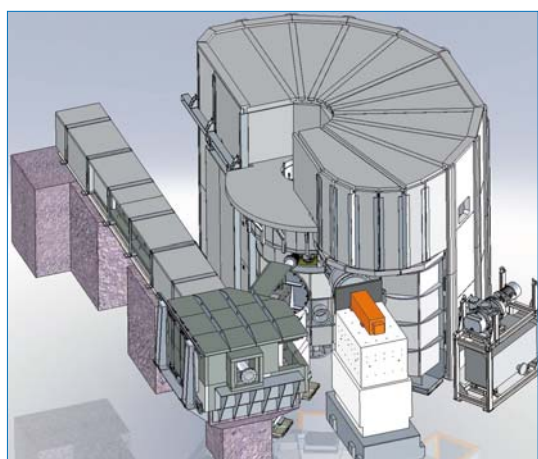


Figure 2: Design study for IN16B showing the massive vacuum chamber on the right.

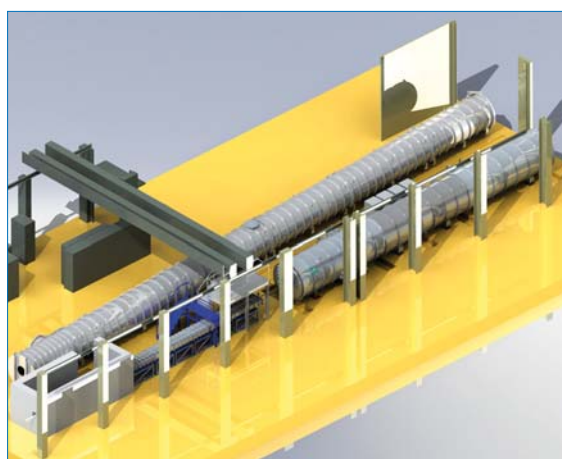


Figure 3: Proposed layout for the projected D33 (foreground) alongside the existing SANS instrument D11.

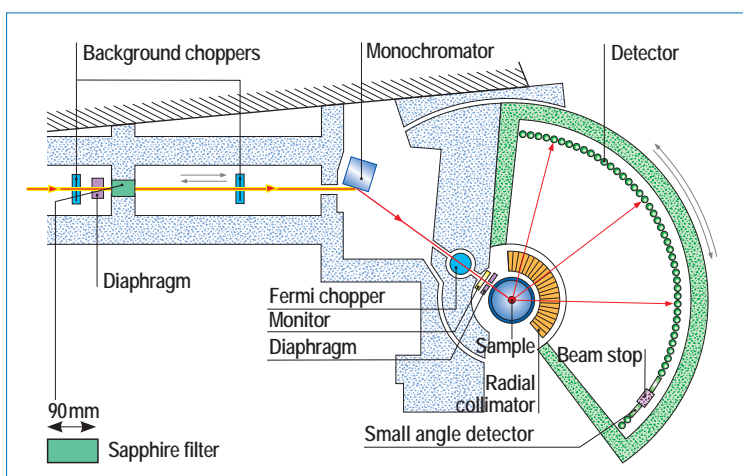
Other projects of the second phase (M-1) of the Millennium Programme are in their design or construction phase. In particular, IN16B has completed its feasibility study and entered the construction phase. Most of IN16B's main components, in particular the Phase Space Transformer (PST) and the massive vacuum chamber, will be ordered in 2009. The assembly and testing of the different components will begin in May 2010, and neutron commissioning is scheduled from September 2011 onwards. The definition and design of the associated neutron delivery system (H112 guide) is almost complete; this new guide will be ordered at the beginning of 2009.

D33, the new SANS instrument devoted to materials science and biology is still being examined in a detailed feasibility study, in order to validate the various technical options available and ensure that the anticipated scientific goals are achieved. A feasibility study is also being conducted for the associated guide H14 in order to produce an optimal design able to supply the best possible solution to a number of different instruments. H14 will in fact be split into three different guides, with different sizes in order to supply neutrons to three instruments: H141 to IN11 (or LADI), H142 to D33 and H143 to IN12.

Most of the M-1 upgrade projects are progressing according to schedule. In particular, D17 is ready for the installation of its new neutron guide, which was delivered by the supplier in December 2008. The new detector, based on similar technology to the FIGARO detector, is under construction and the first neutron tests are expected in mid-2009.

The IN4C project has begun with the installation of a new sapphire filter which has already produced a significant improvement to IN4's enduring background problem. This suggests that further additional shielding for the detector will not be necessary. The new control electronics for the Fermi chopper are currently being manufactured by the chopper supplier and should be installed in the middle of 2009. The main cause for concern at the moment is the ageing positioning electronics of the same Fermi chopper (including the positioning sensors). Work is currently focused primarily on the new monochromator mechanics. A completely new design for the mechanics of the focusing monochromator is under development. The new monochromator system is due to be completed by mid-2009.

Figure 4: Schematic diagram of IN4C showing the newly installed sapphire filter.



The LAGRANGE project (an upgrade of the IN1 beryllium filter secondary spectrometer) completed its feasibility phase in 2008. A new concept for LAGRANGE has been developed in order to be able to compete with similar instruments at ISIS (TOSCA) and SNS (VISION). LAGRANGE's design is based on a large array of analyser crystals that follow an elliptical surface. Due to the specific characteristics of the ellipse, the sample is placed at one focal point and the scattered beam is automatically focussed on the detector positioned at the second focal point of the ellipse. This special geometrical design makes it possible to cover a huge solid angle (2.5 Str.), which greatly increases the counting efficiency while reducing alignment problems. The second advantage of LAGRANGE over its competitors is the possibility it offers to increase or reduce the energy resolution (depending on the primary spectrometer) according to the scientific needs. The global gain of LAGRANGE compared with IN1's previous Be filter is a factor 5 to 6. The project is now in the construction phase and is expected to start the neutron commissioning phase from mid-2010 onwards.

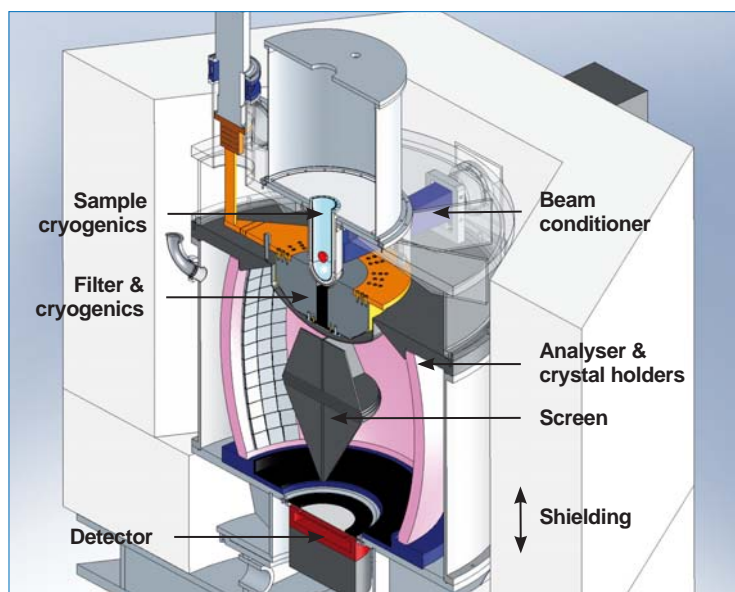


Figure 5: Cross section of the future IN1-LAGRANGE configuration: neutrons scattered by the sample are filtered by a beryllium filter at 100 K, then analyzed and focused on the detector by the elliptical graphite analyzer. An absorbing screen prevents neutrons coming from the sample or from the filter reaching the detector without being analyzed.

GRANIT, a spectrometer devoted to the study of gravitational states, is making good progress. The cleanroom area to house the spectrometer in the reactor hall is almost finished. The new neutron delivery guide (H171) has been installed. The Ultra-Cold Neutron (UCN) source is also in the commissioning phase, as is the monochromator based on intercalated graphite crystals. The analyser mirror and the detector are being constructed. Initial neutron commissioning is planned for June 2009.

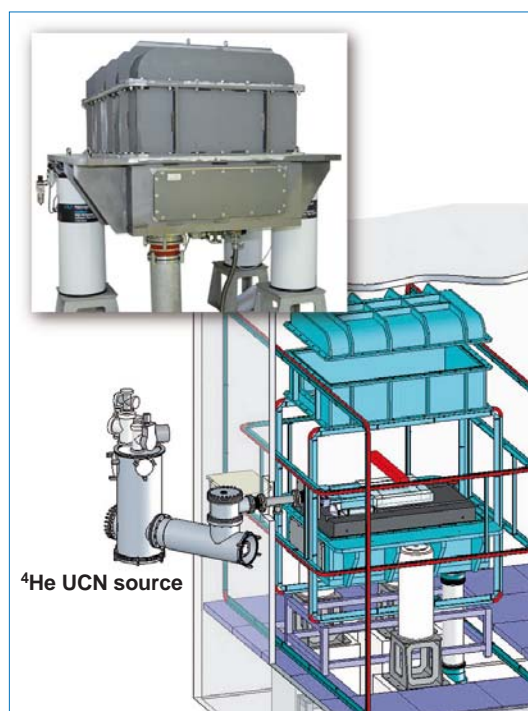


Figure 6: Drawing of the GRANIT spectrometer under construction in the specially-designed clean room inside the reactor hall. The inset photo shows the mirror housing already installed on its vibration-proof supports.

The projects relating to the H5 guide system and the ILL 22 guide hall are planned for the second part of the M-1 phase (from 2011 to 2013). Most of these projects are therefore in the pre-project phase. In particular for THALES, the new triple-axis spectrometer optimised for cold neutrons, work continues on the conceptual design of the different parts of the spectrometer.

Conceptual studies are still under way for WASP, a wide-angle spin echo spectrometer. In particular a small prototype of the supermirror analyser assembly with the corresponding polarizing magnets was tested in the Helmholtz-Zentrum Berlin in early summer 2008 with very good results.

The feasibility phase of the SuperADAM project, a polarized reflectometer being funded as a CRG by the Universities of Bochum and Uppsala, has been completed and the execution phase has already begun. Most of the components have been ordered, in particular the intercalated graphite crystals for the monochromator. The experimental area of SuperADAM will be rebuilt in order to make it possible to change the take-off angle from the monochromator with a corresponding change in resolution.



In 2008 work on rejuvenating the Institute's sample environment facilities continued. A new assembly of liquid nitrogen and helium level meters was designed, built and tested, as were new electronics for controlling the 'orange' cryostat cold valve. The new cryogenic levelmeters and control system are now ready to be installed on the ILL suite of instruments. New CERNOX thermometers were also installed and calibrated on the majority of the 'orange' cryostats. ILL's old 'homemade' temperature controllers are gradually being replaced by new commercial models from the firm Lakeshore.

The process of replacing the cryomagnets continued in 2008. A new 10 T asymmetric cryomagnet was ordered and will be delivered in 2009. A new 7T cryomagnet, optimised for reflectometry, is to be ordered in collaboration with the SuperADAM CRG team.

New power control electronics are now available for the ILL furnaces. These have improved performance and reliability significantly compared with the previous system. Finally, a great deal of effort continues to be devoted to improving the high-pressure capability at ILL. A new high-precision pressure control system for continuously loaded high pressure cells is under construction in collaboration with the CNRS in Grenoble. Moreover a new high-pressure Paris-Edinburgh cell was purchased and is now fully operational.

Figure 7: View of the instrument housing for the SuperADAM project showing the high and low resolution configurations.



Figure 8: Cryogenic control systems showing the cryogenic fluid values and cold valve pressure.

Completion of the IN5 spectrometer project and first results

The modernised IN5 spectrometer received its first neutrons in July this year, marking a milestone toward the completion of the project. The new position-sensitive detector (PSD) array gave encouraging first results that were confirmed later during the commissioning phase. Testing and commissioning took place between July and October and the regular user programme started in November 2008. The opening of this fully upgraded spectrometer to the user community marks the completion of almost 10 years of work to keep IN5 as the world leader in its field.



Figure 1:
Careful positioning of the central part of the time-of-flight chamber after lowering through the opened roof of the ILL7 building.

The intense preparatory work completed last year [1] greatly facilitated the final installation of the time-of-flight chamber, the detectors, the electronics and all the ancillary equipment at the instrument position. The most delicate phase was the installation in early March of the heavy time-of-flight chamber through the opening in the roof of the ILL7 building. Fortunately, on this occasion, the weather was on our side with the sun shining and almost no wind to perturb the delicate lifting operations (**figure 1**).

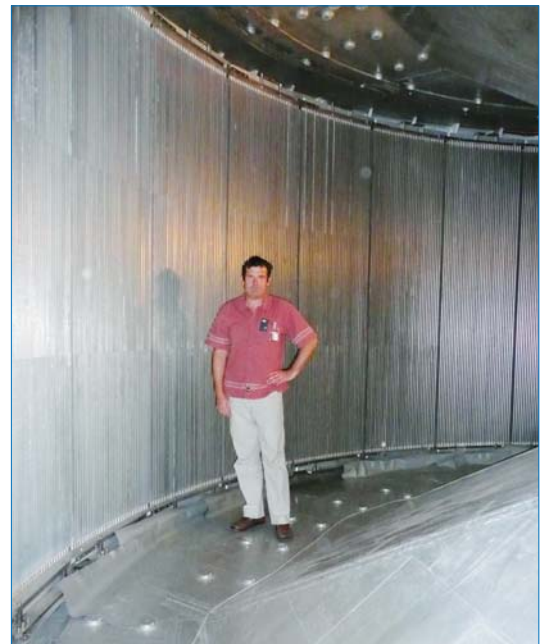


Figure 2: *The detector array in place, ready to work. L. Didier (BE-ILL), 1.80 m tall, shows the scale of the detector surface.*

After fitting the cadmium lining to the internal surfaces, the detectors were mounted on the accurately positioned supports (**figure 2**). The positioning was checked to be within the tolerance of a few millimetres of the ideal 4 m sample-axis to detector-axis distance.

Only a few debugging steps were necessary after cabling and installation of the detector electronics to get the whole 30 m² of detector surface working.

Measurements, using a narrow slit in an absorbing material placed on the detector units, have shown that the spatial resolution is better than 25 mm in the equatorial plane and better than 30 mm at tube edges. Both the efficiency

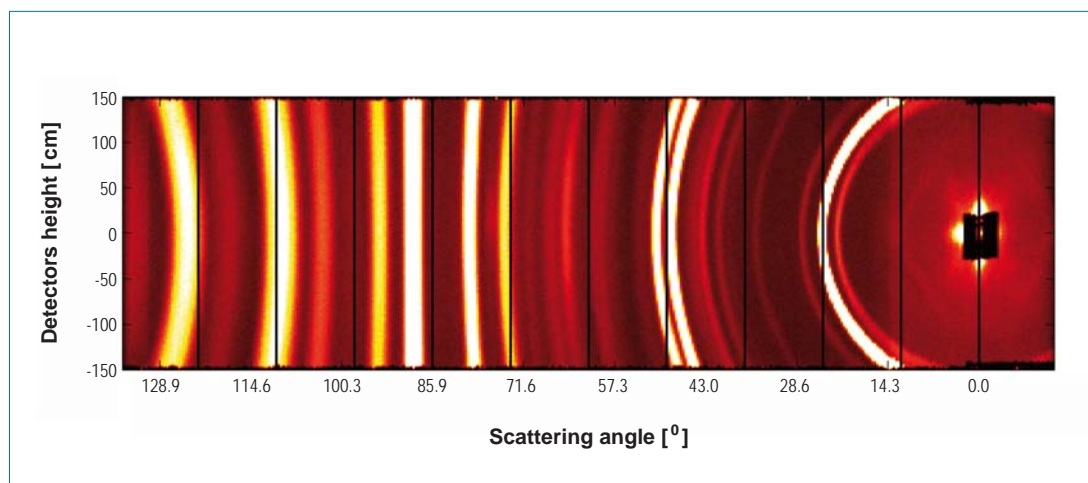


Figure 3: The rich diffraction pattern from an alkali osmate sample at low temperature shows the curved impact of the Debye-Scherrer powder cones with the cylindrical detector surface (image courtesy of H. Mutka).

and gamma discrimination have been found to be excellent with essentially no difference from the former single detector tubes. This characteristic, together with the < 3% tube length spatial resolution, are much better than the initial requirements, thanks to the highly-competent technical development carried out at the ILL detector laboratory. The overall target count-rate gain factor of 60 compared to the former instrument (including the primary spectrometer upgrade) will be easily achieved.

The new vacuum pumps enable the sample environment to be changed in less than 3 hours. The time loss is thus minimal despite the 80 m³ to be evacuated to a working pressure of less than 10⁻² mbar after each change.

New acquisition hardware has been installed to accommodate the 400 Mb to 800 Mb of data coming out from the 10⁵ pixels with time-of-flight analysis. To meet this challenge the NOMAD software has been modified to store the raw data in an efficient compressed format, reducing the data storage needs by a factor of 5 to 10 compared to the initial uncompressed data.

The software developed with the help of the Computing for Science (CS) group, necessary for the analysis of the huge data sets coming out of the new IN5, is fully operational for processing the standard data into a form more familiar to time-of-flight users, while development is under way for single crystal data analysis. Routines are written in the IDL language and integrated into the LAMP package. After a period of validation they are included automatically in the runtime version of the LAMP software allowing any IN5 user to process the data outside of the ILL.

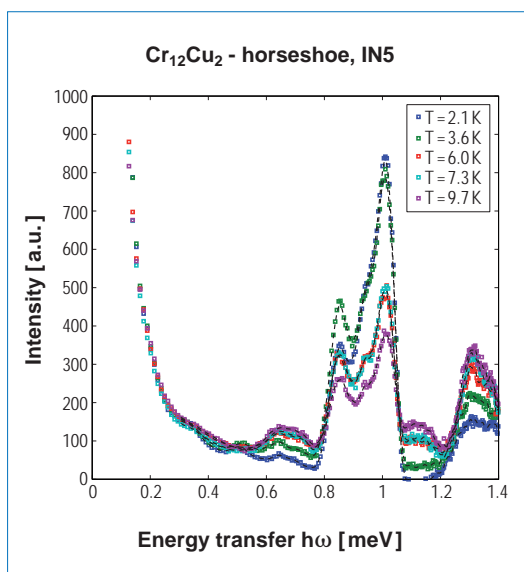


Figure 4: Complexity of the transition line pattern of Cr₁₂Cu₂-horseshoe molecular magnet revealed for the very first time on IN5. The peak maximum at about 1 meV transfer is only of the order of 10⁻³ of the elastic peak height, illustrating the excellent signal to noise capacity of the renewed instrument (image courtesy of M. Baker).

The potential of the densely packed array of detectors in the vacuum chamber is already revealed in the diffraction patterns (figure 3) showing that IN5 is also now a rather good powder diffractometer. Besides, inelastic measurements carried on K-osmates during the commissioning period, on methyl tunnelling with the first regular users and more recently on the Cr₁₂ horseshoe molecular magnet (figure 4), have highlighted the acquisition rate and the excellent quality of the data in terms of signal-to-noise ratio.

References

- [1] J. Ollivier, L. Didier, H. Mutka, ILL Annual Report 2007

D11 reborn — a new benchmark for SANS

The small-angle neutron-scattering instrument D11, one of the first M-1 phase Millennium Projects, has been completely redesigned and rebuilt during an 11-month shutdown in 2008. The work included installation of a new detector on a new trolley inside a new larger and longer aluminium vacuum tank, as well as a complete replacement of 39 m of glass neutron guides on the collimation side. This unique 80 m SANS instrument is now reborn and the upcoming user programme in 2009 will create a new benchmark for SANS.



Figure 1: Jean Aleo aligning the new collimating guides.

Introduction

D11 is the archetype of a long pinhole-geometry instrument, designed for small angle neutron scattering (SANS) studies of large scale structures in chemistry, biology, materials science and solid state physics. D11 has been in operation since 1972 and its unique broad range of momentum transfer, low background and high flux make it the world's leading neutron instrument of its kind.

Although D11 has undergone continual renewal for the past three decades, a major refurbishment has been performed over recent years. The overall strategy for the 3 SANS instruments at ILL (the existing D11 and D22 combined with the upcoming D33 project) ensures the broad versatility of SANS capability at the ILL, while emphasising the particular strengths of each individual instrument. In this respect D11, which has always been widely used for soft matter and biological research, is now being improved to give even higher performance in the particular field of soft matter. Plans for the future include the option of installing a multi-beam USANS.

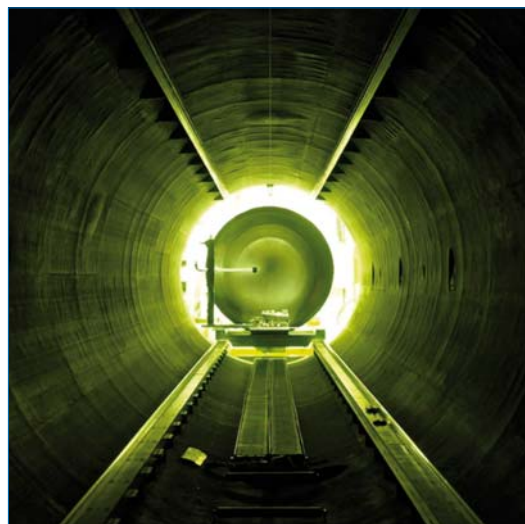


Figure 2: The position-sensitive ^3He multidetector inside the detector tank.

The collimation renewal

The collimation of the incident beam is carried out on D11 by a system of moveable neutron guides, following the principles described by Ibel *et al.* [1, 2]. Significant flux gains were predicted recently at D11 for the whole range of collimation distances with McStas simulations based on new collimation geometry [3]. The complete collimating neutron guide section has now been replaced by an innovative guide design: the 39 m of straight glass guides with constant cross section were replaced with an uncoated Borofloat guide system with a diverging section, increasing the guide width over the first metres by about 50% (to 45 x 50 mm width x height), and a focusing section over the last few metres. Part of the guide housing (18 m) has been replaced with a new aluminium housing and the mechanical stability of the guide movement has been greatly improved over the whole 39 m (**figure 1**).

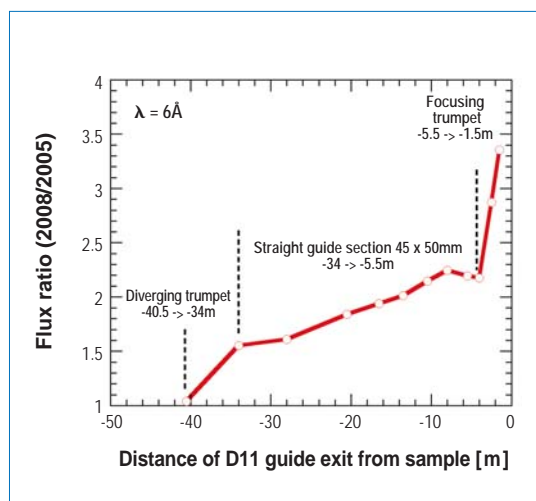


Figure 3: Measured flux gain (2008) compared to 2005.

First results show that the instrument performs with the new guides even better than estimated. **Figure 3** shows the gain in neutron flux measured at the sample position as a function of the collimation distance (= guide length in front of the sample position), compared to 2005. The gain of more than 50 % has been measured for long (≤ 34 m) to intermediate collimation distances. At short collimation distances (≤ 5.5 m) the flux increases very strongly due to the performance of the focusing guide section. The maximum flux for wavelength $\lambda = 6 \text{ \AA}$ (FWHM $\Delta\lambda/\lambda = 9\%$) is now $9.7 \times 10^7 \text{ n cm}^{-2} \text{ s}^{-1}$ (compared to $2.8 \times 10^7 \text{ n cm}^{-2} \text{ s}^{-1}$ in 2005).

Furthermore, new collimation distance positions have been introduced, thus providing optimised flexibility for the choice of the operating conditions: the measurable range of momentum transfer regarding low Q now allows for an easier overlap with results from other scattering techniques like light scattering. A new system of beam-defining apertures along the collimation section has increased the flux for ultra-low Q measurements by a factor of 10.

A larger and faster SANS detector

Another highlight of the recent upgrade step is the development of a larger and faster ^3He detector [4] (used by D22 before its electronic upgrade). This new detector (**figure 2**) is installed on a new compact trolley in a new detector tube with both increased diameter (2.20m) and length (40m), thus raising the dynamic range and the resolution each by a factor of 2. The new detector enables count-rates 6 times higher than at present and the range of momentum transfer Q is extended to both to higher and lower Q for a given geometry.

The measured flux gain at the sample position is well transported to the detector. The comparison with the old installation is illustrated in **figure 4**. Shown is an example of the operating range of D11 for a standard wavelength of 10 \AA , scaled to the same detector resolution (enhanced area bounded by the red lines: new instrument ≥ 2008 , black: old ≤ 2007). Results are interpreted in terms of the "instrumental constant" $C(\lambda)$ (flux on the detector per unit detector cell solid angle) as a function of the available range of momentum transfer. $C(\lambda)$ characterises the performance of the instrument for a given configuration (wavelength, selector bandwidth, collimation distance, sample-to-detector distance, detector efficiency and detector resolution).

At the new D11, with its extended range of momentum transfer Q (due to the larger size of the new detector) only 3 sample-to-detector distances are necessary for measuring the complete scattering curve from Q_{\min} to Q_{\max} , compared to 4 distances before. At the same time, the flux on the detector is significantly increased.

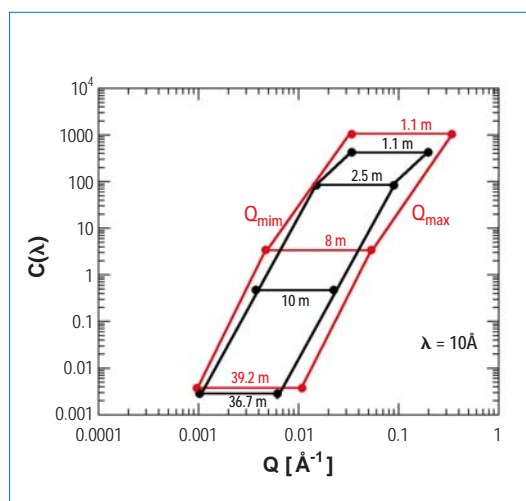


Figure 4: The operating range of D11: instrumental constant vs. momentum transfer. Black: ≤ 2007 . Red: ≥ 2008 . $C(\lambda)$ is the flux on the detector per unit detector cell solid angle.

References

- [1] K. Ibel, J. Appl. Cryst. 9 (1976) 296 - 309
- [2] P. Lindner, R. P. May, P. A. Timmins, Physica B 180 & 181 (1992) 967 - 972
- [3] K. Lieutenant, P. Lindner, R. Gahler, J. Appl. Cryst. 40 (2007) 1056 - 1063
- [4] P. Lindner & R. Schweins, ILL Technical Report (2006) ILL06 LI 02T

■ Authors

R. A. Campbell, I. Sutton, S. Wood,
R. Cubitt, G. Fragneto and the FIGARO team

The commissioning of FIGARO

The commissioning of FIGARO with neutrons started in the last cycle of 2008. This year has seen the installation of the majority of the components of this new reflectometer, devoted to the study of soft matter and biology at horizontal surfaces. Reflectometry measurements started in December 2008, but the instrument will be delivered in its final configuration at the start of the first cycle of 2009. 70 days beamtime were allocated at the last proposal round. The current status of the instrument is described below.

Guide: During the long winter shutdown (early 2008) the H171 neutron guide that feeds FIGARO was extended out from the reactor hall right up to the instrument. The guide is coated with M=2 supermirrors on the sides while the coating changes progressively from M=2 to M=1 on the top/bottom surfaces and its section is $15 \times 80 \text{ mm}^2$ ($w \times h$) at the reactor exit and $30 \times 80 \text{ mm}^2$ at the start of the instrument. The greater height at the instrument takes into account the vertical divergence of the beam. The guide geometry is tailored to the needs of the reflectometer and special attention has been paid to ensure the transport of a high intensity beam devoid of fast neutrons and radiation. The installation was achieved in two phases by teams of technicians from the ILL DPT and guide manufacturers Swiss Neutronics. The end result was a high-performance guide delivered in time to commission FIGARO with a measured flux ($1.5 \times 10^{10} \text{ n/cm}^2/\text{s}$ from gold foil measurements) about 10% above theoretical predictions.

Frame-overlap mirrors: Two frame-overlap mirrors with nickel-coated silicon mirrors inclined at 2° and 3° remove neutrons with wavelengths above 20 and 30 Å, respectively. The guides were installed during the summer and October shutdowns. It will be possible to switch remotely between the two mirrors during the course of an experiment.

Choppers: The four chopper discs and guides have been installed and tested with neutrons. In the final configuration, where the maximum TOF distance is 8505 mm, chopper speeds of 960-1560 rpm provide pulses of neutrons with a choice of 6 different $\Delta\lambda/\lambda$ values in the range 1.3-11.5%.

Deflector mirrors: The two deflector mirrors were installed during the summer shutdown. The first guide is 1450 mm and the second 805 mm long. They are coated on all four

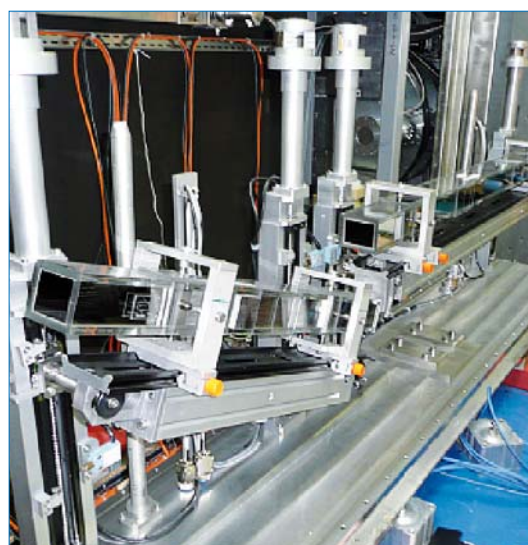


Figure 1: The two deflecting guides

internal faces with M = 4 supermirrors with reflectivities better than 0.8 to allow for reflection up or down at the sample position. They are both 50 mm high and focus the beam in the horizontal direction with a width decreasing linearly from 80 to 60 mm. **Figure 1** shows a picture of the guides being installed.

Collimation guide: The collimation guide was installed during the October shutdown. It is a two-metre guide focusing the beam from 60 to 40 mm in the horizontal direction thanks to M = 4 supermirrors. The reflectivity of the mirrors is about 0.8 everywhere. On the top and bottom faces, the guide is made of glass with B₄C blades stopping reflected neutrons. A μm -precision collimation slit is mounted at the start of the guide.



Figure 2: Sample area: The goniometer is visible on top of the vertical translation rig. The yellow lead door is closed during measurements.

Sample area: A purpose-built goniometer with horizontal translation drive was mounted on a vibration-damping stage (ILL high-precision super-stiff vertical drive) fitted in a 3 m pit below the sample position, isolated from the floor. Sample environments (with a weight capacity up to 1000 kg) will sit on an anti-vibration table (Halcyonics) and can be translated 500 mm in the direction perpendicular to the beam to enable automatic sample changing. An optical alignment device will help optimise reflection conditions during experiments with free liquids. A μm -precision slit and a monitor are situated in front of the sample. Another slit will be installed after the sample in front of the detector nose.

Sample environment: FIGARO will have a range of sample environments. A Langmuir trough, which is ready for measurements, will be used for the study of insoluble films at different surface pressures. Simultaneous images of lateral organisation may be acquired *in situ* using a Brewster angle microscope. A suite of 6 thermalised adsorption troughs will be available next year to enable the study of adsorption phenomena over a range of temperatures. The reflection-down configuration of the instrument will be used for the study of solid/liquid and liquid/liquid applications where it is important to have a horizontal geometry of the solid substrate. Work will also be carried out to develop a dynamic flow cell for the study of adsorption kinetics.

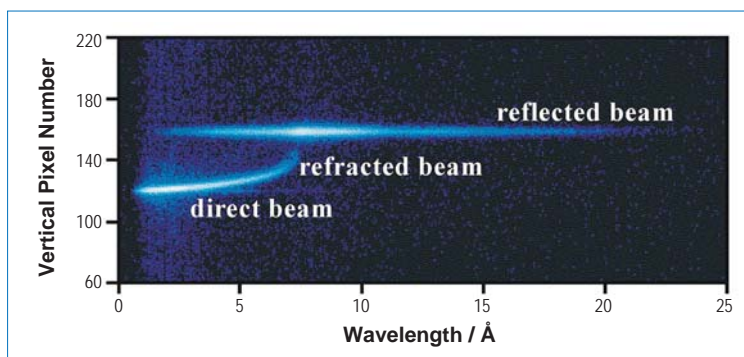


Figure 3: Time-of-flight reflectivity image of a free D_2O surface acquired at the beam axis incident angle of 0.67 degrees to the horizontal.

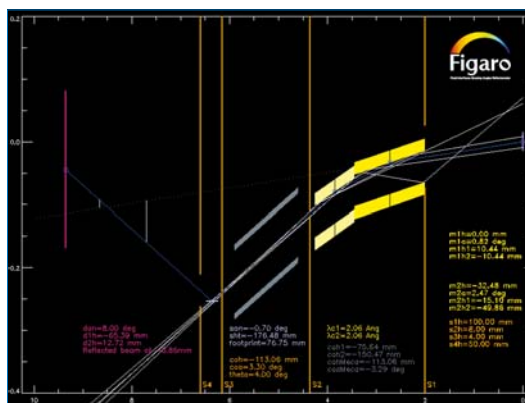


Figure 4: Output IDL programme which shows the positions of all the axes when the incoming angle is changed.

Detector: The 2D aluminium monoblock detector has been installed for commissioning, positioned two metres from the sample, but will be repositioned at three metres in the final instrument configuration from the first cycle of year 2009. The monoblock detector comprises 64 holes, 250 mm in length and with a $6.9 \times 6.9 \text{ mm}^2$ square section. The block is filled with ^3He and provides a resolution along the tubes better than 2 mm. A Time-of-Flight reflectivity image of a free D_2O surface acquired at the beam axis incident angle of 0.64 degrees to the horizontal is shown in **Figure 3**.


Software: NOMAD software is being implemented on the instrument. All motors can be driven and data acquired with this software. A programme was written in IDL to calculate the motors positions that control the deflector mirrors, collimation guide, slits, sample and detector. **Figure 4** shows an example of the output from this programme.

We wish to thank everyone in the team for their effort and enthusiasm in building and commissioning the instrument.

■ Authors

E. Lelièvre-Berna, E. Bourgeat-Lami, T. Hansen, M. Thomas, X. Tonon, J. Torregrossa, F. Bordenave, P. Courtois, D. Jullien, P. Mouveau and G. Manzin (ILL)
A. S. Wills and A. Poole (University College London, UK)

Spin-polarised powder diffraction



The polarised neutron technique used on D3 is a very sensitive method and certainly the most powerful tool for determining magnetisation distributions in the whole volume of the unit cell. The measurement of polarisation-dependent cross-sections reveals unambiguously the spin delocalisation, the polarisation sign, the density shape and the effects of magnetic interactions. Combined with specific data analysis tools, it gives access to very precise quantitative results. It is even sometimes possible to separate precisely the spin and orbital contributions. However, it only applies to single crystals that are magnetically ordered in a ferro- or ferri-magnetic phase under an applied magnetic field or to particular antiferromagnets. The lack of installation on a powder diffractometer has, in the past, prevented the investigation of most molecular magnets and nano-systems. We present here the realisation of a high-flux polarised neutron diffractometer with variable resolution taking advantage of the recent ^3He spin filter developments.

We have implemented a polarised neutron option on the powder neutron diffractometer D20 [1] for investigating molecular magnets, biological samples and nano-systems. A first very successful attempt [2] had been accomplished on the instrument D1B with the magnetostatic cavity **Cryopol** hosting a ^3He neutron spin filter in the stray field of a cryomagnet [3]. Motivated by the results, we have constructed a second-generation Cryopol, a spin rotator optimised for the 20 cm high monochromator and guiding coils.

Cryopol-II is a cryogen-free cryostat that fits perfectly the beam profile of D20 (**figure 1**). It consists in a superconducting Nb cylinder surrounded by soft magnetic screens. We trap inside the Meissner chamber a homogeneous magnetic field that is used to maintain the polarisation of the ^3He gas polarised on Tyrex [4]. The neutron beam entering Cryopol-II is polarised by the ^3He cell. At the exit, a magnetic field is applied parallel or anti-parallel to the field trapped in Cryopol-II. This way, we flip the neutron polarisation with perfect efficiency whatever the field applied on the sample or the wavelength used.

The incident beam polarisation is monitored permanently using two nitrogen monitors M_1 and M_2 located before and after Cryopol-II. The polarising efficiency ε is simply deduced from the counts of these two monitors with the expression $\varepsilon^2 = 1 - (M_{20}/M_{10})^2 / (M_2/M_1)^2$ where M_{10} and M_{20} are the monitor values measured with the ^3He gas depolarised.

With the world's largest spin filter cells built specifically for D20 ($10 \times 8 \times 22 \text{ cm}^3$), the relaxation decay is about 120 hours at 2.2 bar, which is clearly enough for powder diffraction measurements lasting a few hours. During an experiment, care must be taken to check the absence of beam depolarisation between Cryopol-II and the sample position due to instrument imperfections. This is performed using a Heusler crystal taped on the vanadium can of the sample. The depolarisation in the sample itself is also measured by rotating the sample can by 180° . The experiment consists in collecting [+] and [-] spectra following the [+][-][+] repeated sequence so that we do not integrate the decay of the beam polarisation into the data (first order correction).

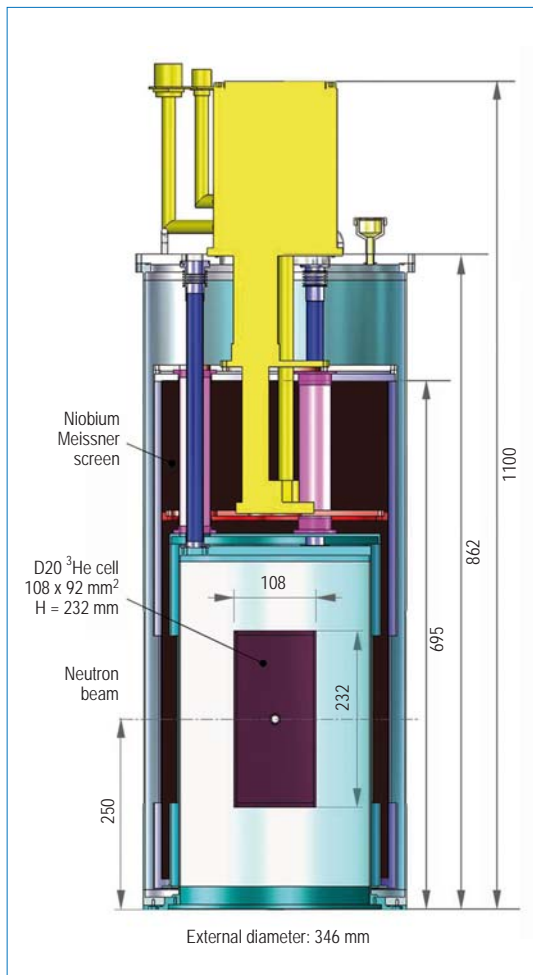


Figure 1: Drawing of Cryopol-II. The volume of the D20 spin cell is represented inside the chamber.

The polarisation decay being quite small inside one sequence, we calculate the difference of the [+] and [-] spectra for each sequence. The difference spectra obtained are then corrected for the transmission of the ^3He gas and the polarising efficiency of the spin filter that are time-dependent functions. The data can then be averaged over all collected

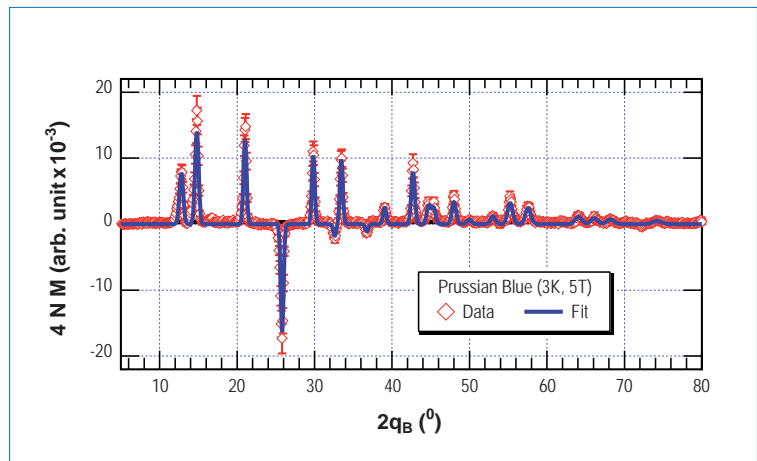


Figure 2: Difference diffraction spectra collected in 8 hours on Prussian Blue at 3K, 5T and 1.30 Å.

sequences and corrected for the transmission of the glass of the cell and depolarisation factor of the sample. We obtain difference spectra proportional to the interference term of the scattering cross-section 4.N.M whose scale factor is identical to the one of the spectrum collected in the nuclear phase with a non-polarised beam (i.e. without cell). **Figure 2** shows the first difference spectrum collected with Cryopol-II in 8 hours on Prussian Blue at 3K under 5T. This new polarised neutron option is now available on the high-flux powder diffractometer D20.

References

- [1] T. C. Hansen, P. F. Henry, H. E. Fischer, J. Torregrossa and P. Convert, *Meas. Sci. Technol.* 19 (2008) 034001
- [2] A. S. Wills, E. Lelièvre-Berna, A. Sella, F.G. Cloke, P.L. Arnold, F. Tasset, J. Schweizer and R. Ballou, *Physica B* 356 (2005) 254
- [3] J. Dreyer, L. P. Regnault, E. Bourgeat-Lami, E. Lelièvre-Berna, S. Pujol, M. Thomas, F. Thomas and F. Tasset, *Nuc. Inst. Met. Phys. Res. A* 449 (2000) 638
- [4] K. H. Andersen, D. Jullien, A. K. Petoukhov, P. Mouveau, F. Bordenave, F. Thomas and E. Babcock, *Physica B*, in press

■ Authors

P. M. Bentley and K. H. Andersen (ILL)

J. Saroun (Nuclear Physics Institute, Rez, Czech Republic)

Speeding up instrument simulations: from 25 hours to 55 milliseconds in 8 months

Simultaneous optimisation of all adjustable instrument parameters is becoming increasingly attractive and feasible using modern, fast computing hardware. Artificial Intelligence algorithms such as genetic algorithms or particle swarms are particularly good at these tasks. The bottleneck is the time taken for one evaluation of the instrument, because many evaluations are needed. During the last eight months, we have made significant progress in speeding up instrument modelling. Here we present an overview of two user-friendly techniques.



Figure 1: Optical ray tracing: 'The wet bird', by Gilles Tran © 2000 www.oyonale.com

Monte-Carlo (MC) simulations trace the progress of neutrons outwards from a moderator through an instrument. They include all important physical details, and these days the agreement between simulations and real experiments is quite good, allowing scientists to perform 'virtual experiments' with realistic samples and detectors.

In optical ray-tracing, used for many years in the arts and movies (e.g. **figure 1**), the tracing direction is the opposite to that used for neutrons: rays are traced outwards from the focal point of the camera. Tracing rays outwards from the sources of light would be wasteful because only a tiny fraction of light trajectories reach the camera. Similarly, most neutron trajectories leaving the moderator don't reach the sample. To have a high flexibility, the beam properties are defined close to the sample by passing through narrow slits, monochromators, or choppers. This means that most of the 'throwing away' is done near the sample to define the resolution. If all these neutron trajectories are traced from the moderator only to be discarded right at the last moment then there are a lot of wasted CPU cycles.

To give an idea, a MC simulation of the D22 SANS instrument with 12% uncertainty on the flux takes around 11 minutes with the finest resolution settings, even when trajectories are generated so they all enter the guide. Starting with 100 000 000 trajectories leaves only 70 or so that reach the sample! Things get worse if we want smaller uncertainty: 25 hours are needed for <1% errors, which is crucial for fine-tuning instrument parameters.

The same 1% simulation when run in reverse, i.e. starting at the sample, takes just 2.8 seconds, and from 500 000 starting trajectories ~15 000 remain. We have shown [1] that tracing should start at the place with the most restrictive geometry. At early stages the correct simulation direction may indeed be to begin at the moderator for guides, but if a sample is included then the direction should probably be reversed.



Figure 2:
Polygon graphics rendering in Half Life 2, Valve Software © 2008.

Optical ray-tracing can take many minutes or hours, but polygon methods can render convincing scenes (**figure 2**) at 30 frames per second or more. If we could apply a raster-type method to neutron simulations, grouping similar trajectories into polygon bunches, we should get a similar speed increase. The question is how best to group the bunches. Acceptance diagrams can help here: they are parameter space maps of position and divergence regions that are transmitted by modules.

To follow guide reflectivity curves with high accuracy, polygon division should also occur along discontinuities, e.g. one cut along $m = 1$ (the critical angle for air-Ni surfaces) and the other at the critical angle for a supermirror. Our calculation method called neutron acceptance diagram shading (NADS) is based on these methods [2]. The calculations for the bunches, even including gravity, are four simple operations: reflection, translation, cutting and shearing. The same kind of speed improvement as for computer graphics is found for neutrons: the 25 hour simulation of D22 takes around 30 seconds with NADS. If we model backwards by starting the trajectories at the sample, then the D22 calculation takes just 55 milliseconds.

Using these methods, a whole instrument optimisation can be performed on one CPU core in minutes. It will be put to the test by optimising the design of the H5 guide splitter, simultaneously optimising the instruments D22, IN15, WASP, ThALES, SuperADAM and D16 as part of the Millennium Programme.

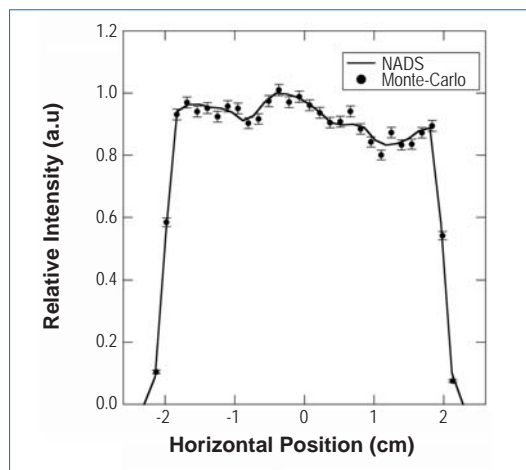


Figure 3: Agreement between ray-tracing and NADS for neutrons. This graph shows the variations in beam intensity (caused by a curved guide) as a function of horizontal position for the SANS instrument D22.

References

- [1] P. M. Bentley, J. Saroun, K. H. Andersen, in preparation for submission to NIMA
- [2] P. M. Bentley, K. H. Andersen, accepted for publication in NIMA (January 2009)

Neutron detector development



The emergence of Linear Position-Sensitive Detectors (LPSD) has contributed to enhancing the quality of neutron instruments in Small-Angle Neutron Scattering (SANS) and Time-Of-Flight (TOF) spectrometry. These detectors provide a cost-effective solution for covering a large sensitive area with a high counting rate capability at a modest but acceptable spatial resolution. However, single crystal diffractometers (SXD) and reflectometers are still limited by the position resolution of their detector and/or its maximum sustained counting rate. Although applying the best available detector technology to build a new instrument or to upgrade an existing one does not contribute to the evolution of the technology, introducing innovation into instrument projects often means taking risks. New concepts can only be integrated into such projects when they have proved their performance and reliability within an acceptable confidence level. In this article we describe recent contributions by ILL to neutron detector development in four types of project having different levels of innovation risk: instrument upgrades, new instruments, small-scale R&D projects and international collaboration projects.

Instrument upgrades

For an existing instrument, there is always the risk of losing users due to competition from more recent, higher-performance instruments in the same field. Innovation is then vital if an instrument is to maintain its level of excellence. Several instruments have been upgraded at the ILL over the last few years through the addition of state-of-the-art detectors, in particular MSGCs (Micro-Strip Gas Chambers) and Multitubes. It is interesting to look at some aspects of how instrument upgrade projects have been managed.

The **D20** instrument's position as leader in powder diffraction is partly due to the unequalled performance of its MSGCs, which began stable operation in 2000. MSGCs are better than other detectors for counting rate capability, uniformity of response, and gamma insensitivity. The D20 detector upgrade project encountered a series of technical difficulties, which thwarted all our attempts to adhere to a strict timetable. The MSGC development was supported firstly because it immediately produced promising results but also since no alternative solution was in sight. 12 years of epic development work have resulted in the most significant innovation in the field of radiation gas detectors since the MWPC (Multi Wire Proportional Chamber). The MSGC was the starting point for several MPGDs (Micro-pattern Gas

Detectors) currently being studied for high energy physics. After operating the D20 detector for 9 years, we can now say that the MSGC technique, although sensitive to handle, is a mature, reliable, high-performance and underexploited technique. In 2008, demands to increase the counting rate for neutron reflectometry have prompted the study of a new MSGC, which will be described later in this article.

The **D22** instrument is the leader in SANS instrumentation, in particular due to its combination of a high flux and a fast detector. The so-called multi-LPSD, in operation since 2004, was developed with the support of the TECHNI project within the European FP5 framework programme. It is composed of 128 LPSDs mounted side by side on a mechanical support. A counting rate of 3 MHz has been measured with negligible efficiency loss. A new detector, known as the Multitube, came into being during this project. Here, the stainless steel tubes are welded at both ends to two gas-tight vessels, sharing the same gas volume. This design makes it possible to reduce fabrication and material costs compared to LPSDs.

In 2008, the **IN5** time-of-flight chopper spectrometer was upgraded a very large Multitube system. The detection system consists of 12 identical modules placed side by side, each made up of 32 stainless steel tubes 25.4 mm



Figure 1: The 3 m-long tubes of the IN5 detector welded on the flange with the orbital weld head.

in diameter, 0.5 mm thick and 3 m long. The IN5 detector is the largest ever built for neutron instrumentation: it covers an angular range of 150° of a 3 m high cylinder and has a sensitive area of 30 m^2 ; the total volume of ^3He is 3000 litres. The IN5 project is an exceptional achievement considering the production constraints that had to be satisfied: the average production time for a module is around one month. This very tight schedule was made possible by carrying out several tasks in parallel. In fact, 3 modules were handled at the same time at different stages in their production: assembly, outgassing and testing. Each of these stages was the subject of quality controls. Although the fabrication process was well mastered, the main risk concerned the organisation of the production process.

New instruments

Building a new instrument involves assembling many separate parts, including new functionalities. Scientists usually prefer not to add the additional risk of a non-proven detector. The duration of the pre-study phase of the project, between budget approval and finalisation of the design, is generally less than one year. This leaves enough time to optimise a technical solution that is close to maturity, but not to invent a new concept. For the new **FIGARO** detector, this period was dedicated to the study of the "Multitube monoblock", where tubes are carved from an aluminium monoblock via Wire Cut EDM (Electron Discharge Machining). Compared to the previous Multitube, the new one is more robust and provides better mechanical fabrication accuracy. Because aluminium is more transparent to neutrons than stainless steel, a minimum of neutrons is lost in the entrance window. The detection efficiency is further increased by machining the tubes with a square or rectangular section. FIGARO's detector has 64 square channels, $6.9 \times 6.9\text{ mm}^2$, 300 mm long (250 mm active length), separated by walls 0.5 mm thick. The detector's entrance window is 5 mm thick; the gas mixture contains $8 \times 10^5\text{ Pa}$ of ^3He and $2 \times 10^5\text{ Pa}$ of CF_4 .



The wires, 20 microns in diameter, are stretched in the middle of the channels and held in position using polyimide supports. The new FIGARO detector was installed on the instrument at the end of 2008, and has already measured its first reflections.

Figure 2: Walking in the TOF chamber of IN5 fully equipped with the 12 Multitube modules.

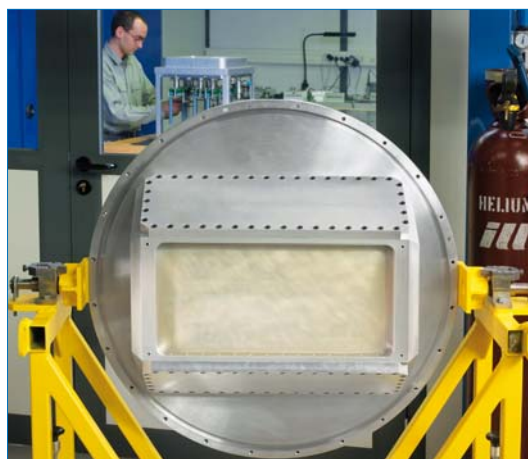


Figure 3: The FIGARO Monoblock Multitube being tested on the CT2 test beam line; for this test, the detector was mounted on the flange of the vacuum flight tube of the instrument. The charge division electronics are mounted behind the tube flange. The sensitive window is materialised by the rectangle in the centre of the photo. The tubes are machined vertically by spark erosion into a single block of aluminium. Gas tightness is provided by two plates mounted with elastic metal seals.

Small-scale R&D projects

Over and above large-scale projects, small R&D projects, managed in laboratories without any formal planning process and with a small budget, are the source of most innovations. Work progresses at a natural rate, which depends mainly on the workload in the laboratory and the funding available, and is often slowed down by a lack of resources. One such project, the MSGC200_ddc detector, began in 2001. Its objective was to combine the high resolution power of MSGCs with the high counting rate capability of parallel cells by charge division readout. A “virtual cathode” layout, with anodes on the front side, and cathodes on the rear side, was used to make the connection of the anodes at both ends easier for charge division readout. A resolution of 1.3mm FWHM was measured in the direction of the anodes, but the detector could not be used for reflectometers because of its count rate limitation: A degradation of the detection efficiency started to occur above 3kHz per mm of anode strip. This effect was due to the charging up of the substrate inducing electric field distortions and thus a local decrease of the amplification gain. The project was therefore put on hold after these preliminary tests. It was reactivated in 2008 with the fabrication of a new MSGC using the same readout scheme and standard photolithography (anodes and cathodes on the same side). First tests are planned at the beginning of 2009. Small R&D projects can also sometimes offer unexpected solutions to old technical problems. As an example, the honeycomb Multitube

Figure 4:

The honeycomb multitube is made of 37 hexagonal tubes, 20 cm long, machined by Electron Discharge Machining from a single piece of aluminium. Anode wires, centred in each tube, will be connected to individual amplifier and comparator circuits.

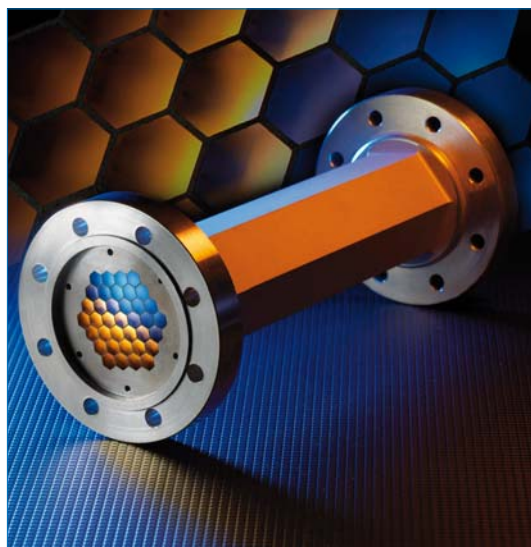


(figure 4), has the functionality of a single counter, but is segmented into independent cells to sustain a count rate of 500 kHz, a factor of 20 better than with a single wire counter. EDM provides a very efficient way to segment a large diameter detector without introducing dead zones. A prototype of this new detector was made shortly after the ILL was equipped with an ED machine for mechanical development.

International collaboration: the MILAND detector for SXD and reflectometers

The MILAND (Millimetre Resolution Large Area Neutron Detector) Joint Research Activity started in 2004 within the NMI3 project (Integrated Infrastructure Initiative for Neutron Scattering and Muon Spectroscopy) with the aim of improving neutron detectors for single crystal diffractometers (SXD) and reflectometers. More than thirty people, coming from seven European institutes (BNL, FRM-II, GKSS, ILL, ISIS, LIP, LLB), plus Tokyo University, took part in this development. Several techniques, all based on the capture of neutrons in ^3He , were studied in parallel during the first two years. The MWPC with individual readout offered the best compromise between technical risk and performance levels. The detector (figure 5) has a sensitive area of 320 mm x 320 mm, and a pixel size of 1 mm x 1 mm. It is based on a MWPC with a wire pitch of 1 mm, mounted inside a pressure vessel filled with a gas mixture of ^3He and CF_4 at 15×10^5 Pa. The pressure vessel is separated into 2 distinct volumes: the detection chamber and a gas buffer with a spherical window in front of it. Each volume is connected to a pressure compensation system which overcomes the effects of temperature gradient or gas leaks. The high gas pressure combined with the thin active volume (5mm) reduces the parallax error and thus enables the sample-to-detector distance to be minimised without compromising spatial resolution. This is particularly interesting for SXD instruments which require both a large angular coverage and a high spatial resolution. The active volume of the detector is extendable to 20mm by simply applying a negative voltage on the back drift electrode. This mode of operation, suitable for reflectometers, enables the detection efficiency to be increased for short wavelength neutrons. 20 feed-through connectors, with 32 pins each, are welded onto the stainless-steel flange to connect individually the 640 sensing wires to the front-end electronics; Time-Over-Threshold (TOT) signals delivered by the fast amplifiers and comparators are processed in FPGA cards: the position of a neutron is measured by selection of the channel carrying the maximum of charge (longest TOT).



Figure 5: The MILAND detector undergoing tests in the detector laboratory.

The detection parameters were characterised on the CT2 beam line: The detector was scanned with the neutron beam of CT2 collimated with two slits of 0.2mm width. The spatial resolution FWHM is 1.4mm in average on the anodes and 1.2mm on the cathodes. The position centroid accuracy - defined as the 'standard deviation of errors from beam position measurements (given by fitting the detector response)' - is 11 μm on the anodes, and 15 μm on the cathodes. By irradiating the detector uniformly and measuring the standard deviation of the counting rate, we measured a homogeneity of 0.9% for the anodes and 6.5% for the cathodes; the global count rate capability is 0.7MHz with only 10% efficiency loss; and finally the gamma sensitivity is less than 3×10^{-8} for 661 keV gammas. Compared to current technology, the MILAND detector improves the spatial resolution (relative to the size of the detector) by 2.5 and the counting rate by 5. The detector has been installed on the D16 diffractometer of the ILL for evaluation in real experimental conditions. The measurement with a Lysozyme crystal at 35 cm from the detection plan shows the ability of the MILAND detector to cover a large solid angle with a high angular resolution (**figure 6**). At this short distance, the MILAND detector covers a solid angle which is equal to that covered by the large curved MWPC of the D19 SXD instrument. 40 years after its invention, the MWPC revisited by the MILAND project, can still be considered as a very high-performance and constantly evolving technique for neutron detection.

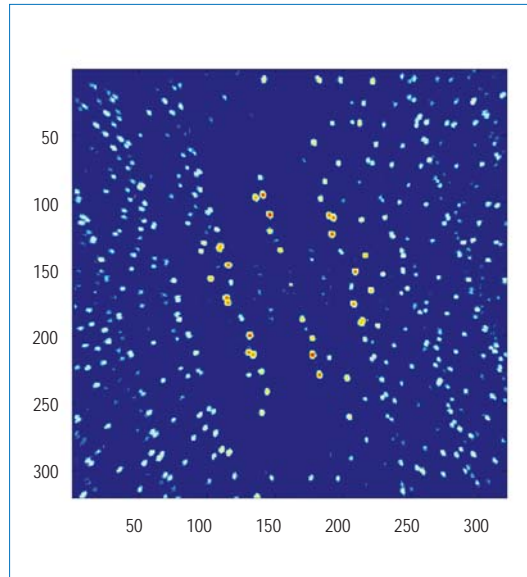


Figure 6. Image obtained on the D16 instrument with a lysozyme crystal, by superimposing images obtained during an angular scan. The detector was mounted at 35 cm from the sample. The neutron flux on the sample was 4×10^4 n/sec, and the total acquisition time was 16 hours.

Considering that the intensity of a neutron source is cost dependent, increasing the sensitivity of the instruments by improving their detector performance is beneficial to all existing neutron facilities. Technical teams in neutron research centres are primarily resourced to set up and maintain instrumental components whereas prospective research is a fringe activity. Merging resources and know-how from several institutes in the framework of international projects to support prospective and risky development in detector techniques can result in significant and exploitable progress which would be of immediate benefit to neutron science. We believe this is well illustrated by the MILAND project, and more generally by all JRAs of NMI3, but to quote Robert McGreevy (Neutron News, Vol 19, issue 4) 'with the reduction in funding across the EU Research Infrastructures Programme, neutron facilities need to rely more on their own initiative'.

We are grateful to the ESRF and the LPSC, who have contributed to the fabrication of the anode and cathode frames. The MILAND JRA was supported by the European Commission under the 6th Framework Programme through the Key Action: Strengthening the European Research Area, Research Infrastructures. Contract n°: RII3-CT-2003-505925.

5. Experimental and user programme

ILL member countries in 2008

- France
- Germany
- United Kingdom

- Austria
- Belgium
- Czech Republic
- Hungary
- Italy
- Poland
- Spain
- Sweden
- Switzerland



User programme

Beamtime allocation

Instrument performance

Instrument list

The ILL User Support Team is there to assist all our users. If you are coming to the ILL to carry out experiments, the User Office is here to give you the organisational and administrative support you need for the successful operation of your experiments. Neutron beams and instrument facilities are free of charge for proposers of accepted experiments. Scientists affiliated to ILL member countries will also, in general, be assisted with necessary travel and daily subsistence for a limited period. The User Support Team makes all arrangements for accommodation and will process claims for expenses after you have completed your experiment.

Extensive information about the ILL, its facilities and application for beamtime is available on our web-site.

(<http://www.ill.eu/users>)

- The Scientific Council Subcommittees examined 1118 proposals for 2008 of which 766 were allocated beamtime.

User programme

(1) If you are not yet registered in the Visitors Club and you wish to join it, you can register directly at <http://club.ill.eu/cv/>.

The ILL Visitors Club

All administrative tools for our scientific visitors are grouped together and directly accessible on the web, thanks to the Visitors Club. All information is presented in a user friendly environment. After having logged in with your own personal identification⁽¹⁾, you will have direct access to all the available information which concerns you. Users with particular responsibilities have privileged access to other tools, according to their role. The ILL Visitors Club includes the electronic proposal and experimental reports submission procedures, and electronic peer review of proposals. Additional electronic services have also been put in place: acknowledgement of proposals, subcommittee results, invitation letters, user satisfaction forms and so on.

Proposal submission

There are different ways of submitting a proposal to the ILL:

- Standard submission – twice a year – via the Electronic Proposal System (EPS)
- Long-Term Proposals – once a year – via the Electronic Proposal System (EPS)
- EASY access system (EASY) throughout the year
- Director's Discretion Time (DDT) throughout the year
- Special access for proprietary research and industrial users.

Submission of a standard research proposal

Applications for beamtime should be submitted electronically, via our Electronic Proposal Submission system (EPS), available on the Visitors Club web-site. Proposals can be submitted to the ILL twice a year, usually in March and in September. The web system is activated two months before each deadline.

Submitted proposals are divided amongst the different colleges (see box) according to their main subject area.

Proposals are judged by a Peer Review Committee of the Subcommittees of the ILL Scientific Council. Subcommittee members are specialists in relevant areas of each College and they evaluate the proposals for scientific merit and recommend to the ILL Management the award of beamtime to the highest-priority proposals.

Before the meeting, the subcommittee receives a report on the technical feasibility and safety of a proposed experiment from the appropriate College at the ILL. Two proposal review rounds are held each year, approximately six weeks after the deadline for submission of applications.

There are normally 4 reactor cycles a year, each of which lasts 50 days. Accepted proposals submitted by March will receive beamtime in the second half of the year and those submitted by September, in the first half of the following year. More detailed information on application for beamtime and deadlines is given on our website at <http://www.ill.eu/users/proposal-submission/>.

The ILL scientific life is organised into 10 colleges:

- College 1** - Applied Physics, Instrumentation and Techniques
- College 2** - Theory
- College 3** - Nuclear and Particle Physics
- College 4** - Magnetic Excitations
- College 5A** - Crystallography
- College 5B** - Magnetic Structures
- College 6** - Structure and Dynamics of Liquids and Glasses
- College 7** - Spectroscopy in Solid State Physics & Chemistry
- College 8** - Structure and Dynamics of Biological Systems
- College 9** - Structure and Dynamics of Soft-condensed Matter

Easy Access System

The Easy Access System (EASY) grants diffraction beamtime to scientists from ILL member countries, who need a rapid structural characterisation of samples and data analysis. Access is open all year long, and it does not go through the ILL standard proposal round and consequent peer review system.

The system offers one neutron day per cycle, on four instruments (D1A, D2B, VIVALDI and OrientExpress) to perform very short experiments (a maximum of 4h per cycle) at room temperature. The users will not be invited to the ILL, but will send their samples to one of two designated ILL scientists (one for powder and one for single-crystal experiments), who will be responsible for the measurements and sample radiological control. The ILL will ship back the sample once the measurement is finished. You can apply for EASY beamtime on the Visitors Club. More information is available at http://club.ill.eu/cvDocs/EASY_Guidelines.pdf.

Long-Term Proposals

The ILL has recently decided to allow users from its member countries to apply for extended periods of beamtime, by submitting a Long-Term Proposal (LTP). The purpose of the scheme is to facilitate users to develop instrumentation, techniques or software through the award of beamtime over several cycles. Both the ILL Scientific Council and the

ILL Management believe that LTPs could be beneficial to the ILL community as a whole, bringing extra resources or capabilities, so it was launched for a trial period of three years in the scheduling round of autumn 2008. The total amount of beamtime that may be allocated to LTPs on any particular instrument is capped at 10%, and beamtime is not awarded to LTPs to perform science beyond essential testing.

LTPs can be submitted once a year at the autumn proposal round using the specific LTP application form. The primary criterion for acceptance of a LTP is the excellence of the science that it will ultimately enable. The length of LTP projects is expected to be 3 years typically, with continuation approved at the end of each year, based on an annual report; a final report is also required at the end of the project. Each LTP must have a Principal Investigator who is affiliated to a scientific institution of an ILL member country.

Beamtime for accepted LTPs becomes available during the following scheduling period, i.e. the first and second cycles of the following year. More details are given on our web site at <http://www.ill.eu/users/proposal-submission/>

Submission of a proposal to the Director's Discretion Time

This option allows a researcher to obtain beamtime quickly, without going through the peer-review procedure. DDT is normally used for 'hot' topics, new ideas, feasibility tests and to encourage new users. Applications for Director's Discretion Time can be submitted to the Head of the Science Division, Prof. Andrew Harrison, at any time, (harrison@ill.eu).

Access for proprietary research and industrial users

The ILL's mission is to provide neutrons for both public and industrial research. Our Industrial Liaison and Consultancy Group (ILC) ensures rapid access and total confidentiality for industrial companies, and provides specialised technical and scientific support. The ILC Group is composed of scientists with considerable experience and expertise in neutron techniques applied to industrial R&D, and it facilitates and coordinates all aspects of industrial R&D at the ILL: initial enquiries, contractual questions, planning, experimental operations. To apply for proprietary beamtime, please contact the ILC Group at industry@ill.eu or consult the web site under <http://www.ill.eu/industry/>.

Experimental reports

Users are asked to complete an experimental report on the outcome of their experiments. Following a recommendation of the ILL Scientific Council, the submission of an experimental report is now compulsory for every user who is granted ILL beamtime. Failure to do so may lead to rejection in case of application for beamtime for a continuation proposal.

All ILL Experimental Reports are archived electronically and accessible via the web server as PDF files (under <http://club.ill.eu/cv/>). You can search for a report by experimental number, instrument, college, date of experiment, title, institute, experimental team or local contact.

Experimental reports for experiments performed in 2008 are included in the CD-ROM of this year's Annual Report.

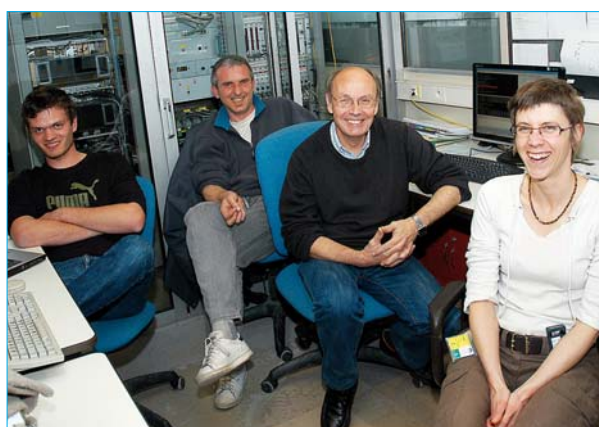
Out of hours support

We have actively strengthened the level of technical support outside working hours. To date, Out of Hours Support (OHS) has been implemented within the Instrument Control Service, the Detector Service and the Sample Environment Service.

Collaborative Research Group instruments

The ILL provides a framework in which Collaborating Research Groups (CRGs) can build and manage instruments on ILL beamlines to carry out their own research programmes. CRGs represent a particularly successful form of long-term international scientific collaboration.

CRGs are composed of scientists from one or two research disciplines, and often multinational, carrying out a joint research programme centred around a specific instrument. CRGs enjoy exclusive access to these instruments for at least half of the beamtime available. The CRGs provide their own scientific and technical support and cover the general operating costs of these instruments. If there is demand from the user community and the resources are available, the beamtime reserved for ILL can be made accessible to users via the subcommittees.



Nicolas Martin, Eric Ressouche and Louis-Pierre Regnault (CEA CRG group) with Virginie Simonet (CNRS) in the IN22 cabin.

Beamtime allocation

The ILL User Community

The ILL welcomed 1247 users from 43 countries in 2008, including 294 from France, 212 from Germany and 296 from the UK (**figure 1**). Many of our visitors were received more than once (for a total of 2002 visits).

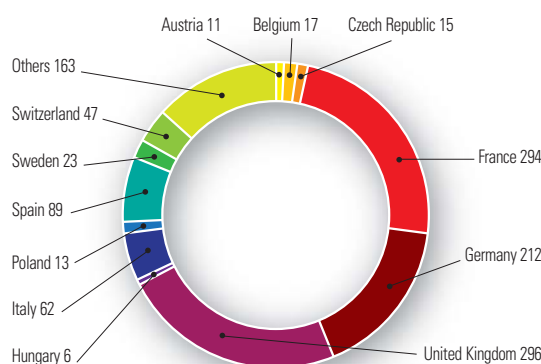


Figure 1: National affiliation of ILL users in 2008.

We value feedback from our users as an indicator of how well our facility is fulfilling their needs and to initiate actions when this is not the case.

The **User Satisfaction Form** is a means of finding out what our users think of the facility. Users who have just finished an experiment at the ILL are asked to complete the questionnaire on the Visitors Club and give us their views on different topics.

User comments are made available to managers for their information and actions when appropriate.

Instruments

The instrumental facilities at the ILL are shown in the schematic diagram on page 99.

Besides the 27 ILL instruments, there are 10 CRG-instruments, which are operated by external Collaborating Research Groups to carry out their own research. There are currently three different categories of CRG instruments.

- CRG-A in which the external group leases an instrument owned by the ILL. They have 50% of the beamtime at their disposal and for the remaining 50% they support ILL's scientific user programme.
- The CRG-B category owns their instrument and retains 70% of the available beamtime, supporting the ILL programme for the other 30%.
- Finally, CRG-C instruments are used full time for specific research programmes by the external group, which has exclusive use of the beam.

DB21, LADI and IN15 have a special status, since they are joint ventures of the ILL with other laboratories: in the case of DB21 and LADI with EMBL and for IN15 with FZ Jülich and the Helmholtz-Zentrum Berlin.

- powder diffractometers: D1A, D1B*, D2B, D20, SALSA
- liquids diffractometer: D4
- polarised neutron diffractometers: D3, D23*
- single-crystal diffractometers: D9, D10, D15*
- large scale structures diffractometers: D19, DB21, LADI, VIVALDI
- small-angle scattering: D11, D22
- low momentum-transfer diffractometer: D16
- reflectometers: ADAM*, D17, FIGARO
- diffuse scattering and polarisation analysis spectrometer: D7
- three-axis spectrometers: IN1, IN8, IN12*, IN14, IN20, IN22*
- time-of-flight spectrometers: BRISP*, IN4, IN5, IN6
- backscattering and spin-echo spectrometers: IN10, IN11, IN13*, IN15, IN16
- nuclear physics instruments: PN1, PN3, Cryo-EDM*
- fundamental physics instruments: PF1, PF2, S18*

* CRG instruments are marked with an asterisk.

<http://www.ill.eu/instruments-support/instruments-groups/>

Beamtime allocation & utilisation for 2008

Overall, the Subcommittees of the Scientific Council examined 1118 proposals requesting 7960 days for 2008. 4506 days of beamtime were allocated for 766 peer-reviewed proposals.

The distribution of beamtime requested and allocated amongst the different countries is shown in **table 1**. In 2008, the member countries of the ILL were: France, Germany, UK, Austria, Belgium, the Czech Republic, Hungary, Italy, Poland, Spain, Sweden and Switzerland

In calculating the statistics of beamtime per country, shown in **table 1a**, the attribution is based on the location of the laboratory of the proposers, not their individual nationality. For a proposal involving laboratories from more than one member country, the total number of days is weighted by the number of proposers from each country.

In **table 1b**, the beamtime requested by and allocated to scientists from ILL, ESRF or EMBL is allocated to the member countries according to a weighting system based on the fractional membership of the country to the institute concerned.

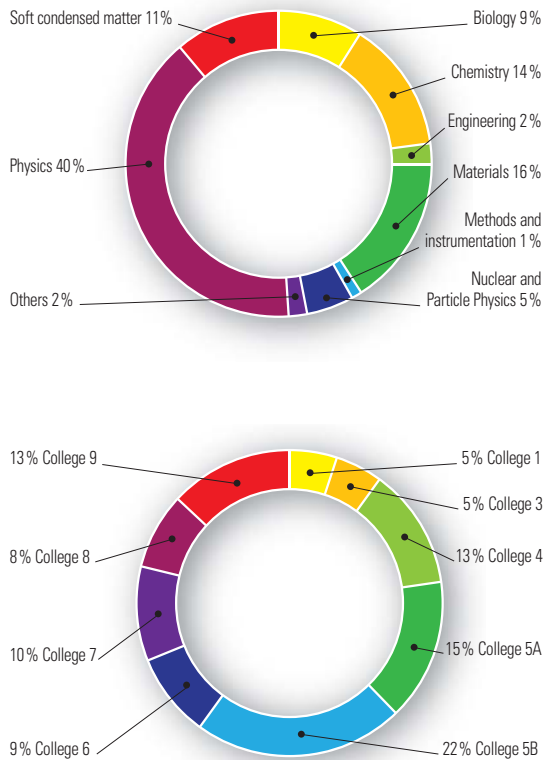


Figure 2: Beamtime allocation in 2008: distribution amongst the different research areas and colleges.



Christiane Alba-Simionesco in discussion with Richard Wagner at the Scientific Council, November 2008.

All countries		Before national balance		After national balance		
Country	Requested days	Requested in %	Allocated days	Allocated in %	Allocated days	Allocated in %
AR	1.92	0.02	1.33	0.03	1.33	0.03
AT	41.29	0.52	18.27	0.40	18.27	0.40
AU	97.80	1.23	65.05	1.42	65.05	1.43
BE	31.80	0.40	17.33	0.38	17.33	0.38
BG	2.96	0.04	3.04	0.07	3.04	0.07
BR	4.73	0.06	2.13	0.05	2.13	0.05
BY	3.43	0.04	2.10	0.05	2.10	0.05
CA	42.75	0.54	21.18	0.46	21.18	0.46
CH	196.79	2.47	145.66	3.19	145.66	3.20
CN	21.50	0.27	16.50	0.36	16.50	0.36
CZ	60.70	0.76	40.61	0.89	24.97	0.89
DE	1154.48	14.50	644.87	14.10	646.59	14.28
DK	24.48	0.31	23.60	0.52	19.75	0.52
ES	398.39	5.01	184.32	4.03	190.32	4.18
ESRF	41.79	0.53	15.76	0.34	16.36	0.36
FI	23.83	0.30	13.00	0.28	13.00	0.29
FR	1251.75	15.73	775.12	16.95	777.25	17.23
GB	1620.92	20.36	998.08	21.82	1010.21	22.17
HU	15.10	0.19	14.90	0.33	14.90	0.33
IL	23.67	0.30	12.80	0.28	12.80	0.28
ILL	599.99	7.54	362.56	7.93	357.15	8.01
IN	713.64	8.97	366.00	8.00	368.83	8.10
IT	241.91	3.04	116.80	2.55	117.80	2.59
JP	220.22	2.77	122.68	2.68	129.08	2.83
KR	47.22	0.59	33.45	0.73	31.62	0.69
LV	7.40	0.09	0.00	0.00	0.00	0.00
NL	22.75	0.29	7.58	0.17	7.58	0.17
NO	28.98	0.36	20.29	0.44	20.29	0.45
NZ	9.33	0.12	7.80	0.17	7.80	0.17
PL	80.03	1.01	36.27	0.79	36.27	0.80
PT	16.54	0.21	20.14	0.44	8.64	0.44
RU	278.96	3.50	156.35	3.42	151.55	3.33
SE	102.20	1.28	65.42	1.43	65.42	1.44
SG	12.50	0.16	2.25	0.05	2.25	0.05
SK	1.00	0.01	0.50	0.01	0.50	0.01
TN	3.17	0.04	0.00	0.00	0.00	0.00
UA	15.00	0.19	0.00	0.00	0.00	0.00
US	485.35	6.10	229.43	5.02	172.41	3.78
ZA	13.90	0.17	10.07	0.22	10.07	0.22
Total	7959.67	100.00	4573.25	100.00	4506.00	100.00

Table 1a: Distribution amongst the different countries of beamtime requested and allocated in 2008 by the Subcommittees of the Scientific Council.

Only member countries		Before national balance		After national balance		
Country	Requested days	Requested in %	Allocated days	Allocated in %	Allocated days	Allocated in %
AT	62.15	0.81	30.59	0.69	30.81	0.69
BE	40.82	0.53	22.64	0.51	22.65	0.51
CH	269.86	3.53	189.60	4.28	189.66	4.24
CZ	76.16	1.00	55.69	1.26	55.66	1.24
DE	1801.37	23.56	1015.39	22.91	1022.00	22.83
ES	518.68	6.78	246.58	5.56	252.52	5.64
FR	1900.26	24.85	1144.44	25.82	1156.02	25.82
GB	2210.95	28.91	1324.39	29.88	1336.99	29.86
HU	44.02	0.58	26.19	0.59	26.20	0.59
IT	498.40	6.52	251.62	5.68	258.56	5.78
PL	90.88	1.19	42.48	0.96	42.48	0.95
SE	132.98	1.74	83.40	1.88	83.42	1.86
Total	7646.53	100.00	4432.97	100.00	4476.97	100.00

Table 1b: Distribution amongst the Associate and scientific-member countries of beamtime requested and allocated in 2008 by the Subcommittees of the Scientific Council.

Scientific support laboratories & instrument performance

Scientific support laboratories

Deuteration Laboratory

A common ILL/EMBL deuteration laboratory is available to external users. The aim of the laboratory is to provide a focus for European scientists wishing to make their own deuterated materials for neutron scattering or NMR experiments. Information about the availability of this facility for external users is given at: http://www.ill.eu/fileadmin/users_files/Other_Sites/deuteration/index.htm. Please contact the Head of the Deuteration Facility, Dr Michael Härtlein (haertlein@ill.eu) for further details.

Materials Science Support Laboratory

The joint ILL-ESRF Materials Science Support Laboratory provides a range of support to our users, from advice with experiment proposals to advanced sample metrology. In particular, the Laboratory works with users to optimise the experimental methodology before the start of an experiment. This takes the form of standardised specimen mounting, digitisation of samples, definition of measurement macros and liaising with the instrument responsible. It is recommended that users arrive at the ILL a day or two prior to the start of an experiment to enable these off-line preparations to be performed. The extra subsistence costs may be available from the SCO if requested beforehand. More information about this support may be found on the MSSL's website <http://www.ill.eu/others/mssl/>

Partnership for Structural Biology

The Partnership for Structural Biology (PSB) is a collaboration between the ILL, ESRF, EMBL and the neighbouring *Institut de Biologie Structurale* (IBS). As a centre of excellence in the field of structural genomics, the PSB concentrates its research programmes on proteins and other biomolecules selected for their medical interest. It shares its office and laboratory space (located in the Carl-Ivar Bränden Building, CIBB) with the *Institut de Virologie Moléculaire et Structurale* (IVMS) of the Joseph Fourier University. Further details are provided on its website <http://www.psb-grenoble.eu/>

Partnership for Soft Condensed Matter

A Partnership for Soft Condensed Matter (PSCM) is being established with the ESRF, drawing some of its inspiration from the success of the PSB. Its primary aim is to enable users to characterise samples before their experiments at the ILL and ESRF, and to facilitate the performance of complementary *in situ* measurements. It will also develop complex sample environments for carrying out advanced surface and solution science experiments.

More details can be found on page 115.

Instrument performance

Table 2 also gives a summary of instrument performance for 2008. For each cycle, a record is kept of any time lost from the total available beamtime and the reasons for the lost time are analysed for all the instruments. The table gives a global summary for the year.

Overall 5978 days were made available to our users in 2008 on ILL and CRG instruments, which represents about 79% of the total days of operation. 460 days were used by ILL scientists to carry out their own scientific research. About 10% of the total beamtime available on the ILL instruments is allowed for tests, calibrations, scheduling flexibility, minor breakdowns recuperation. 6438 beam days were delivered for all users including CRGs and internal research. 4506 of these days were delivered for peer-reviewed experiments.

A total of 833 experiments were scheduled. During 2008 the reactor operated for 4.0 cycles, representing 198 days of neutrons.

In 2008, about 442 out of 7594 days were lost due to various malfunctions, which represent about 5% of the total available beamtime. The breakdown by reasons for beamtime losses is shown in **figure 3b**.

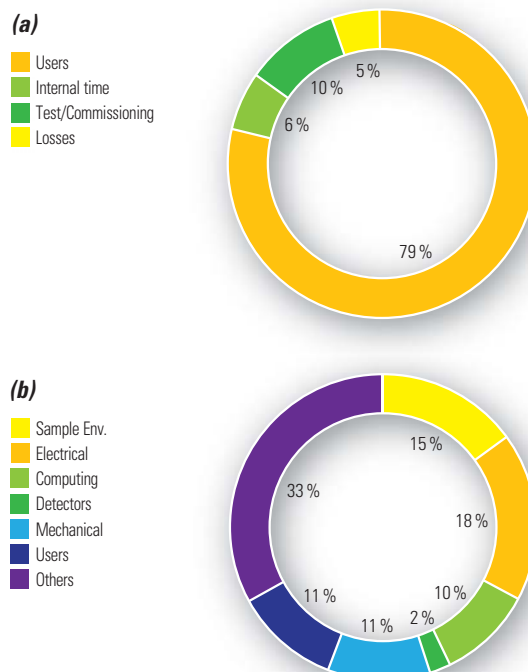


Figure 3 (a) Use of ILL beamtime (b) Reasons for beamtime losses.

Instrument	Days requested	Days allocated*	Number of scheduled experiments	Available days **	Days used for users***	Days lost	Days for commissioning /test/training	Days for internal research
ADAM	91	60	12	198	194	0	4	0
BRISP	72	48	4	198	147	5	10	36
D10	223	138	21	198	182	1	9	6
D11	99	58	24	0	0	0	0	0
D15	27	33	5	198	144	9	16	29
D16	103	100	15	198	135	26	33	4
D17	246	137	41	198	148	0	38	12
D19	102	110	16	198	131	0	39	28
D1A	91	100	30	198	130	0	6	62
D1B	130	85	29	198	168	3	16	11
D20	312	135	56	198	171	0	20	7
D22	474	148	57	198	161	20	14	3
D23	80	53	7	198	180	0	18	0
D2B	258	137	57	198	183	1	7	7
D3	240	146	18	198	159	7	13	19
D4	213	94	20	134	120	7	7	0
D7	200	139	21	198	155	23	16	4
D9	184	129	19	198	134	25	19	20
DB21	66	66	3	198	92	43	40	23
FIGARO	54	25	7	0	0	0	0	0
IN1	59	38	8	64	55	0	4	5
IN10	122	136	17	198	165	7	12	14
IN11	382	143	23	198	158	4	16	20
IN12	142	49	6	198	174	4	16	4
IN13	145	82	15	198	173	6	11	8
IN14	262	144	22	198	169	6	9	1
IN15	196	72	11	198	136	20	33	9
IN16	333	146	27	198	152	26	8	13
IN20	215	142	19	198	161	5	30	2
IN22	106	57	7	198	193	4	1	0
IN4	203	150	35	198	132	40	23	3
IN5	125	48	12	70	32	2	36	0
IN6	265	150	40	198	170	8	4	16
IN8	212	140	20	198	147	23	27	1
LADI	257	153	17	198	146	16	22	14
PF1B	358	188	6	198	153	38	0	7
PF2****	378	150	14	198	153	0	34	11
PN1	311	140	14	198	156	21	21	0
PN3	291	164	7	198	110	12	47	29
S18	0	0	0	198	178	10	7	3
SALSA	152	130	26	198	164	0	18	16
VIVALDI	182	143	25	198	167	20	11	0
Total (days)	7961	4506	833	7594	5978	442	715	460
Percentage of the total available beamtime					79%	5%	10%	6%

* days allocated refers to only those days reviewed by the subcommittees (i.e., excluding CRG time for CRGs).

** available days refers to the days of reactor operation in 2008.

*** days used refers to the total number of days delivered to users (i.e., including CRG days for CRGs and DDT).

**** PF2: 5 different experimental positions in 2008 where experiments can run simultaneously. The values given are averaged for these 5 positions. D11, FIGARO and IN5 were commissioned in 2008.

Detailed comments on the larger beamtime losses (above 25 days):

- D16 26 days lost due to illness of key staff.
- DB21 the loss of 42 days was mainly due to mechanical problems related to motors and encoders. Also some beamtime was lost due to failure of the new monochromator.
- IN4 40 days lost due to a problem on the Fermi chopper control electronics.
- IN16 a large number of days were lost due to unsuccessful user sample preparation and other user errors. There were also frequent difficulties with sample environment equipment.
- PF1 38 days lost due to a problem with a user cryostat.

Table 2 shows beamtime requests and allocation as well as the number of scheduled experiments.

The effective number of days given to our users takes into account also Director's Discretion Time (DDT) and CRG time for CRG instruments. The instruments D4 and IN1 share a beam.

Table 2:
Beamtime request/
allocation
by instrument.
CRG instruments
are in blue.

Instrument list - December 2008

ILL instruments		
D1A (50%)	powder diffractometer	operational
D2B	powder diffractometer	operational
D3	single-crystal diffractometer	operational
D4 (50% with IN1)	liquids diffractometer	operational
D7	diffuse-scattering spectrometer	operational
D9	single-crystal diffractometer	operational
D10	single-crystal diffractometer	operational
D11	small-angle scattering diffractometer	operational
D16	small momentum-transfer diffractometer	operational
D17	reflectometer	operational
D19	single-crystal diffractometer	operational
D20	powder diffractometer	operational
D22	small-angle scattering diffractometer	operational
FIGARO	reflectometer	operational
IN1 (50% with D4)	three-axis spectrometer	operational
IN4	time-of-flight spectrometer	operational
IN5	time-of-flight spectrometer	operational
IN6	time-of-flight spectrometer	operational
IN8	three-axis spectrometer	operational
IN10	backscattering spectrometer	operational
IN11	spin-echo spectrometer	operational
IN14	three-axis spectrometer	operational
IN16	backscattering spectrometer	operational
IN20	three-axis spectrometer	operational
PF1	neutron beam for fundamental physics	operational
PF2	ultracold neutron source for fundamental physics	operational
PN1	fission product mass-spectrometer	operational
PN3	gamma-ray spectrometer	operational
SALSA	strain analyser for engineering application	operational
VIVALDI	thermal neutron Laue diffractometer	operational

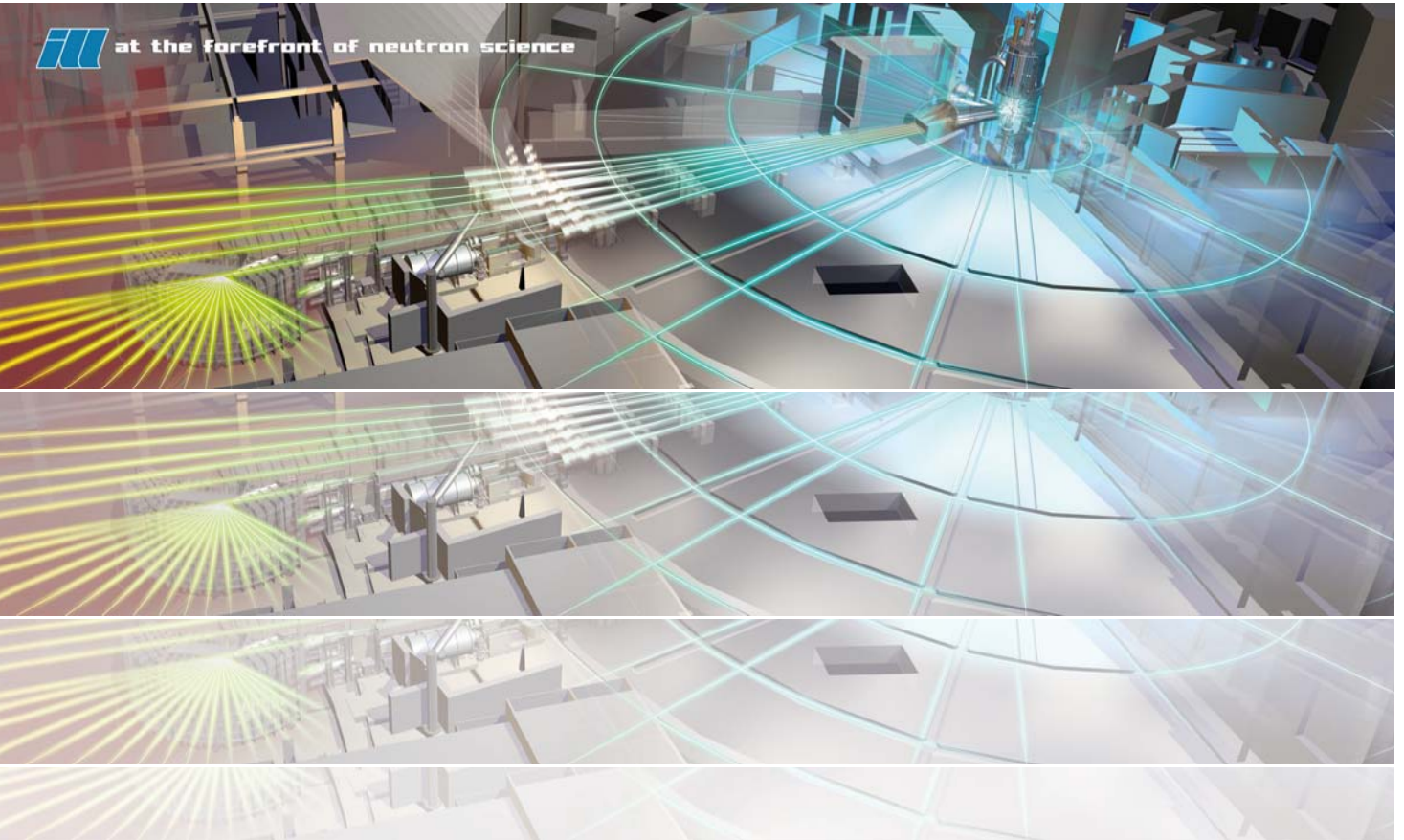
CRG instruments		
ADAM	reflectometer	CRG-B operational
BRISP	Brillouin spectrometer	CRG-B commissioning
CRYO EDM	installation for the search of the neutron electric dipole moment	CRG-C operational
D1B	powder diffractometer	CRG-A operational
D15	single-crystal diffractometer	CRG-B operational
D23	single-crystal diffractometer	CRG-B operational
GRANIT	gravitation state measurement	CRG under construction
IN12	three-axis spectrometer	CRG-B operational
IN13	backscattering spectrometer	CRG-A operational
IN22	three-axis spectrometer	CRG-B operational
S18	interferometer	CRG-C operational

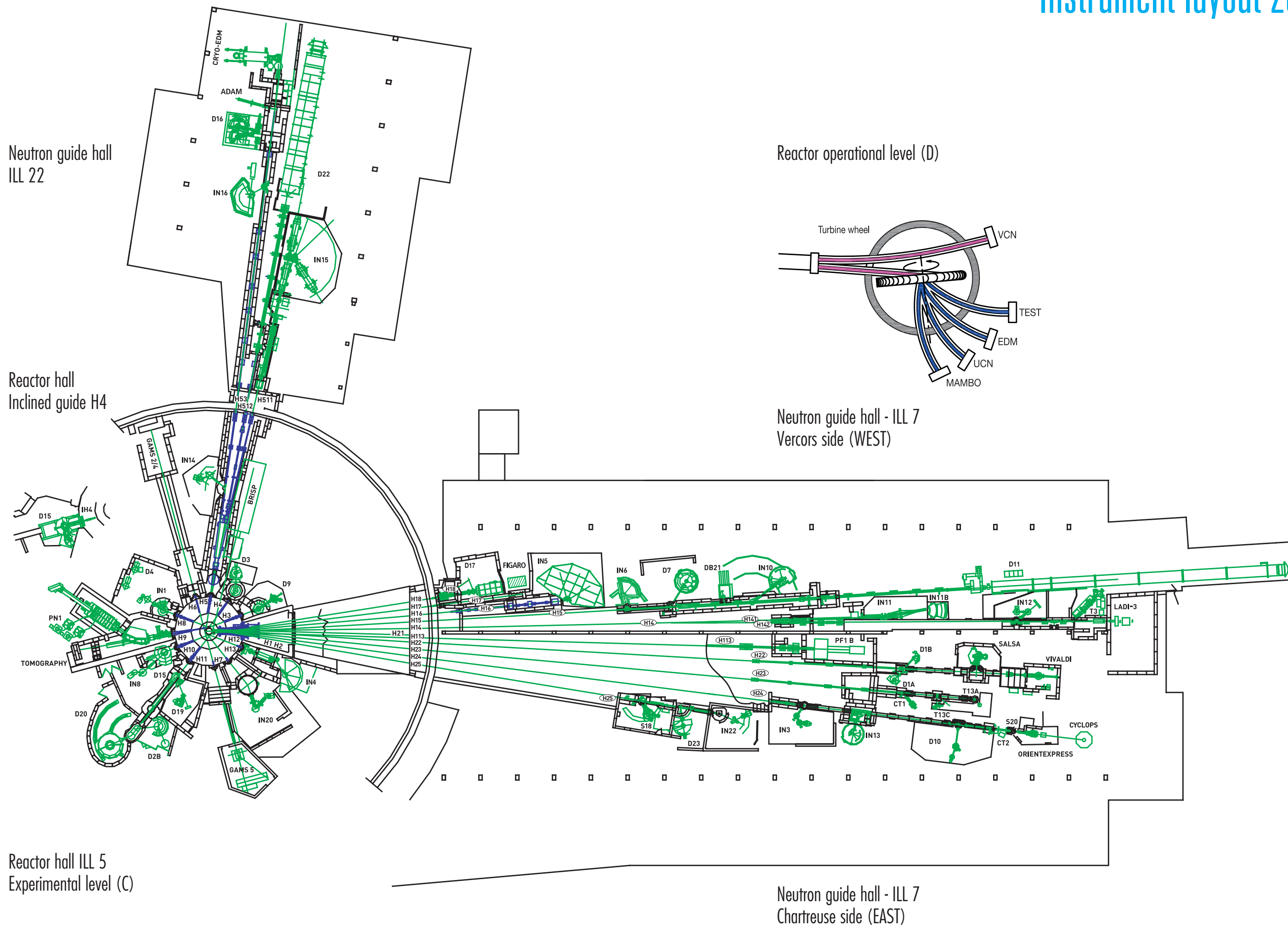
Jointly funded instruments		
DB21 (50%)	single-crystal diffractometer	operational with EMBL
LADI (50%)	Laue diffractometer	operational with EMBL
IN15	spin-echo spectrometer	operational with FZ Jülich and HMI Berlin


Test and characterisation beams	
CT1, CT2	detector test facilities
CYCLOPS	Laue diffractometer
TOMOGRAPHY	neutrography
OrientExpress	Laue diffractometer
T3	neutron optics test facility
T13A, C	monochromator test facility
T17	cold neutron test facility

Instrument layout 2008

 at the forefront of neutron science







6. Reactor operation



The ILL's neutrons are generated by its high-flux reactor

This reactor was refurbished between 1993 and 1995 and produces the most intense neutron flux in the world: 1.5×10^{15} neutrons per second per cm^2 , with a thermal power of 58.3 MW.

The reactor operates 50-day cycles, with each cycle of operation followed by a shutdown period during which the fuel element is changed and a number of checks are carried out. Occasional longer shutdowns allow for equipment maintenance. There are normally 4 reactor cycles per year, supplying 200 days of neutron flux for scientific use.

As part of the ILL's determination to guarantee the safety and reliability of its facilities over future years, the Reactor Division runs a 'key reactor components programme', the aim of which is to ensure the development and replacement as necessary of the essential main components of the reactor. The current plans under this programme cover the period up to 2016.

■ The ILL reactor operates four 50-day cycles per year, producing 200 days of beamtime for the experimental programme



Bruno Desbrière and Hervé Guyon during the reactor emergency exercise.

Reactor operation

The four reactor cycles scheduled in 2008 provided for 198 days of scientific activity. They raised no significant problems. The start of the first cycle was delayed by 4 days as a consequence of the heavy work schedule programmed for the winter shutdown, an unavoidable cut in the water supply a few days before start-up, and minor pre-start-up testing woes. The cycle was therefore extended by 3 days

in compensation. The second cycle followed hard on the tail of the first, with only a 10-day break. It was nevertheless affected by a cut in the mains electrical supply; the 58-hour shutdown this caused (xenon poisoning) was offset by an extension of 2 days in the cycle length. The following 2 cycles passed without a hitch.

Cycle no.	Start of cycle	End of cycle	Number of days of operation/scheduled	Number of EFPD ¹ scheduled	Number unscheduled shutdowns
150	01.04.08	23.05.08	49.2/50	46/46	0
151	03.06.08	25.07.08	49.6/50	45.5/46	1
152	27.08.08	16.10.08	50/50	46/46	0
153	30.10.08	19.12.08	50/50	46/46	0
TOTAL			198.8/200 (99.4%)	181.5/182	1

¹EFPD: Equivalent Full Power Days



Conclusion of the Refit Programme

On 11 October 2007 the ILL met with the nuclear safety authorities' *Groupe Permanent*. The purpose of the meeting was to present the studies and work carried out over the last few years to satisfy the requirements and recommendations the *Groupe* had made in May 2002. The meeting was successful and the next major round of safety inspections will not be performed before 2017.

The recent reactor refit and the additional upgrade measures we have planned will ensure safe operating conditions for the facility until the 2030s. The dossiers outlining the ILL's current plans were sent to the safety authorities in 2008.

Key Reactor Components Programme

The Reactor Division is now pursuing a new programme – the Key Reactor Components programme – designed to ensure the long-term safety and reliability of the reactor. The aim is to replace or improve a number of key components; the programme is to run until 2016.

One of the aims was to undertake a major renovation of the ILL's decontamination facilities. Rising costs however have led to a change in the plans, with the aim to treat ILL's heavy water externally.

The long 2008 winter shutdown was used to perform a number of important operations. In the course of a few weeks we were able to:

1. replace the high tension antenna, cells and transformers, with a conversion from 15 to 20kV (part of the Key Reactor Components programme)
2. remodel the supervision system
3. replace the valves and sensors on the hot and cold sources
4. clean and inspect the water tube lane and cooling pumps used by the ILL, ESRF and CNRS.

Evacuation of radioactive waste	Quantity
Decay bin (60l)*	0
5 m ³ pre-concreted crate (low- and intermediate level waste)	0
5 m ³ crate (low- and intermediate-level waste)	0
200l drums of 'incineratable' (low-level waste)	0
120l HDPE drums (low-level waste)	7

* Waste stocked in these decay bins is still quite active and requires several years of interim storage before meeting ANDRA's specifications for processing as intermediate-level waste.

Gaseous effluents	Released in 2008
Tritium	13 TBq
Rare gas	1.3 TBq
Carbon 14	0.68 TBq
Iodine	6.8 MBq
Aerosols	0.20 MBq

Liquid effluents	Released in 2008
Tritium	0.22 TBq
Carbon 14	0.23 GBq
Iodine	2.0 MBq
Other activation products	90 MBq

A full-scale emergency exercise

8 April was the day the nuclear safety authorities had chosen for a national emergency-response exercise. This is a three-yearly event organised to keep the local authorities and nuclear operators fully alert and to test the emergency procedures set up for high-risk installations, including the off-site emergency response plan.

The scenario detailed a major challenge for the teams, who were faced with the extremely rare case of a major nuclear accident.

The Prefect and safety authorities declared that the ILL's management of the scenario was entirely satisfactory! The next emergency exercise will take place in three years' time.





Chronicle 2008

Workshops

A year in photos

Scientific support laboratories

Site development

7. More than simply neutrons

■ ILL chronicle 2008

31 January

Signature of a Memorandum of understanding between ILL and LPSC (*Subatomic Physics and Cosmology Laboratory*)

17 February - 20 March

HERCULES: Higher European Research Course for Users of Large Experimental Systems

17 March

Visit of a Spanish delegation

20 March

Visit of a Hungarian delegation

8 April

Reactor safety exercise

9 April

Visit of a Swedish delegation (City of Lund and Skåne region)

15-18 April

Meetings ILL Scientific Council and its Subcommittees

6 May

Visit of an ESS Danish task force

18 June and 12 December

DS/DPT Heads of 'Service' outdoor meetings

25-26 June

Steering Committee meeting

7 July

Renaissance of the time-of-flight spectrometer

8 September

Visit of a Slovakian delegation

14 October

Visit of the German Consul General

22 October

Agreement with the Grenoble University Joseph Fourier on an Associate professorship chair for scientists from the ESRF and ILL

4-7 November

Meetings ILL Scientific Council and its Subcommittees

14-16 November

French Science Festival week, ILL stand in the centre of Grenoble

15 November

French colloquium on Women in Science, Grenoble

26-27 November

Steering Committee meeting

28 November

Celebration at PSI of the 20th anniversary of Switzerland joining the ILL

8 December

Delivery of the new fast CCD neutron Laue detector CYCLOPS

10 December

FIGARO's first reflection using a silicon crystal

Workshops in which ILL was a major player in 2008

2008 was an extremely busy year for workshops, with 11 events taking place in the first six months of the year, most of which were held at the ILL.

Simulations on Disordered Systems

M. Johnson (ILL) and A. Pasturel (LPMC)
31 January-1 February

Advanced Neutron Diffraction Data Treatment (FullProf School)

J. Rodriguez-Carvajal, M.H. Lemée-Cailleau and G. Cuello (ILL)
11-15 February

Powder Diffraction with 2-Dimensional Detectors

H. Fischer and J. Rodriguez-Carvajal (ILL)
25-26 February

Highly Frustrated Magnetism (HFM)

A. Harrison (ILL), C. Lacroix, P. Lejay, P. Bordet (CNRS) and C. Berthier (UJF)
3-6 March

Spectroscopy of Neutron-rich Isotopes

U. Koester (ILL) and G. Simpson (LPSC)
16-21 March 2008

Neutron Scattering Investigations in Condensed Matter

Poznan (Poland)
6-10 May 2008

ILL-Slovenia Workshop in Ljubljana

20-22 May 2008

Surfaces & Interfaces in Soft Matter & Biology

G. Fragneto (ILL), S. Clarke, J. -R. Lu, J. Penfold (ISIS) and A. R. Rennie (Uppsala)
21-23 May

Sample Environment at Neutron Scattering Facilities

E. Lelièvre (ILL)
26-29 May

Particle Physics with Slow Neutrons

C. Plonka and T. Soldner (ILL)
29-31 May

Scattering Methods Applied to Soft Condensed Matter

P. Lindner (ILL)
7-14 June

Biological Physics at Large Facilities

J. Zaccai (ILL), S. McSweeney (ESRF) and P. A. Lindgard
28-23 October

Hercules School on Soft Matter

G. Fragneto, P. Timmins (ILL), A. Madsen and C. Riekel (ESRF)
16-23 November

More than simply neutrons

Atomic scale simulations on disordered systems. (SiMaDes-II)

Liquids and glasses, constitute a considerable challenge for experimentalists looking to establish atomistic detail of structure and dynamics. Atomistic simulations, combined with experimental investigations, therefore have an important role to play.

SiMaDes-II followed on from a one-day meeting held in Strasbourg in 2006, which focused uniquely on simulations and theory. The 2008 meeting was held at the ILL to bring in local experimentalists. However about 60 people attended the meeting which resulted in a very busy 24-hour schedule.

Complementary neutron scattering and X-ray results were presented, covering structure and dynamics, the latter via collective excitations and vibrational densities of states. Experiment provides the reference data for simulations and theoretical models which can then be extended to extreme conditions of pressure and temperature. The systems studied ranged from favourites like silica (and related systems) to molecular, ionic and metallic systems.

FullProf School-2008



Precise crystallography has significantly contributed to the success of recent developments in materials science, solid state physics and chemistry. Among the available programs for diffraction data analysis, the FullProf Suite appears as one of the packages most widely used by the scientific community working in these fields. By creating a regular hands-on

school, our aim is to directly contribute to the training of the upcoming generation of scientists on analysis with the FullProf Suite of diffraction data coming from powders, single crystals, time-of-flight diffraction, with neutron as well as X-rays. In 2008 the FPSchool was mainly devoted to powder diffraction, in particular to the treatment of large amount of diffraction data, coming in particular from phase transformation studies. 40 students attended the 2008 session which took place at the ILL over 5 days: three were dedicated to general applications plus two, more focused on the specialised topic. Theoretical introductory lectures were followed by hands on practical computing sessions very well appreciated.

<http://www.ill.eu/news-events/workshops-events/fpschool/>

Powder Diffraction with 2-Dimensional Detectors (PD2DD)

The first international workshop on Powder Diffraction with 2-Dimensional Detectors (PD2DD) took place at the ILL on 26 and 27 February 2008.

About 80 scientists from 12 different countries participated in a workshop programme that included 12 invited talks and 20 posters.

Although the main theme of the PD2DD workshop was neutron powder diffraction, the programme was enriched by the participation of several X-ray diffractionists, as well as single-crystal diffractionists. The subject range of well-prepared presentations included new instruments at several central facilities and the latest developments in 2-D detectors and corresponding sample environments, as well as scientific applications like texture analysis, time-resolved diffraction, high-pressure studies and phase transitions.

More information can be found at the PD2DD workshop website:

<http://www.ill.eu/news-events/workshops-events/pd2dd/>

Particle Physics with Slow Neutrons

The International Workshop on Particle Physics with Slow Neutrons, jointly organised by the Institut Laue Langevin, the LPSC Grenoble, and the Technical University Munich, took place from 29-31 May, 2008 at the ILL. 110 participants from all over the world discussed theoretical motivation, latest results, and new projects in the fields 'few body systems', 'weak interactions', 'CP violation', 'new interactions' and 'new techniques'. These topics were animated by inspiring invited talks. Many questions remain to be answered, by experiments with slow neutrons!



Delegates to the workshop on Sample Environments at Neutron Scattering Facilities seen here in the Vercors mountains near Grenoble.

Sample Environments at Neutron Scattering Facilities

The 5th international workshop on sample environments at neutron scattering facilities was held on 26-28 May in the Vercors mountains near the ILL. We had a record gathering of 68 scientists from neutron scattering facilities worldwide and representatives from a few companies discussing: cryogenic systems, high-temperature furnaces, high-pressure generators and cells, magnetic and electric fields, sample positioning and orienting, sample-reaction environments, sample preparation and encapsulation, in situ measurements and (remote) control. The booklet, posters and viewgraphs are available from the web pages of the workshop at <http://www.ill.eu/sane/home/events/sensf-2008/>. The next workshop will be organized by FRM II at Munich during the Octoberfest.

Materials for Frustrated Magnetism

The ILL and the Louis Neel Laboratory of the CNRS both play prominent roles in the study of frustrated magnetic materials so it was natural for them to organise jointly a workshop on Materials for Frustrated Magnetism, funded largely by the European Science Foundation. About 90 delegates descended on the ILL between 3 - 5 March to attend talks on a wide range of materials that display magnetic frustration, from intermetallics, metal oxides and salts, to co-ordination compounds and organic materials. The aim was to bring together those who design and synthesise such materials – primarily chemists and materials scientists – with those from the physics community who traditionally focus more on measuring and rationalising their behaviour. 10 international leaders in their fields, drawn from across Europe, as well as Canada, the USA and Japan provided focal points for the meeting through invited talks, and we also enjoyed strong participation from PhD students and early-career researcher, a very promising pointer for this field's future health.

<http://mffm.neel.cnrs.fr/>



Joe Zaccai (with the hat) with Prof. Don Engelman of Yale, preparing to give the opening lecture of the Biological Physics at Large Facilities Workshop held in Grenoble in October 2008.

Hercules School on Soft Matter

The Hercules Specialised Course 9 (HSC9) 'Scattering and Imaging Studies of Soft Matter Systems Using Synchrotron Radiation and Neutrons' took place at the ESRF/ILL site from 16-23 November 16-23, 2008. The course was opened by a series of lectures providing an introduction to the various techniques with relevant examples of applications in soft condensed matter research. Following safety training courses at both ILL and ESRF two full days were dedicated to practical sessions on four beamlines/instruments. The last day of the school was devoted to lectures from local scientists on either complementary or 'novel' techniques in neutron and synchrotron radiation important for soft matter. Feedback from the participants was very positive. They confirmed that it was a good idea to combine scattering and imaging techniques in this school and to obtain an insight in both neutron and synchrotron radiation techniques.

More than simply neutrons

Surfaces and Interfaces in Soft Matter and Biology



Bob Thomas clearly enjoying being among old friends.



Julia Higgins makes her point to Andrew.

The Symposium on 'Surfaces and Interfaces in Soft Matter and Biology - The Impact and Future of Neutron Reflectivity' was held on 21-23 May 2008 at the ILL in honour of Bob Thomas (Oxford University), who has retired this year. The Symposium was organised jointly by ILL and ISIS and was attended by around 120 scientists from Europe and further afield. The event was a resounding success, with excellent international speakers, lively discussions and a host of new ideas. The quality of the speakers is testimony to their respect for Bob Thomas and the high degree of interest in the subject. Both Andrew Harrison and Andrew Taylor welcomed the participants. The after-dinner speech at the Château de la Commanderie was given by John White, former ILL director and Bob Thomas' former tutor. Proceedings are being published in a special issue of *Langmuir*.

Scattering Methods Applied to Soft Condensed Matter

From 7-14 June 2008, the 9th European Summer School on 'Scattering Methods Applied to Soft Condensed Matter' was organized through ILL and held at the remote vacation centre RelaiSoleil 'Les Bruyères' in Carcans-Maubuisson. This series of 'Bombannes' summer schools proposes since 1990, with a period of 2 years, advanced training for young European researchers and for researchers with a working place in European laboratories, at post-graduate and post-doctoral level. It is devoted to a practical 'state-of-the-art' approach to scattering methods, using neutrons, as well as X-ray and light sources – today's key techniques to study structure and dynamics in 'soft matter', i.e. systems containing colloids, polymers, surfactants and biological macromolecules. The scope of the 'Bombannes' school is to introduce on a fundamental level the current methodology of static and dynamic scattering techniques and their application to soft matter systems. In this year's event 16 well-recognized soft matter experts presented their lectures to 40 PhD-students from all over Europe, with a gender mix of 53% female/male and a peak of the age distribution at 27 years. The next event is planned for June 2010.

Further information on the 'Bombannes' school can be found at <http://www.ill.fr/Events/bombannes>.

Biological Physics at Large Facilities: from molecule to cell

The aim of this workshop, organised by ESRF and ILL, was to bring together the Biology and Physics communities for a discussion on the state-of-the-art and future perspectives of physics instrumentation and methods for the study of biological structures and dynamics at neutron sources and synchrotron radiation facilities. The impact of using physics methods in the study of biological systems is growing rapidly with unique opportunities offered by new instrumentation and methodology at large facilities worldwide. Both ESRF and ILL are planning considerable upgrades, with biophysical methods at the forefront. An integrated approach is essential to understand the physics of biological processes.

About eighty participants registered for the event; there were 35 oral presentations and a poster session. It was appreciated that the sessions were organised in order to avoid topic specialisation, which ensured multidisciplinary participation and cross-fertilisation of ideas. The workshop was opened by the President of the Division of Life Sciences of the EPS, who discussed



The workshop on Biological Physics at Large Facilities, jointly organised by the ERSF and the ILL brought together scientists from both the physics and the biology communities.

the different length and time scales that are relevant to understanding biological processes, which span from atomic sizes to the metre size of organisms, and from the 10-13 sec of fast electronic processes involved in sight or respiration to the several minutes of cell division. The development of neutron and synchrotron radiation methodology and instrumentation appropriate to the study of each level of organisation were discussed in several contributions. Biological topics discussed included the molecular structures and dynamics of proteins, biological membranes and the large molecular machines that are the basis of function inside living cells. At the larger size level there were contributions from groups that image cells and from paleontology, in which synchrotron radiation images of ancient fossils revealed the earliest evidence of human life developmental history.

N = 52: a new "magic" number?

A workshop on spectroscopy of neutron-rich nuclei was held from 16 to 21 March 2008 in Chamrousse to honour the career of Jean-Alain Pinston (formerly ILL, then CEN Grenoble and finally ISN/LPSC Grenoble) and Janine Genevey (ISN/LPSC Grenoble) who made important contributions to nuclear physics in Grenoble and retired in 2008. Enthusiastic presentations were given about recent experiments, results and ideas for future work on exotic nuclei at nuclear physics facilities in Europe and the U.S. using beta-decay, isomer, in-beam, mass and laser spectroscopy, as well as lifetime and magnetic moment measurements.

The workshop also provided time to reinforce current collaborations, and discuss new ones in different areas. The workshop was sponsored by the ILL, LPSC, UJF, INPG and Heinzinger Electronic and was attended by 52 participants from 26 different institutes and universities. Hopefully this number of 52 will really prove to be 'magic' by creating enough momentum to bring a large gamma detector array to the ILL for a measurement campaign of neutron-rich nuclei produced in neutron-induced fission.



Workshop on spectroscopy of neutron-rich nuclei held from 16 to 21 March 2008 in Chamrousse to honour the career of Jean-Alain Pinston and Janine Genevey.

All in a day's work

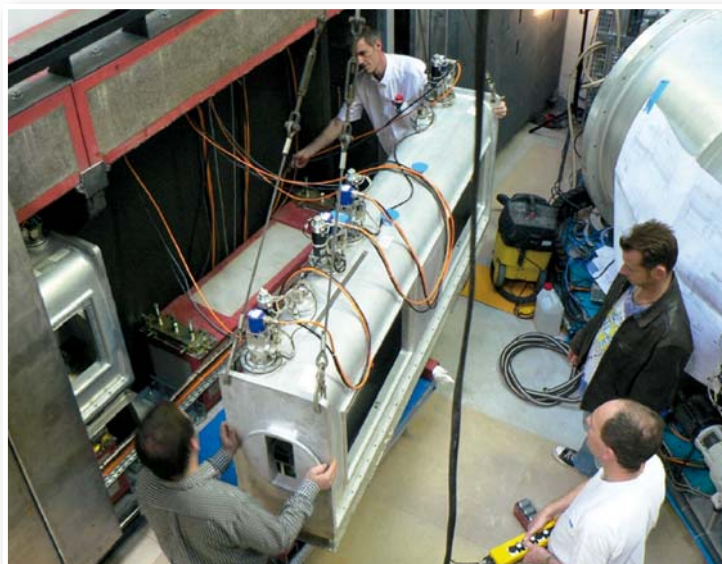
Mind your head

Peter Lindner leads journalists inside D11.



Gently does it

Richard Campbell, Mark Jacque, Simon Wood and Bob Cubitt nudge the beam deflector into place on FIGARO.



Meltdown

Pascal Mouveau seals a cell in the ³He laboratory.



Hang in there

Jerome Nucci guides the 3m-long detector unit into the IN5 flight chamber. Each detector unit weighs about 300 kg.



Hands on

David Bowyer helps position the new D11 tank into place.

Keeping cool

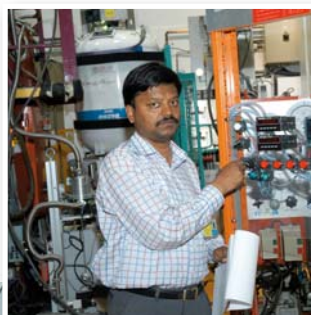
Laurent Brayer and his team check the latest data during the reactor safety exercise.



Happy scientists and users



Kristine Niss (left) and her two Danish colleagues prepare a high-pressure experiment on D20 with Alain Daramsy (right).



Ranjan Mittal sets up his experiment on IN6.



Anna Carnerup, Viyeka Alfredsson and Nina Reichhardt from Lund with Beate Klösgen from South Denmark working on D16 in the summer of 2008.



The prize for the most original T-shirt goes to D1B user Pedro Gorria from Spain. The T-shirt was designed by Kukuxumusu, a well known Basque artist.



Maurits van der Grinten and Michael McCann working on the guide system of the Cryo-EDM experiment.



Charles Dewhurst and Vikash Venkataramana, a PhD student from St Andrews University at the control computer of D22.

More than simply neutrons

Women in science at the ILL



Nuria Rebolledo, Isabel Galán and Lina María Toro from Madrid add colour to D1B.



Kathrin Zielske, Isabelle Grillo and Peggy Heunemann processing data in the D22 cabin.



Andrea Severing happily watching data output on the monitor screen of IN20.



The two Amys: Amy Poole and Amy Dee with a smiling Andrew Wills on D20.



Cécile Poulain, checking her LOHENGRIN data.

Susana Teixeira (left) and Giuliana Manzin (2nd from right) among delegates to a colloquium in Grenoble on Women in Science and Technology.



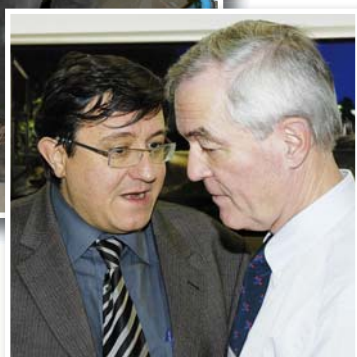
■ Visits and events



Thomas Hansen shows Ingo Radcke, the German Consul General from Lyon, around the reactor hall.



Richard Wagner thanking Michel Mollier after many years of service as Secretary of the ILL Work's Committee.



José-Luis Martínez makes his point to Paul Zinsli at the Steering Committee meeting.



Andrew Harrison, Virginie Guérard and Giovanna Cicognani at the Grenoble Science Festival in November.



Unmistakeable in their red T-shirts: Trevor Forsyth, Virginie Guérard, and Susana Teixeira on a joint ILL/ERSF stand at the American Crystallographic Association in Knoxville (USA).

The first-floor girls wish Carmen a happy retirement.



Sasha Ivanov explains some low temperature physics to Pavol Balgevy, a member of the Slovakian delegation.

More than simply neutrons

Scientific support laboratories

Materials Science Support Laboratory

In 2002, the Facility for Materials Engineering was formed at ILL-ESRF, led by a consortium of UK universities and proved invaluable for materials science experiments. In 2008 it was renamed the Materials Science Support Laboratory. Although the focus for the laboratory remains in the field of materials science and engineering, the service is available to both the Science Division and the Projects and Techniques Division.

A recent addition to the metrology suite, the portable Faro CMM arm can be used *in situ* when required. The arm has a reach of 2.4 m (which can be extended indefinitely by overlap measurements) and a precision of approximately 25 micrometres. **Figure 2** shows the arm in use on the hexapod of the SALSA beamline.

Figure 1:
The IN8 monochromator being measured using the laboratory-based CMM.



At the core of metrology of the laboratory are two coordinate measuring machines (CMM). The laboratory-based Mitutoyo 776 CMM is equipped for precise inspection or rapid digitisation of samples/components. When used with a Renishaw single-point touch probe, the precision is of the order of several micrometres. For digitisation purposes, a Metris LC50 non-contact laser scanner is available to rapidly scan a surface, visualising features as small as 10-15 micrometres. An example of

the use of the CMM is the measurement of the crystal orientations for the focusing IN8 monochromator (**figure 1**). Correct alignment of each of the 99 faces is crucial for beam optimisation. The CMM was used to determine the precise alignment of each face, indicating the faces that were out of tolerance and needing adjustment.

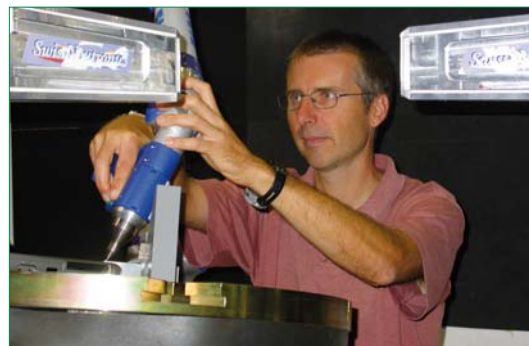


Figure 2: Steven Rowe using the portable CMM arm on the SALSA hexapod.

The laboratory is equipped with a Leica metallographic microscope and Buehler micro-hardness testing machine as well as the associated sample preparation tools. A good example of its use is shown in the work of ILL student Marc Pissard who is studying modern Damascene steels which are produced from two distinct powder grades using a rapid solidification process. **Figure 3** shows the typical banding from the two grades (RWL34 and PMC27) as well as the associated profile of micro-Vickers hardness for the quenched and slow-cooled material.

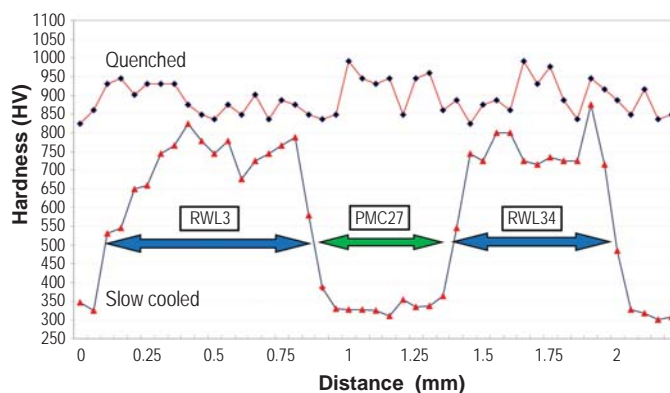
The Materials Science Support Laboratory is open to all users of ILL and ESRF. More information about this support may be found on the MSSL's website <http://www.ill.eu/others/mssl/>. For further information please contact S. Rowe (rowe@ill.fr) or D.J. Hughes (hughes@ill.fr).

Figure 3:
(a) Microscopic image showing typical banding of the two phases. Diamond indents by the hardness testing machine are highlighted.
(b) Variation of micro-Vickers hardness for the quenched and slow cooled Damascene steels.

a



b

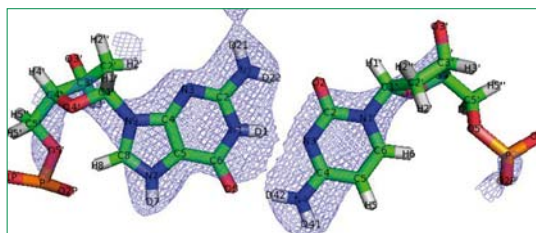


Scientific support laboratories

The Partnership for Structural Biology

The Partnership for Structural Biology (PSB) contains a powerful set of technology platforms that are contributed by the various partner institutes (ILL, ESRF, EMBL, IBS, and the unit for host-pathogen interactions). These platforms include advanced capabilities that complement the powerful neutron scattering facilities available to ILL users: synchrotron X-rays, electron microscopy, NMR, high-throughput methods (soluble expression and crystallisation), and a range of biophysical techniques such as isothermal calorimetry and surface plasmon resonance. A joint SANS/SAXS platform is being developed and there is also an initiative to develop a joint X-ray/neutron low resolution crystallography capability.

The aim of the PSB is to enhance the interdisciplinary capabilities of each of the facilities co-located on the site. Of particular interest to ILL's biology users is the ILL-EMBL Deuteration Laboratory (<http://www.ill.eu/deuteration>), managed by M. Härtlein (haertlein@ill.eu). This platform has had a decisive impact on biological neutron scattering at the ILL. A high proportion of all biology-related beamtime proposals now involve deuterated samples made in the laboratory.



G-C base pair in the LADI-III study of A-DNA shows unexpected protonation at the guanine 7 position.

Work on IN5 has been published in Phys. Rev. Lett. by A. Paciaroni (Perugia) and colleagues on the ice-like behaviour of water in complex with protein. Another project carried out by R. Leal (Keele, UK), together with colleagues from ILL and ESRF, has demonstrated the existence of novel protonation states in the base-pairs of A-DNA using data from LADI-III. A very interesting *in vivo* study carried out by M. Jasnin (IBS) has used deuterated *E. coli* cells to study intracellular water dynamics. Further dynamics work has been carried out by K. Wood (IBS) *et al.* who used incoherent scattering experiments to study the dynamic coupling between proteins and hydration water (Proc. Natl. Acad. Sci.). In another LADI-III study, A. Podjarny *et al.* (Strasbourg) have defined proton pathways in human aldose reductase (Proc. Natl. Acad. Sci.). A further example is SANS work on D22 by H. Niemann (Braunschweig, Germany) on the interaction between the Met Receptor and a *Listeria* invasion protein (J. Mol. Biol.). None of these of these experiments would have been possible without the Deuteration Laboratory and the PSB. For further information please contact: T. Forsyth (tforsyth@ill.fr) (Head of ILL's Neutron-Biology programme in the PSB)

The Partnership for Soft Condensed Matter

The Partnership for Soft Condensed Matter (PSCM) is an initiative first discussed back in 2004 that has seen considerable progress in the last few years, progress that witnessed an exponential trend in 2008. It involves mainly the ILL and ESRF with possible contribution by Associate Laboratories and Industry.

The PSCM is intended as a structure where samples to be used on soft matter instruments can be prepared and characterised before use with neutron and synchrotron radiation techniques. It will also represent a place for meetings and exchange for the soft matter communities of the two facilities (including both members of staff and users). Besides a number of laboratories it will comprise space for a seminar room, offices for students, post-docs and scientists on sabbatical.



The award of the ESFRI grant has tremendously boosted the activity around this project. This grant, awarded to contribute to the preparatory phase of planning for the overall upgrade of the ILL, has allowed the creation of a Senior Fellow position in Soft Matter to establish scientific partnerships with research centres focusing on soft matter, extreme sample conditions and materials science but who are not expert in the use of neutrons.

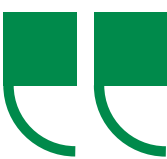
Part of the CPER grant (Contrat de Projets État-Région), recently awarded by French Local Authorities to renew the ILL/ESRF site, will be used for the PSCM building. The ESRF has always been seen as the natural partner for the ILL in this project. A milestone for the project has been the final support to the initiative by the ESRF Science Advisory Committee, obtained last November. As a result a re-organization of the ESRF Soft Matter Group has taken place with the activities led by the new group leader T. Narayanan.

At the moment, laboratories are being set up both at the ILL and ESRF to host pieces of equipment that will eventually move to the new building. In 2008, after consultation with the user community, the ILL acquired a light scattering apparatus and an ellipsometer for checking both bulk samples and interfaces prior to use with scattering methods.

ILL and ESRF have agreed a framework to take the collaboration forward: to jointly develop the scientific scope and content of the partnership; to demonstrate the feasibility of the partnership having well defined scientific activities; and to prepare a Memorandum of Understanding. This partnership provides for mutual, long-term commitment of ILL and ESRF in establishing and maintaining the PSCM laboratory. For further information please contact Giovanna Fragneto (fragneto@ill.fr).

More than simply neutrons

Grenoble and the future



The Grenoble metropolitan authorities have launched an ambitious development plan, aiming to reinforce links between research institutes, universities and local business. The city's two main hives of intellectual activity, the university campus and the *Polygone Scientifique* science park where ILL has its home, are to benefit from a major redevelopment programme. A sizeable portion of the city's surface area is to be transformed in what is one of France's top five urban development initiatives.

closer to the city centre via improved transport and housing infrastructure. This implies a major urban requalification of the site which accommodates major research centres (ESRF, CEA Grenoble, Institut de Biologie Structurale, engineering schools and the Minatec hub). The ILL is of course deeply involved.

Linked to the town centre via an underground boulevard and a new tramline and to the northern bypass the *Polygone*, which could be renamed 'peninsula of the future', will provide lodgings,

Architect's view of the Grenoble peninsula project for 2020[©] CEA/Grenoble/Vasconi.



Future specialised areas on the Grenoble High Technology peninsula.



- Large-Scale Research Infrastructures
- ST Microelectronics
- Fundamental Sciences
- Energy
- Nano-electronics
- Health-biology

shops, parks and sports grounds. The project plans are firmly underpinned by principles of sustainable development and high environmental, architectural and urban quality.

The urban services and equipment, as well as the teaching and research facilities, will be refurbished to meet international standards. It is this international orientation that is particularly satisfying for ILL, which was the first international facility to settle in Grenoble.

From a scientific point of view, the project will be based on specialised activity clusters. The laboratory and university structures in the fields of biotechnology or energy, for example, will be relocated together to improve the potential for synergy and the links with industrial partners. ILL will also benefit from the pooling of local skills and resources.

The *Polygone Scientifique* is to be developed both in economic terms – to multiply the links between research and industry – and through major replanning by bringing the *Polygone*

The changes to come will have a major and highly beneficial social impact on the science park as a whole, and our users will be amongst the happy beneficiaries.

The ILL 20/20 project

ILL 20/20 is part of the European Strategy Forum for Research Infrastructures (ESFRI) Road Map, the European Commission's strategic initiative to develop the scientific integration of Europe and to strengthen its international outreach. The mission of ESFRI is to support a coherent and strategy-led approach to policy-making on research infrastructures and to facilitate multilateral initiatives leading to the better use and development of research infrastructures in Europe.

Assisted by EU infrastructure funding, the ILL 20/20 project has a budget of 171 M€. It focuses on the maintenance of key neutron source components and the construction of beamlines and instruments and aims to boost the average efficiency of the ILL instruments by a factor of more than 10.



The Minatec nanotechnology centre. CEA®.



Research in a cleanroom at the CEA. Artechnique®



P. Conche®

Future development of the ILL site

The ILL and ESRF have launched an ambitious project to extend the facilities already offered by our international site.

Both institutes have agreed on a joint plan defining the facilities required to modernise the site and further boost its scientific appeal.

The plan includes scientific partnerships on soft condensed matter and materials science, along with a chemistry laboratory.

The new scientific and technological installations will be complemented with other more general improvements:

- A new site entrance
- A despatch and reception platform
- A visitors' centre
- A restaurant
- Internal roadways

Under the French *Contrat de Projets entre l'Etat et la Région*, significant funding is available for projects in our Rhône-Alpes region. The two institutes have signed an agreement with Rhône-Alpes under the CPER scheme for a total amount of 15 M€. Of this sum 9 M€ will be contributed by the Rhône-Alpes Region, 4.5 M€ by the *Métro* (the 'greater Grenoble council') and 1.5 M€ by the *Ville de Grenoble*. Some 850 k€ will also be granted through ESFRI, the European Strategy Forum on Research Infrastructures.

A joint ILL-ESRF Steering Group has been set up to pilot the project. A Building Programme has been outlined, and fifteen architects have been invited to participate in a prequalification exercise. It is planned to launch the 12-month study phase in October 2009 and the construction work in October 2010. Final delivery is expected in April 2012.

8 Administrative matters

Administration Division

In addition to its three separate services, covering human resources, finance and purchasing, and building and site maintenance activities, the Administration Division provides language, administrative and legal support. It also performs the role of secretariat to the Steering Committee, participates actively in the management of the CPER project (*Contrat Projet Etat Région*) for modernising the site's infrastructure, and from 2009 onwards will for the first time take over the chairmanship of the Workplace Health and Safety Committee (CHSCT). In 2008 the Division devoted a great deal of time to the introduction of new audit procedures at the ILL and continued its efforts to streamline administrative controls and procedures in order to better serve both its internal and external customers.

Human Resources

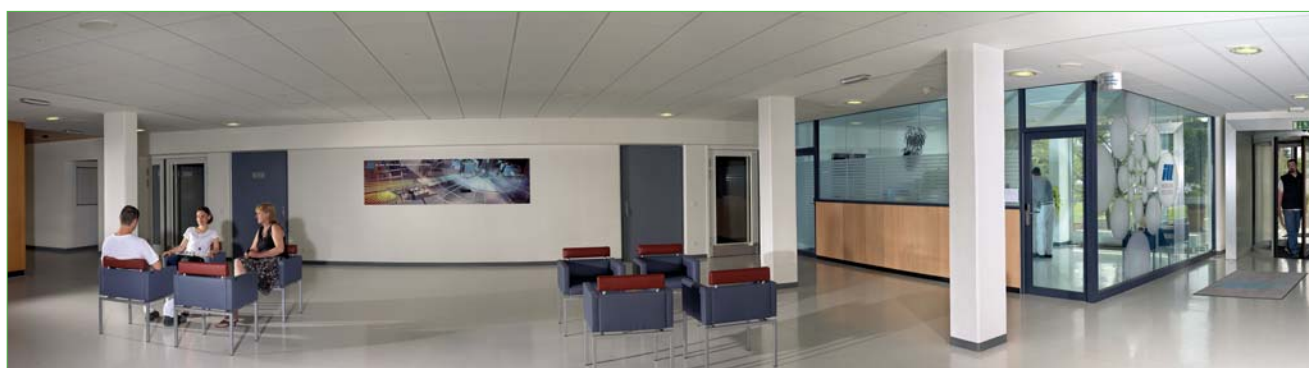
For the Human Resources Service, 2008 was marked by the successful conclusion of a number of separate sets of negotiations concerning the time-saving accounts, out-of-hours support, work by scientists at weekends and on bank holidays, the employment of disabled people, and the introduction of a three-year fixed-term project-based contract for 'cadres' and engineers. Furthermore, changes to French labour law meant that ILL had to modify the terms of its Collective Agreement regarding the length of notice periods in force during probationary periods for various categories of staff.

A new project to upgrade the ILL's promotion and job profiling system was started with the close involvement of Management, the Human Resources Service, the heads of service and the staff. The aim of the project is to give staff clear and well-structured career prospects, increase openness and transparency in the annual assessment process, and encourage an even greater degree of teamwork. To help it complete this project successfully, the ILL has called on the support of an outside firm of consultants with a proven track record of international experience in this area. Efforts will continue to focus on fine-tuning the new system in the first half of 2009 before final negotiations with the trade unions and implementation.

Due to the retirement of a large number of staff, recruitment was a major activity in 2008 and aimed to satisfy the dual constraints of providing the Institute with the best qualified personnel and managing the balance of nationalities, something which remains a major challenge for ILL. A comprehensive study of this issue was carried out during the course of the year and one of the recommendations made was the introduction of international cross-divisional interview panels. This recommendation has since been implemented and efforts to improve the balance of nationalities will continue in 2009. The coming year is also set to be another busy year in terms of collective bargaining as we aim to provide the ILL with a modern collective agreement in keeping with the expectations and image of a world-leading international research institute.

Finance and Purchasing

Following their merger into the newly formed Finance and Purchasing Service, the accounts and purchasing groups focussed on strengthening their collaboration and on upgrading the accounting and financial software tools and procedures in place. On the finance side, the first contractual audit of the ILL's accounts for 2007 was conducted by the external firm of auditors KPMG. Their report and the procedures implemented were examined by the ILL's Audit Commission and the 2007 accounts were approved by the ILL's Steering Committee in December 2008. The Committee of Experts on Fiscal Matters also carried out its annual examination of the Institute's tax and customs procedures and operations, and forwarded its report to the tax authorities. The finance group was involved in a number of major ongoing activities, such as the updating of the CEA study on the evaluation of the cost of decommissioning the ILL's nuclear installations and reporting to the French administrative authority on the securing of the financing of nuclear costs.



On the purchasing side, an organisational audit of the purchasing group was conducted by an outside consultant at the beginning of the year and the UK National Audit Office also carried out a review of the purchasing function, which confirmed that the group was functioning well.

At the beginning of the year, a contract was signed with the firm CERCA for the manufacture of the next 15 fuel elements. Negotiations were also successfully concluded at the end of 2008 on the amendment to the contract with AREVA for the reprocessing of spent fuel for the years 2009 to 2013.

The campaign to recruit a head of purchasing and a junior buyer in order to bolster the purchasing team was successfully concluded. The new head of the purchasing group will take up her duties on 1st March 2009.

Building and Site Maintenance

The Building and Site Maintenance Service's most noteworthy activity in 2008 was the civil engineering work associated with the installation of D11 and the biological shielding work required for the instrument FIGARO. The third phase of the seismic refit programme was completed in the first quarter, as were the re-landscaping of the grounds in front of the ILL/EMBL office building and the creation of controlled radiation protection areas in ILL 7 and ILL 22. During the second half of the year a building for offices and labs was inserted between ILL 7 and 22 and a new building for the Reactor Division compressors was built. The Building and Site Maintenance Service was also involved in the start of work on the basement of ILL 17 (radiation protection laboratories); this will be completed in the first half of 2009.

Translation

The translation office continued to translate a wide variety of documents into and out of the Institute's three official languages – English, French and German. The office's work covers the translation of technical specifications, safety notices, administrative documents, and brochures and leaflets aimed at the general public. Recurring activities include the translation of preparatory documents for the meetings of the ILL's statutory bodies (SAQ, Steering Committee and Audit Commission) and the provision of interpreting services for these meetings. The office also copy edits technical and scientific papers prior to their submission for publication. A major and ongoing project in 2008 was the translation of the ILL's new intranet and internet sites.

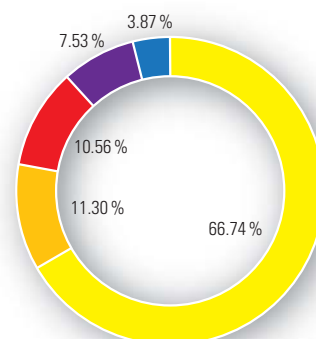
9 Facts and figures

Staff

- 478 people including 67 experimentalists in the scientific sector and 25.5 thesis students
- 319 French, 54 German, 50.5 British, 36 from Scientific Member countries and 18.5 from others

Staff numbers on 31/12/2008		%
France	319.0	66.74
Germany	54	11.30
United Kingdom	50.5	10.56
Scientific Members	36	7.53
Others	18.5	3.87
Total	478	100

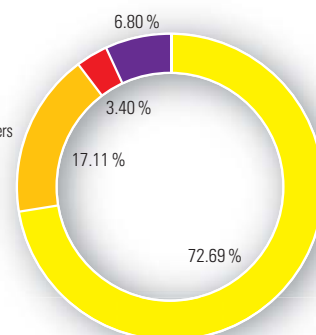
■ France
■ Germany
■ United Kingdom
■ Scientific Members
■ Others



Budget 2008 (excluding taxes)

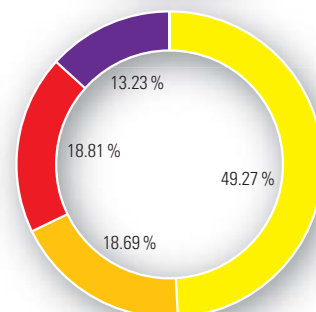
Income	M€	%
Income from Associates	59.9	72.69
Income from Scientific Members	14.1	17.11
Own income	2.8	3.40
Carry forward to 2008	5.6	6.80
Total	82.4	100

■ Income from Associates
■ Income from Scientific Members
■ Own income
■ Carry forward to 2008



Expenditure	M€	%
Staff costs	40.6	49.27
Operating costs	15.4	18.69
Investment costs	15.5	18.81
Fuel cycle	10.9	13.23
Refit Programme	0	0
Total	82.4	100

■ Staff costs
■ Operating costs
■ Investment costs
■ Fuel Programme

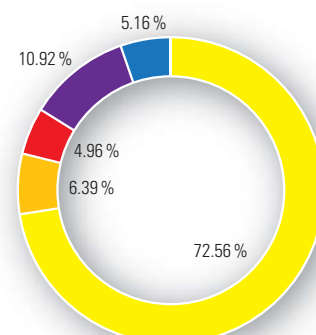


Distribution of ILL purchases

(without French captive market: 12M€)

Purchases	M€	%
France	18.27	72.56
Germany	1.61	6.39
United Kingdom	1.25	4.96
Scientific Members	2.75	10.92
Others	1.3	5.16
Total	25.18	100

■ France
■ Germany
■ United Kingdom
■ Scientific Members
■ Others



Name
Institut Max von Laue - Paul Langevin (ILL)

Founded
17 January 1967. International Convention (renewal)
signed until 31 December 2013.

Associates
France
Commissariat à l'Énergie Atomique (CEA)
Centre National de la Recherche Scientifique (CNRS)

Germany
Forschungszentrum Jülich (FZJ)

United Kingdom
Science & Technology Facilities
Council (STFC)



Countries with Scientific membership

Spain
Ministerio de Ciencia e Innovación (MICINN)

Switzerland
Staatssekretariat für Bildung und Forschung (SBF)

Italy
Istituto Nazionale per la Fisica della Materia (INFN)
Consiglio Nazionale delle Ricerche (CNR)

CENI (Central European Neutron Initiative)
Consortium, composed of:
- Austria: Österreichische Akademie der Wissenschaften
- Czech Republic: Charles University of Prague
- Hungary: Research Institute for Solid State Physics and
Optics affiliated to the Budapest Neutron Centre (BNC-RISP)

BELSWENI
- Belgium: Belgian Federal Science Policy Office (BELSPO)
- Sweden: Swedish Research Council (SRC)

Poland
The Henryk Niewodniczański Institute of Nuclear Physics
(Polish Academy of Sciences)

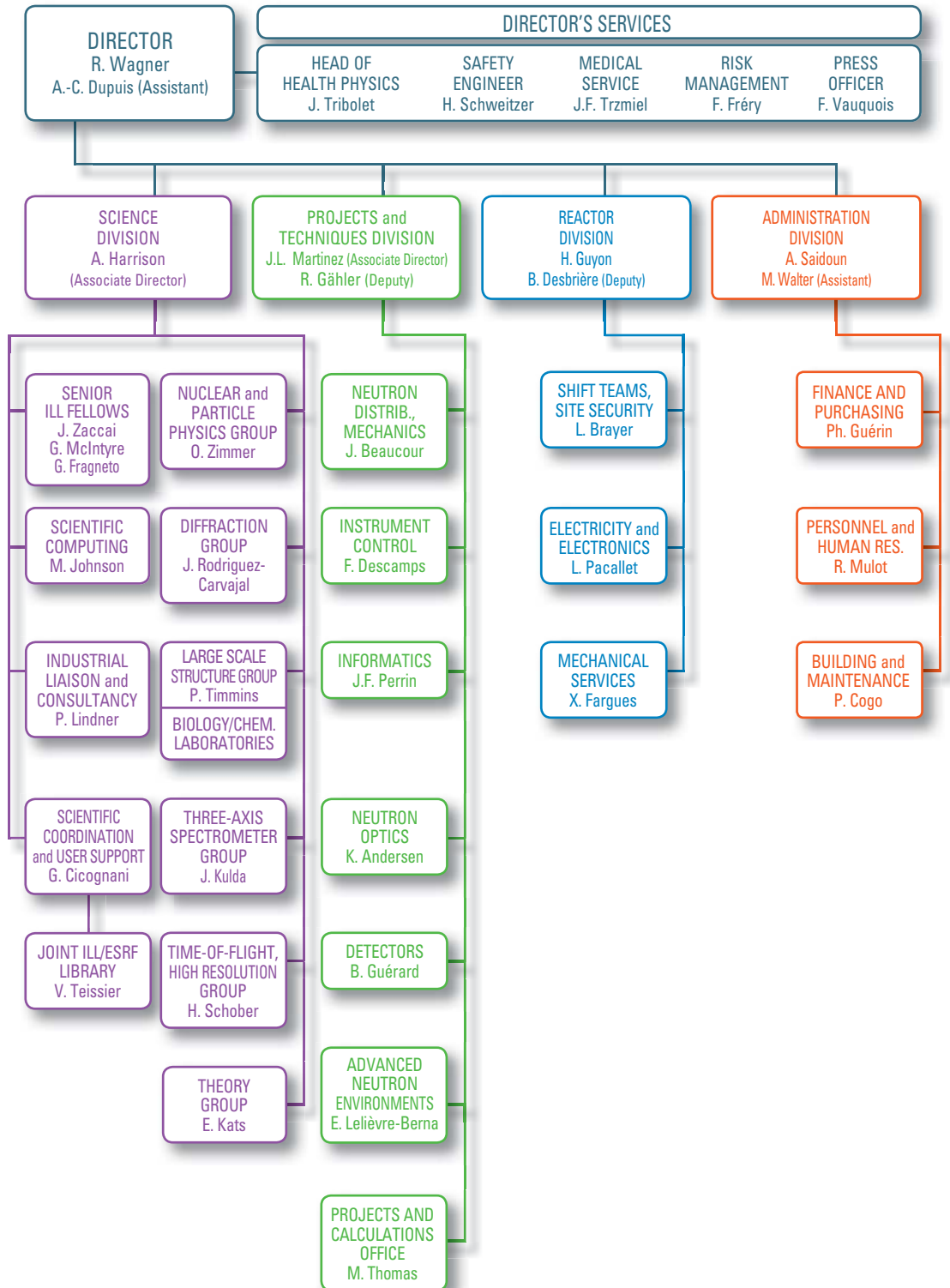
- Supervisory and Advisory Bodies**
- Steering Committee, meeting twice a year
 - Subcommittee on Administrative Questions,
meeting twice a year
 - Audit Commission, meeting once a year
 - Scientific Council with 9 Subcommittees,
meeting twice a year

Reactor
- 58 MW, running 4 cycles in 2008 (with cycles of 50 days)

Experimental Programme
- 833 experiments (allocated by subcommittees)
on 27 ILL-funded and 10 CRG instruments
- 1247 visitors coming from 43 countries
- 1118 proposals submitted and 766 accepted

Facts and figures

Organisation chart - December 2008



Publications

In 2008, the ILL received notice of 599 publications by ILL staff and users

The distribution by subject is as follows:

Applied physics, instrumentation and techniques	44
Materials science and engineering	42
Theory	25
Nuclear and particle physics	41
Magnetic excitations	43
Crystallography	64
Magnetic structures	84
Liquids and glasses	40
Spectroscopy in solid state physics and chemistry	77
Biology	56
Soft matter	83

PhD students and theses

PhD students at ILL in 2008	37
PhD theses completed in 2008	12



■ More than simply neutrons...

